SIMULATED HEAT-PIPE VAPOR DYNAMICS

DISSERTATION

W. Jerry Bowman
Captain, USAF

AFIT/DS/ENY/87

DEPARTMENT OF THE AIR FORCE
AIR UNIVERSITY
AIR FORCE INSTITUTE OF TECHNOLOGY

Wright-Patterson Air Force Base, Ohio

SIMULATED HEAT-PIPE VAPOR DYNAMICS

DISSERTATION

W. Jerry Bowman
Captain, USAF

AFIT/DS/ENY/87

AFIT/DS/ENY/87

SIMULATED HEAT-PIPE VAPOR DYNAMICS

DISSERTATION

Presented to the Faculty of the School of Engineering

of the Air Force Institute of Technology

Air University

In Partial Fulfillment of the

Requirements for the Degree of

Doctor of Philosophy

W. Jerry Bowman

Captain, USAF

May 1987

AFIT/DS/ENY/87

SIMULATED HEAT-PIPE VAPOR DYNAMICS

W. Jerry Bowman, B.S., M.S.E.
Captain, USAF

Approved by:	Date
James E. Hitchcock	7 May 1987
James E. Hitchcock, Chairman	
Milton E. Franke	7 May 1987
Milton E. Franke	
Alan V. Lair	7 May 1987
Alan V. Lair	
E. T. Mahefkey	11 May 87
E. T. Mahefkey	
Jerry E. Beam	11 May 87
Jerry E. Beam	
Eric J. Jumper	8 MAY 1987
Eric J. Jumper	

Accepted:

J S Przemieniecki	11 May 1987
Dean, School of Engineering	

Acknowledgements

The purpose of this research was to obtain further understanding of heat-pipe vapor dynamics. Numerical investigations of steady state and transient phenomena as well as experimental investigations of steady-state behavior were performed.

The project was sponsored by the Power Technology Group, Air Force Aero-Propulsion Laboratory of the Air Force Wright Aeronautical Laboratories, Wright-Patterson Air Force Base, Dayton, Ohio. I greatly appreciate their constant support, especially when my computer account ran dry. The project also received unofficial support from the Aerodynamics Branch, Air Force Flight Dynamics Laboratory, WPAFB. Dr. Joe Shang provided priceless support during the numerical portions of the research.

I would like to thank the members of my research committee who aided me during the ordeal, Dr. Jerry Beam, Dr. Alan Lair, Dr. Milton Franke, and Dr. Tom Mahefkey. I would also like to thank the Dean's representative, Dr. Eric Jumper, for his help in editing the final draft of this document. Special thanks goes to Dr. James Hitchcock who on a daily basis sat in counsel with me and shared his infinite wisdom. Without his support this project may have never been completed. If it had, it could never have been as good.

Table of Contents

List of Figures

Notation

A	pipe area
A	porous pipe property (Eq 2.12)
AR	aspect ratio (Eq 6.27)
B	porous pipe property (Eq 2.12)
C	coefficient of discharge (Eq 2.6)
c_v	specific heat at constant volume (Eq 4.22)
c_p	specific heat at constant pressure (Eq 4.24)
c	speed of sound (Eq 5.8)
D	pipe inside diameter
d	orifice plate hole diameter
E	specific total energy (Eq 4.14)
Ec	Eckert number (Eq 6.6)
e	specific internal energy
F_a	thermal expansion coefficient (Eq 2.5)
$\vec{F}$	axial terms, Navier-Stokes eqs (Eq 4.15)
$\vec{F}_t$	axial terms, turbulent Navier-Stokes eqs (Eq 4.49)
f	friction coefficient (factor) (Eq 6.1)
f	arbitrary variable
f^*	turbulent friction coefficient
$\vec{G}$	radial terms, Navier-Stokes Eqs (Eq 4.15)
$\vec{G}_t$	radial terms, turbulent Navier-Stokes eqs (Eq 4.49)
$\vec{H}_t$	extra terms, Navier-Stokes eq (Eq 4.15)
$\vec{H}$	extra terms, turbulent Navier-Stokes eqs (Eq 4.49)
K	flow coefficient (Eq 2.6)
k	thermal conductivity
L	total pipe length

M	momentum (Eq 6.3)
Ma	Mach number
$\dot{m}$	mass flow rate
p_o	total pressure
p	pressure
Pr	Prandtl number (Eq 4.20)
Pr_t	turbulent Prandtl number (Eq 4.48)
$\vec{q}$	heat flux vector
q_r	radial component, heat flux vector (Eq 4.17)
q_z	axial component, heat flux vector (Eq 4.18)
R	radius of pipe
R	gas constant
Re	axial Reynolds number (Eq 6.6)
Re_w	radial Reynolds number (Eq 1.1)
r	radial coordinate
T	temperature
t	time
u	axial component of velocity vector
$\vec{U}$	unknowns vector, Navier-Stokes eqs (Eq 4.15)
$\vec{U}_t$	unknowns vector, turbulent Navier-Stokes eqs (Eq 4.49)
$\vec{V}$	velocity vector
v	radial component of velocity vector
x	axial coordinate
$\bar{x}$	normalized streamwise coordinate (Eq 4.60)
Y	compressibility expansion factor (Eq 2.11)
y	axial coordinate
β	wall blowing/suction parameter

β'	wall blowing/suction parameter (Eq 6.27)
β_d	ratio of diameters (Eq 2.5)
γ	ratio of specific heats (Eq 4.25)
Γ	fraction of transition to turbulent flow (Eq 4.59)
Δt	time step (Eq 5.6)
Δt_{CFL}	stability time step (Eq 5.7)
λ	second coefficient of viscosity (Eq 4.16)
λ_t	eddy viscosity (second coefficient) (Eq 4.49)
μ	first coefficient of viscosity
μ_t	eddy viscosity (first coefficient) (Eq 4.50)
ξ	blowing distribution parameter (Eq 6.6)
$\overleftrightarrow{\Pi}$	unit normal tensor (Eq 4.5)
ρ	density
σ	safety factor, stability time step (Eq 5.6)
$\overleftrightarrow{\tau}$	viscous stress tensor (Eqs 4.8 to 4.11)
τ_w	wall shear stress (Eq 6.1)
σ_{ij}	stress tensor (Eq 4.4)
ϕ	momentum flux factor (Eq 6.22)
Ω	extent of the transition region (Eq 4.61)

Superscripts and Subscripts:

a	Mach number equation (Eq 7.1)
b	total pressure equation (Eq 7.1)
E	condenser entrance (Eq 6.15)
f	pertaining to friction term (Eq 7.1)
j	radial grid index (Eq 5.1)
k	axial grid index (Eq 5.1)
$\bar{k}$	axial grid index, corrector step (Eq 7.12)
n	time iteration (predictor step) (Eq 5.1)
$\bar{n}$	time iteration (corrector step) (Eq 5.2)
o	condition at upstream end of evaporator (Eq 2.1)
p	predictor step (Eq 7.10)
T	turbulent (Eq 6.15)
t	turbulent (Eq 7.18)
t,i	initiation of turbulence (Eq 4.60)
t,f	full transition to turbulent flow (Eq 4.60)
$\dot{m}$	change in mass flow rate term (Eq 7.1)
*	choked flow condition (Eq 2.3)
+	normalized variable (Eq 6.5)
–	time averaged variable (Eq 4.39)
'	fluctuation about time averaged value (Eq 4.37)
~	mass averaged value (Eq 4.40)
"	fluctuation about mass averaged value (Eq 4.30)

Abstract

This dissertation describes work done to establish functional relationships for friction coefficients that can be used in simple, one-dimensional heat-pipe vapor models. Expressions for friction coefficients were derived that can be used to design heat pipes for compressible-flow situations (Mach numbers as high as one) with very large mass injection/extraction rates (radial Reynolds numbers ranging from ±100 to ±20,000).

In order to establish these relationships, a simulated heat pipe was studied. Pressure variations axially and velocity variations axially and radially along the simulated heat pipe were experimentally measured. Turbulent transition in the heat pipe was also experimentally studied. The experimental data was used to show that numerical solutions gave valid results.

Vapor flow in the simulated heat pipe was numerically modeled. The compressible, non-steady, axisymmetric, Navier-Stokes equations were solved numerically using MacCormack's explicit finite difference method. The friction coefficient expressions developed using the numerical data were shown to give excellent results when used in a one-dimensional model to predict flow dynamics resulting from mass injection/extraction.

I. Introduction

This introductory chapter is divided into three sections. First, a brief history of heat pipes will be presented along with a brief description of how they operate. Next, literature relating to heat pipe vapor flow will be reviewed. Lastly, an outline of the research reported in this work will be presented.

History and Operation of Heat Pipes

A heat pipe is a device which, without moving mechanical parts, is able to transport large amounts of energy over a significant distance with a small temperature difference. The energy transfer is achieved by means of the evaporation of fluid at one location and condensation of the vapor at a different location. Capillary forces in a wick aid in returning the liquid to the evaporator region. The first recorded use of a device similar to a heat pipe was by Perkins in 1897 (1:1,2). Perkins' pipes are wickless heat pipes. They rely on gravitational forces to return the liquid from the condenser to the evaporator.

In 1942 Gaugler invented a heat pipe that worked in a similar manner to a Perkins pipe except that the working fluid was circulated with the aid of a wick. Even though the idea had been around since 1942, it wasn't until 1963 that Grover and his co-workers at the Los Alamos Laboratory began serious research on these devices. It was this group that first introduced the term heat pipe. From 1963 on, the amount of research done on heat pipes grew quickly with work now being done in nearly all developed nations (1:1,2).

A heat pipe has four parts: a container, a wick, a vapor region and a working fluid. A typical container is a right circular cylinder with a large length to diameter ratio enclosing the wick, working fluid, and vapor region. One end of the heat pipe is called the evaporator and the other end is called the condenser. The evaporator and condenser can be separated by an adiabatic region (Figure 1.1).

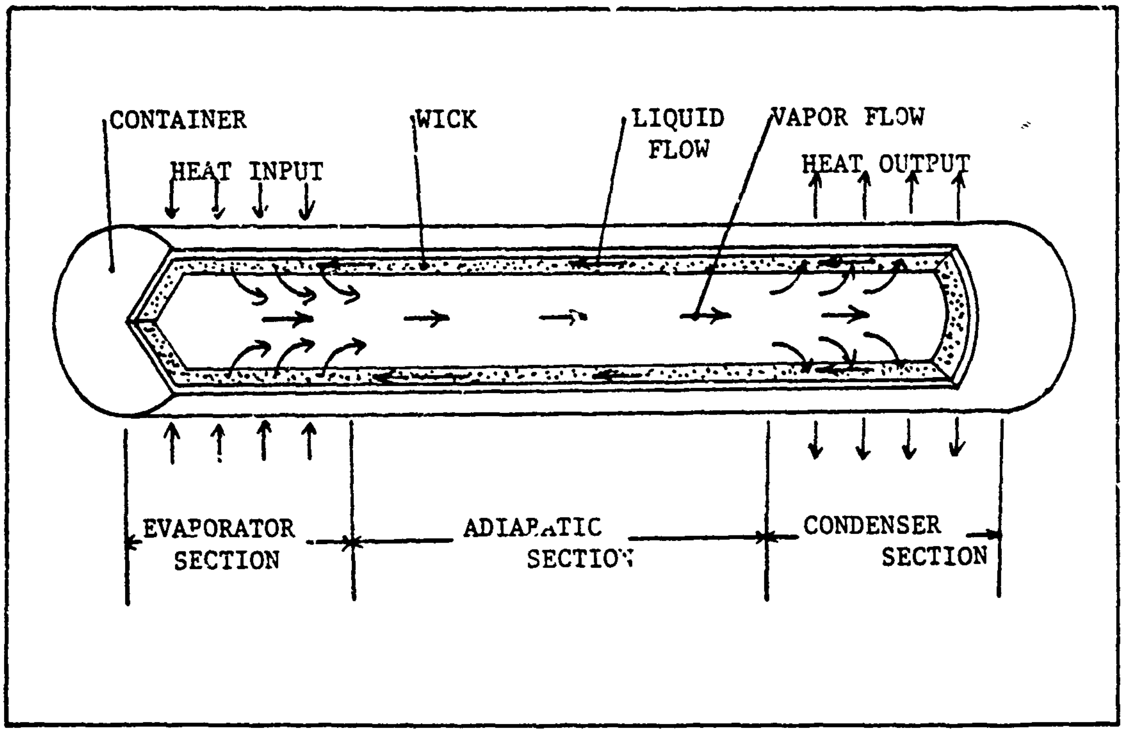

Figure 1.1 Basic Heat Pipe

As the evaporator end of a heat pipe is heated, working fluid evaporates from the wick. The pressure in the evaporator end of the heat pipe rises above the pressure in the condenser. The vapor responds to the pressure gradient and flows from the evaporator to the condenser. To maintain the condenser at a lower pressure than the evaporator, vapor is condensed. As vapor condenses, the resulting liquid must be returned to the evaporator. If the liquid does not return, the evaporator drys out and the cycle stops. Capillary forces in the wick aid in transporting the liquid from the condenser to the evaporator.

Literature Review

The available literature pertaining to heat-pipe vapor dynamics, and the closely related topic of flow in pipes with mass extraction/injection at the pipe wall, is discussed in this section. The literature is grouped into the following categories 1) steady laminar flow in pipes with mass injection/extraction, 2) steady heat-pipe vapor dynamics, 3) experimental studies, 4) transient heat-pipe studies, and 5) the effect of mass injection/extraction on steady turbulent flow in pipes.

Laminar Flow in Pipes With Mass Injection/Extraction. In 1953, ten years before the name heat pipe was coined, research on the fluid dynamics of flow in porous pipes with mass injection/extraction at the wall began. Since 1953 several analytical studies have been performed to help better understand these phenomena. Articles (2),(4)-(9), describe studies in incompressible, laminar flow in porous tubes with uniform mass transfer at the walls. Berman (2) was the first to solve the Navier-Stokes equations for a channel having a rectangular cross-section and two equally porous and opposite walls. With the assumption of uniform extraction (suction) at the walls, an exact solution of the flow equations was obtained. He found that the velocity profile deviates from the Hagan-Poiseuille parabola (3:85-87), being flatter at the center of the channel and steeper in the region close to the walls. The degree of deviation is dependent on a radial Reynolds number. The radial Reynolds number is a Reynolds number based on the velocity of the flow through the channel wall and the hydraulic diameter.

$$Re_w = \frac{\rho_o v_o D}{\mu} \qquad (1.1)$$

where ρ_o is the fluid density, v_o is the radial (extraction) velocity at the wall, D is the hydraulic diameter and μ is the fluid viscosity.

Brady (4) studied the effect of the inlet velocity profile on incompressible flow in a porous channel with uniform extraction. He showed that above a critical radial Reynolds number of 2.3 (a positive radial Reynolds Number corresponds to mass extraction from the pipe), the structure of the flow throughout the entire tube was influenced by the inlet profile. This result is of interest to heat-pipe designers in that it points out the importance of solving the evaporator and condenser problems simultaneously.

Friedman and Gillis (5) studied steady-state, axisymmetric flow of an incompressible liquid in a straight pipe with absorbing walls. They used a vorticity-stream-function approach to solve the coupled

Navier-Stokes equations. They studied the class of problems with axial Reynolds numbers ranging from 0 to 500 and radial Reynolds numbers ranging from 0 to -20 (a negative value corresponds to mass injection). Unlike a heat pipe, the pipe they studied was open at both ends. They did include in their study cases where total absorption occured. Total absorption is when all of the fluid entering the inlet of the pipe is extracted through the pipe wall. Total absorption occurs in all heat pipes because the down stream end of the pipe is blocked. In heat pipes, all fluid entering the condenser must be condensed onto the condenser wall/wick. For the total absorption case, Fredman and Gillis noticed flow reversals along the extraction surface (Figure 1.2).

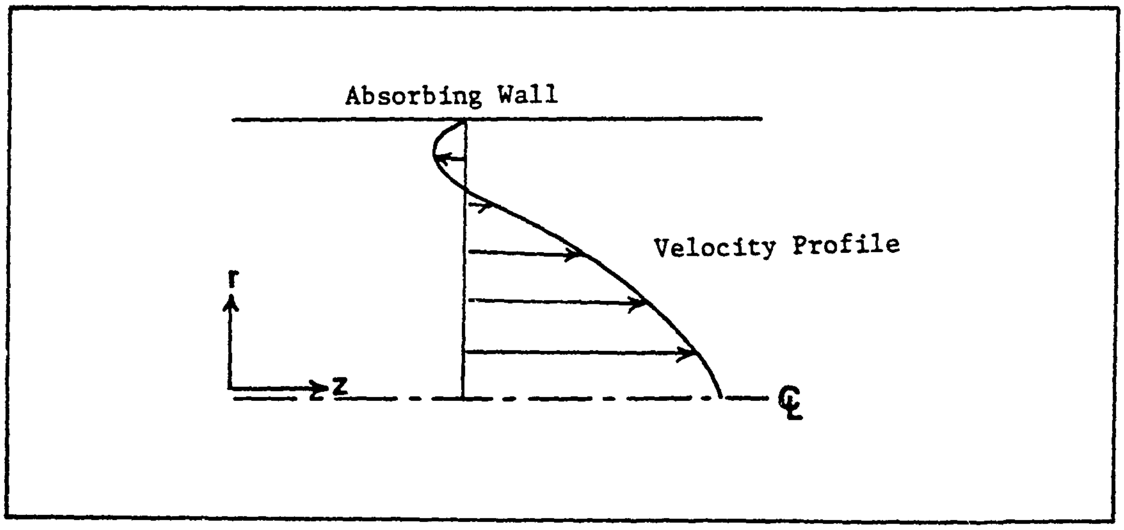

Figure 1.2 Example of a Velocity Profile in a Heat Pipe with Flow Reversal

Kinney (6) numerically determined the friction and heat-transfer characteristics for fully-developed, laminar flow, in circular porous tubes. He assumed a constant property fluid and uniform wall mass transfer. He presented friction factor results for radial Reynolds numbers from -4.618 to 20. The tubes studied were open at both ends. Kinney, extrapolating from his results, estimated that at a radial Reynolds number of -4.626 the friction factor would be zero. This would correspond to an onset of flow reversal in the pipe.

Rathby (7) analytically studied laminar flow in pipes and rectangular ducts with mass injection/extraction. Equations representing the friction coefficient were presented for both geometries for radial Reynolds numbers in the range of -20 to 40. Where earlier authors had predicted a decrease in friction with small extraction rates in pipes, he found that for duct flow, in a region with an adverse pressure gradient, the velocity profile became flatter with a steeper gradient near the wall. This led to an increase in friction.

Some interesting results of the above studies have been summarized by Terrill and Thomas (8). They found that two distinct analytical solutions to the governing differential equations exist for radial Reynolds numbers in the range of 0.0 to 2.3046 and for radial Reynolds numbers between 9.1045 and about 50. No analytical solutions could be found in the range of 2.3046 to 9.1045. Where the two solutions existed, at least one of the solutions predicted flow reversal in the pipe's mass extraction region.

Most recently R. M. Terrill (9),(10) has solved the incompressible, laminar Navier-Stokes equations for axisymmetric flow in a porous tube with non-uniform injection/extraction. The result was used to obtain a fully-developed solution for flow in a porous pipe with axially varying injection/extraction. Prior to these works, all researchers had limited their work to uniform extraction or injection.

Heat-Pipe Vapor Dynamics. Since 1963 a body of literature has developed about heat pipes. Five International Heat Pipe conferences have been held. Three books on heat pipe design and theory are now available (1),(11),(12). Numerous papers have been written about the different aspects of heat-pipe operation including the dynamics of vapor flow which is the topic of this research.

The first major paper on heat pipes was written by Cotter in 1965 (13). Cotter based his vapor flow analysis on the work of Yuan and Finkelstein (14) for radial Reynolds numbers much less than one and on the work of Knight and McInteer (15) for radial Reynolds numbers much greater than one. Both analyses assumed incompressible laminar flow with uniform injection/extraction. Yuan and Finkelstein (14) showed that the pressure gradient would be close to that obtained for Hagan-Poiseuille flow (3:85-87) where the velocity profile is parabolic. The gradient would be slightly larger for the case of evaporation (mass injection) and smaller for condensation (mass extraction). For large radial Reynolds numbers, Knight and McInteer (15) showed that the velocity profiles could no longer be assumed to be close to parabolic. They developed an expression for the axial pressure gradient at high radial Reynolds numbers which was experimentally verified by Wageman and Guevara (16).

Since that time other authors have used incompressible flow models. Bankston and Smith (17) solved the two-dimensional, incompressible Navier-Stokes equations for steady-flow in a heat pipe. They used a vorticity-stream-function approach so that radial pressure gradients would not be ignored and so that flow reversals could be permitted. They concluded that for radial Reynolds numbers larger than 2, accurate prediction of axial pressure loss requires the solution of the complete two-dimensional equations. For small radial Reynolds numbers, simpler approaches could be used. They limited their study to laminar flow in heat pipes.

Van Ooijen and Hoogenborm (18) studied vapor flow in a flat-plate heat pipe. The vapor region was a rectangular channel. The lower plate contained the wick, evaporator and condenser. The top plate of their heat pipe was assumed to be an adiabatic wall. For their numerical work they assumed steady, incompressible, two-dimensional, laminar flow. They concluded that for small radial Reynolds numbers (less than 25) accurate pressure and velocity profiles could be obtained by using the simple Hagan-Poiseuille flow model (i.e., parabolic velocity profile). For larger radial

Reynolds numbers, a more complicated approach was needed. In a later article, (19), Van Ooijen and Hoogenborm compared experimental pressure data they obtained for flow in a flat plate heat pipe with their numerical results reported in Ref (18) (discussed above). The comparison was fair.

The effects of compressibility on flow with mass injection/extraction have also been studied. One-dimensional, frictionless, compressible-flow models have been developed by several authors. Levy (20) studied the behavior of vapor in the evaporator section of a heat pipe using a steady, one-dimensional, compressible-flow analysis. He was interested in knowing if gas dynamic choking could limit heat-pipe performance. He studied two vapor models, a perfect-gas model and an equilibrium two-phase model, and compared his results with the experimental data of Kemme (21) obtained from a horizontal sodium heat pipe. Levy concluded that at low vapor pressures sonic velocities could be obtained at the entrance to the heat-pipe condenser thus limiting the amount of energy transport achievable by a heat pipe.

Bystor and Popov (22) were also interested in the compressibility effect in supersonic flows of high temperature heat pipes. They developed a steady, one-dimensional, frictionless, compressible model to study these effects. In their model they also compared the two gas models studied by Levy. They found that assuming thermodynamic equilibrium of the two phase flow was valid when compared with unpublished experimental data obtained from a sodium heat pipe by Ivonovsky and Sorokin and their colleagues at the Physics and Power Institute. The experimental data was in the form of temperature fields measured with a movable thermocouple located in a capillary tube mounted inside the vapor channel near the wick surface. The experimental data suggested the presence of a normal shock in the condenser. This indicated the presence of supersonic velocities in the condenser.

Two-dimensional, steady, compressible models have also been developed. The first was developed by DeMichele (23). He solved the governing equations by using an integral transformation closely related to the stream-function transformation first introduced by R. Von Mises (24). He simplified the governing equations by assuming the boundary-layer assumptions applied. When compared to unpublished experimental data obtained by J. Kemme at the Los Alamos Scientific Laboratories, the method was shown to give good results.

Tien and Rohani (25) also solved the Navier-Stokes equations for steady, two-dimensional, compressible flow in a cylindrical heat pipe. They did not assume the boundary-layer assumptions applied. They used a vorticity-stream-function approach similar to the incompressible-flow method used by Bankston and Smith (17). They claim that, for high evaporation and condensation rates, their model gave better results than similar models that made boundary-layer assumptions.

Recently Busse and Prenger (26) wrote a computer code, AGATHE, which was intended to evaluate the vapor flow in axially-symmetric, vapor-limited heat pipes. They used a steady, two-dimensional, compressible, boundary-layer model which assumed that the vapor was an isothermal perfect gas. Their program was the first to model both laminar and turbulent flows. Upon comparing their results with experimental and numerical results from other sources [(17), (27) c.f. below], they concluded that their model did a good job of predicting pressure recovery in heat pipes. Since Busse and Prenger published their paper, Haug and Busse (27) have further validated the model with the latest experimental heat-pipe vapor data that was available.

Experimental Results. Although some data is available, review of the heat-pipe literature reveals that the experimental data available to validate numerical models are still incomplete. It should be noted that the available data are in two forms: actual heat-pipe data; and simulated heat-pipe data employing air flow with injection/extraction in porous-wall pipes. Wageman and Guevara (16) were among the first to act on the need to experimentally validate early theoretical studies. They simulated a heat-pipe evaporator by injecting air through a porous-wall pipe. They found that their experimental results closely matched the laminar flow theory of Yuan and Finkelstein (14) even for axial Reynolds numbers up to 100,000, where turbulence should have been well established. In their work, no Mach numbers above 0.16 were attained nor did they study the effects of mass extraction.

The most widely referenced experiment is that done by Quaile and Levy (28). They simulated a heat-pipe condenser in a similar way to the condenser studied by Wageman and Guevara (16). They measured axial pressure drop in a porous pipe as well as radial variations in the axial velocity at several axial locations. They found that extraction caused the flow to become turbulent at axial Reynolds numbers lower than 2000 which generally denotes the lower limit of the region of turbulent flow. They observed transition at axial Reynolds numbers lower than 370 when the radial Reynolds number was 6. Transition refers to the region in a flow field where the flow is changing from fully laminar to fully turbulent.

Experiments on flow in a porous pipe with extraction (i.e., simulated heat-pipe condensers) have also been reported by Aggarwal, Hollingsworth and Mayhew (29). They measured the pressure gradient obtained with air flow in a porous tube of circular cross-section with a fully-developed turbulent profile at the entrance of the mass extraction region and with uniform mass extraction through the pipe wall. Their experiments covered inlet axial Reynolds numbers ranging from 11,000 to 101,000 (inlet axial Reynolds number refers to the Reynolds number based on mean axial velocity and pipe diameter at the entrance to the pipe) with a ratio of the transverse velocity at the wall to the mean axial velocity at the inlet ranging from 0 to about 0.027. The form of the velocity profile was found to depend upon extraction rate, becoming more flat at modest rates of extraction, but less flat at high rates. Extraction also caused the relative turbulence level to increase at all radii, except for some reduction in the region of the wall at very low rates of extraction. Friction-coefficient values for flow with extraction are graphically presented in the paper. At a fixed axial Reynolds number, friction-coefficient values were found to increase markedly with suction as compared to typical non-porous pipe friction coefficients (for example, at an axial Reynolds number of 80,000, the friction coefficient was as high as 10 times the expected turbulent rough pipe friction coefficient).

Transient Heat-Pipe Studies. During the literature review, no papers were found that model non-steady vapor flow in heat pipes. Three papers, one by Beam (30), one by Chang (31) and the last by Colwell (32) all presented studies on transient heat-pipe operation; however, their work was aimed at understanding transient wick phenomena. At the Fourth Symposium on Space Nuclear Power Systems, Albuquerque, New Mexico, January 1987, five papers (33)-(37) were presented on work currently being done to model heat-pipe transients. All of the models discussed were still in the development stages. The majority of the models being considered assume the vapor flow is one-dimensional.

Turbulence Studies. Several of the previously-mentioned articles discussed the existence of turbulence in heat-pipe vapor flow. The articles that will now be discussed (38)-(42),(44),(45) pertain specifically to the modeling of turbulence in regions of mass injection/extraction or with adverse/favorable pressure gradients.

Five of the papers (38)-(42) proposed modifications to the Van Driest dampening factor, Ref (43), used in conjunction with Prandtl-mixing-length theory of turbulence modeling. Van Driest introduced a useful modification to Prandtl's-mixing-length theory which provides a continuous velocity and shear distribution for turbulent flow near a wall. The Van Driest dampening factor (a value used in Van Driest's model) relates to the thickness of the laminar sublayer. The same general trends were noted in all papers. They suggested that a favorable pressure gradient (accelerating flow) caused an increase in the dampening factor. This is manifest in a thicker laminar sublayer which leads to lower skin-friction as compared to flow over a flat plate. The reverse was noted for an adverse pressure gradient (decelerating flow), that is the dampening factor was decreased. All five papers also concluded that mass extraction had a similar effect to that of a favorable pressure gradient while mass injection had a similar effect to that of an adverse pressure gradient. Each paper presented a slightly different formula for modifying the Van

Driest dampening factor to account for these effects. All five papers limited their range of study to small mass transfer rates and small pressure gradients.

Brosh (44) experimentally studied turbulent flow in a tube with mass extraction. He verified the trends relating to extraction discussed above; however, he noted that this was only true in very long pipes after fully-developed flow had been established. In pipe entrance regions the opposite trend prevailed; i.e., mass extraction caused a thin laminar sublayer which lead to higher skin friction as compared to flow over a flat plate. He stated that the flow seems to be much more complex than originally thought; that more experimental work, especially in the transition zone, was clearly indicated.

The most recent attempt to model turbulent flow in a pipe with extraction was by Eroshenko, Ershov, and Zaichik (45). They chose to deviate from Prandtl-mixing-length theory, feeling that a more complex model was needed. In their paper a three-parameter model of turbulence was used. Upon comparing their results with the experimental data of Aggarwal et. al. (29) they felt that a fairly satisfactory description of the flows' turbulence characteristics was obtained with the three-parameter turbulence model.

Objective of This Research

The main thrust of the present work was to establish functional relationships for friction coefficients that can be used in simple, one-dimensional formulations to model heat-pipe performance in operating regions not formerly well understood. These regions include compressible-flow situations where Mach numbers can approach one somewhere in the pipe. Such regimes are usually brought on by large mass injection/extraction rates; thus the friction coefficient relations must be able to account for such rates.

In order to establish reliable relationships a simulated heat pipe was studied. Pressure variations axially and velocity variations axially and radially along the simulated heat pipe were experimentally measured. The experimental data was used to show that numerical solutions (c.f. below) gave valid results.

To gain more detailed information about the flow field being studied, vapor flow in the simulated heat pipe was numerically modeled. The compressible, non-steady, axisymmetric Navier-Stokes equations were solved numerically. The compressible form of the equations was used because of the vapor density changes in heat pipes at high Mach numbers and during power transients. MacCormack's explicit finite-difference method was used to solve the equations.

From the results of the numerical simulations, expressions for friction coefficients were derived that can be used by heat-pipe designers to design heat pipes for compressible-flow situations with very large mass injection/extraction rates (radial Reynolds numbers from 100 to 20,000). The expressions developed were shown to give excellent results when used in a one-dimensional model to predict flow dynamics.

II. Experimental Approach

The goal of the experimental portion of the present work was to gain a better understanding of vapor dynamics in a heat pipe at Mach numbers near one. This goal was achieved by measuring the vapor pressure and velocity distributions in a simulated heat pipe operating in the sonic range, and by trying to characterize the turbulence patterns encountered. These data formed the basis for comparison with the numerical model of vapor behavior discussed in detail in a later chapter. In this chapter a discussion on how the heat-pipe vapor flow was simulated will be given. Following this, the experimental set up is discussed. Finally a discussion is given on how turbulence was measured.

Simulated Heat Pipe

It is well documented that measurement of vapor dynamics in actual heat pipes presents a number of experimental difficulties (c.f. below). Following the work of Wageman and Guevara (16) and Quale and Levy (28), an alternative to studying vapor dynamics in a heat pipe is to simulate heat-pipe vapor flow by blowing air through a porous pipe to model an evaporator, and extracting the air via suction through a different section of the porous pipe to simulate a condenser. Figure 2.1 is a schematic representation of this idea. Such a system is relatively simple to build and test, and has been shown (Ref (16)

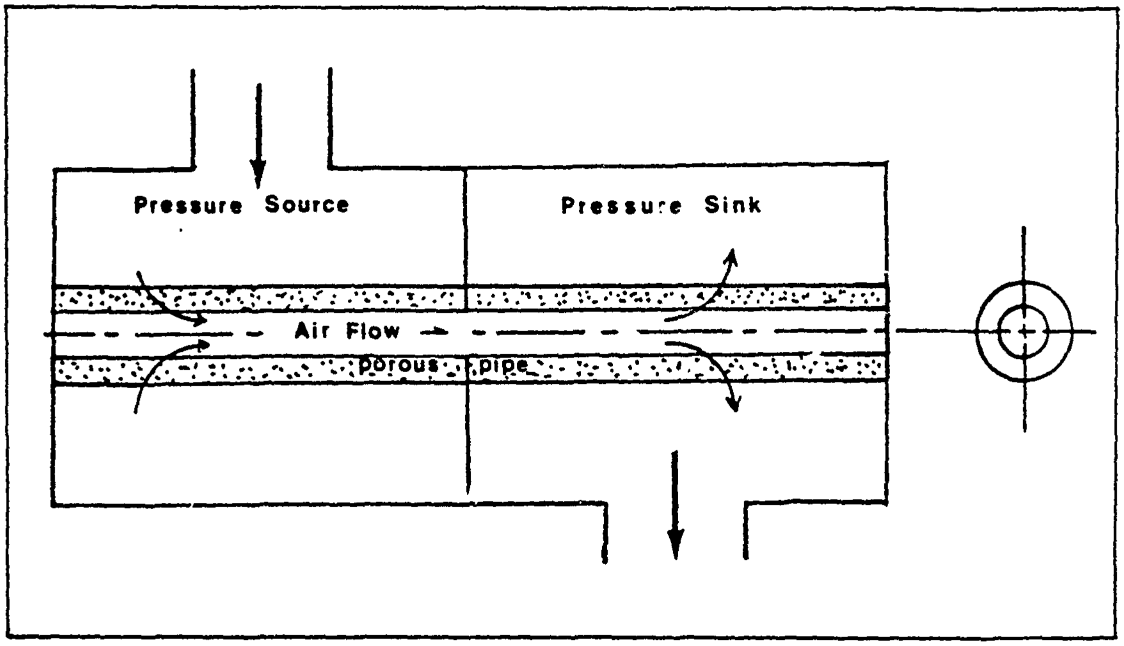

Figure 2.1 Porous Pipe Concept

and (28)) to closely model heat-pipe vapor dynamics.

Because heat pipes are carefully sealed from their environment, it is difficult to measure the velocity field in the vapor region. For the porous pipe set up, velocity probes can be easily introduced into the vapor region to measure the gas velocity. Because heat pipes are able to operate at very low pressures with very small axial pressure variations, pressure measurements can be hard to make. Since the porous pipe is operated at higher pressures with larger pressure changes, this problem is avoided. Finally, with the porous pipe, no complicated heating and cooling equipment is needed, nor is a liquid return mechanism (like the wick in a heat pipe) required. For all the above reasons, a porous-wall heat-pipe simulator was used to obtain the required data for this study.

Porous-Wall Heat-Pipe Simulator Design

The first consideration in the porous-pipe design was the compressed air supply available for the testing. At AFIT, compressors were available that could continuously supply 1 lbm/sec of air at 100 psig. The pressure sink was the laboratory atmosphere. Choked mass flow rate versus upstream pipe pressure for various sizes of pipes are plotted in Figure 2.2, along with the operating limits of the pressure supply. Figure 2.2 assumes that air enters the upstream end of the pipe at 560 R, and that one-dimensional, compressible flow relations for flow with mass injection/extraction (c.f. below) were valid. Such considerations led to the selection of a 0.650 inch inside diameter porous pipe for use in the experiment.

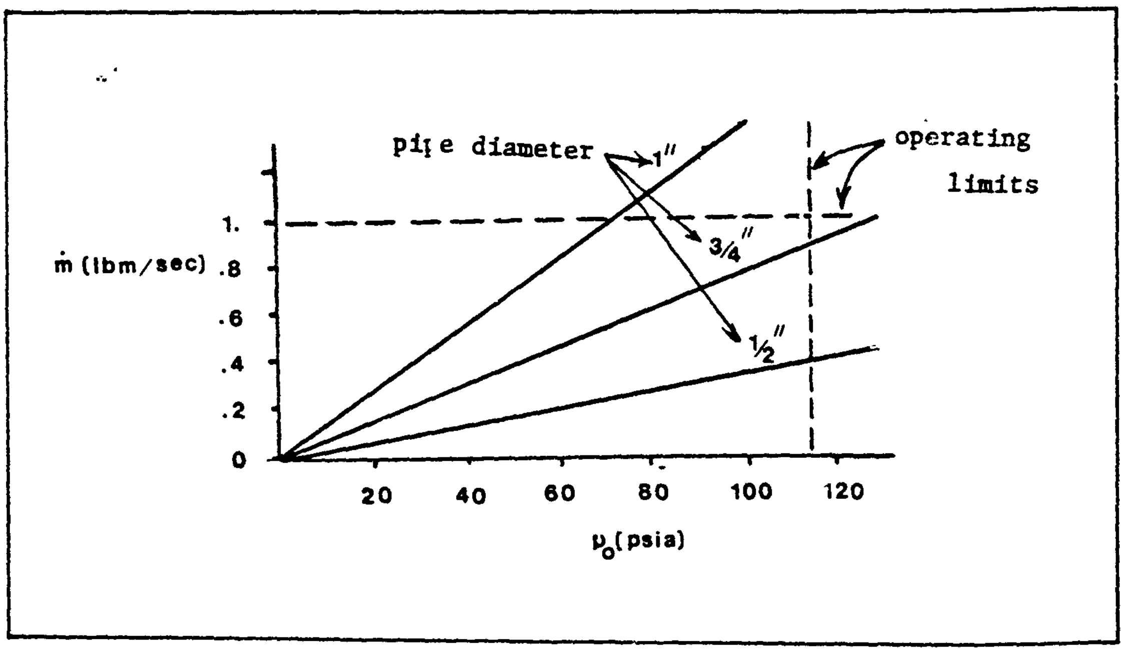

Figure 2.2 Pipe Size Limitation

Frictionless, One-Dimensional, Compressible Flow with Mass Injection/Extraction

Property variations with Mach number for frictionless, one-dimensional, compressible flow with simple gas injection may be found following Shapiro (46), by

$$\frac{p}{p_o} = \frac{1}{1 + \gamma Ma^2} \tag{2.1}$$

$$\frac{T}{T_o} = \frac{1}{1 + \frac{\gamma - 1}{2} Ma^2} \tag{2.2}$$

$$\frac{\rho}{\rho_o} = \frac{p\,T_o}{p_o T} \tag{2.3}$$

$$\frac{\dot{m}}{\dot{m}^*} = Ma\left[\frac{1 + \frac{\gamma - 1}{2} Ma^2}{1 + \frac{\gamma - 1}{2}}\right]^{\frac{1}{2}}\left[\frac{1 + \gamma}{1 + \gamma Ma^2}\right] \tag{2.4}$$

where p is the pressure, T is the temperature, ρ is the density, $\dot{m}$ is the mass flow rate, Ma is the Mach number and γ is the ratio of specific heats. The subscript "o" refers to the upstream pipe conditions (Ma=0) and the subscript "*" refers to choked flow (Ma=1.0). Sample pressure distributions for a pipe with uniform injection and extraction are shown in Figure 2.3 by curves 1, 2, 2A, and 2B.

In a cylindrical heat pipe, mass addition in the evaporator causes the axial mass flow rate to increase down the pipe. This results in a decrease in pressure. As mass is removed in the condenser, the mass flow rate desreases and the pressure increases. If friction is ignored, the pressures at the two ends of the pipe must be equal.

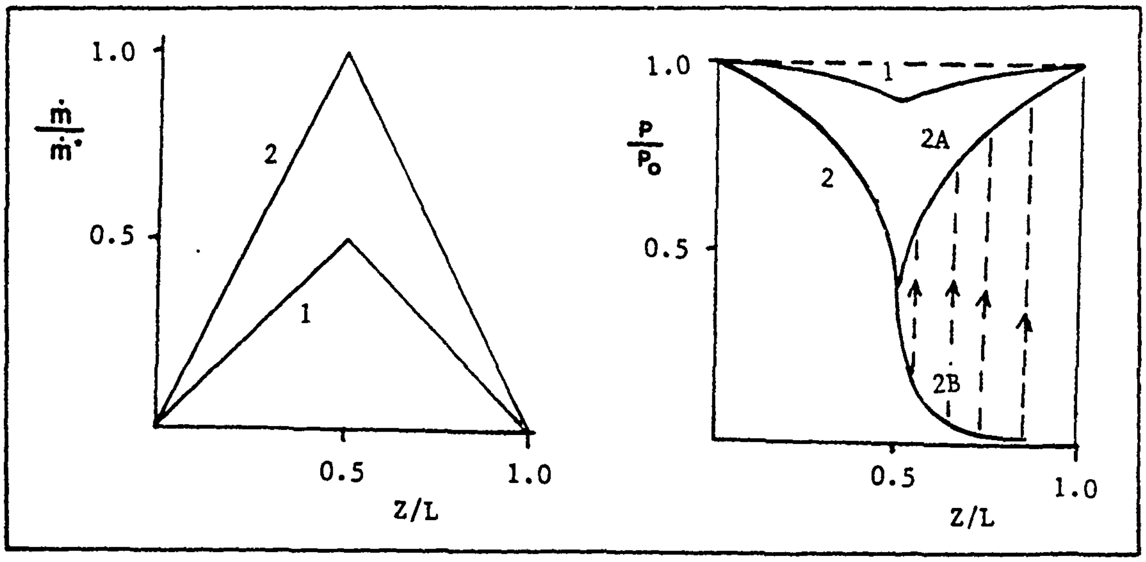

Figure 2.3 Sample Axial Pressure Distributions for Ideal One-Dimensional Vapor Flow in a Heat Pipe

A force balance performed on the control volume containing the heat-pipe vapor region shows that only friction can cause the end pressures to be different (Figure 2.4).

Curve 1 in Figure 2.3 illustrates the axial variation of pressure in a heat pipe for the case where sonic velocities are never attained. As mass injection/extraction increased, Curve 2, the axial velocity in the evaporator increases until sonic velocity is achieved at the entrance to the condenser (heat pipe throat). For Curve 2, a pressure ratio of Ø.417 is reached at the condenser entrance. As the sonic flow enters the condenser, mass extraction can cause the flow to either deccelerate (Curve 2A) or accelerate (Curve 2B).

For Curve 2A the flow is subsonic in the condenser. As the flow slows, the pressure in the condenser rises. Assuming no friction, the pressure must rise to the evaporator entrance pressure. Complete pressure rise is called total pressure recovery. For Curve 2B, the flow accelerates, becoming supersonic in the condenser entrance region. As the flow accelerates, the pressure decreases. Because the flow velocity must be zero at the end of the condenser, the flow must deccelerate somewhere in the condenser. The flow decceleration is initiated by a shock. It is interesting to note that there is no unique shock location if the flow is assumed to be frictionless, and the mass extraction distribution for the subsonic and supersonic cases are the same. The pressure jump across the shock causes the pressure to increase to the subsonic pressure for the given mass flow rate for any shock location in the condenser. After the shock, once again, total pressure recovery occures. If friction is considered, the condenser end pressure would be less than the evaporator end pressure. The larger the frictional forces, the larger the pressure drop between the ends of the pipe.

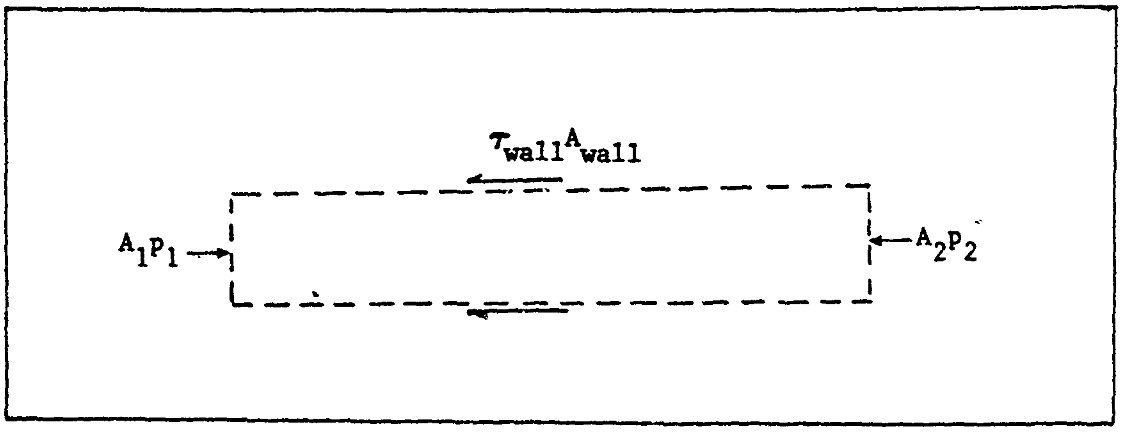

Figure 2.4 Control Volume for Force Balance

Pressure and Temperature Measurements

All pressure measurements were made using a T-type Scanivalve, from Scanivalve Corporation. A Model PDCR42 differential pressure transducer with a pressure range of 0-100 psig was used in the Scanivalve. The pressure measurements were accurate to within 0.2 psi. This system allowed for 36 pressure measurements with the one pressure transducer. The disadvantage of the system was that only steady-state or slowly changing pressures could be measured. The pressure transducer was calibrated using two 100 inch mercury manometers connected in series as a standard.

Data Acquisition

Data acquisition was done via an S-100 based computer. Pressure transducer input into the computer was digitized through a Dual Systems Control model AIM12 analog-to-digital card in the computer. An offset option on the card and amplification were set so signals from 0 to +100 millivolts could be read with a resolution of 0.024 millivolts. Shielded cables were used to reduce noise introduced to the system. Noise was further reduced by averaging 30 data samples. Once the data had been read and averaged by the computer, it could be displayed on a monitor, stored on disk, or processed as desired.

Mass-Flow-Rate Measurements

The total mass flow rate entering the test section was measured using a square edged orifice. Ten feet (40 pipe diameters) of straight pipe preceded the orifice plate. Three (3) feet (12 pipe diameters) of straight pipe were down stream of the orifice. When the orifice plate was installed, the inside of the pipe was inspected. The pipe inside had to be ground with a hand grinder to remove weld slag from where the pipe was welded to the orifice plate flanges. The grinding process left the inside of the pipe smooth and free from obstructions. Upstream of the orifice plate the pipe diameter was 3.062±0.002 inches. The downstream pipe diameter was 3.056±0.002 inches. Orifice plates with hole diameters varying from 0.25 inches to 1.0 inches were used. Orifice plate holes were varied so that for a given mass flow rate an easily measured pressure drop across the orifice was created. The holes also had to be varied so that the flow would not be choked at the orifice hole.

Flange taps and a water manometer were used to measure the pressure differential across the orifice plate. The following expressions were used to calculate the mass flow rate (47):

$$\dot{m} = 0.5202\left(\frac{C\,Y\,d^2\,F_a}{\sqrt{1-\beta_d^4}}\right)\sqrt{\rho_1(p_1-p_2)} \qquad (2.5)$$

where $\dot{m}$ is the measured mass flow rate in lbm/sec, p_1 and p_2 are the upstream and down stream pressures in psia, ρ_1 is the upstream density in lbm per cubic foot, β_d is the ratio of diameters d/D where d is the orifice plate diameter in inches, D is the inside pipe diameter in inches, C is the coefficient of discharge, Y is a compressibility expansion factor, and F_a is the metal's thermal expansion factor. The discharge coefficient is given by

$$C = K\sqrt{1-\beta_d^4} \qquad (2.6)$$

where K is the flow coefficient defined as

$$K = K_o\left(1 + \frac{A}{Re}\right) \qquad (2.7)$$

where Re is the axial Reynolds number and K_o is the limiting value of K for any specific value of D and β_d, when Re becomes infinitely large. It is defined as

$$K_o = K_e\left(\frac{10^6 d}{10^6 d + 5A}\right) \qquad (2.8)$$

where

$$K_e = .5993 + \frac{.007}{D} + \left(.364 + \frac{.076}{\sqrt{D}}\right)\beta_d^4$$
$$+ .4\left(1.63 - \frac{1}{D}\right)\left[\left(.07 + \frac{.5}{D}\right) - \beta_d\right]^{\frac{5}{2}}$$
$$-\left(.009 + \frac{.034}{D}\right)\left(.5 - \beta_d\right)^{\frac{3}{2}} + \left(\frac{65}{D^2} + 3\right)\left(\beta_d - .7\right)^{\frac{3}{2}} \qquad (2.9)$$

and

$$A = d\left(830 - 5000\beta_d + 9000\beta_d^2 - 4200\beta_d^3 + \frac{530}{\sqrt{D}}\right)$$

The axial Reynolds number can be expressed in terms of mass flow rate as

$$Re = \frac{48\,\dot{m}}{\pi \mu D} \qquad (2.10)$$

Finally, the compressibility factor, Y, is given by

$$Y = 1 - (.41 + .35\beta_d^4)\frac{x}{\gamma} \tag{2.11}$$

where x is the differential pressure ratio $\frac{\Delta p}{p_1}$ and γ is the ratio of specific heats for the gas.

Air Supply Manifold

A manifold was designed and built to supply air to the porous pipe as shown conceptually in Figure 2.1. Figure 2.5 is a detailed sketch of the manifold used. Fortyeight valves allowed for metering flow in/out of 12 chambers axially along the pipe. The valves were used in an attempt to control the axial distribution of the air to and from the pipe.

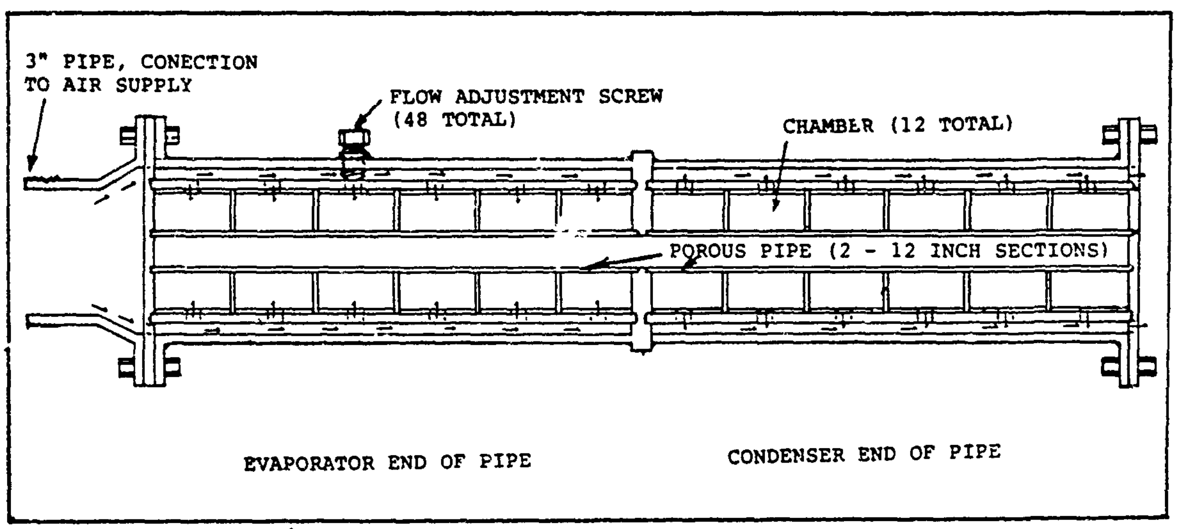

Figure 2.5 Air Supply Manifold

Porous Pipe

Inexpensive polyethylene porous pipe produced by Porex Technologies was selected for the experiment because of its uniform properties. A design pressure drop across the pipe of 30 psi was selected. The higher the pressure drop used, the more uniform the extraction and injection in the pipe; however, too large of a pressure drop would restrict flow to an extent that sonic flow could not be achieved in the pipe core. The final test configuration had a one foot long evaporator and a one foot long condenser. The porus pipe had an inside diameter of 0.650 inches and an outside diameter of 1.00 inches with an average pore size of 35 microns.

Pipe Calibration

Muskat (48) states that for the flow of a compressible gas through a porous medium, the mass flux (ρv) can be related to the pressure difference across the porous medium by the expression:

$$\Delta(p^2) = A(\rho v)^2 + B(\rho v) \qquad (2.12)$$

Four samples of 35 micron porous pipe were installed in the manifold shown in Figure 2.6. $\Delta(p^2)$ and ρv were measured for each sample of pipe for various mass flow rates. The results are shown in Figure 2.7.

Using least-squares techniques to curve fit the experimental data in Figure 2.7, the constants A and B in Equation (2.12) were found to be 3.639×10^9 and 1.7015×10^8, respectively. Determination of the constants A and B was needed for the injection and extraction boundary conditions used in the computer model (c.f. Chapters IV,V). The flow characteristics varied for the four samples by ±8%.

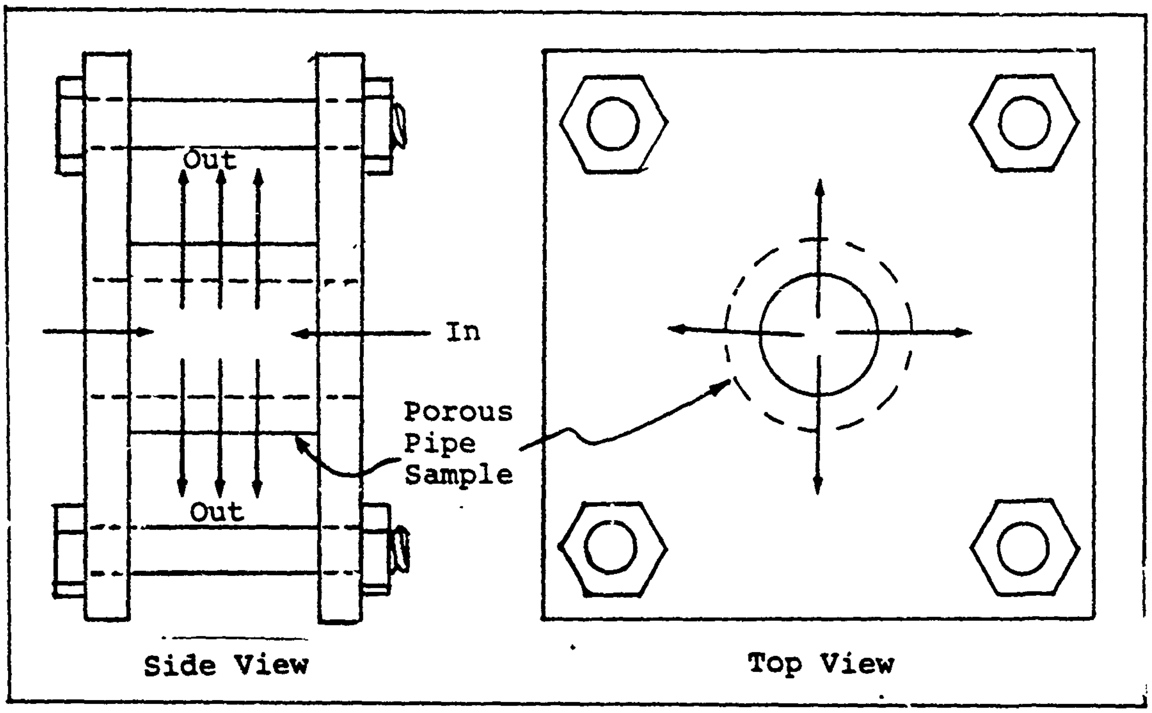

Figure 2.6 Porous Pipe Calibration Manifold

The samples were selected from different parts of a three foot section of pipe. One sample from each end and two samples were selected from the middle. A final calibration coefficient was needed so the experimental and numerical nass flow rates would be the same. It was found that a factor of 1.07 times the mean value represented by Eq (2.12) best described the mass flow rate.

Installation of the Porous Pipe in the Manifold

To prevent air from blowing between the ends of the porous pipe and the pipe manifold wall (to force all air to go through the porous pipe) great care was taken to insure good seals between the pipe and the manifold wall. Figure 2.8 illustrates how the seals were made.

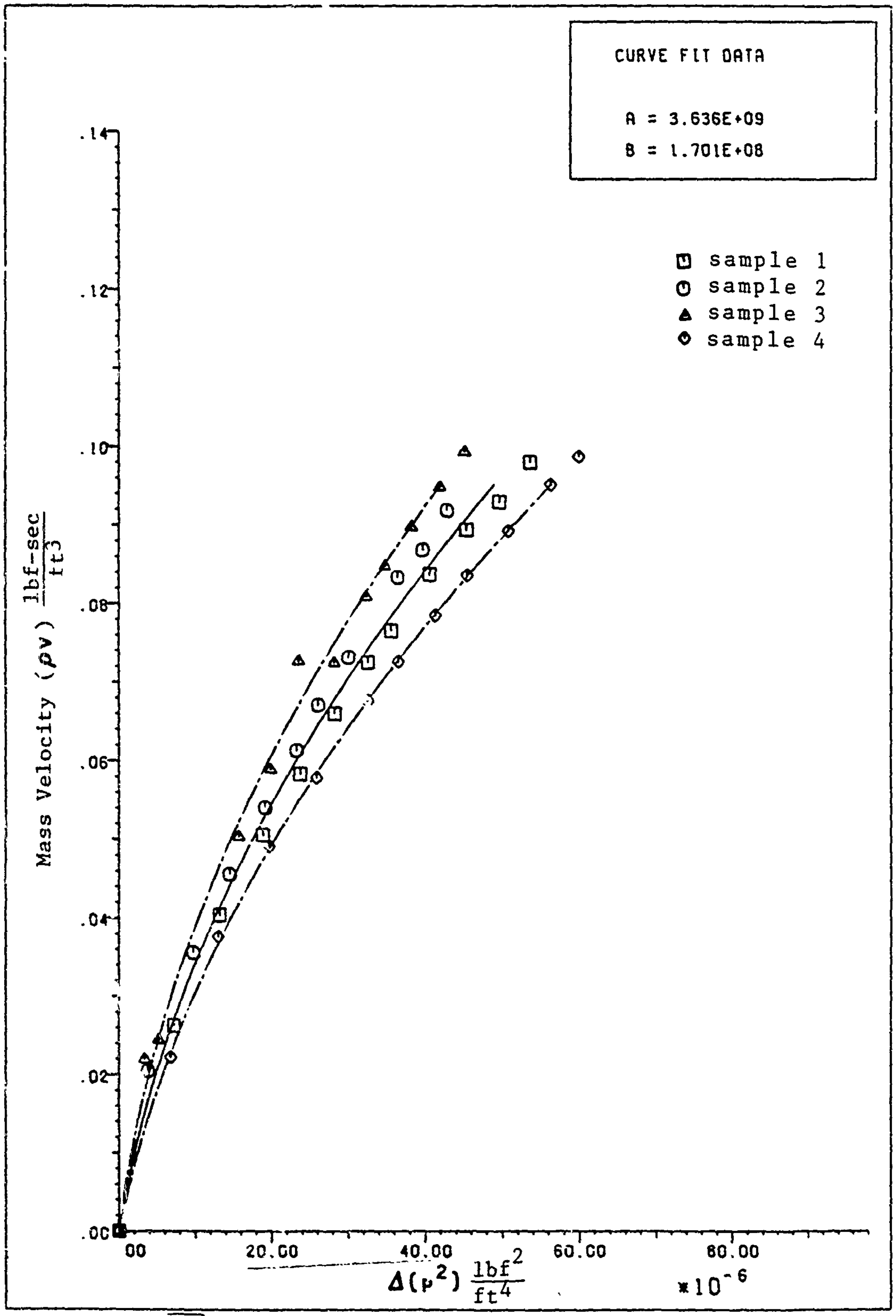

Figure 2.7 35 Micron Porous Pipe Calibration Results

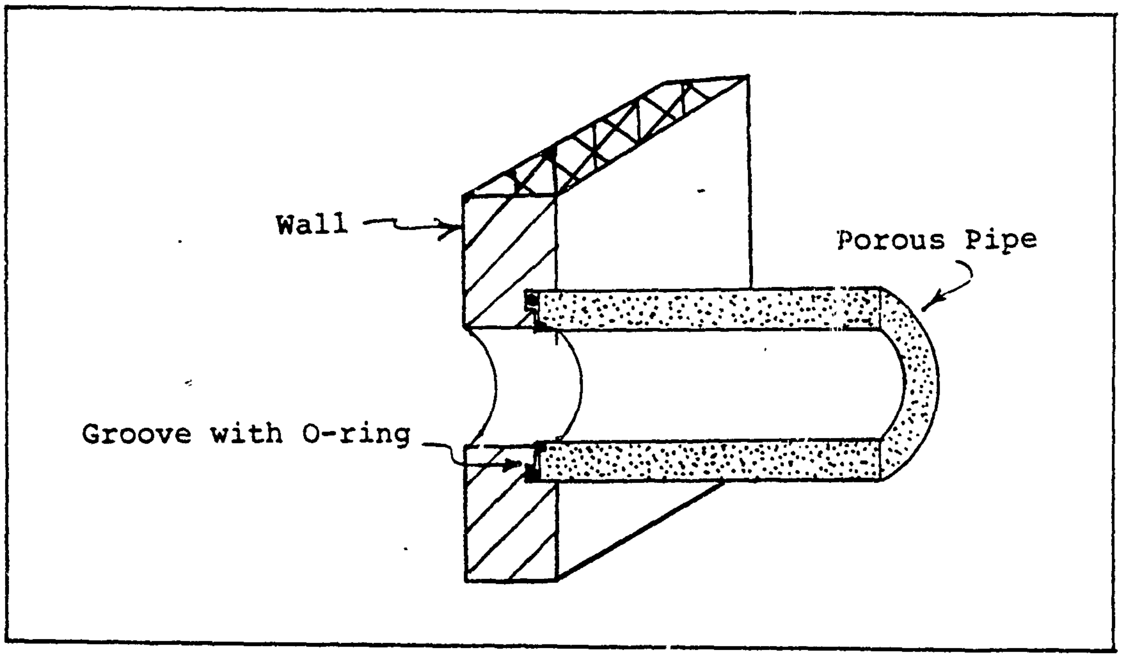

Figure 2.8 Porous Pipe End Seals

As can be seen from Figure 2.8, whenever the porous pipe was butted up against a wall, a grove was cut in the manifold to hold the porous pipe. The grove had an o-ring in it and was also filled with a silicone-base sealant that further inhibited leaks.

Pressure Taps

Pressure taps were installed in the porous pipe by cementing 1/2 inch long 0.069 inch outside diameter stainless steel tubes force fit into 0.058 inch diameter drill holes resulting in a snug fit. The stainless steel tube was inserted into the porous pipe so that its end was flush with the inside of the porous pipe. The pressure taps were located as shown in Figure 2.9. The actual pressure tap locations are given in Appendix A, Figure A.1.

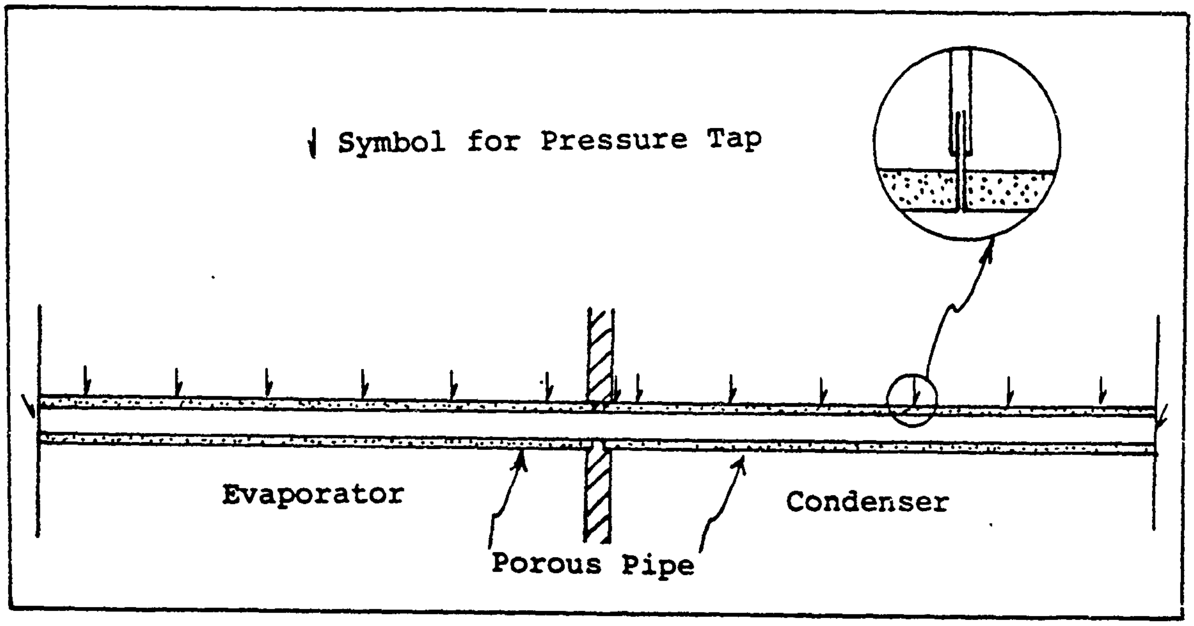

Figure 2.9 Pressure Tap Locations

Velocity Measurements

Seven total pressure tubes were combined to form a rake that was used for velocity measurements. The rake is shown in Figure 2.10.

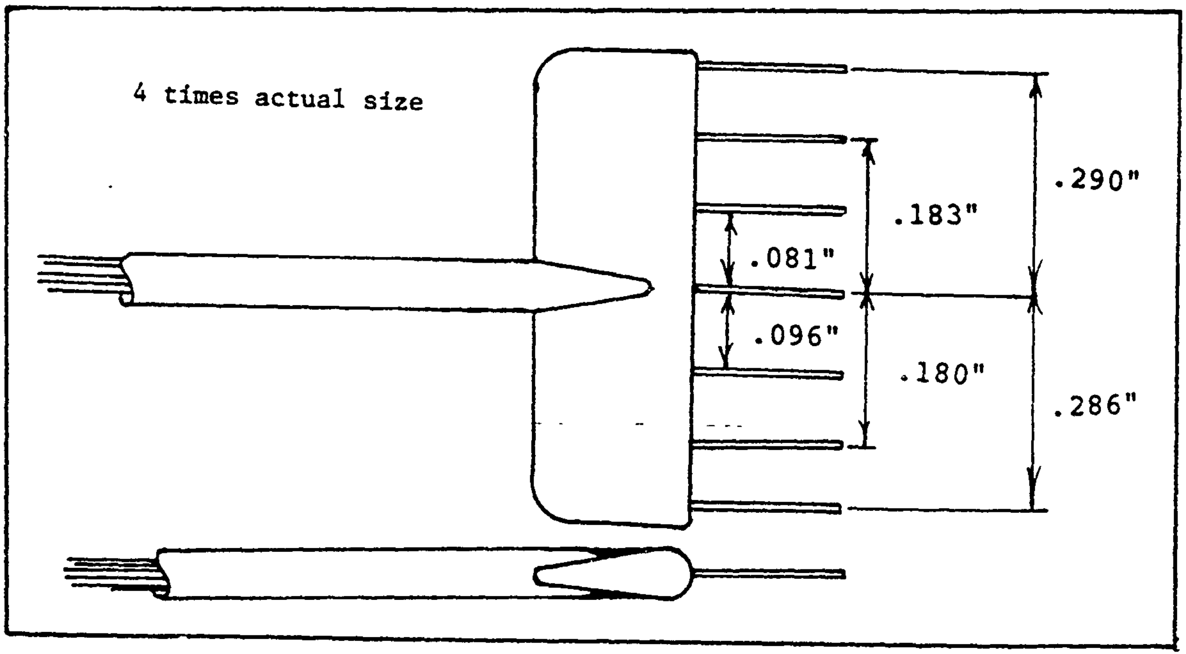

Figure 2.10 Velocity Rake

During the experiment, the rake was located so that the ends of the total pressure probes were adjacent to one of the static pressure ports (thus velocity profiles could be measured at any of 15 locations along the pipe). The axial velocities were calculated using the following equations.

$$u = Ma\sqrt{\gamma R T} \qquad (2.13)$$

$$\frac{p_s}{p} = \left(1 + \frac{\gamma - 1}{2} Ma^2\right)^{\frac{\gamma}{\gamma - 1}} \qquad (2.14)$$

$$\frac{T_o}{T} = 1 + \frac{\gamma - 1}{2} Ma^2 \qquad (2.15)$$

Where p_s is the stagnation pressure, p is the static pressure, T_o is the total temperature, and Ma is the Mach number.

Turbulence Measurements

To measure the effect of injection, extraction, and pressure gradient on the flow field's turbulence, the velocity rake was replaced by a hot-film anemometer. A Model 1050, constant temperature anemometer manufactured by TSI Incorporated was used with a TSI 1212.10 hot-film anemometer. A TSI Model 1076 digital voltmeter was used to measure the mean voltage (velocity) values while a B&K Precision Dual Time Base Oscilloscope model 1570A was used to visualize the fluctuating velocity component. A second TSI Model 1076 digital voltmeter was used to find the RMS (root-mean square) of the fluctuating voltage (velocity).

The anemometer was limited to the center line of the test section by a lateral support which was attached to the probe to ensure it did not come in contact with the pipe wall. The support was located four inches from the end of the probe. This prohibited measurements closer than four inches from the downstream end of the test section.

III. Experimental Results

The purpose of the experiment was to gather data to be used to validate the numerical models. First, the experimental pressure and velocity data will be presented. Next, the effect of the velocity rake and hot-film anemometer on the flow field will be discussed. Lastly, the results of the turbulence studies will be presented.

Axial Pressure Data

One of the primary goals of this research was to gain a better understanding of the effect of injection and extraction on the wall shear stress and thus the pressure variations in a compressible flow. Figure 3.1 shows how the pressure varied axially along the simulated heat pipe (c.f. Chapter II). The cases shown represent five typical cases with different mass flow rates. The pressure varied due to shear-stress as well as momentum effects. From the discussion of ideal (shear-stress free) flow with mass injection/extraction (c.f. Chapter II), the pressure at the end of the pipe matched that at the beginning. This had to be the case because, without shear stress, no other forces were present to make the end pressures other than equal. In ideal flow, pressure variations are due only to momentum (acceleration/deceleration) effects. In Figure 3.1, then, it is clear that shear is present and such "friction" effects are manifest in the pressure drop between the pipe ends. The friction pressure drop increases with mass flow

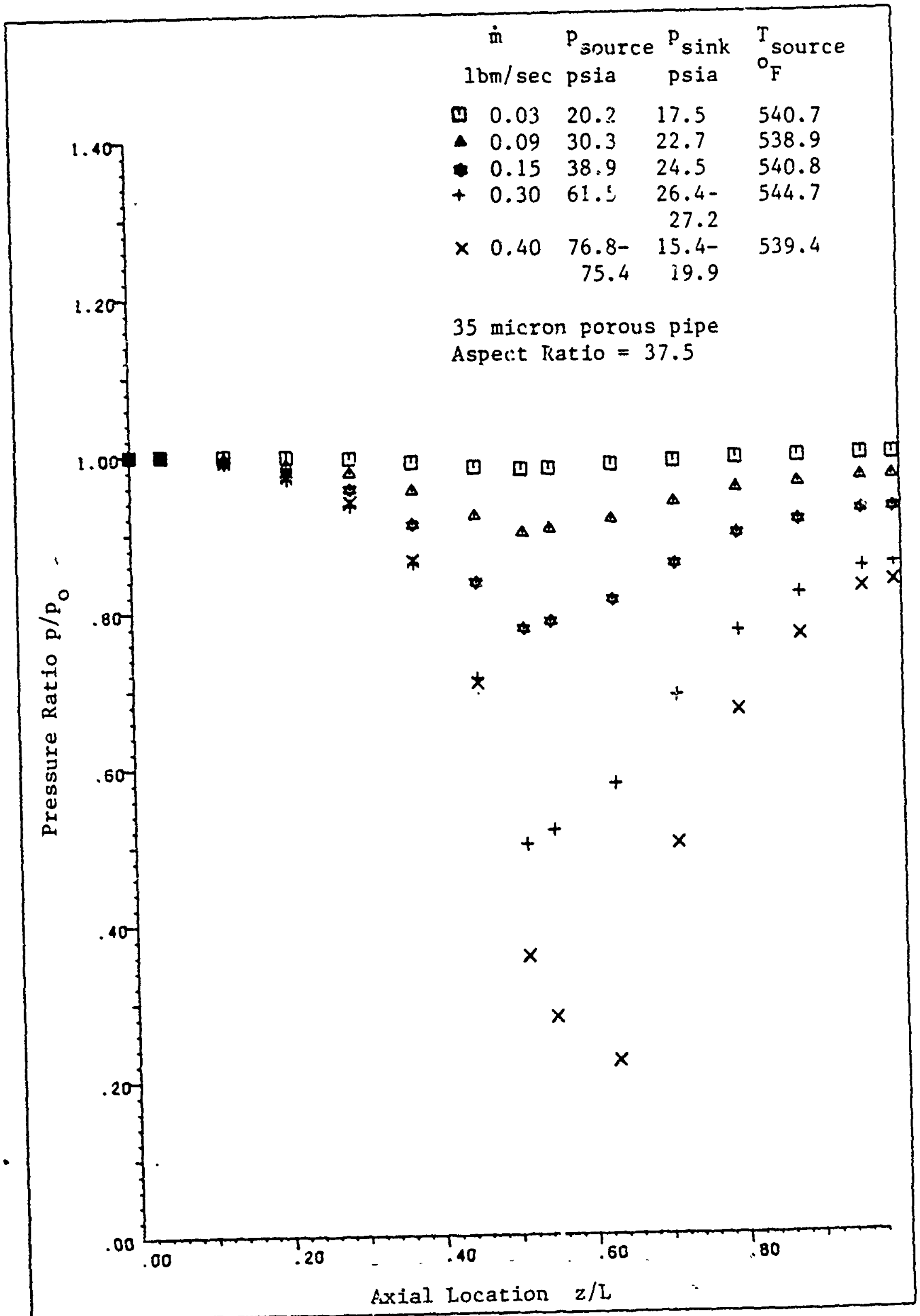

Figure 3.1 Effect of Increasing Mass Flow Rate on Pressure

rate. Momentum effects can be seen in all of the cases shown. Most interesting is the highest mass-flow-rate case. In the evaporator region, $0 < Z/L < 0.5$, the pressure drops with increasing Z/L as the fluid accelerates due to mass addition. At the end of the evaporator, the pressure ratio was very close to 0.416, the pressure ratio predicted by frictionless flow theory. This corresponds to sonic velocity at the "throat" (evaporator/condenser junction) and choked flow. Theoretically, the mass removal in the condenser can either decelerate or accelerate the flow (c.f. Chapter II). For the highest mass-flow-rate case shown, the pressure continues to drop in the entrance region of the condenser. Referring again to the discussion in Chapter II, this corresponds to the flow continuing to accelerate to supersonic velocities. For the four subsonic cases shown, the mass removal caused the flow to decelerate and the pressure ratio to rise. For the supersonic case, the sharp increase in pressure between Z/L's of 0.63 and 0.72 is due to a normal shock which is required to deccelerate the flow before it reaches the pipe end.

Because of the compressible nature of the flow, non-uniform mass injection and removal occur along the pipe studied. In Chapter II it was shown that the amount of wall mass transfer depends on the pressure difference across the pipe wall as described by Equation (2.12). As mass was added in the evaporator, the flow accelerated down the pipe and the pressure dropped (Figure 3.1). Because the external pressure was constant along the pipe and the internal pressure varied axially along the pipe, the mass injection and removal varied along the pipe. The mass injection was smallest near the upstream end of the evaporator and highest near the evaporator/condenser junction. Similarly, the mass removal was smallest at the condenser/evaporator junction and greatest at the downstream end of the condenser.

In the evaporator the effect of the increasing mass injection was to increase the rate of pressure drop axially along the pipe. An attempt was made to create a flow situation with uniform mass injection and extraction. This was done by axially varing the external pressures along the outside of the test section. This turned out to be difficult to do; however, the trend of approaching uniform mass transfer was to linearize the pressure variation in the evaporator. Smaller changes were noted in the condenser pressure distribution, probably due to larger friction forces affecting the pressure in that region.

Velocity Data

The velocity rake described in Chapter II was used to measure the radial variation in the axial velocity at different axial locations along the test section. Figures 3.2 through 3.6 are the velocity results which correspond to the five axial pressure distributions shown in Figure 3.1. The five profiles shown are at axial locations of 7, 11, 13 3/8, 17 3/8, and 21 3/8 inches (measured from the upstream end of the pipe).

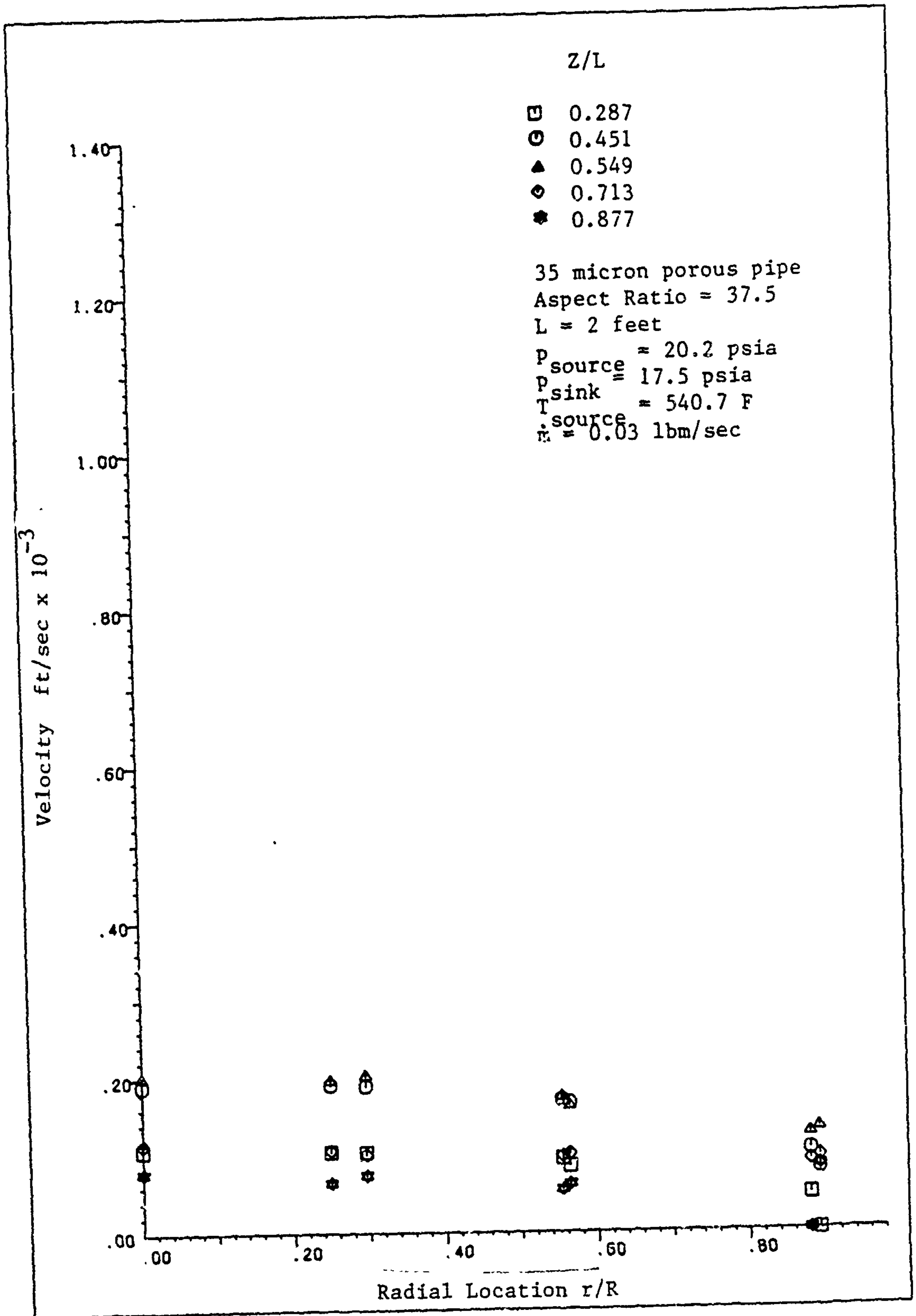

Figure 3.2 Experimentally Measured Velocity Profiles
$\dot{m}$ = 0.03 lbm/sec

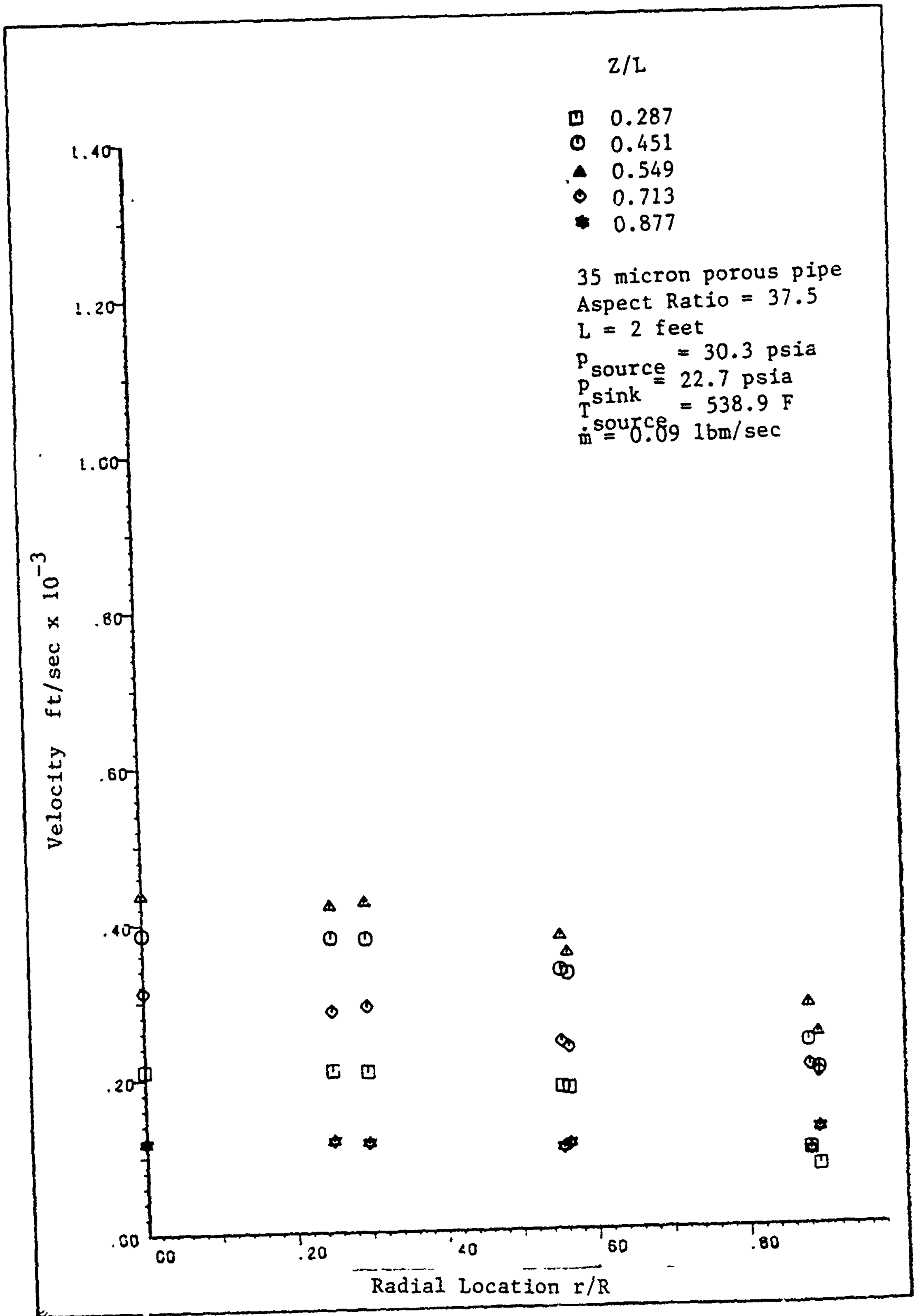

Figure 3.3 Experimentally Measured Velocity Profiles

$\dot{m}$ = 0.09 lbm/sec

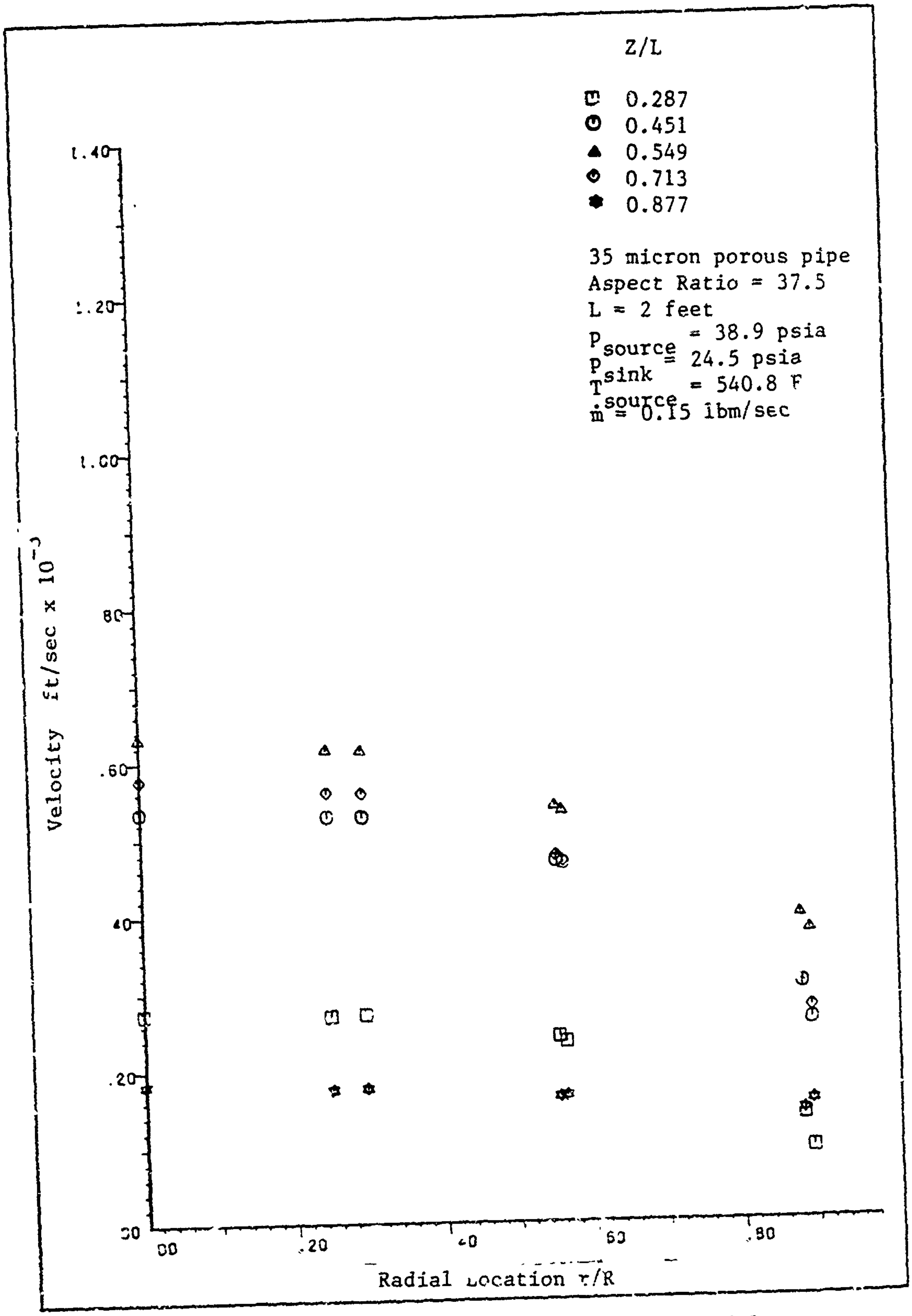

Figure 3.4 Experimentally Measured Velocity Profiles
$\dot{m}$ = 0.15 lbm/sec

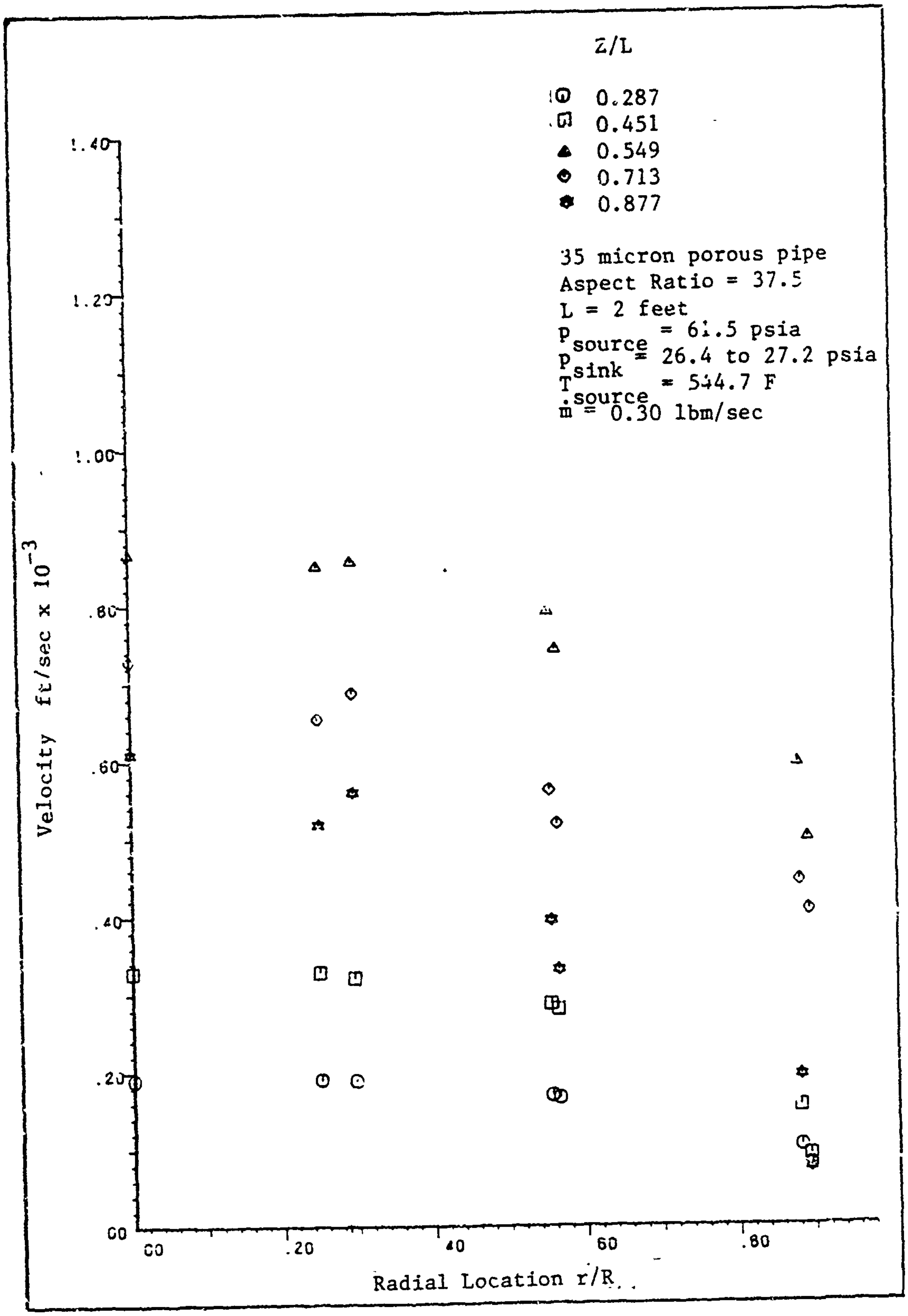

Figure 3.5 Experimentally Measured Velocity Profiles
$\dot{m}$ = 0.30 lbm/sec

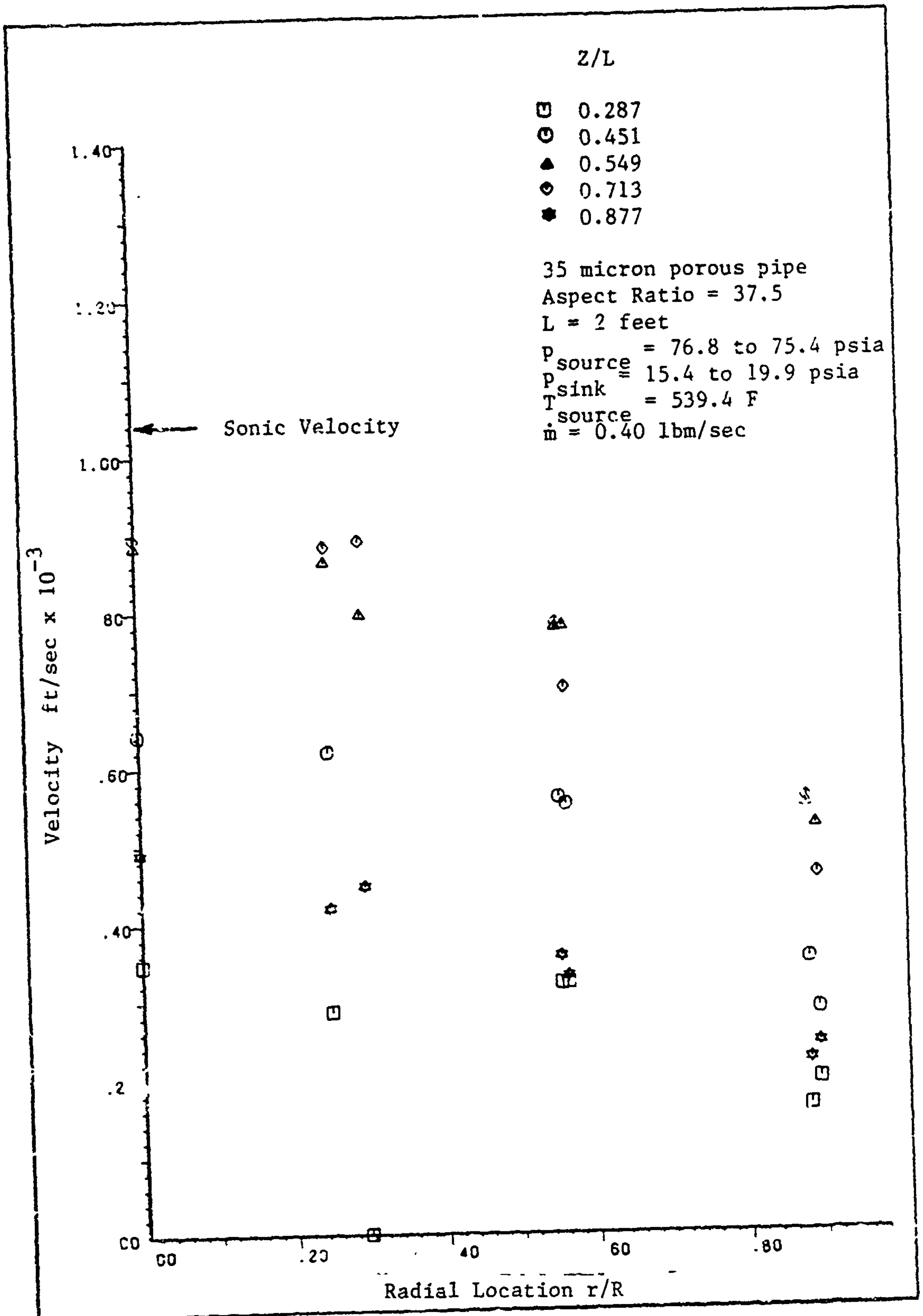

Figure 3.6 Experimentally Measured Velocity Profiles
$\dot{m}$ = 0.40 lbm/sec

The velocity rake was 0.010 inches narrower than the inside diameter of the porous pipe. Thus, the radial location of the velocity probes was known to within 0.010 inches.

By examining Figures 3.2 through 3.6, several velocity trends can be noted. The most obvious trends are 1) increasing velocities occur at higher mass flow rates and 2) the axial variation in the velocities was increasing through the evaporator and then decreasing in the condenser. The supersonic case (Figure 3.6) does not indicate supersonic velocities. This is believed to be due to experimental error caused by the velocity rake influencing the flow field. Studies conducted with a hot-film anemometer indicated that small disturbances in the supersonic evaporator flow would cause the flow to become subsonic. As will be discussed later, the velocity probe also affected the static pressures measured along the pipe. This would be another source of error in the implied velocity measurements.

The last observation to be discussed relates to the effect of mass injection and removal on the velocity profiles. In four out of the five cases shown, the velocity profiles in the condenser, when compared to those in the evaporator, are flatter in the center of the pipe with steep gradients near the pipe wall. Later this will be shown to be due in part to turbulence in the condenser (as compared to laminar flow in the evaporator) and in part due to the mass removal in the condenser.

Effect of Velocity Probe on Flow Field

As inferred from the above discussion, the velocity probe and the hot-film anemometer affected the flow field. Figure 3.7 demonstrates how the axial pressure distribution was affected by the velocity probe. These pressure disturbances can be divided into two parts, that caused by the velocity rake and that caused by the probe shaft. When the velocity rake was in a region of large air velocities it would disturb the flow more than the probe shaft. Longer lengths of shaft produced greater pressure disturbances than shorter lengths.

Turbulence Measurements

When numerically modeling the problem it was observed that a totally-turbulent flow model would over predict the friction pressure loss, while a totally-laminar model under predicted the pressure loss [this has also been noted by Busse (26)]. To understand which parts of the flow were turbulent and which were laminar a hot-film anemometer was used to measure turbulence levels. A digital volt meter measured the RMS of the hot-film's alternating voltage output. It was found that the RMS of the alternating voltage was constant and small in the evaporator, consistent with the interpretation of laminar flow. As the hot-film anemometer was moved into the condenser region, the RMS of the alternating voltage rose sharply over a small but

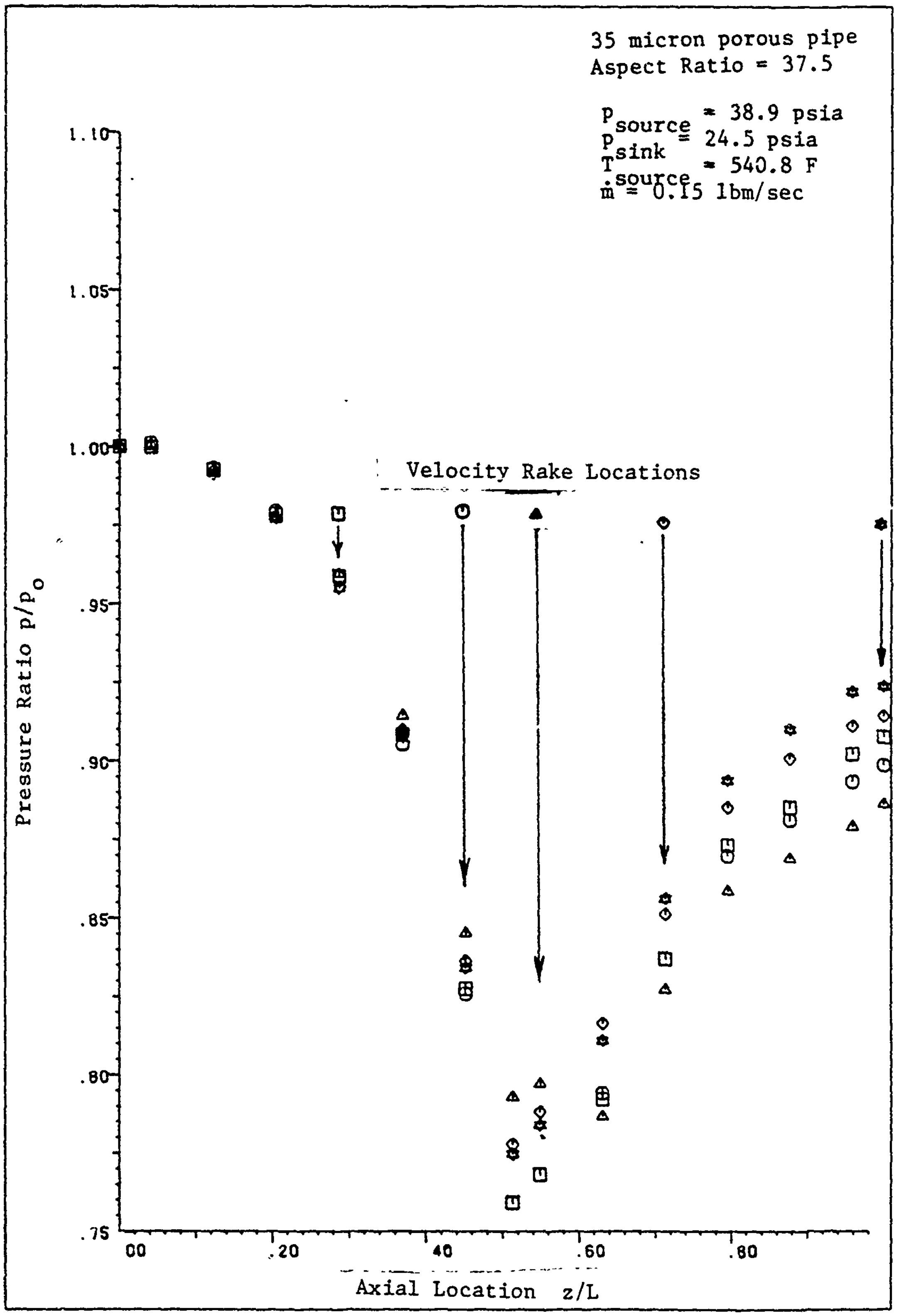

Figure 3.7 Effect of Velocity Rake on Flow

defined length of the pipe, indicating a region of transition in character of the flow from fully laminar to fully turbulent.

Figure 3.8 gives some representative examples of the measurements made. In Figure 3.8, the RMS of the alternating voltage measured is normalized with respect to the RMS of the alternating voltage measured in the fully turbulent region. For all cases studied (up to Reynolds numbers based on pipe diameter of 1,000,000), the flow was always laminar in the evaporator region [Wageman and Guevara (16) observed a similar phenomenon]. This is believed to be due to the strong favorable pressure gradient in the evaporator. From Figure 3.8 it can also be seen that once the flow enters a region with an adverse pressure gradient in the condenser, the flow becomes turbulent. Except in the supersonic case (c.f. below), the transition region always started at the entrance to the condenser ($Z/L = 0.5$ in Figure 3.8) near the pipe wall and then stretched down stream toward the center of the flow channel where it was measured by the hot-film anemometer. At higher flow rates, transition in the center of the flow channel moved down stream. Figure 3.9 illustrates what the flow field may look like.

Such a description of the character of the flow is consistent with the fact that at higher flow velocities the beginning of the transition region moved down stream at the center of the pipe.

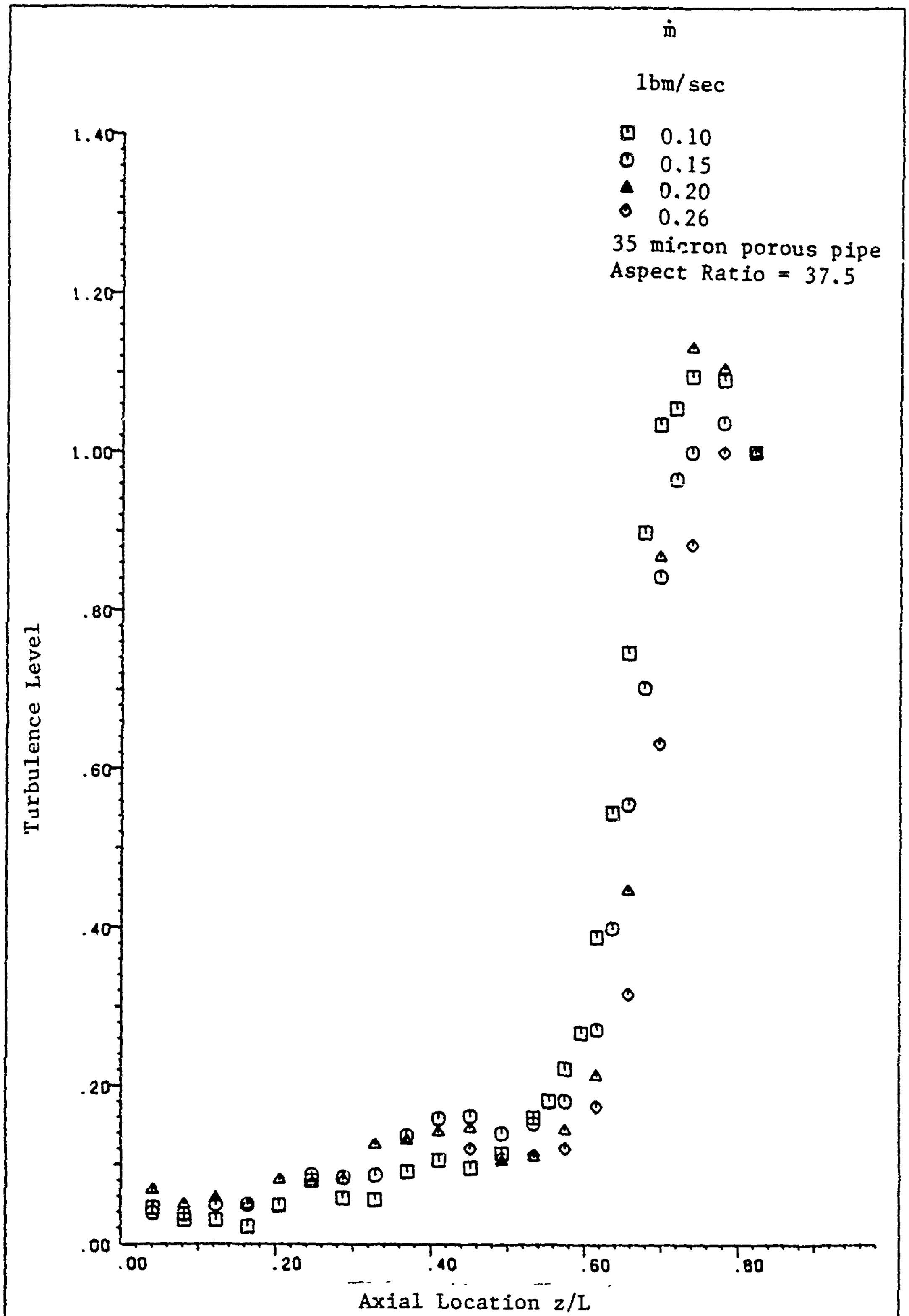

Figure 3.8 Turbulence Intensity During Transition From Laminar to Turbulent Flow

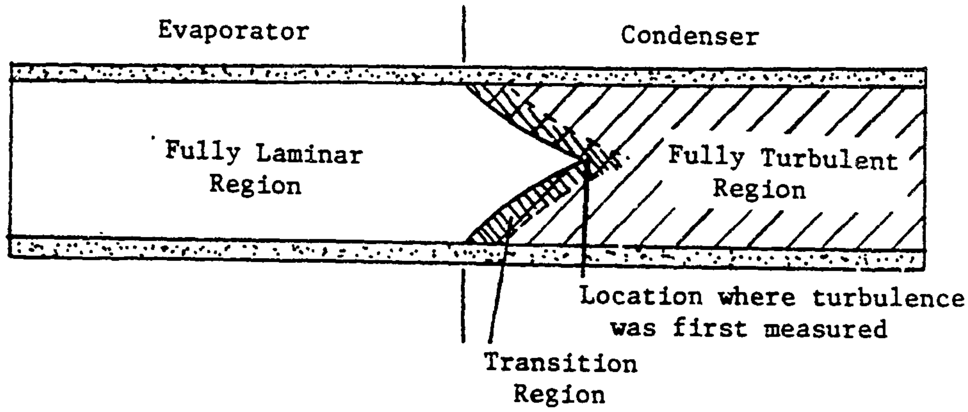

Figure 3.9 Turbulence Character of the Flow

All of the turbulence data followed the above trend except for the case where the flow became supersonic in the condenser. For the supersonic case the flow remained totally laminar until the shock was reached and then transition to turbulent flow abruptly occurred (i.e. no extended "transition region appeared to be present).

A second set of turbulence experiments was conducted to determine the axial Reynolds number , Eq (2.10), at which the condenser flow would remain laminar. With the hot-film anemometer located in the condenser at the location Z/L = 0.67, the system flow rate was decreased until the flow became laminar. Figure 3.10 contains the results. As can be seen, at axial Reynolds numbers below about 12,000 the flow was laminar. When the axial Reynolds number was 12,000, the Mach number at the simulated heat pipe's throat was 0.06, well in the subsonic range.

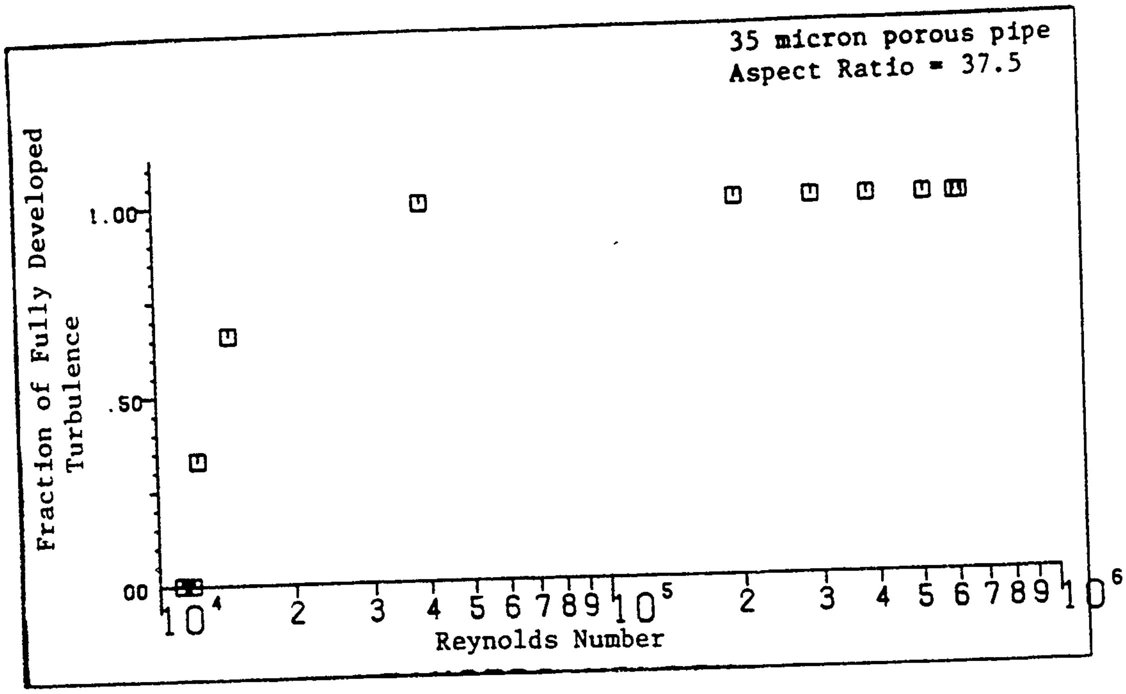

Figure 3.10 Turbulence Vs. Reynolds Number in the Condenser

IV. Mathematical Flow Description

The flow field to be modeled is mathematically described in this chapter. The chapter is divided into five sections. First the general continuity, momentum and energy equations are presented in both vector and cylindrical form. Second, the closure relations needed to complete the set of equations will be presented. Third, the boundary conditions which relate to steady and transient simulated heat-pipe operation will be described. Fourth, the Reynolds-Averaged continuity, momentum and energy equations that were used for describing the turbulent flow will be developed. Lastly, there will be a discussion of how turbulence modeling was accomplished.

Governing Equations

The equations governing the motion of an unsteady, compressible, viscous gas with no body forces and no heat sources are derived from conservation laws of mass, momentum and energy (49:181-206).

The continuity equation in conservation form and using vector notation is:

$$\frac{\partial \rho}{\partial t} + \text{div}\{\rho\vec{V}\} = 0 \qquad (4.1)$$

Where ρ is the density, t is time, and $\vec{V}$ is the velocity vector. When written in cylindrical coordinates, the equation becomes

$$\frac{\partial \rho}{\partial t} + \frac{1}{r}\frac{\partial\{r\rho v\}}{\partial r} + \frac{\partial\{\rho u\}}{\partial z} = 0 \qquad (4.2)$$

Where r is the radial position, z is the axial position, v is the radial velocity and u is the axial velocity. The azimuthal terms have been eliminated from the general cylindrical continuity equation. Throughout the rest of this paper, cylindrical will refer to the general cylindrical form of an equation minus the azimuthal terms.

Conservation of momentum in conservation form and using vector notation is

$$\frac{\partial\{\rho\vec{V}\}}{\partial t} + \text{div}\{\rho\vec{V}\vec{V}\} = \text{div}\{\bar{\tau}\} - \text{grad}\{p\} \qquad (4.3)$$

Where p is the pressure, and $\bar{\tau}$ is the viscous stress tensor defined by

$$\bar{\tau} = \mu[\nabla\vec{V} + \nabla\vec{V}^T] + \lambda\,\text{div}\{\vec{V}\}\bar{\Pi} \qquad (4.4)$$

μ is the viscosity, λ is the second coefficient of viscosity and $\bar{\Pi}$ is the unit normal tensor defined by

$$\bar{\Pi} = \begin{bmatrix} 1 & 0 & 0 \\ 0 & 1 & 0 \\ 0 & 0 & 1 \end{bmatrix} \qquad (4.5)$$

When written in cylindrical coordinates, Equation (4.3) becomes

$$\frac{\partial\{\rho v\}}{\partial t} + \frac{1}{r}\frac{\partial\{r\rho v^2\}}{\partial r} + \frac{\partial\{\rho u v\}}{\partial z} = \frac{1}{r}\left[\frac{\partial\{r\sigma_{rr}\}}{\partial r} + \frac{\partial\{r\sigma_{zr}\}}{\partial z}\right] - \frac{\sigma_{\theta\theta}}{r} \qquad (4.6)$$

$$\frac{\partial\{\rho u\}}{\partial t} + \frac{1}{r}\frac{\partial\{r\rho u v\}}{\partial r} + \frac{\partial\{\rho u^2\}}{\partial z} = \frac{1}{r}\left[\frac{\partial\{r\sigma_{rz}\}}{\partial r} + \frac{\partial\{r\sigma_{zz}\}}{\partial z}\right] \qquad (4.7)$$

The stress terms are defined as

$$\sigma_{rr} = -p + 2\mu\frac{\partial v}{\partial r} + \lambda\left[\frac{1}{r}\frac{\partial\{rv\}}{\partial r} + \frac{\partial u}{\partial z}\right] \tag{4.8}$$

$$\sigma_{\theta\theta} = -p + 2\mu\frac{v}{r} + \lambda\left[\frac{1}{r}\frac{\partial\{rv\}}{\partial r} + \frac{\partial u}{\partial z}\right] \tag{4.9}$$

$$\sigma_{zz} = -p + 2\mu\frac{\partial u}{\partial z} + \lambda\left[\frac{1}{r}\frac{\partial\{rv\}}{\partial r} + \frac{\partial u}{\partial z}\right] \tag{4.10}$$

$$\sigma_{rz} = \sigma_{zr} = \mu\left[\frac{\partial v}{\partial z} + \frac{\partial u}{\partial r}\right] \tag{4.11}$$

Conservation of energy in conservation form, assuming no internal energy generation and no radiation heat transfer, can be written as

$$\frac{\partial}{\partial t}\left\{\rho\left[e + \frac{V^2}{2}\right]\right\} + \mathrm{div}\left\{\rho\vec{V}\left[e + \frac{V^2}{2}\right]\right\} = -\,\mathrm{div}\left[p\vec{V}\right] + \mathrm{div}\left[\bar{\tau}\cdot\vec{V}\right] + \mathrm{div}\left[\vec{q}\right] \tag{4.12}$$

Where e is the internal energy per unit mass, and $\vec{q}$ is the conduction heat transfer per unit area. When written in cylindrical coordinates, the equation becomes

$$\frac{\partial[\rho E]}{\partial t} + \frac{\partial}{\partial z}\left\{\rho u E - u\sigma_{zz} - u\sigma_{zr} + q_z\right\} + \frac{1}{r}\frac{\partial}{\partial r}\left\{r\left[\rho v E - v\sigma_{rr} - v\sigma_{rz} + q_r\right]\right\} = 0 \tag{4.13}$$

where,

$$E = e + \frac{1}{2}\left\{u^2 + v^2\right\} \tag{4.14}$$

Equations (4.2), (4.6), (4.7) and (4.13) are the governing equations for the problem in conservation form. They can be written in vector form as

$$\frac{\partial \vec{U}}{\partial t} + \frac{\partial \vec{F}}{\partial z} + \frac{1}{r}\frac{\partial}{\partial r}\left\{ r\vec{G} \right\} = \frac{\vec{H}}{r} \quad (4.15)$$

where:

$$\vec{U} = \begin{bmatrix} \rho \\ \rho u \\ \rho v \\ \rho E \end{bmatrix} \qquad \vec{F} = \begin{bmatrix} \rho u \\ \rho u^2 - \sigma_{zz} \\ \rho uv - \sigma_{zr} \\ \rho uE - u\sigma_{zz} - u\sigma_{zr} + q_z \end{bmatrix}$$

$$\vec{G} = \begin{bmatrix} \rho v \\ \rho uv - \sigma_{rz} \\ \rho v^2 + \sigma_{rr} \\ \rho vE - v\sigma_{rr} - v\sigma_{rz} + q_r \end{bmatrix} \qquad \vec{H} = \begin{bmatrix} 0 \\ 0 \\ -\sigma_{\theta\theta} \\ 0 \end{bmatrix}$$

Closure Relations

Upon examining equation (4.15), it can be seen that additional relations are needed to form a closed set of equations.

Stokes analogy can be used to relate the second coefficient of viscosity to the viscosity.

$$\lambda = -\frac{2}{3}\mu \quad (4.16)$$

Fourier's law of heat conduction can be used to represent the energy flux as a function of temperature.

$$q_r = -k\frac{\partial T}{\partial r} \quad (4.17)$$

$$q_z = -k\frac{\partial T}{\partial z} \quad (4.18)$$

where k is the thermal conductivity of the fluid.

The viscosity and thermal conductivity can be expressed as functions of temperature. For example, Sutherland's formula for viscosity is given by

$$\mu = C_1 \frac{T^{3/2}}{T + C_2} \tag{4.19}$$

where C_1 and C_2 are constants for a given gas. The Prandtl number

$$Pr = \frac{c_p \mu}{k} \tag{4.20}$$

can be used to find the thermal conductivity once the viscosity and specific heat at constant pressure are known. This is possible if Prandtl number is assumed to be constant, which is a fair assumption for most gases.

The additional relationships come from assuming that the vapor is a perfect-gas. The perfect gas equation of state is

$$p = \rho R T \tag{4.21}$$

where R is the gas constant. Also for an perfect gas, $e = e(T)$, or the internal energy is a function of temperature only. The following relations hold true for a perfect gas.

$$c_v = \frac{de}{dT} \tag{4.22}$$

$$c_v = \frac{R}{\gamma - 1} \tag{4.23}$$

$$c_p = \frac{\gamma R}{\gamma - 1} \tag{4.24}$$

$$\gamma = \frac{c_p}{c_v} \tag{4.25}$$

where c_v and c_p are the specific heats at constant volume and pressure, respectively, and γ is the ratio of specific heats defined by Equation (4.25). Using Equations (4.22) to (4.25), Equation (4.21) can be rewritten in the forms:

$$p = [\gamma - 1]\rho e \tag{4.26}$$

$$T = \frac{[\gamma - 1]e}{R} \tag{4.27}$$

These last expressions complete the set of equations.

Equation (4.15) presented earlier applies to many cylindrical problems. The boundary conditions which apply to a given problem distinguish it from other problems which use Equation (4.15). Next the boundary conditions which apply to a heat pipe will be described.

Boundary Conditions

At the ends of the simulated heat pipe, both the radial and axial velocity components were assumed to be zero, or

$$u[r,0] = u[r,L] = v[r,0] = v[r,L] = 0 \tag{4.28}$$

Where L is the length of the heat pipe.

The axial pressure gradient at the heat pipe-ends was handled in one of two different ways. One way was to set it equal to zero.

$$\frac{\partial p}{\partial z}[r,0] = \frac{\partial p}{\partial z}[r,L] = 0 \qquad (4.29)$$

This technique has been reported to aid in the numerical stability of finite-difference solutions and is a good assumption because the axial pressure gradient should be small at the heat-pipe ends. It gave the same results as the second method described below. A more complicated approach was to solve Equation (4.7), the axial momentum equation, for the axial pressure gradient term and then estimate the pressure gradient by approximating the expression using finite differences at z=0 and z=L.

$$\frac{\partial p}{\partial z} = -\frac{\partial\{\rho u^2\}}{\partial z} + \frac{4}{3}\mu\frac{\partial^2 u}{\partial z^2} \qquad (4.30)$$

This method required more computer time and did not improve the results. For this reason, the quicker, simpler approach was used.

The fourth boundary condition needed at the pipe ends was that for the total energy. The temperature was assumed to have no axial gradient at the pipe ends.

$$\frac{\partial T}{\partial z}[r,0] = \frac{\partial T}{\partial z}[r,L] = 0 \qquad (4.31)$$

Along the length of the heat pipe, the "no-slip" condition for the axial component of velocity was assumed to apply (i.e.,mass injection/extraction was assumed to be in the radial direction only). This led to the expression

$$u[R,z] = 0 \qquad (4.32)$$

where R is the radius of the vapor space. The radial velocity component at the wall was dependent on the rate of vapor injection or extraction at the wall and could be varied axially along the pipe. The variation was specified as a funtion of position and time. This was done by specifying the pipe's outside enviornment pressure (source and sink pressure). The radial velocity at the wall was found from Equation (4.33).

$$\Delta(p^2) = A(\rho v)^2 + B(\rho v) \qquad (4.33)$$

A and B are properties of the porous pipe, $\Delta(p^2)$ is the inside wall pressure squared minus the outside pressure squared. Further details on the above equation can be found elsewhere (48:55-119).

The radial pressure gradient at the wall was found in a similar manner to the axial pressure gradient at the heat-pipe ends. One method was to set it equal to zero.

$$\frac{\partial p}{\partial r}[R,z] = 0 \qquad (4.34)$$

The other alternative was to isolate the radial pressure gradient term in the radial momentum Equation (4.6) and then evaluate the expression at the heat pipe wall.

$$\frac{\partial p}{\partial r} = -\rho v\frac{\partial v}{\partial r} + \frac{4}{3}\mu\left(\frac{\partial^2 v}{\partial r^2} + \frac{1}{r}\frac{\partial v}{\partial r} - \frac{v}{r} + \frac{\partial^2 v}{\partial z^2}\right) \qquad (4.35)$$

Both methods gave comparable results, thus the first, which used the least amount of computer, time was picked.

Along the axis of symmetry, symmetry boundary conditions were applied to all variables.

$$\frac{\partial \rho}{\partial r} = \frac{\partial u}{\partial r} = \frac{\partial v}{\partial r} = \frac{\partial E}{\partial r} = 0 \qquad (4.36)$$

An alternative to applying the symmetry boundary condition to the radial velocity was to set the radial velocity equal to zero along the pipe's center line. Both methods were tried. The symmetry condition gave the better results probably because of the numerical grid picked to handle the singular point in the governing equations at the centerline ($r = 0$). In order to avoid the singular point, a grid network was constructed which straddled that point. When using the no radial velocity method, the radial velocity at the nodes closest to the centerline was set equal to zero. This prohibited mass from entering or leaving the center most section of the pipe. With the symmetry boundary condition, this problem was avoided. It was also observed that with the symmetry boundary condition, the radial velocity at the center of the pipe was always zero. Thus, the one boundary condition achieved both goals.

Reynolds-Averaged Navier-Stokes Equations

For turbulent flow problems, an averaging process is used to solve for the mean motion which was of primary interest. According to Cebeci and Smith (50:49) this averaging is valid for both steady and unsteady flows, provided that the interval over which the average is taken is long in comparision with the reciprocal of the mean frequency of the turbulenes.

Cebeci and Smith (50:47-61) introduced an averaging procedure which leads to a convenient form of the equations. The dependent variables are written in terms of time averaged mean and fluctuating terms

$$\begin{aligned} \rho &= \bar{\rho} + \rho' \\ p &= \bar{p} + p' \\ \sigma &= \bar{\sigma} + \sigma' \\ q &= \bar{q} + q' \end{aligned} \qquad (4.37)$$

and mass averaged mean and fluctuating quantities

$$\begin{aligned} u &= \tilde{u} + u'' \\ v &= \tilde{v} + v'' \\ e &= \tilde{e} + e'' \\ k &= \tilde{k} \\ \mu &= \tilde{\mu} \\ \lambda &= \tilde{\lambda} \end{aligned} \qquad (4.38)$$

Note that the momentum and energy transport coefficients have been assumed to have no fluctuating components.

For any variable, f, the time average is defined as

$$\bar{f} = \frac{1}{T}\int_{t_o}^{t_o+T} f \; dt \qquad (4.39)$$

In mass averaging, the mass flux is written as a single term and the mean velocity is defined as

$$\tilde{u} = \frac{\overline{\rho u}}{\bar{\rho}} \qquad (4.40)$$

Expressions similar to Equation (4.40) may also be written for the radial velocity and the internal energy. Upon substituting the variables, in terms of mean and fluctuating quantities, into Equations (4.2), (4.6), (4.7) and (4.13) and time averaging, the following mean flow equations result:

$$\frac{\partial \bar{\rho}}{\partial t} + \frac{1}{r}\frac{\partial\{r\bar{\rho}\tilde{v}\}}{\partial r} + \frac{\partial\{\bar{\rho}\tilde{u}\}}{\partial z} = 0 \qquad (4.41)$$

$$\frac{\partial\{\bar{\rho}\tilde{v}\}}{\partial t} + \frac{1}{r}\frac{\partial}{\partial r}\left\{r\left[\bar{\rho}\tilde{v}^2 + \overline{\rho v''^2}\right]\right\} + \frac{\partial}{\partial z}\left\{\bar{\rho}\tilde{u}\tilde{v} + \overline{\rho u''v''}\right\} =$$

$$\frac{1}{r}\left[\frac{\partial}{\partial r}\left\{r\left[-\bar{p} + 2\tilde{\mu}\frac{\partial\tilde{v}}{\partial r} + \tilde{\lambda}\left(\frac{1}{r}\frac{\partial\{r\tilde{v}\}}{\partial r} + \frac{\partial\tilde{u}}{\partial z}\right)\right]\right\} + \frac{\partial}{\partial z}\left\{r\tilde{\mu}\left(\frac{\partial\tilde{v}}{\partial z} + \frac{\partial\tilde{u}}{\partial r}\right)\right\}\right]$$

$$-\frac{1}{r}\left\{-\bar{p} + 2\tilde{\mu}\frac{\tilde{v}}{r} + \tilde{\lambda}\left[\frac{1}{r}\frac{\partial\{r\tilde{v}\}}{\partial r} + \frac{\partial\tilde{u}}{\partial z}\right]\right\} \qquad (4.42)$$

$$\frac{\partial\{\bar{\rho}\tilde{u}\}}{\partial} + \frac{1}{r}\frac{\partial}{\partial r}\left\{r\left[\bar{\rho}\tilde{u}\tilde{v} + \overline{\rho u''v''}\right]\right\} + \frac{\partial}{\partial z}\left\{\bar{\rho}\tilde{u}^2 + \overline{\rho u''^2}\right\} = \frac{1}{r}\left[\frac{\partial}{\partial r}\left(r\tilde{\mu}\left[\frac{\partial\tilde{v}}{\partial z}\right.\right.\right.$$

$$\left.\left.\left. + \frac{\partial\tilde{u}}{\partial r}\right]\right)\right] + \frac{\partial}{\partial z}\left(-\bar{p} + 2\tilde{\mu}\frac{\partial\tilde{u}}{\partial z} + \tilde{\lambda}\left[\frac{1}{r}\frac{\partial\{r\tilde{v}\}}{\partial r} + \frac{\partial\tilde{u}}{\partial z}\right]\right) \qquad (4.43)$$

$$\frac{\partial[\bar{\rho}\tilde{E}]}{\partial t} + \frac{\partial}{\partial z}\left\{\bar{\rho}\tilde{u}\tilde{E} + \overline{\rho u''E''} - \tilde{u}\bar{\sigma}_{zz} - \tilde{u}\bar{\sigma}_{zr} + \bar{q}_z\right\}$$

$$+ \frac{1}{r}\frac{\partial}{\partial r}\left\{r\left[\bar{\rho}\tilde{v}\tilde{E} + \overline{\rho v''E''} - \tilde{v}\bar{\sigma}_{rr} - \tilde{v}\bar{\sigma}_{rz} + \bar{q}_r\right]\right\} = 0 \quad (4.44)$$

where $\tilde{E} = \tilde{e} + \frac{1}{2}\left(\tilde{u}^2 + \tilde{v}^2\right)$. In the developement of Equation (4.44), the following terms were assumed to be small enough to ignore.

$$\overline{\frac{\rho u''}{2}\left(u''^2 + v''^2\right)}$$

$$\overline{\frac{\rho u''}{2}\left(\frac{u''^2 + v''^2}{\bar{\rho}}\right)}$$

Eqs (4.41) to (4.44) differ from their laminar counterparts in that they contain the additional terms:

$$\left.\begin{matrix}\overline{\rho u''v''} \\ \overline{\rho u''} \\ \overline{\rho v''^2}\end{matrix}\right\} \quad \text{Reynolds Stress} \qquad (4.45)$$

$$\left.\begin{matrix}\overline{\rho u''e''} \\ \overline{\rho v''e''}\end{matrix}\right\} \quad \text{Reynolds Heat Flux} \qquad (4.46)$$

These terms represent the effect of the turbulent fluctuations on the mean motion.

Turbulence Model

The turbulent fluctuating averages are additional unknowns for which there are no corresponding equations. The equations must be closed by appropriate expressions for the unknowns. Most methods to date have been based upon the eddy viscosity concept. In this method, the Reynolds stress is modeled as being proportional to the laminar stress of the mean flow, with the coefficient of proportionality being defined as the eddy viscosity. For example:

$$\overline{\rho v''^2} = 2\tilde{\mu}_t\frac{\partial \tilde{v}}{\partial r} + \tilde{\lambda}_t\left(\frac{1}{r}\frac{\partial\{r\tilde{v}\}}{\partial r} + \frac{\partial \tilde{u}}{\partial z}\right)$$

$$\overline{\rho u''^2} = 2\tilde{\mu}_t\frac{\partial \tilde{u}}{\partial z} + \tilde{\lambda}_t\left[\frac{1}{r}\frac{\partial\{r\tilde{v}\}}{\partial r} + \frac{\partial \tilde{u}}{\partial z}\right] \quad (4.47)$$

$$\overline{\rho u''v''} = \tilde{\mu}_t\left[\frac{\partial \tilde{v}}{\partial z} + \frac{\partial \tilde{u}}{\partial r}\right]$$

A similar eddy conductivity (k_t) for heat flux can be defined as

$$\overline{\rho u''e''} = \gamma \frac{\mu_t}{Pr_t}\frac{\partial \tilde{e}}{\partial z}$$

$$\overline{\rho v''e''} = \gamma \frac{\mu_t}{Pr_t}\frac{\partial \tilde{e}}{\partial r} \quad (4.48)$$

$$Pr_t = \frac{c_p \mu_t}{k_t} = 0.9$$

Upon substituting Equations (4.47) and (4.48) into Equations (4.41) through (4.44) the Reynolds-averaged cylindrical Navier-Stokes equations may be written as

$$\frac{\partial \vec{U}_t}{\partial t} + \frac{\partial \vec{F}_t}{\partial z} + \frac{1}{r}\frac{\partial}{\partial r}\left\{r\,\vec{G}_t\right\} = \frac{\vec{H}_t}{r} \quad (4.49)$$

where

$$\vec{U}_t = \begin{bmatrix} \bar{\rho} \\ \overline{\rho u} \\ \overline{\rho v} \\ \overline{\rho E} \end{bmatrix} \qquad \vec{F}_t = \begin{bmatrix} \bar{\rho}\tilde{u} \\ \bar{\rho}\tilde{u}^2 - \bar{\sigma}_{zz} \\ \bar{\rho}\tilde{u}\tilde{v} - \bar{\sigma}_{zr} \\ \bar{\rho}\tilde{u}\tilde{E} - \tilde{u}\bar{\sigma}_{zz} - \tilde{u}\bar{\sigma}_{zr} + \bar{q}_z \end{bmatrix}$$

$$\vec{G}_t = \begin{bmatrix} \bar{\rho}\tilde{v} \\ \bar{\rho}\tilde{u}\tilde{v} - \bar{\sigma}_{rz} \\ \bar{\rho}\tilde{v}^2 + \bar{\sigma}_{rr} \\ \bar{\rho}\tilde{v}E - \tilde{v}\bar{\sigma}_{rr} - \tilde{v}\tilde{u}_{rz} + \bar{q}_r \end{bmatrix} \qquad \vec{H}_t = \begin{bmatrix} 0 \\ 0 \\ -\bar{\sigma}_{\phi\phi} \\ 0 \end{bmatrix}$$

and where

$$\bar{\sigma}_{rr} = -\bar{p} + 2[\tilde{\mu} + \mu_t]\frac{\partial\tilde{v}}{\partial r} + [\tilde{\lambda} + \lambda_t]\left[\frac{1}{r}\frac{\partial\{r\tilde{v}\}}{\partial r} + \frac{\partial\tilde{u}}{\partial z}\right]$$

$$\bar{\sigma}_{\phi\phi} = -\bar{p} + 2\tilde{\mu}\frac{\tilde{v}}{r} + \tilde{\lambda}\left[\frac{1}{r}\frac{\partial\{r\tilde{v}\}}{\partial r} + \frac{\partial\tilde{u}}{\partial z}\right]$$

$$\bar{\sigma}_{zz} = -\bar{p} + 2[\tilde{\mu} + \mu_t]\frac{\partial\tilde{u}}{\partial z} + [\tilde{\lambda} + \lambda_t]\left[\frac{1}{r}\frac{\partial\{r\tilde{v}\}}{\partial r} + \frac{\partial\tilde{u}}{\partial z}\right]$$

$$\bar{\sigma}_{rz} = \bar{\sigma}_{zr} = [\tilde{\mu} + \mu_t]\left[\frac{\partial\tilde{v}}{\partial z} + \frac{\partial\tilde{u}}{\partial r}\right]$$

$$\tilde{E} = \tilde{e} + \frac{1}{2}\left\{\tilde{u}^2 + \tilde{v}^2\right\}$$

$$q_z = -\left(\frac{\tilde{\mu}}{P_r} + \frac{\mu_t}{P_{r_t}}\right)\frac{\partial e}{\partial z} \qquad q_r = -\left(\frac{\tilde{\mu}}{P_r} + \frac{\mu_t}{P_{r_t}}\right)\frac{\partial e}{\partial r}$$

A model proposed by Baldwin and Lomax (51) was used to model the eddy viscosity. The turbulence model proposed by Baldwin and Lomax is patterned after that of Cebeci and Smith (50) with modifications that avoid the necessity for finding the edge of the boundary layer. It is a two-layer algebraic eddy viscosity model in which μ_t is given by

$$\mu_t = \begin{cases} (\mu_t)_{inner} & y \le y_{cr} \\ (\mu_t)_{outer} & y > y_{cr} \end{cases} \qquad (4.50)$$

where y is the normal distance from the wall and y_{cr} is the smallest value of y at which μ_t values from the inner and outer formulas are equal.

The Prandtl-Van Driest formulation is used in the inner region

$$(\mu_t)_{inner} = \rho l^2 |\omega| \tag{4.51}$$

where $l = ky\left[1 - \exp\left\{\frac{-y^+}{A^+}\right\}\right]$ and $|\omega|$ is the magnitude of the vorticity

$$|\omega| = \sqrt{\left(\frac{\partial \tilde{v}}{\partial z} - \frac{\partial \tilde{u}}{\partial r}\right)^2} \tag{4.52}$$

also

$$y^+ = \frac{\sqrt{\rho_w \tau_w}}{\mu_w} y \tag{4.53}$$

For the outer region

$$(\mu_t)_{outer} = KC_{cp} \rho F_w F_k(y) \tag{4.54}$$

where K is the Clauser constant, C_{cp} is an additional constant, and

$$F_w = \left\{ \begin{array}{c} y_{max} F_{max} \\ \text{or} \\ C_{wk} y_{max} \frac{U_{dif}}{F_{max}} \end{array} \right\} \text{smallest} \tag{4.55}$$

The quantities F_{max} and y_{max} are determined from the function

$$F(y) = y|\omega| \left[1 - \exp\left(\frac{-y^+}{A^+}\right)\right] \tag{4.56}$$

The quantity F_{max} is the maximum value of F(y) that occures in a profile and y_{max} is the value of y at which it occurs. The function $F_k(y)$ is the Klebanoff intermittency factor given by

$$F_k(y) = \left[1 + 5.5\left(\frac{C_k\, y}{y_{max}}\right)^6\right]^{-1} \qquad (4.57)$$

The quantity U_{dif} is the difference between the maximum and minimum total velocity in the profile (i.e., at a fixed z station)

$$U_{dif} = \left(\sqrt{u^2 + v^2}\right)_{max} - \left(\sqrt{u^2 + v^2}\right)_{min} \qquad (4.58)$$

The second term in U_{dif} is taken to be zero (except in wakes).

The constants appearing in the foregoing relations were determined by requiring agreement with the Cebeci formulation for constant pressure boundary layers at transonic speeds. The values determined are

$$A^+ = 26$$
$$C_{cp} = 1.6$$
$$C_k = 0.3$$
$$C_{wk} = 0.25$$
$$k = 0.4$$
$$K = 0.0168$$
$$P_r = 0.72$$
$$P_{r_t} = 0.9$$

Transition Region Model

Based on the experimental measurements presented in Chapter III, the flow was found to always be laminar in the evaporator and usually turbulent in the condenser. A transition region model was needed to model the change from fully laminar to fully turbulent flow.

The model used was that of Dhawan and Narasimha (52). The transition region model is

$$\Gamma\left(\bar{x}\right) = 1 - \mathrm{EXP}\left(-0.412\ \bar{x}^2\right) \qquad (4.59)$$

where $\bar{x}$ is the normalized streamwise coordinate in the transition region

$$\bar{x} = \left[\left(x - x_{t,i}\right) / \Omega\right] \qquad x_{t,i} < x < x_{t,f} \qquad (4.60)$$

$x_{t,i}$ and $x_{t,f}$ denote the initial and final locations of the transition zone. Ω is a measure of the extent of the transition region defined by

$$\Omega = x_{\Gamma=3/4} - x_{\Gamma=1/4} \qquad (4.61)$$

In the above mentioned model, three parameters are required, namely $x_{t,i}$, $x_{\Gamma=1/4}$ and $x_{\Gamma=3/4}$. For the present purpose, these parameters were obtained from experimental data.

V. Numerical Solution Technique

The numerical approach that was used to solve the system of equations developed in chapter IV will be discussed in this chapter. The general solution procedure was that developed by MacCormack in 1969 (53). It is known as the Explicit MacCormack Method. The general procedure used by MacCormack will be described in the first part of this chapter. The presentation is paraphased from the presentation by Anderson, Tannehill and Pletcher (49:482-485). After the method has been described, the computer code that was used to solve the problem will be outlined. Lastly, the finite-difference grid that was used for the problem solution will be introduced.

Explicit MacCormack Method

When the MacCormack scheme is applied to the compressible Navier-Stokes equation given by Equation (4.15) the following algorithm results:

Predictor:

$$U_{j,k}^{\overline{n+1}} = U_{j,k}^{n} + \frac{\Delta t}{\Delta z}\left(F_{j,k+1}^{n} - F_{j,k}^{n}\right) - \frac{1}{r}\frac{\Delta t}{\Delta r}\left[r\left(G_{j+1,k}^{n} - G_{j,k}^{n}\right)\right] + \Delta t\, H_{j,k}^{n} \tag{5.1}$$

Corrector:

$$U_{j,k}^{n+1} = \frac{1}{2}\left[U_{j,k}^{n} + U_{j,k}^{\overline{n+1}} - \frac{\Delta t}{\Delta z}\left(F_{j,k}^{\overline{n+1}} - F_{j,k-1}^{\overline{n+1}}\right) - \frac{1}{r}\frac{\Delta t}{\Delta r}\left\{r\left(G_{j,k}^{\overline{n+1}} - G_{j-1,k}^{\overline{n+1}}\right)\right\} + \Delta t\left(H_{j,k}^{n} + H_{j,k}^{\overline{n+1}}\right)\right] \tag{5.2}$$

where $z = k\Delta z$, and $r = j\Delta r$. This explicit scheme is second-order accurate in both space and time. In the present form of this scheme, forward differences are used for all spatial derivatives in the predictor step while backward differences are used in the corrector step.

The derivatives appearing in the viscous terms of $\vec{F}$ and $\vec{G}$ must be differenced correctly in order to maintain second-order accuracy. This is accomplished in the following manner. The z derivative terms in $\vec{F}$ are differenced in the opposite direction to that used for $\frac{\partial \vec{F}}{\partial z}$ while the r derivatives are approximated with central differences. Likewise, the r derivative terms appearing in $\vec{G}$ are differenced in the opposite direction to that used for $\frac{\partial \vec{G}}{\partial r}$, while the cross-derivative terms in $\vec{G}$ are approximated with central differences. For example, consider the following term in $\vec{F}$ which corresponds to the z-momentum equation

$$F_3 = \rho uv - \mu \frac{\partial u}{\partial r} - \mu \frac{\partial v}{\partial z} \tag{5.3}$$

In the predictor step, given by Equation (5.1), the term is differenced as

$$(F_3)^n_{j,k} = \left(\rho uv\right)^n_{j,k} - \left[\left(\frac{u^n_{j+1,k} - u^n_{j-1,k}}{2\,\Delta r}\right) + \left(\frac{u^n_{j,k} - u^n_{j,k-1}}{\Delta z}\right)\right]\mu \tag{5.4}$$

while in the corrector step, given by Equation (5.2), the term is differenced as

$$(F_3)^{\overline{n+1}}_{j,k} = \left(\rho uv\right)^{\overline{n+1}}_{j,k} - \left[\left(\frac{u^{\overline{n+1}}_{j+1,k} - u^{\overline{n+1}}_{j-1,k}}{2\,\Delta r}\right) + \left(\frac{u^{\overline{n+1}}_{j,k+1} - u^{\overline{n+1}}_{j,k}}{\Delta z}\right)\right]\mu \tag{5.5}$$

Because of the complexity of the compressible

Navier-Stokes equations, as yet, it has not been possible to obtain a closed-form stability expression for the MacCormack scheme applied to these equations; however, the following empirical formula can normally be used

$$\Delta t \leq \sigma(\Delta t)_{CFL} \tag{5.6}$$

where σ is a safety factor ($\leq$ 0.9), $(\Delta t)_{CFL}$ is the inviscid CFL condition

$$(\Delta t)_{CFL} = \left(\frac{|u|}{\Delta z} + \frac{|v|}{\Delta r} + c\sqrt{\left(\frac{1}{\Delta z}\right)^2 + \left(\frac{1}{\Delta r}\right)^2} \right) \tag{5.7}$$

and c is the local speed of sound

$$c = \sqrt{\frac{\gamma p}{\rho}} \tag{5.8}$$

Before each iteration the time step can be computed for each grid point using Equation (5.6). The smallest of these time steps is then used to advance the solution over the entire mesh.

After each predictor and corrector step, the primitive variables (ρ , u, v, e, p, T) are found by decoding the $\vec{U}$ vector

$$\vec{U} = \begin{bmatrix} U_1 \\ U_2 \\ U_3 \\ U_4 \end{bmatrix} = \begin{bmatrix} \rho \\ \rho u \\ \rho v \\ \rho E \end{bmatrix} \tag{5.9}$$

in the following manner

$$\rho = U_1$$

$$u = \frac{U_2}{U_1}$$

$$v = \frac{U_3}{U_1}$$

$$E = \frac{U_4}{U_1}$$

$$e = E - \frac{1}{2}\left(u^2 + v^2 \right) \qquad (5.10)$$

$$p = p[\rho, e]$$

$$T = T[\rho, e]$$

For both the predictor and corrector sweeps, artifical damping (a numerical smoothing term) was calculated and added to the problem variables. This damping was necessary to ensure a stable solution. The technique used for determining the amount of damping was that presented by MacCormack and Baldwin (54). The method uses a damping term that is proportional to the second derivative of pressure and is of significant magnitude only in regions of pressure oscillation, where truncation error is already adversely affecting calculation.

Computer Code

Figure 5.1 is a flow chart of the computer code used. The code was written by Dr. Joe Shang of the Flight Dynamics Laboratory, Wright Patterson Air Force Base. Appendix A contains a listing of the code.

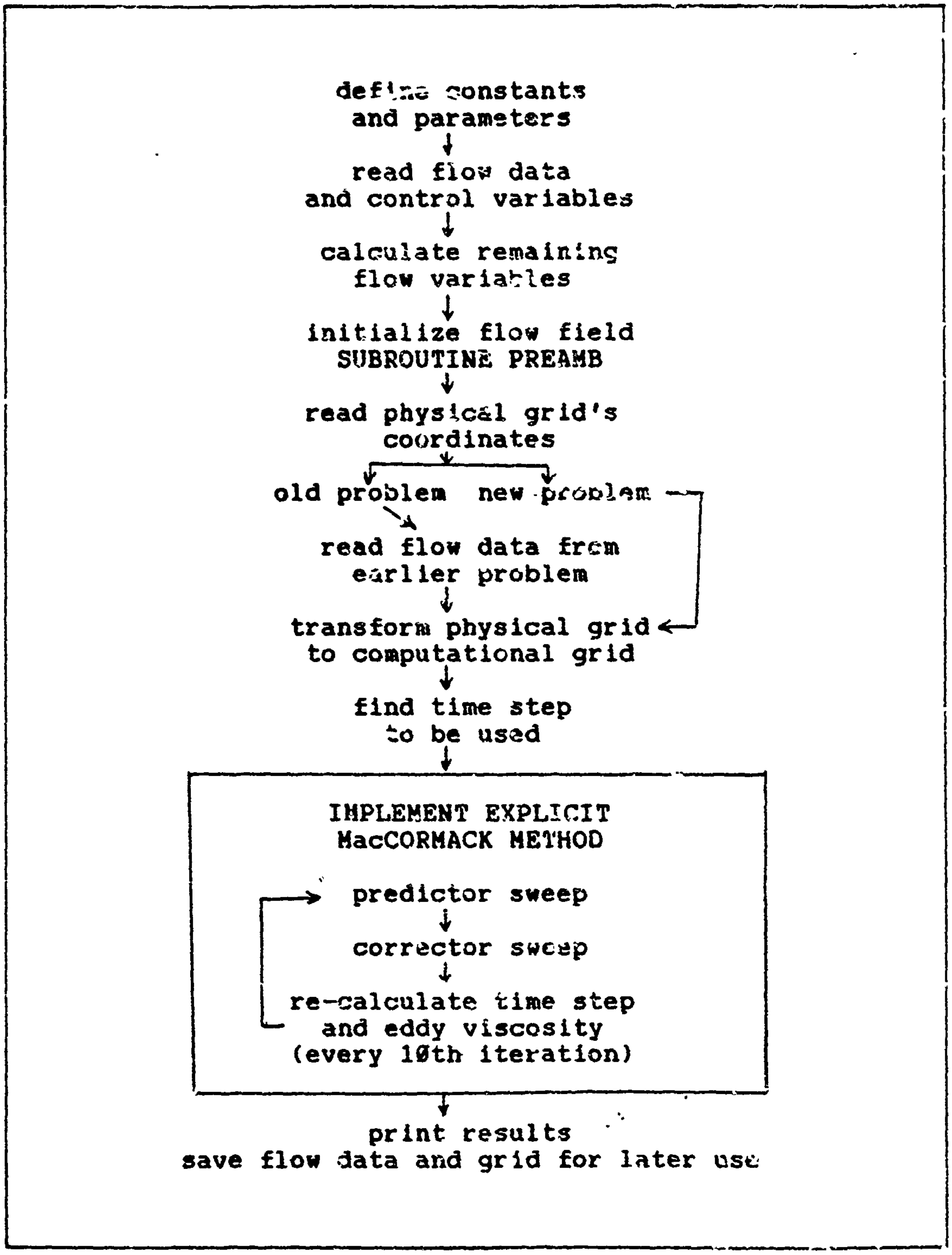

Figure 5.1 Program Flow Chart

Physical Grid

Initially, the grids used took advantage of early heat-pipe vapor flow solutions by clustering grid points into areas where large gradients were expected. Numerical experiments were performed to compare the grid with clustering to a uniform grid. The non-uniform grid had round off errors larger than those found with the uniform-grid by four orders of magnitude. The uniform-grid solutions seemed to give more stable results despite the coarse grid in the regions of large gradients. The grid used for most of the calculations had uniform spacing with 96 axial grid points and 25 radial grid points.

VI. Numerical Results

The results of the numerical simulation will be discussed in this chapter. First, there will be a discussion of the solution to the unsteady problem. Secondly, the steady-state solutions obtained will be compared with the experimental results. The numerical results were used to estimate friction coefficients that can be used in one dimensional models. The third section of this chapter will describe how this was done and present the results obtained. The chapter will be concluded with a discussion of the applicability of boundary-layer assumptions to heat-pipe vapor flow problems.

Transient Results

One of the original objectives of this research was to better understand the transient vapor dynamics of a heat pipe. The heat-pipe transient modeled was equivalent to an instantaneous lowering of the condenser environment temperature while maintaining the evaporator environment temperature at a constant value. Because the experimental results were for a porous pipe with air injected or extracted through its wall, the actual transient modeled consisted of instantaneously lowering the condenser's external manifold pressure while maintaining the evaporator's external manifold pressure constant. The transient modeled would be equivalent to the heat-pipe transient described if the heat-pipe wall had no thermal capacitance and thus provides a "worst-case" situation.

Figures 6.1 and 6.2 represent the pressure response to the transient. The pressures at three locations in the pipe are plotted during the transient. The three locations are 1) the evaporator end of the pipe, 2) the center of the pipe, i.e., the evaporator-condenser junction, and 3) the condenser end of the pipe. All three points were on the pipe's center line.

As the transient began, mass was removed from the condenser end of the pipe along the entire region. This caused a drop in the condenser pressure. As the condenser's external pressure dropped, an expansion wave moved radially from the wall to the pipe's center line. Upon reaching the center of the pipe, the expansion wave reflected as a compression wave. Upon reaching the outside wall, the compression wave reflected off the pipe wall as an inward moving expansion wave. These radially moving compression and expansion waves can be seen for quite some time in the two lower pressure plots. They are seen superimposed on the overall condenser pressure drop. More important than the radially moving waves are those that move axially in the pipe. Shortly after the transient began, a series of expansion waves began moving from the condenser region toward the evaporator. Also, a compression wave began traveling from the downstream end of the evaporator into the condenser. From Figure 6.2, it can be seen that when the different waves reached the ends of the pipe, the evaporator end pressure began to drop and the condenser end pressure

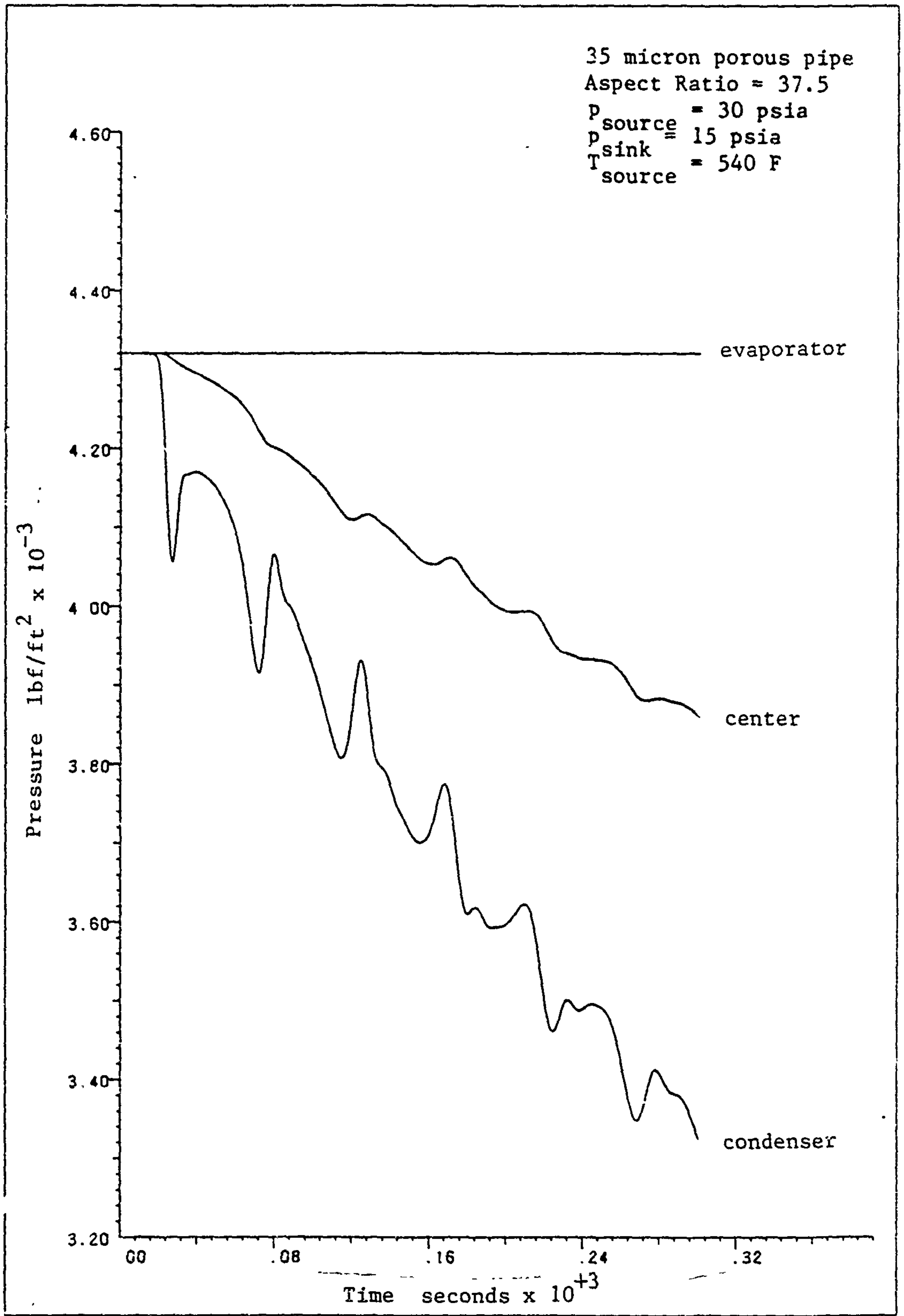

Figure 6.1 Pressure History Early in the Transient

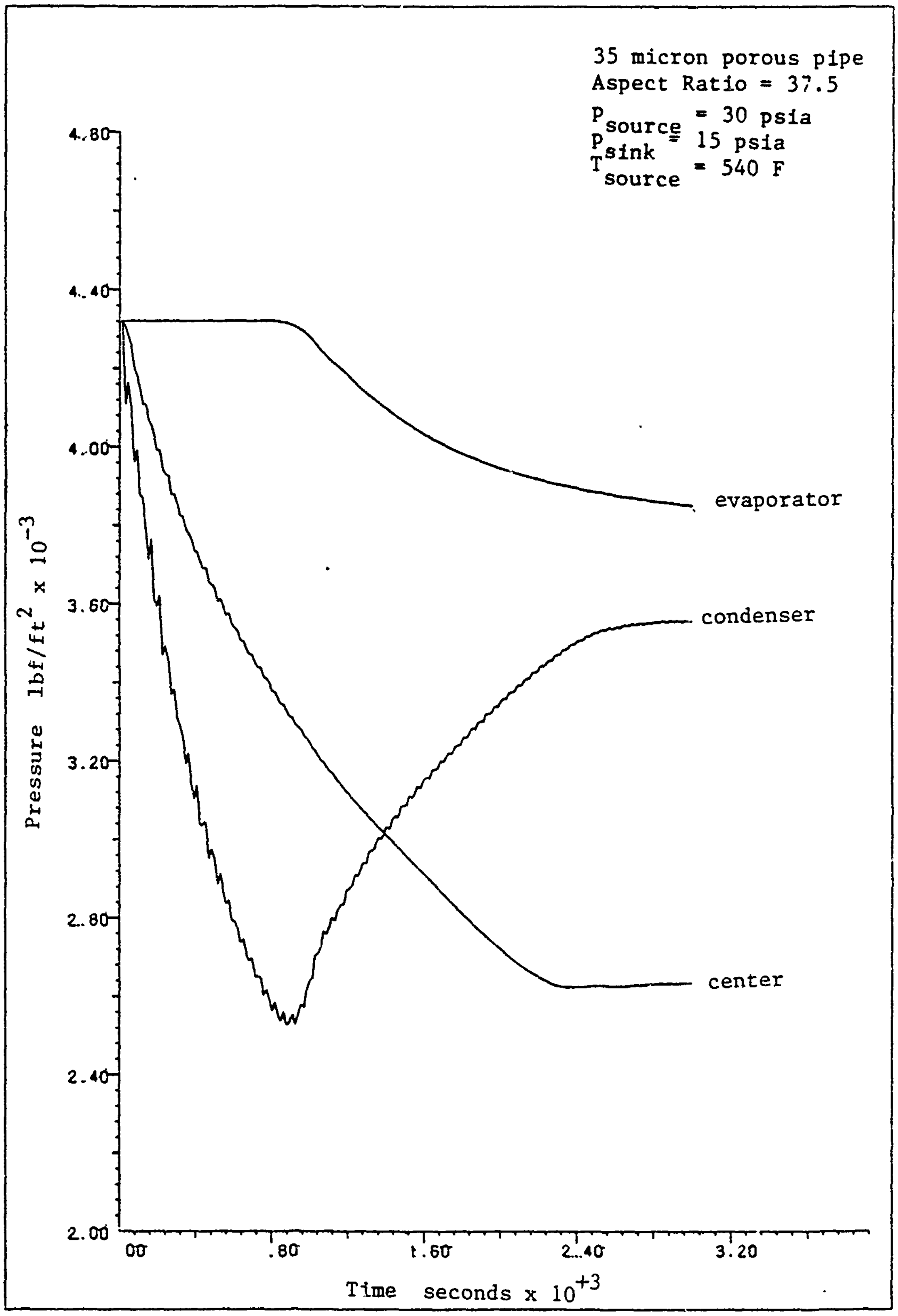

Figure 6.2 Extended-time Pressure History During the Transient

stopped falling and began to rise. As can be seen from Figure 6.2, the pressure waves eventually diminish and steady state was reached. A check was performed to determine if the time for the expansion and compression waves to move the length of the pipe, as predicted by the numerical results, was realistic. Assuming the axial expansion wave was moving at sonic velocity, it should reach the evaporator end of the pipe about 0.9 ms after the transient began. This corresponds well with the results shown in Figure 6.2.

Figures 6.3 and 6.4 are velocity plots for different instants in time during the transient. They show how the expansion and compression waves affect the velocity field in the pipe. The times on Figures 6.3 and 6.4, A to C, correlate with the time scales in Figures 6.1 and 6.2. Figure 6.3A is an expanded view of the condenser. Most of the fluid motion is radially out of the condenser. The expansion wave from the evaporator has moved about 1/7 of the way into the condenser. The resulting flow from the evaporator into the condenser can be seen in the figure. In Figure 6.3B the expansion wave has moved twice as far into the condenser. The fluid is still stationary in the upstream end of the evaporator. The blank region in Figure 6.3B corresponds to stagnant flow. In Figure 6.3C the axial expansion and compression waves have still not reached the pipe ends. At the end of the condenser, the radial flow can be seen to split and move both inward and outward. This may

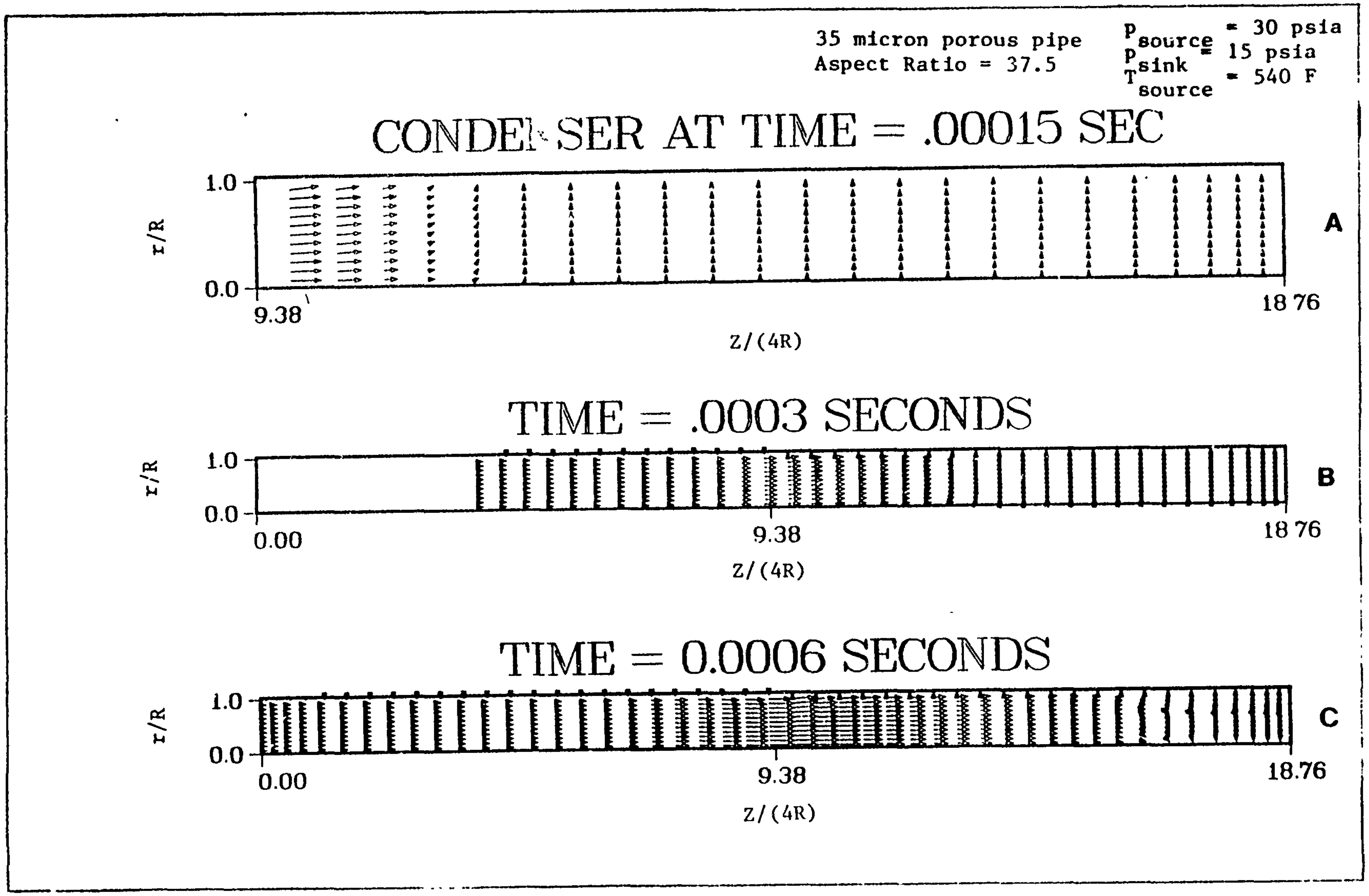

Figure 6.3 Velocity Fields

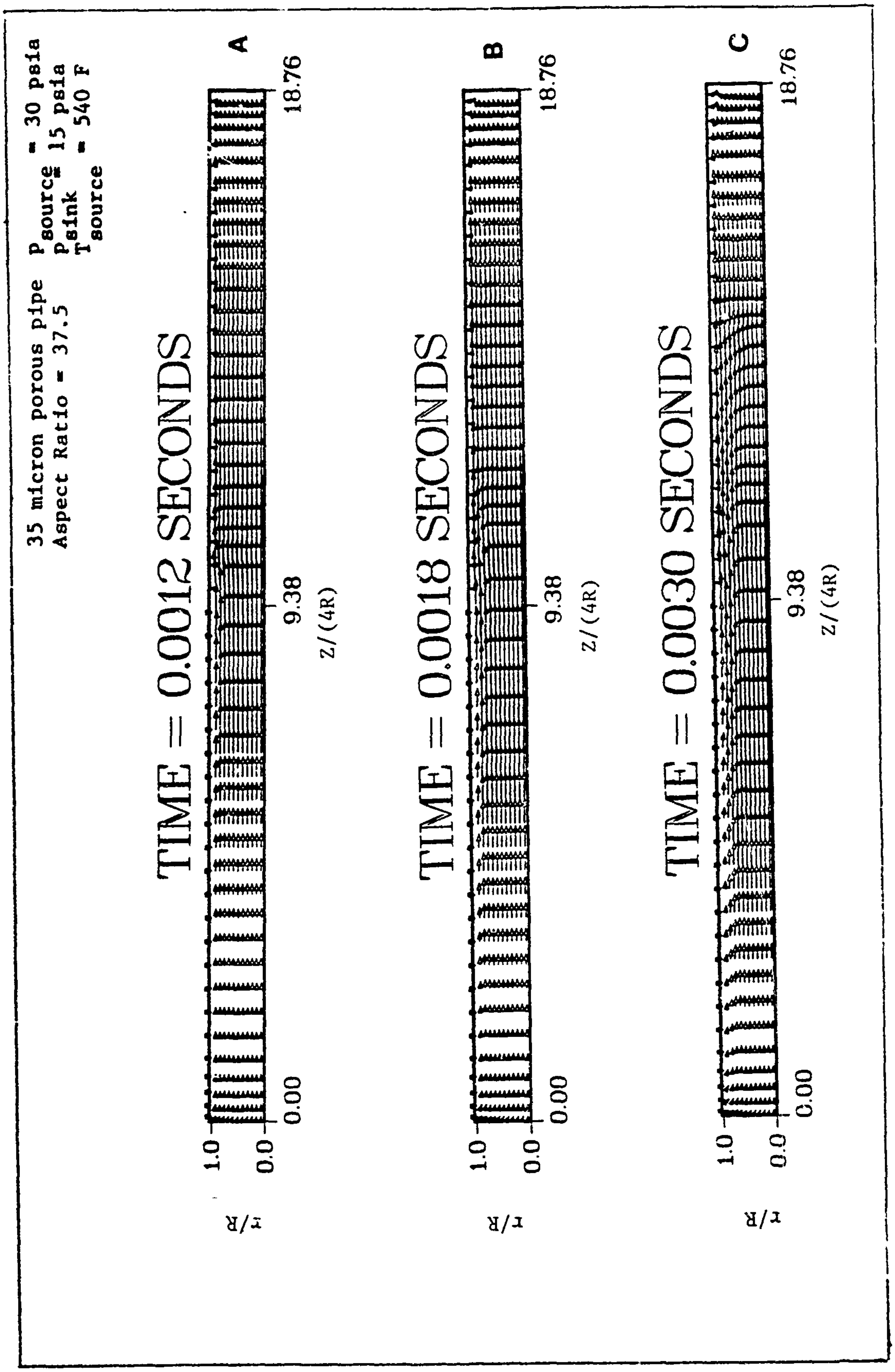

Figure 6.4 Velocity Fields

be due to the radial expansion and compression waves that are still dominant in this region. In Figure 6.4A the axial expansion and compression waves have reached the ends of the pipe. It is interesting to note that at this time the mass moving from the evaporator into the condenser is not all leaving the condenser through the wall. Some of the mass stays in the condenser, helping to raise the condenser pressure to its steady-state distribution. In Figure 6.4B the flow can be seen to continue to develop. In Figure 6.4C steady-state flow is almost reached. It is interesting to contrast the radial variations in velocity between Figure 6.4C and Figure 6.4B. At the later times, the velocity profiles are approaching more of an internal pipe flow profile which has a definite boundary layer region. Earlier in the transient (Figures 6.4A and 6.4B) the velocity profiles are very flat.

From Figure 6.2 it can be seen that after about 3.2 ms, the vapor transient has almost reached the steady-state value. This time is much faster than the time for a heat-pipe wall to respond to a transient. For example, a 1/32 inch thick sheet of copper with a convection heat transfer coefficient of 1000 Btu/hr-ft^2-F has a characteristic response time on the order of 0.24 seconds (assuming a lump parameter model). As a result of the difference between the response times of the vapor and the wall, the vapor is essentially always in steady state when compared to the wall. Thus, we may infer that for most numerical heat-pipe models, it is a good assumption to use a steady heat-pipe vapor model in conjunction with a transient heat-pipe wall model.

Steady-State Solution

The experimental part of this research consisted of measuring steady-state spatial pressure and velocity variations in a simulated heat-pipe vapor region. This section will compare the steady-state numerical results to the experimental measurements. First the pressure data and then the velocity data will be compared.

Pressure Profiles. Figure 6.5 contains the numerically-determined pressures and the experimentally-measured pressures for three cases. The numerical simulations (solid lines) closely matched the experimental results. The maximum Mach numbers obtained in the flow fields for the three cases were 0.175, 0.635, and 1.70. For all three cases axial pressure drops where observed as the flow accelerated in the evaporator region due to mass injection at the wall. For the two subsonic cases, the pressure rose as it decelerated in the condenser due to mass removal. In the supersonic case, mass removal caused a further acceleration of the air in the condenser until a normal shock was encountered. Bystrov and Popov (22) reported observing a similar phenomena by infering the presence of the shock from temperature measurements on the inside of a sodium heat pipe. After the shock, the pressure increased as the flow slowed down. The total frictional

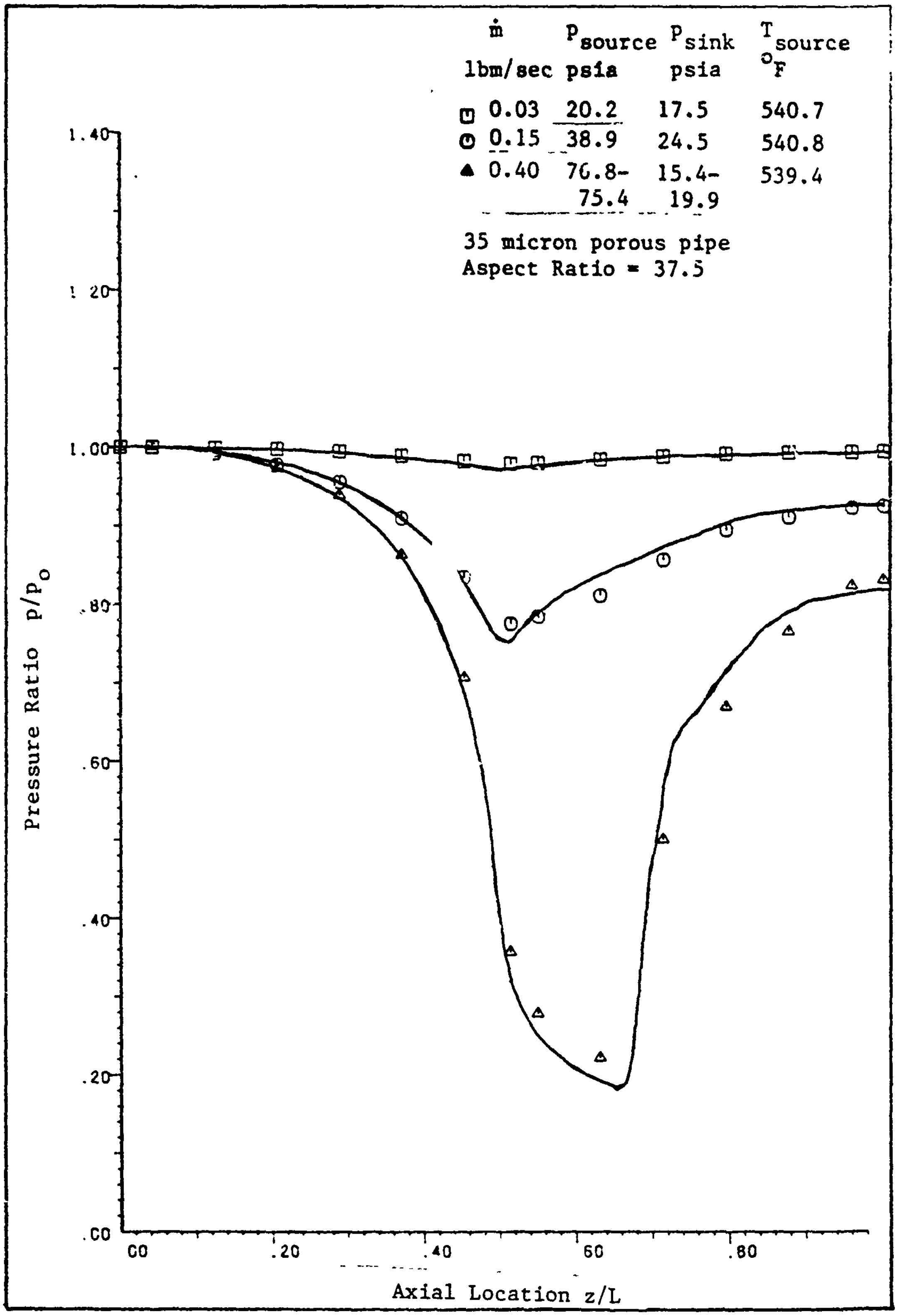

Figure 6.5 Numerical and Experimental Pressure Data

pressure loss is the difference between the pressures at the upstream end and down stream end of the pipe. If no friction was present, total pressure recovery would occur and the two end pressures would have been equal (c.f. Chapter II). It can be seen from Figure 6.5 that the amount of friction increases with flow rate (or Mach number).

From the experimental data, for the low mass flow rate cases studied, the evaporator and condenser manifold pressures were uniform over the exterior of the porous pipe. As the mass flow rate increased, however, the flow resistance into the different chambers caused an axial variation in the manifold pressures. For example, in the evaporator manifold the pressure would decrease from the upstream end of the pipe to the center of the pipe, the evaporator/condenser junction. This was because more flow was trying to go through the porous pipe near the downstream end of the evaporator where there was a lower internal pressure. The higher flow rates through the camber valving (c.f. Figure 2.2) caused a larger pressure drop and thus a lower manifold presssure on the porous pipe. This same phenomenon was noticed in the condenser manifold. There the pressure would increase from the entrance of the condenser to the end of the condenser. To obtain accurate internal pressure variations, the experimentally measured external pressure distribution had to be used as a boundary condition.

Velocity Profiles. Figure 6.6 illustrates a sample of

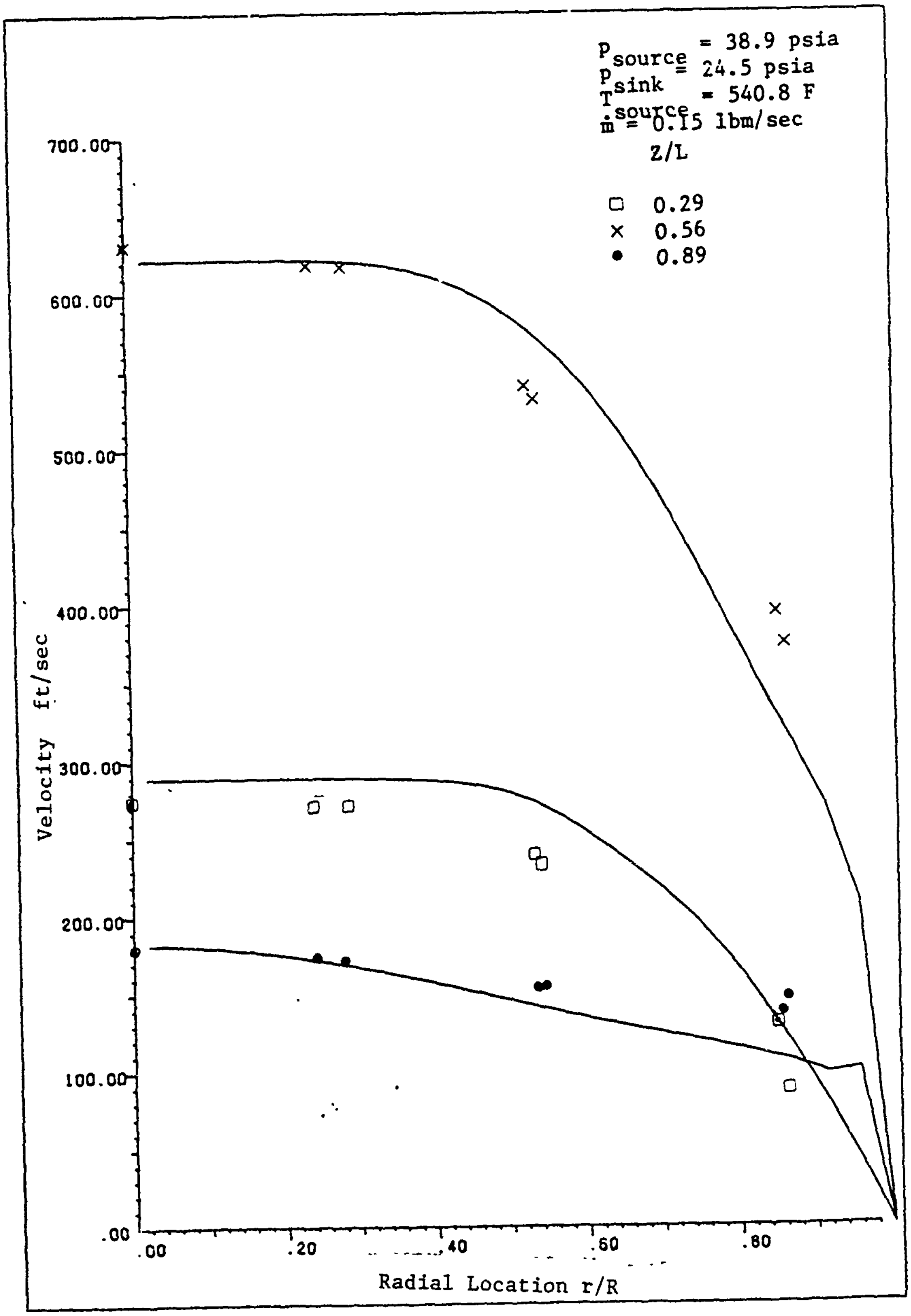

Figure 6.6 Numerical and Experimental Velocity Data

the velocity results obtained. The three radial variations in the axial velocities shown are for three different axial positions along the pipe. The middle line is for the location X/L = Ø.29 or about halfway down the evaporator. The upper most line is for the location X/L = Ø.56 or slightly down stream from the evaporator/condenser junction. The lower curve is for X/L = Ø.89 or near the down-stream end of the condenser. The agreement between the numerical and experimental results is good. The numerical results were best for the evaporator region. In the condenser, the turbulence and mass extraction at the wall cause a very flat velocity profile in the center of the pipe with a sharp velocity gradient at the wall. Because of the relative coarseness of the numerical grid, the sharp velocity gradient along the condenser wall could not be resolved as well as it was in the evaporator.

Numerical studies indicated that by increasing the number of radial grid points, the condenser velocity profile could be more accurately predicted. The problem with doubling the number of grid points was that four times as much computer time was needed to obtain a solution. To obtain the quality of results sought for this work, 25 radial grid points gave sufficient results without requiring excessive computer time.

Figure 6.7 illustrates how the radial velocity varies throughout the flow field for a maximum Mach number of Ø.635. It is interesting to note that the maximum or

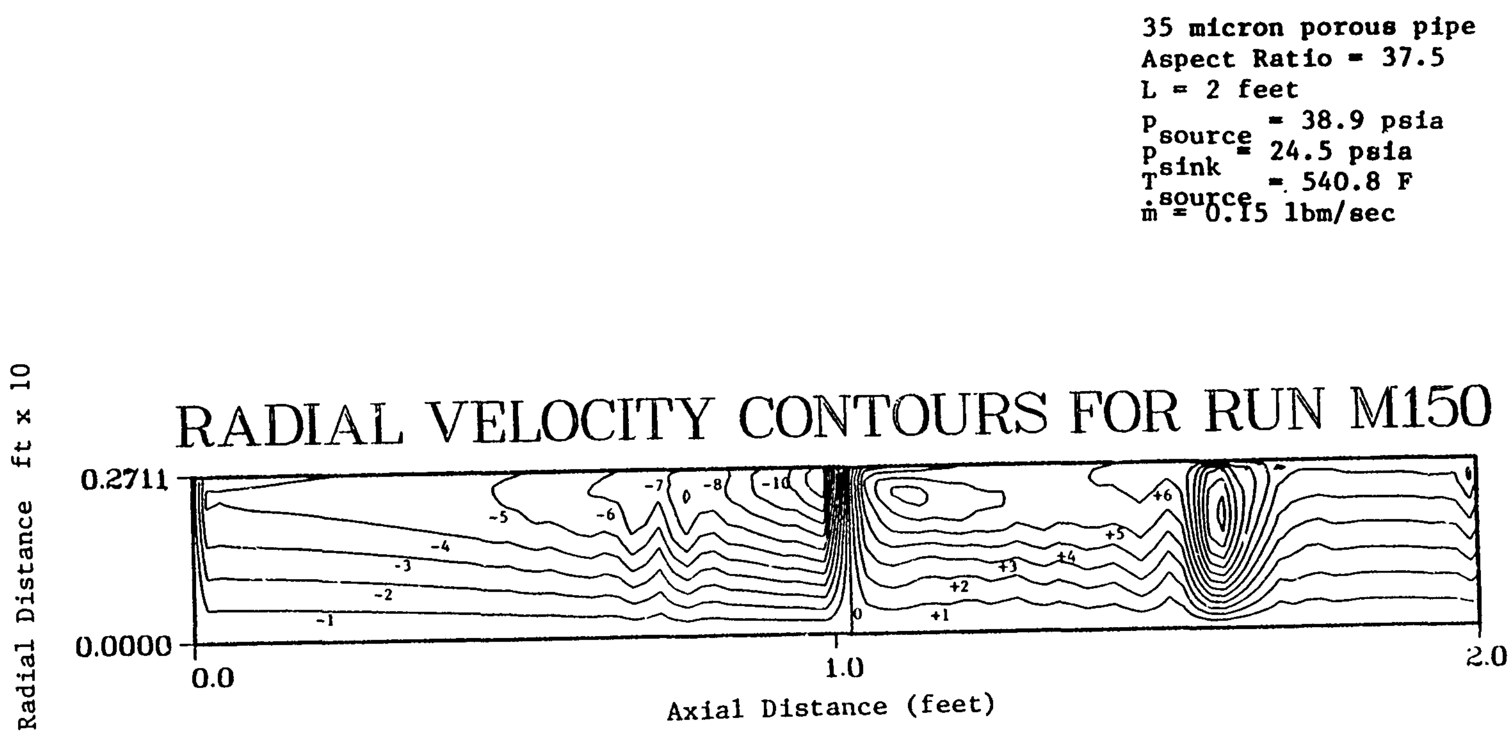

Figure 6.7 Radial Velocity Contour Plot

minimum radial velocity at a given axial location doesn't always occur at the pipe wall as might be expected. As the fluid moves radially toward the center of the pipe in the evaporator, the radial mass flow rate must decrease, becoming zero at the pipe center. It is believed that near the pipe wall the flow area decreases faster than the the mass flow rate. This causes the radial velocity to increase for a short distance. The abnormal behavior noticed in the condenser region is due to transient effects that were still present when the data in Figure 6.7 was obtained.

Friction Coefficients

Once the numerical solutions were shown to be valid, they were used to predict friction coefficients that could be used in simpler, one dimensional models. The friction coefficient found is defined by the equation

$$f = \frac{2\tau_w}{\bar{\rho}\,\bar{U}^2} \qquad (6.1)$$

where τ_w is the shear stress at the pipe wall, $\bar{\rho}$ is the average density and $\bar{U}$ is the average velocity. This section of chapter VI will describe how the friction coefficients were calculated. Also, useful functional representations of the data will be presented.

Method of Calculation. Two methods were used to approximate the friction coefficient defined by Equation (6.1). The two methods used different techniques for finding the wall shear stress. The most straightforward method approximated the shear stress at the wall with the finite difference formula

$$\tau_w = -\mu \frac{\partial u}{\partial r}\bigg|_{r=R} = -\mu \frac{3u_1 - 4u_2 + u_3}{2\Delta r} \qquad (6.2)$$

where u_1, u_2, and u_3 were axial velocities at the pipe wall, one grid point from the wall and two grid points from the wall, respectively. This method worked best for the evaporator region where the experimental and numerical velocity profiles matched the closest. In the condenser, this method was suspected of underestimating the shear stress because of the error in the numerical velocity gradient results near the pipe wall.

In the second method, the shear stress at the pipe wall was approximated using a force balance on an element of fluid in the pipe. Figure 6.8 shows a typical fluid element studied.

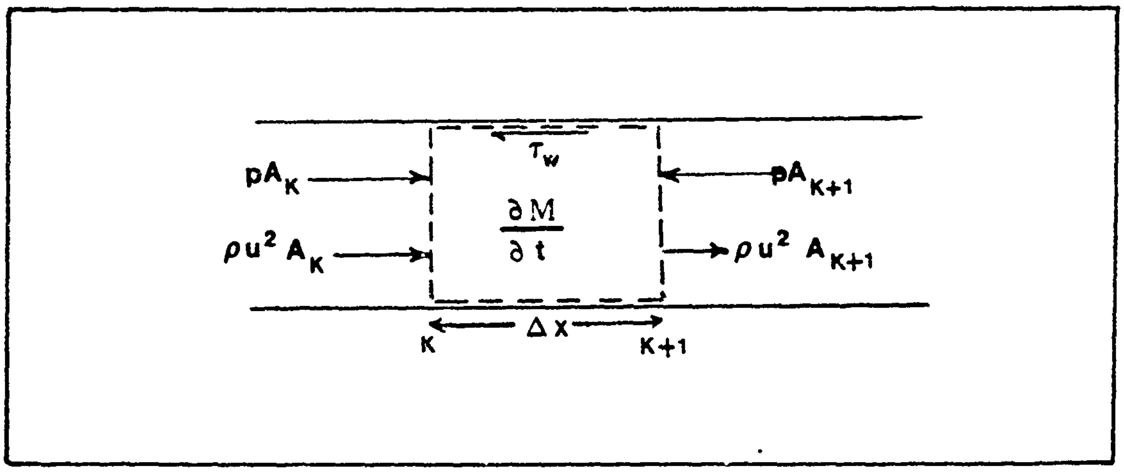

Figure 6.8 Element of Fluid Used For Force Balance

The force balance took the form

Time Rate of change of Momentum in the Element	=	Rate of Flow of Momentum into the Element	−	Rate of Flow of Momentum out of the Element	+	Sum of the Forces on the Element

Symbolically this can be written as

$$\frac{\partial M}{\partial t} = 2\pi\int_0^R \rho u^2\Big|_k r\,dr - 2\pi\int_0^R \rho u^2\Big|_{k+1} r\,dr + 2\pi\int_0^R p_k\, r\,dr - 2\pi\int_0^R p_{k+1}\, r\,dr - \tau_w 2\pi R\Delta x \quad (6.3)$$

or

$$\tau_w = \frac{-1}{R\Delta x}\int_0^R \left(\rho u^2\Big|_{k+1} - \rho u^2\Big|_k + p_{k+1} - p_k\right) r\,dr - \frac{1}{2\pi R\Delta x}\frac{\partial M}{\partial t} \quad (6.4)$$

The wall shear stress in Equation (6.4) was found by numerically integrating the pressure and velocity results from the numerical simulation. Simpson's rule was used for the numerical integration.

When calculating the friction coefficient, the momentum balance was used for the condenser region and the velocity gradient method was used for the evaporator. Figure 6.9 compares the two methods for calculating friction coefficient.

A great deal of time was spent studying and comparing the two methods of finding the friction coefficient. Several factors led to using a combination of methods. From

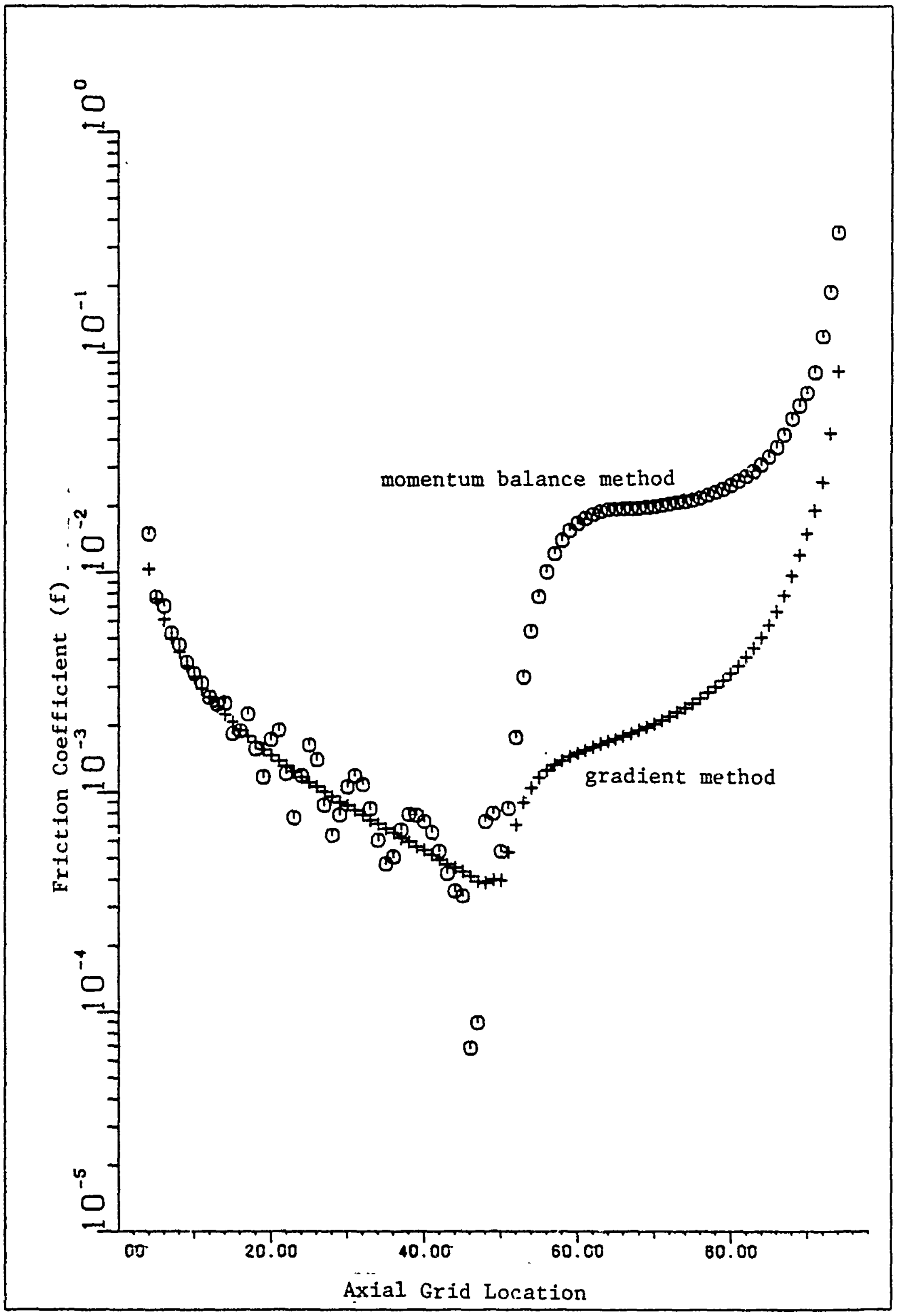

Figure 6.9 Comparison of Friction Calculation Methods

the studies, it was found that either method could have been used in the evaporator region. If the numerical results used to calculate the friction were sufficiently steady (close to a steady-state solution), both methods gave the same result. Because the velocity gradient method was less adversely effected by small non-steady terms, that method was used for calculations in the evaporator region. This resulted in a large savings in computer time because only a near steady-state solution was required.

The two different methods predicted results that varied by about a factor of 10 in the condenser region. It was felt that the coarse numerical grid (25 radial nodes) gave inaccurate near-wall velocity results in the condenser. This led to an under estimation of the shear stress when the velocity gradient method was used. Finer grid systems were studied. As more grid points were clustered near the wall, the velocity gradient method results converged toward the momentum method results. In another study, an overall force balance was performed on the control volume containing the vapor region. The integral of the wall shear stress along the pipe was compared to the pressure drop between the two pipes ends. The velocity gradient method under-predicted the pressure drop (over 95% error) indicating that insufficient friction was being estimated along the pipe. The momentum method accurately predicted the pressure drop (less that 0.1% error). This, along with the grid study, stengthened the selection of the momentum balance method for finding friction coefficients in the evaporator. As will be seen later, the large friction coefficient values predicted by the momentum method compare favorably with research done by others in this area. It will also be shown that they are needed if accurate results are to be obtained from one-dimensional models (c.f. Chapter VII).

Functional Dependence. Before presenting the results of the friction coefficient calculations, the motivation for selecting the variables used in representing the functional form of the friction coefficient data will be discussed. The equations to be studied are Equations (4.2) through (4.13) developed in Chapter IV. The dimensionless variables chosen were:

$$z^+ = \frac{z}{R} \qquad r^+ = \frac{r}{R} \qquad u^+ = \frac{u}{\overline{U}}$$
$$v^+ = \frac{v}{v_o} \qquad \rho^+ = \frac{\rho}{\rho_o} \qquad p^+ = \frac{p}{\rho_o v_o \overline{U}} \tag{6.5}$$
$$T^+ = \frac{T}{T_o} \qquad e^+ = \frac{T}{T_o}$$

where $\overline{U}$ = a local mean axial velocity, R is the pipe radius, v_o is the local blowing or suction velocity at the pipe wall and ρ_o is the local fluid density at the pipe wall. After substituting these dimensionless variables into Equations (4.2) through (4.13), the dimensionless continuity, momentum, and energy equations shown below resulted.

$$\xi \frac{\partial}{\partial z^+}\left(\rho^+ u^+ \frac{\rho_o}{\overline{\rho}}\right) - 2\rho^+ u^+ \frac{\rho_o}{\overline{\rho}} + \frac{1}{r^+}\frac{\partial}{\partial r^+}\left(r^+ \rho^+ v^+\right) = 0$$

$$\xi u^+ \frac{\partial}{\partial z^+}\left(\rho^+ u^+ \frac{\rho_o}{\overline{\rho}}\right) - 2\rho^+ u^{+2} \frac{\rho_o}{\overline{\rho}} - u^+ \frac{Re}{Re_w}\frac{\rho_o}{\overline{\rho}}\frac{\partial \rho^+}{\partial z^+} + \rho^+ v^+ \frac{\partial u^+}{\partial r^+} =$$
$$- \frac{\partial p^+}{\partial z^+} + \frac{2}{Re_w}\frac{1}{r^+}\frac{\partial}{\partial r^+}\left(r^+ \frac{\partial u^+}{\partial r^+}\right) + \cdots$$

$$\frac{Re_w}{Re}\frac{\overline{\rho}}{\rho_o}\rho^+ v^+ \frac{\partial v^+}{\partial r^+} + \rho^+ u^+ \frac{\partial v^+}{\partial z^+} = - \frac{\partial p^+}{\partial z^+} + \cdots$$

(6.6)

$$\rho^+ v^+ \frac{\partial e^+}{\partial r^+} + \rho^+ u^+ \frac{Re}{Re_w}\frac{\rho_o}{\overline{\rho}}\frac{\partial e^+}{\partial z^+} = \frac{Re_w}{Re}\frac{\overline{\rho}}{\rho_o}\frac{\overline{T}}{T_o} Ec\, \gamma\, p^+ \Bigg[\xi \frac{\partial}{\partial z^+}\left(\rho^+ u^+ \frac{\rho_o}{\overline{\rho}}\right)$$
$$- 2\rho^+ u^+ \frac{\rho_o}{\overline{\rho}} - \frac{Re}{Re_w}\frac{\rho_o}{\overline{\rho}}\frac{\partial \rho^+}{\partial z^+}\Bigg] + 4\gamma \frac{Ec}{Re_w}\frac{\overline{T}}{T_o}\left(\frac{\partial u^+}{\partial r^+}\right)^2$$
$$+ \frac{2\gamma}{Re_w Pr}\frac{1}{r^+}\frac{\partial}{\partial r^+}\left(r^+ \frac{\partial T^+}{\partial r^+}\right) + \cdots$$

$$\xi = \frac{-2\int_0^{z^+} Re_w \, dz^+}{Re_w}, \quad Re = \frac{\overline{\rho}\,\overline{u}\, D}{\mu}, \quad Re_w = \frac{\rho_o v_o D}{\mu},$$

$$Ec = \frac{\gamma - 1}{2} Ma^2, \quad Pr = \frac{c_p \mu}{k}$$

From these equations it can be seen that in general

$$u^+ = u^+\left(z^+, r^+, Re, Re_w, Ma, Pr\right) \tag{6.7}$$

By non-dimensionalizing and combining Equations (6.1) and (6.2) it can be shown that

$$f \times Re = -4\mu \frac{\partial u^+}{\partial r^+}\bigg|_{r^+=1} \tag{6.8}$$

thus in general

$$f = f\left(z^+, Re, Re_w, Ma, Pr\right) \tag{6.9}$$

Upon examining the friction coefficient results that follow, one of the tasks was establishing the functional relationship between f and the five dimensionless groups shown in Equation (6.9). This was simplified by studying the results of earlier researchers. First, because all of the cases studied in this work used air as a working fluid, the Prandtl number could be assumed to be nearly constant. Thus, no friction coefficient dependence on Prandtl number was expected. Kinney (6) has shown that in the evaporator, the friction coefficient becomes independent of the radial Reynolds number at large values of blowing. Because this work was done at very high values of blowing, Kinney's assumption applies here also. The last assumption that was used in developing the functional relationship for friction coefficient was that in the evaporator the friction coefficient was inversly proportional to the axial Reynolds number. Kinney (5) showed that this is also true for laminar flow in pipes with blowing

Results. Eleven numerical simulations were run using the two-dimensional Navier-Stokes code. For the different simulations, aspect ratios varying from L/D = 12 to L/D = 96 were modeled. Also the maximum flow velocity in the systems was varied from a Mach number of 0.1 to 1.0. The flow fields generated by the numerical simulation were used to estimate the friction coefficient as described above. Figure 6.10 is a plot of friction coefficient versus axial Reynolds number. The raw data is included as Appendix C.

The results in Figure 6.10 can be divided into three regions. Region 1 is the lower clustering of points. These points represent the friction coefficients predicted in the evaporator region. Region 3 of the data is most of the upper clustering of points. These data points represent the friction coefficients in the fully-developed turbulent flow region in the condenser. The Region 2 data is the friction coeffcient data where the flow is transitioning from laminar to turbulent in the condenser inlet region. In Region 2 the friction coefficient data is independent of axial Reynolds number. This is because the high-axial-Reynolds-number (much higher than 2000) laminar flow entering the condenser quickly transitions to turbulent flow.

Yuan and Finkelstein (14) and Kinney (5) were the first

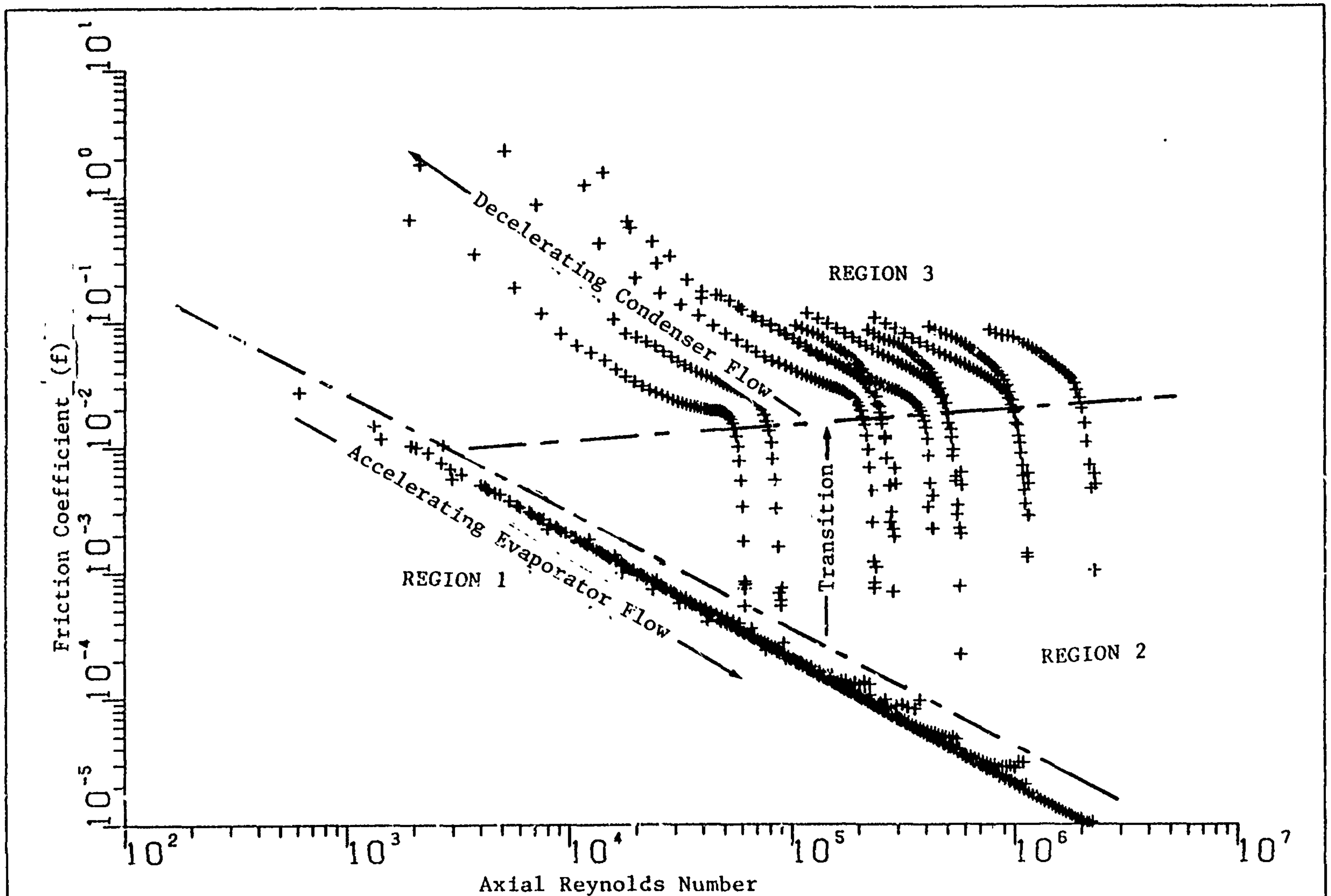

Figure 6.10 Friction Coefficient Vs. Reynolds Number

to study lami -, incompressible flow in pipes with blowing. They showed that blowing caused a slight steepening in the velocity gradients at the pipe wall, which resulted in an increase in friction coefficient. Their results can be represented using the expression

$$f \times Re = 16\left(1.2337 - 0.2337\, e^{0.0363\, Re_w}\right) \qquad (6.10)$$

where Re_w is the radial Reynolds number defined as

$$Re_w = \frac{\rho_o V_o D}{\mu} \qquad (6.11)$$

The data in Region 1 of Figure 6.10 very closely matches the expression predicted by Kinney. The only variation is for large Mach numbers. For large Mach numbers, a compressibility affect needs to be included in the friction model that accounts for a rise in friction coefficient with Mach number. Figure 6.11 show how the friction coefficient in the evaporator region varies with Mach number. The least squares representation of the data including the compressibility affect is

$$f \times Re = 16\left(1.2337 - 0.2337\, e^{0.0363\, Re_w}\right) e^{\frac{6 Ma^2}{5}} \qquad (6.12)$$

where Ma is the Mach number based on the local mean velocity.

The data in Region 3 of Figure 6.10 were studied to

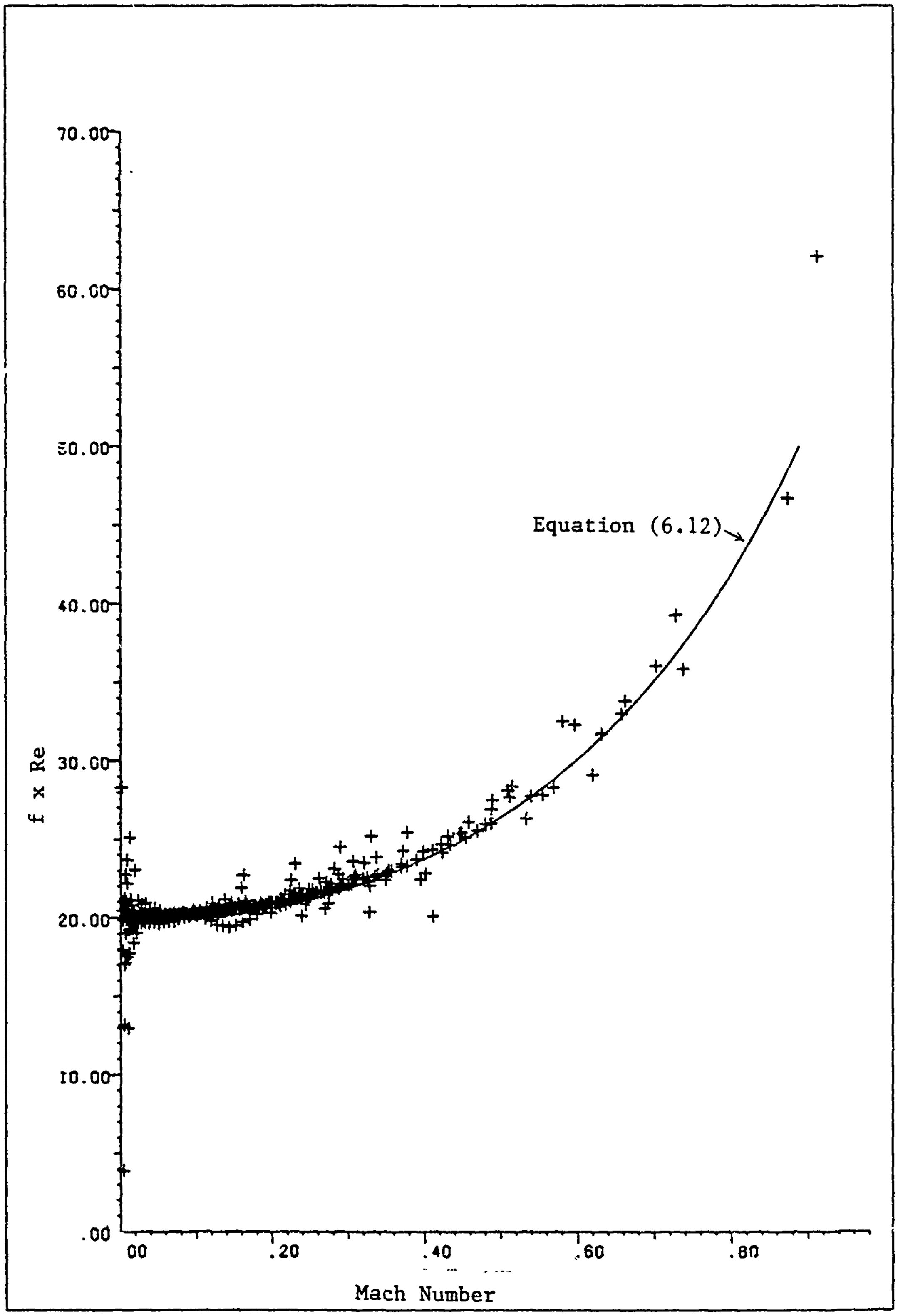

Figure 6.11 Effect of Compressibility on Friction Coefficients in Evaporator

find a convenient way of representing them functionally. The compressible effects were assumed to be the same as in the evaporator. The friction data in the condenser can be functionally represented as

$$f = f^* \left[1 + 55\, Re^{0.1} \left(\frac{V_o}{U}\right)^{0.9} \left(\frac{2L_c}{D}\right)^{0.1} e^{\frac{6Ma^2}{5}} \right] \tag{6.13}$$

$$f^* = \frac{0.046}{Re^{1/5}} \tag{6.14}$$

where L_c is the length of the condenser. This expression predicts the friction coefficient for fully-developed turbulent flow in a pipe with suction at the pipe wall. Figure 6.12 is a graph of the friction coefficient calculated using Equations (6.13) and (6.14) compared with the friction coefficient found from the numerical experiment described above.

The Region 2 numerical data represents friction coefficients for the region where the flow is transitioning from laminar to turbulent and from a region of blowing to a region of suction. This type of behavior has been modeled by Dhawan and Narasimha (52). Equation (6.15) is a modified form of their expression which closely models the friction coefficient in the condenser entrance region.

$$f = f_T + \left(f_E - f_T\right) e^{-0.412\, \bar{x}^2} \qquad x_{t,i} < x < x_{t,f} \tag{6.15}$$

where $\bar{x} = \left[\left(x - x_{t,i}\right) / \Omega\right]$, $\Omega = x_{\Gamma = 3/4} - x_{\Gamma = 1/4}$

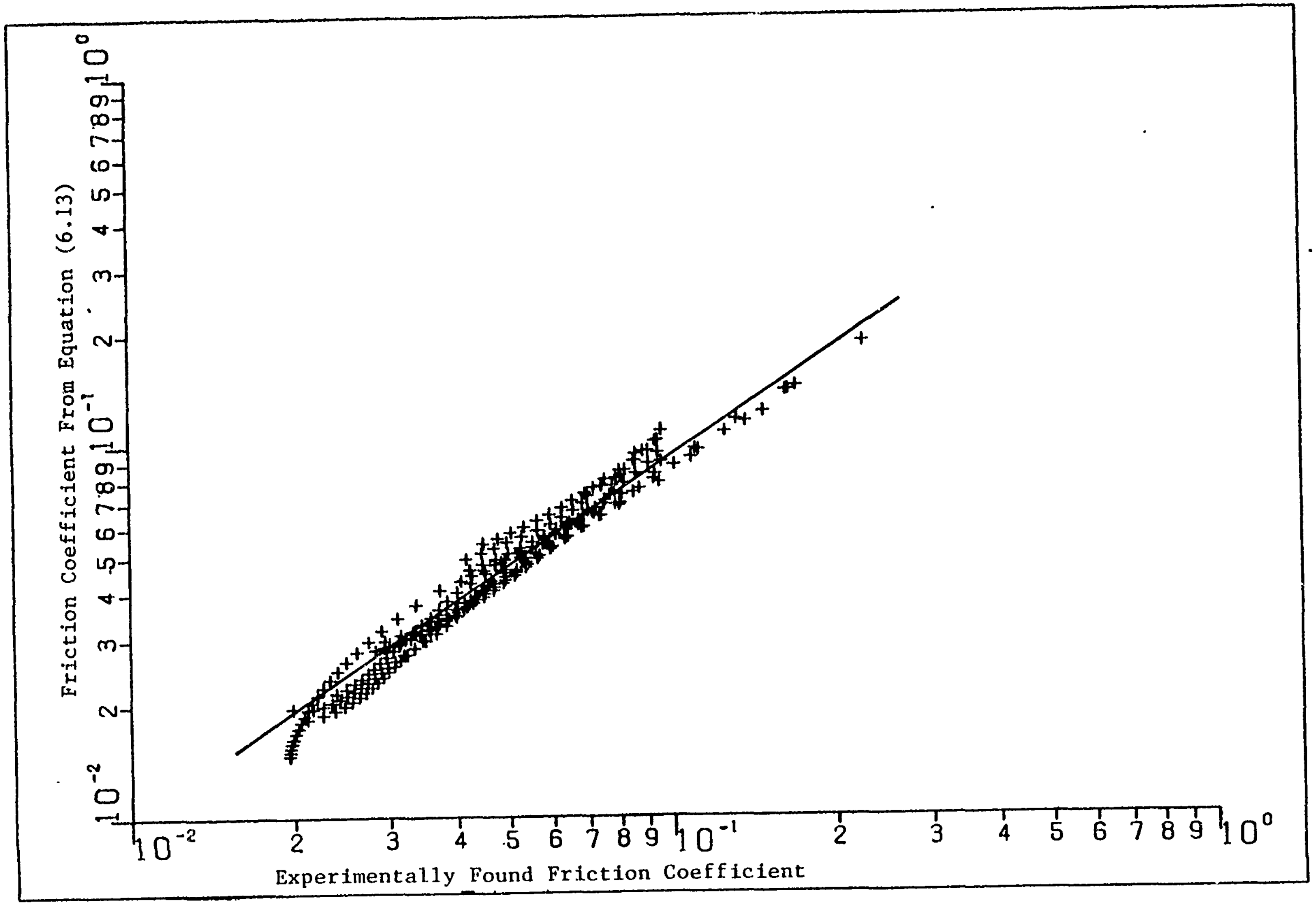

Figure 6.12 Condenser (suction) Friction Coefficient Curve Fit Results

and f_E is the friction coefficient at the entrance to the condenser and f_T is the fully-developed, suction, friction coefficient (Equation (6.13)). The other values shown in Equation (6.15) were defined in the last section of Chapter IV and relate to the location and width of the transition region.

Comparison With Other Results. As mentioned earlier the friction coefficient expression found for the laminar, evaporator section of the pipe has also been reported by other authors. The first to develop such an expression were Yuan and Finkelstein in 1956 (14). They predicted that as mass injection increased, the friction coefficient would increase from the non-blowing friction coefficient. They showed that for laminar incompressible flow with large blowing rates the friction coefficient would approach

$$f = \frac{2\pi^2}{Re} \qquad (6.16)$$

As was shown earlier this agrees very favorably with the results found by this research for small Mach numbers.

Aggarwall, et. al. (29) studied the effect of extraction on friction coefficients in porous pipes. In their experiments, the pipe inlet axial Reynolds numbers varied from 11,000 to 101,000. Their experimental results for axial Reynolds number equal to 80,000 are compared with the results of this research in Figure 6.13.

Another comparison can be made. Kinney and Sparrow (41) analytically studied the effect of suction on turbulent

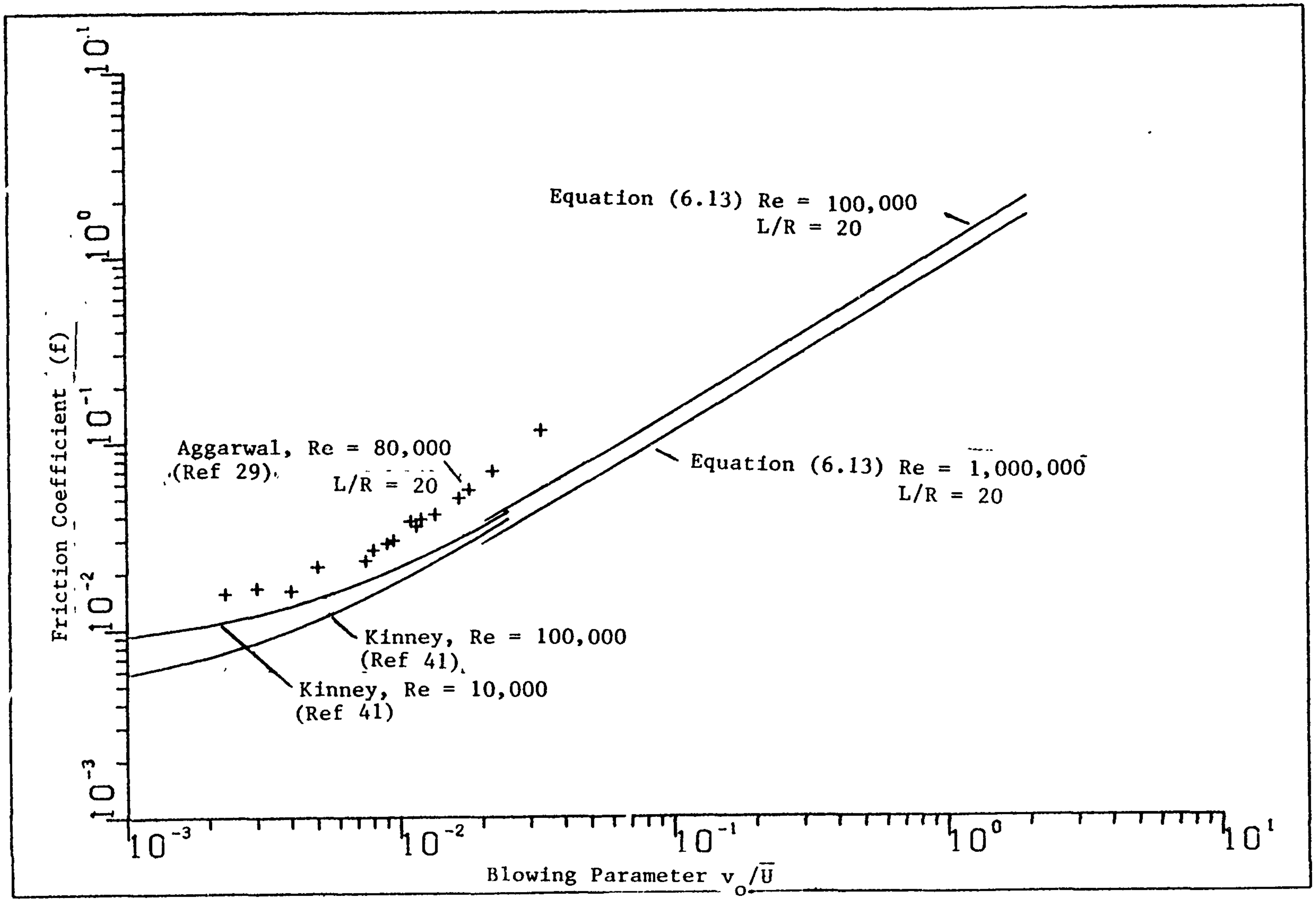

Figure 6.13 Comparison With Other Models

flow in a pipe. Their results are also shown in Figure 6.13. They limited their work to axial Reynolds numbers varying from 10,000 to 150,000 and blowing parameters up to 0.02.

The data used to develop the model presented in this paper was for axial Reynolds numbers between 20,000 and 2,300,000 and for blowing parameters between 0.015 and 2.0. This represents both larger blowing parameters and axial Reynolds numbers than studied by Aggarwal or Kinney.

The difference in the three sets of results, in the region where they overlap, is due to different models used for finding the non-blowing turbulent friction coefficient. Aggarawal et. al. were studying a rough pipe and thus used the Colebrook-White semi-empirical relation

$$\frac{1}{f^{*1/2}} = 3.48 - 4\log\left(\frac{k}{R} + \frac{9.35}{Re\ f^{*1/2}}\right) \qquad (6.17)$$

taking the roughness parameter k/R = 0.0013. Kinney and Sparrow used the Blausius friction law.

$$f^{*} \quad \frac{0.079}{Re^{1/4}} \qquad 5{,}000 < Re < 30{,}000 \qquad (6.18)$$

This research used the high-axial-Reynolds-number, turbulent, non-blowing friction coefficient expression

$$f^{*} = \frac{0.046}{Re^{1/5}} \qquad 30{,}000 < Re < 1{,}000{,}000 \qquad (6.19)$$

<u>Momentum-Flux Factor</u>. When a one-dimensional approach is used to solve a flow problem, the axial momentum at a

given location, k, is calculated using the expression

$$M_k = A\bar{\rho}\bar{U}^2\Big|_k \tag{6.20}$$

In reality, the axial momentum is

$$M_k^* = \int_A \rho u^2 dA\Big|_k \tag{6.21}$$

The ratio of $\frac{M_k^*}{M_k}$ will be defined as the momentum flux factor. In equation form, the momentum flux factor (ϕ) is defined as

$$\phi = \frac{\overline{\rho u^2}}{\bar{\rho}\bar{U}^2} \tag{6.22}$$

The momentum flux factor is useful in understanding the shape of the velocity profile in a pipe. For example, Poiseuille flow in a pipe has a momentum flux factor of 1.33. The flatter the velocity profile, the smaller the momentum flux factor. Slug flow has a value of 1.0. Below will be a brief discussion of how suction, blowing and compressibility effects influence the momentum flux factor for flow in porous pipes.

Figures 6.14 and 6.15 will be used throughout the discussion. They are graphs of momentum flux factor versus Mach number. Figure 6.14 compares three cases where the pipe aspect ratio was constant; however, the rate of injection and extraction varied. Figure 6.15 compares three cases with approximatly the same maximum axial Reynolds

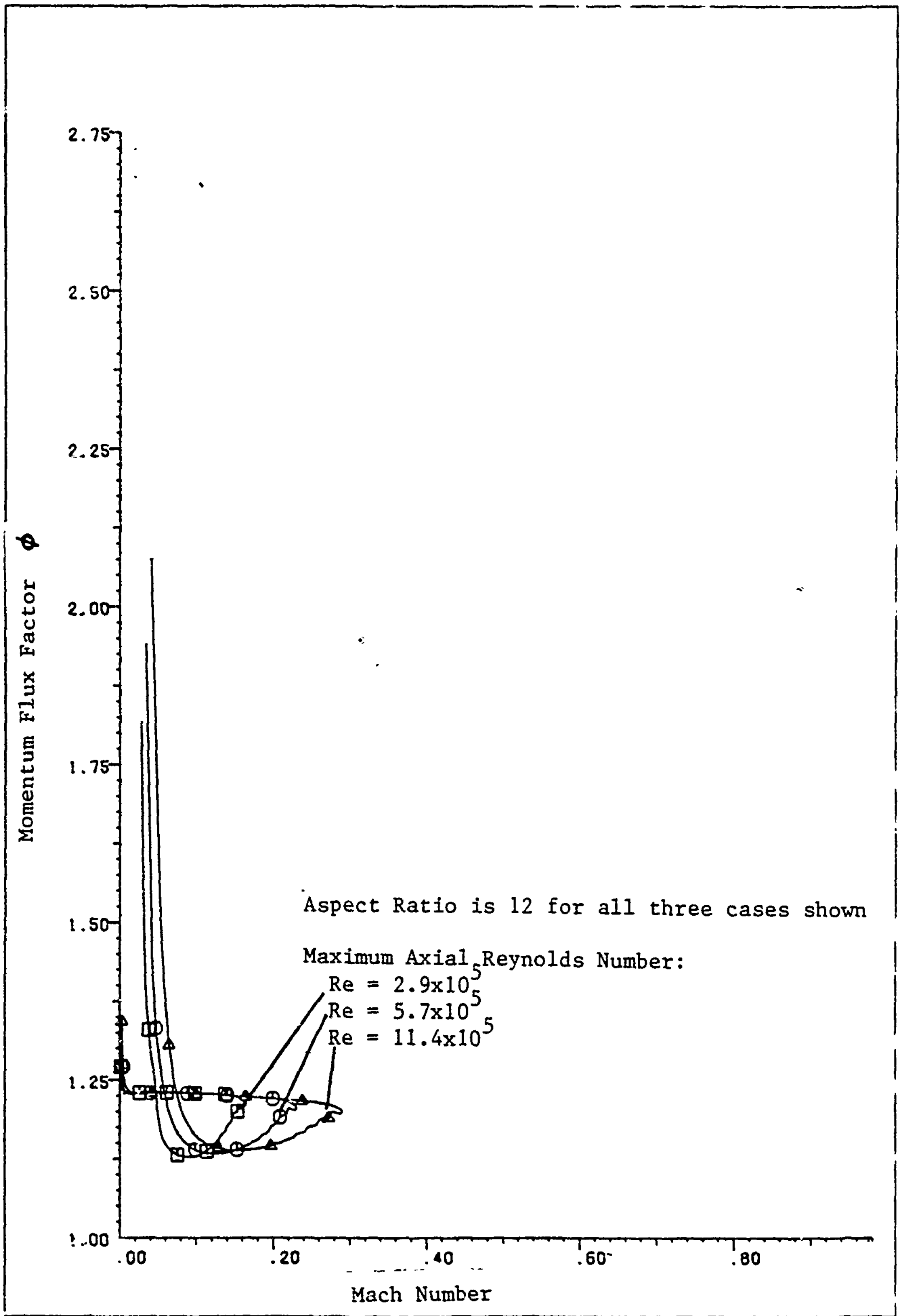

Figure 6.14 Momentum Flux Factor Versus Mach Number (Common Aspect Ratio)

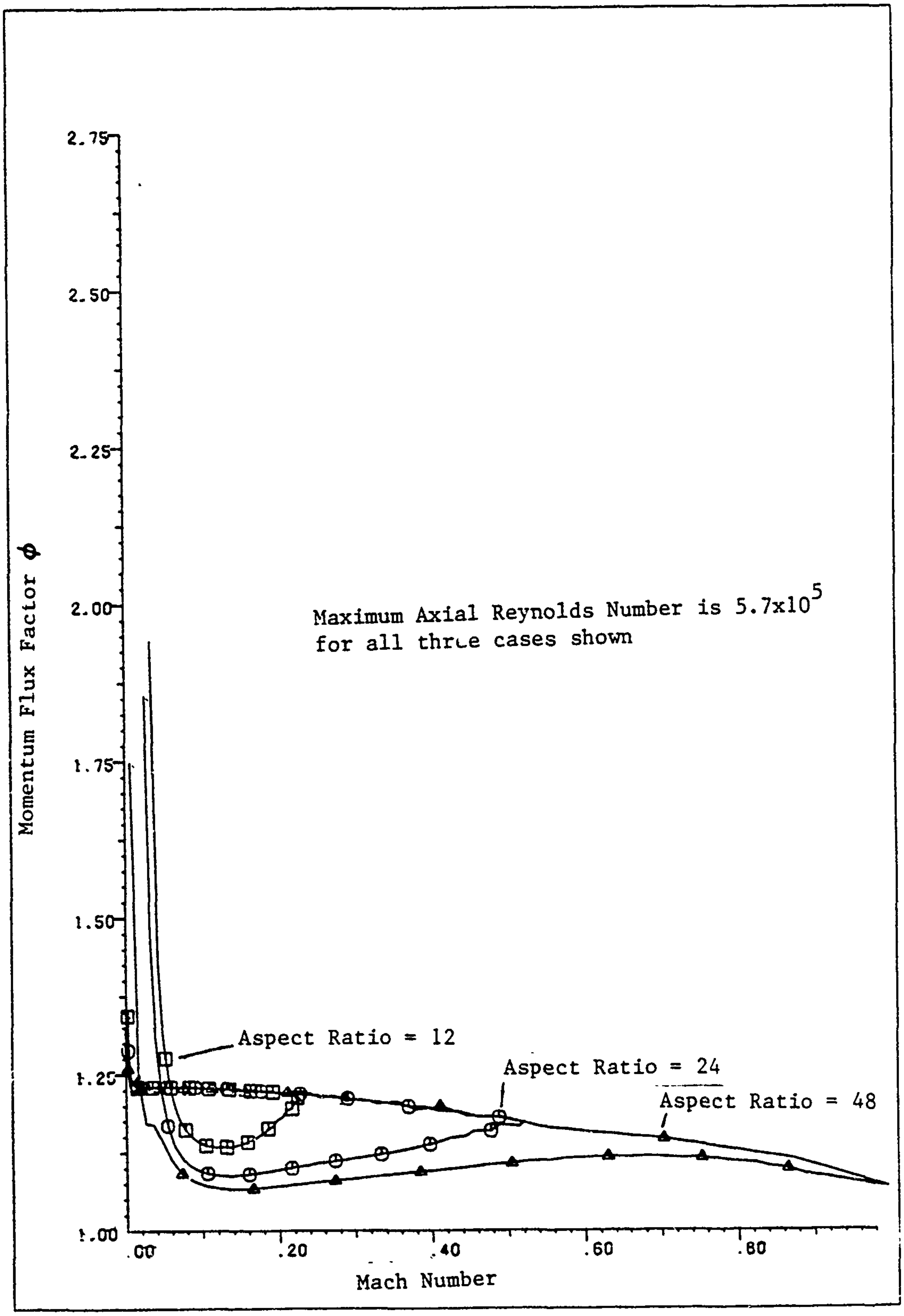

Figure 6.15 Momentum Flux Factor Versus Mach Number
(Common Reynolds Number)

number but with varing pipe aspect ratios.

Several general trends can be seen. Laminar, incompressible flow with large blowing rates produces flow with a momentum flux factor of 1.2337. This was also observed by Yuan and Finkelstein (14). As the Mach number increases in the laminar evaporator flow, the momentum flux factor decreases as a result of the flattening of the velocity profile. As was observed earlier, the flatter velocity profile corresponds to larger friction coefficient values which were seen at higher Mach numbers in the evaporator.

As the flow enters the condenser (a region with suction) and the flow transitions to turbulent flow, the velocity profiles become even flatter (smaller momentum flux factors). The very flat velocity profiles in the condenser correspond to large friction coefficients. From Figure 6.15 it is interesting to note the effect of pipe diameter on the shape of the velocity profiles. As the aspect ratio increases (small diameter pipe) flatter velocity profiles result. At the end on the condenser, the velocity profile becomes less flat due to pipe-end effects. For the large diameter pipe, flow reversal was seen at the end of the condenser. These effects result in very large values of momentum flux factor at the pipe ends.

Term Size

To date, there has been disagreement as to when the full Navier-Stokes equations need to be used and when

Prandtl's boundary-layer equations will yield adequate and less-expensive solutions to heat-pipe vapor-flow problems (25), (26). This section of Chapter VI will describe a study that was performed to help better understand this problem. It will be shown that for short (fat) heat pipes or for pipes with large blowing rates the boundary-layer assumptions are not valid

The problem was addressed by first solving for the vapor flow field in a simulated heat pipe using the full Navier-Stokes solution technique. Once the solution was obtained, finite-difference techniques were used to approximate the size of the different terms in the continuity and momentum equations. To save computer storage, only the absolute value of the largest values calculated for each term were saved. Figure 6.16 is a sample of the results obtained. Figure 6.16 shows 5 different data sets corresponding to 5 different mass flow rates in a pipe 24 inches long and 2 inches in diameter (aspect ratio of 12). The terms are numbered. The numbers correspond to the following terms in the continuity and momentum equations.

$$\underset{\textcircled{1}}{\frac{\partial \rho u}{\partial z}} + \underset{\textcircled{10}}{\frac{1}{r}\frac{\partial r \rho v}{\partial r}} = 0$$

$$\underset{\textcircled{2}}{\frac{\partial \rho u^2}{\partial z}} + \underset{\textcircled{11}}{\frac{1}{r}\frac{\partial r \rho u v}{\partial r}} = -\underset{\textcircled{3}}{\frac{\partial p}{\partial z}} + \underset{\textcircled{13}}{\frac{1}{r}\frac{\partial}{\partial r}\left(r\mu\frac{\partial u}{\partial r}\right)} + \cdots \quad 6.23)$$

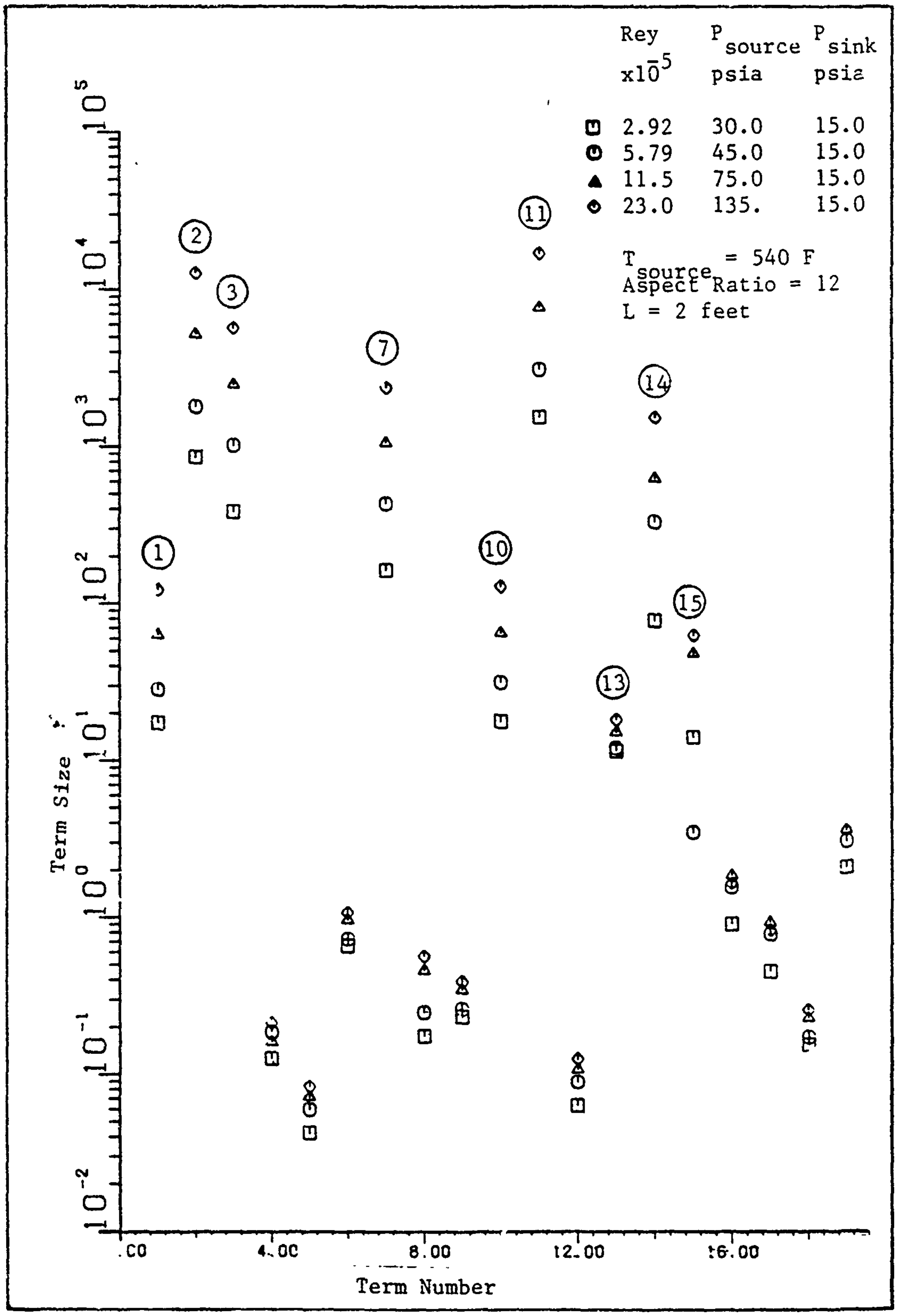

Figure 6.16 Comparison, Term Sizes for Different Mass Flows

$$\frac{\partial \rho v^2}{\partial r} + \frac{\partial \rho u v}{\partial z} = - \frac{\partial p}{\partial r} + \cdots$$

$$\quad (14) \qquad\qquad (7) \qquad\qquad\qquad (15)$$

It can be seen from Figure 6.16 that for increasing axial Reynolds numbers, the terms increase in size.

The steady-state boundary-layer equations in cylindrical coordinates are

$$\frac{\partial \rho u}{\partial z} + \frac{1}{r}\frac{\partial r \rho v}{\partial r} = 0 \tag{6.24}$$

$$\frac{\partial \rho u^2}{\partial z} + \frac{1}{r}\frac{\partial r \rho u v}{\partial r} = - \frac{\partial p}{\partial z} + \frac{1}{r}\frac{\partial}{\partial r}\left(r\mu \frac{\partial u}{\partial r}\right) \tag{6.25}$$

$$\frac{\partial p}{\partial r} = 0 \tag{6.26}$$

Thus, the boundary-layer assumptions assume that only the terms 1, 2, 3, 10, 11, and 13 in Figure 6.16 should be significant. From the figure, it can be seen that terms 7, 14, and 15 from the radial momentum equation are not small.

To gain further insight into the problem the Navier-Stokes equations were non-dimensionalized. The dimensionless variables chosen are

U = maximum axial velocity $\quad u^+ = \frac{u}{U}$

V = average suction velocity $\quad v^+ = \frac{v}{V}$

L = pipe length $\quad z^+ = \frac{z}{L}$

D = pipe diameter $\quad r^+ = \frac{r}{D} \quad$ (6.27)

ρ_0 = source air density $\quad \rho^+ = \frac{\rho}{\rho_0}$

$\quad p^+ = \frac{p}{\rho_0 U^2}$

Aspect Ratio $\quad AR = \frac{L}{D}$

Blowing parameter = $\beta' = \frac{V}{U}$

The resulting steady continuity and momentum equations can be abbreviated as

$$\frac{\partial \rho^+ u^+}{\partial z^+} - \frac{1}{2r^+}\frac{\partial r^+ \rho^+ v^+}{\partial r^+} = 0 \qquad (6.28)$$

$$\frac{\partial \rho^+ {u^+}^2}{\partial z^+} + \frac{1}{2r^+}\frac{\partial}{\partial r^+}\left(r^+ \rho^+ v^+ u^+\right) = \cdots \qquad (6.29)$$

$$\beta' \frac{\partial \rho^+ v^+ u^+}{\partial z^+} + \frac{\beta'}{2r^+}\frac{\partial}{\partial r^+}\left(r^+ \rho^+ {v^+}^2\right) = \cdots \qquad (6.30)$$

The blowing parameter and the aspect ratio were related using conservation of mass.

Mass flow through the wall = Mass flow at the center of the heat pipe

or

$$\frac{\rho \pi D L V}{2} = \frac{\rho \pi D^2 U}{4} \qquad (6.31)$$

$$\beta' AR = 0.5 \qquad (6.32)$$

From Equation (6.30) it can be seen that the two terms in Equation (6.30) are of order β' and $\frac{\beta'}{2}$. This means that for large blowing rates or for small aspect ratios, the boundary-layer assumptions, which ignore these terms, are not valid. This theory was tested by finding how the term sizes varied for different pipe aspect ratios. The results of the study are illustrated in Figure 6.17. In Figure 6.17 the terms in question are normalized with respect to term #2, the axial transport of axial momentum term. It can be

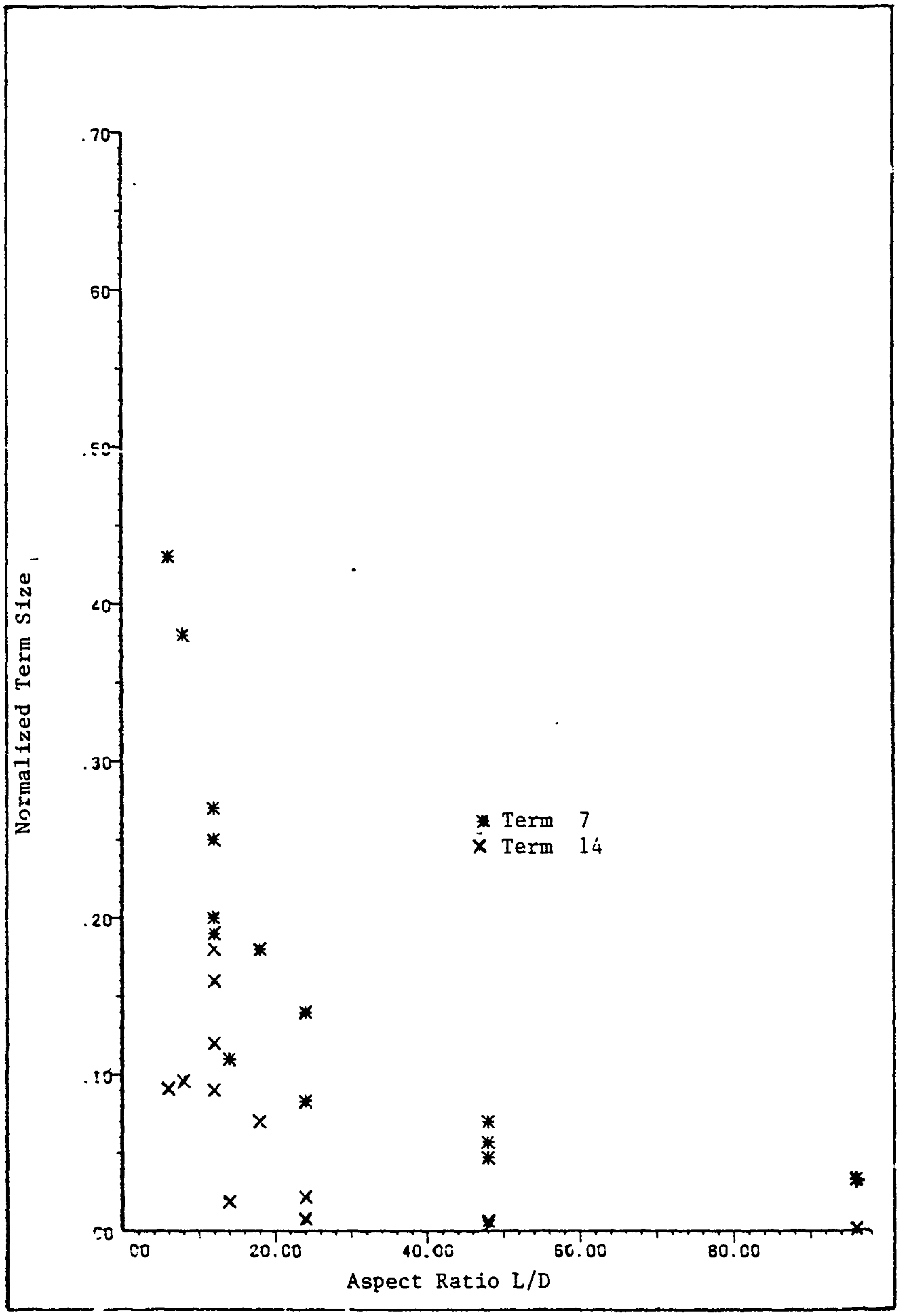

Figure 6.17 Effect of Aspect Ratio on Term Size

seen that as the aspect ratio decreases the boundary-layer assumptions become less valid. In studying the flow fields for the small aspect ratio cases it was found that flow reversals occurred in the downstream end of the condenser (Figure 6.18A). It is felt that the ability to model this behavior is lost when the boundary-layer assumptions are made. Figure (6.18B) is a contour plot that shows how the normalized term # 7 varies throughout the flow field. From Figure 6.18B it can be seen that the boundary-layer assumptions break down in the center of the pipe, between the evaporator and the condenser, and at the pipe ends.

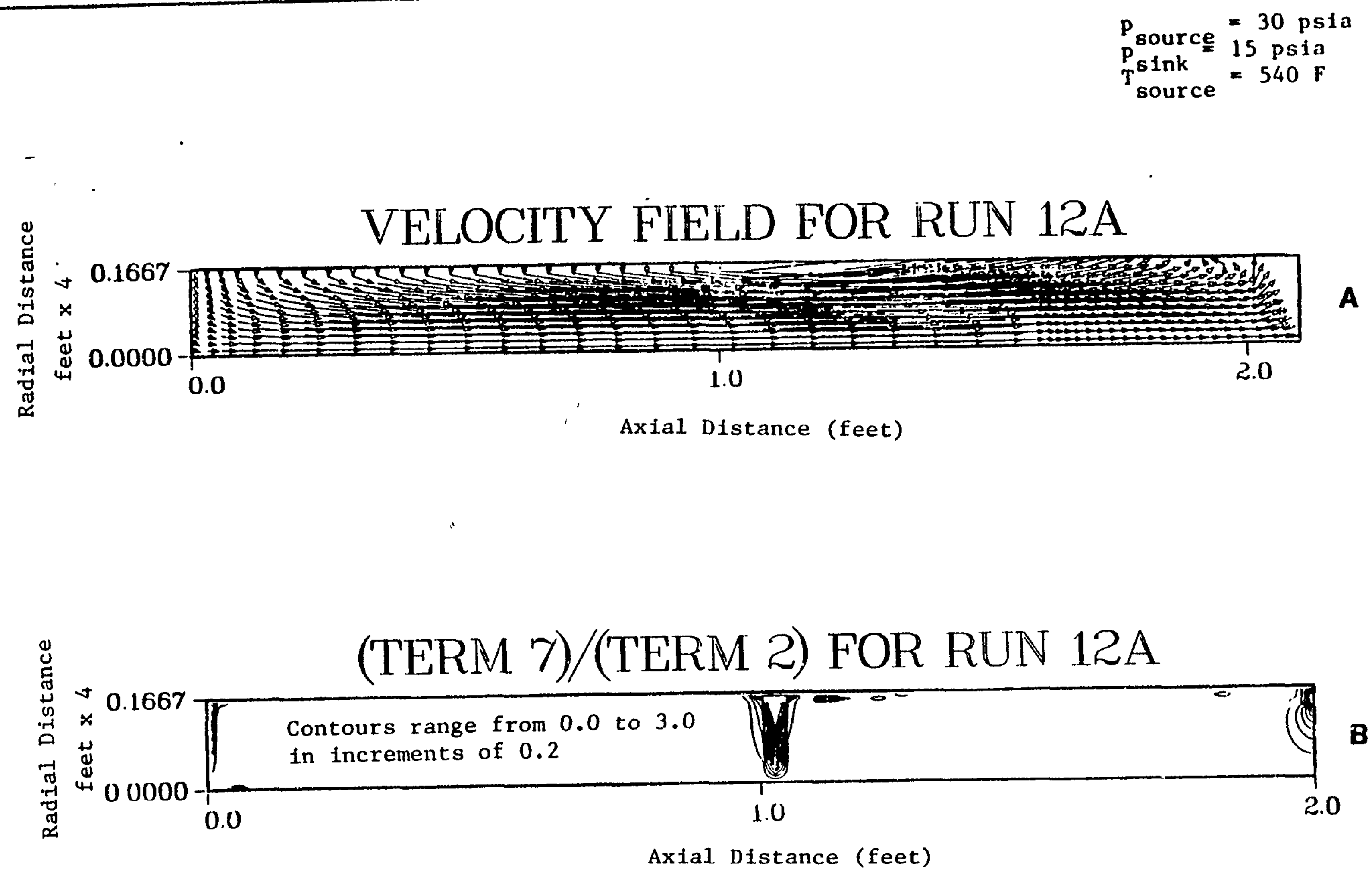

Figure 6.18 Velocity Field and Term Contour Plots

VII One Dimensional Numerical Model

A simplified method for solving the simulated heat-pipe vapor flow problem is described in this chapter. The chapter is divided into three sections. First, the governing equations solved are presented. Second, the solution technique is described. Third, the results obtained are presented.

Governing Equations

For this simplified solution, the flow was assumed to be compressible, one-dimensional, adiabatic, and steady. The form of equations employing influence coefficients presented by Shapiro (46) was used.

$$\frac{dM_a^2}{M_a^2} = F_{f,a} 4f \frac{dx}{D} + F_{\dot{m},a} \frac{d\dot{m}}{\dot{m}} \qquad (7.1)$$

where Ma is the Mach number, and the two influence coefficients are defined as

$$F_{f,a} = \frac{4M_a^2\left(1 + \frac{\gamma - 1}{2} M_a^2\right)}{1 - M_a^2} \qquad (7.2)$$

$$F_{\dot{m},a} = \frac{2\left(1 + \gamma M_a^2\right)\left(1 + \frac{\gamma - 1}{2} M_a^2\right)}{1 - M_a^2} \qquad (7.3)$$

f is a friction coefficient defined early by Eq (6.1). γ is the ratio of specific heats, x is the axial coordinate, D is the hydraulic diameter, and $\dot{m}$ is the mass flow rate. The rate of change of mass flow rate is dependent on the pressure difference across the pipe wall, (Eq 4.33), and can vary with axial location. Eq (7.1) can be solved exactly for the special case where f = Ø (no friction) References

(20),(22). The frictionless solution is presented in Chapter II, Eqs (2.1) to (2.4). For the friction solution, a second expression was needed to relate the change in total pressure (Po) to the change in mass flow rate and to the friction coefficient. From Shapiro (46),

$$\frac{dPo}{Po} = F_{f,b}\, 4f \frac{dx}{D} + F_{\dot{m},b} \frac{d\dot{m}}{\dot{m}} \tag{7.4}$$

where

$$F_{f,b} = \frac{-\gamma M_a^2}{2} \tag{7.5}$$

$$F_{\dot{m},b} = -\gamma M_a^2 \tag{7.6}$$

Other useful relations are

$$\frac{T_a}{T_b} = \frac{1 + \frac{\gamma - 1}{2} M_a^2{}_b}{1 + \frac{\gamma - 1}{2} M_a^2{}_a} \tag{7.7}$$

$$\frac{p_b}{p_a} = \frac{Po_b}{Po_a}\left[\frac{T_a}{T_b}\right]^{\frac{\gamma}{\gamma - 1}} \tag{7.8}$$

$$\frac{\rho_a}{\rho_b} = \frac{p_a T_b}{p_b T_a} \tag{7.9}$$

These relate properties between two different locations, a and b, in the flow field.

Solution Technique

A marching technique was used to solve for the flow properties along the pipe. Initial properties were assumed at the upstream end of the pipe. Eqs (7.1) and (7.4) were integrated to find the Mach number and total pressure at locations along the pipe. Once the Mach number and total pressure were known, Eqs (7.7) to (7.9) were used to find the temperature, static pressure, and density.

A predictor-corrector, finite-difference method of marching was used to obtain a solution or Eqs (7.1) and (7.4). First the influence coefficients were predicted based on the known Mach number at a previous solution location. Also, the change in mass flow rate between two grid points was predicted using Eq (4.33) with the pressure found at the last grid point and an external manifold pressure specified in the problem statement. Defining the grid points where properties were known with the subscript k and where they were sought by the subscript k+1, Eqs (7.1) and (7.4) for the predictor step were

$$Ma^2_{k+1,p} = Ma^2_k + \exp\left\{ F_{f,a}|_k \, 4 f_k \frac{\Delta x}{D} + F_{\dot{m},a}|_k \ln\left(\frac{\dot{m}_{k+1,p}}{\dot{m}_k} \right) \right\} \qquad (7.10)$$

$$Po_{k+1,p} = Po_k + \exp\left\{ F_{f,b}|_k \, 4 f_k \frac{\Delta x}{D} + F_{\dot{m},b}|_k \ln\left(\frac{\dot{m}_{k+1,p}}{\dot{m}_k} \right) \right\} \qquad (7.11)$$

The corrector step in the solution repeated the above operations with the exception that the mass flow rate and the influence coefficients were re-calculated based on the average between the predicted and the previously known Mach number and static pressure

$$Ma_{\bar{k}} = \frac{Ma_k + Ma_{k+1,p}}{2} \qquad (7.12)$$

$$p_{\bar{k}} = \frac{p_k + p_{k+1,p}}{2} \qquad (7.13)$$

$$Ma^2_{k+1} = Ma^2_k + \exp\left\{ F_{f,a}|_{\bar{k}} 4 f_{\bar{k}} \frac{\Delta x}{D} + F_{\dot{m},a}|_{\bar{k}} \ln\left(\frac{\dot{m}_{k+1}}{\dot{m}_k}\right)\right\} \qquad (7.14)$$

$$Po_{k+1} = Po_k + \exp\left\{ F_{f,b}|_{\bar{k}} 4 f_{\bar{k}} \frac{\Delta x}{D} + F_{\dot{m},b}|_{\bar{k}} \ln\left(\frac{\dot{m}_{k+1}}{\dot{m}_k}\right)\right\} \qquad (7.15)$$

Difficulties were encountered in solving the problem near Mach numbers of one. From a truncation error analysis, it was found that the lowest order truncation error term was of order $\frac{\Delta x}{[1 - Ma^2]^2}$. Thus, as the Mach number approached unity, the truncation error became very large. To solve this problem, Δx was decreased faster than the Mach number approached one. The expression

$$\Delta x = n[1 - Ma^2]^2 \qquad (7.16)$$

where n=0.010 was used. Even though the truncation error was now less of a problem, the solution time increased rapidly when the flow velocity approached sonic velocity.

Another difficulty encountered was starting the matching technique. At the first grid location, the Mach number was always zero. Using zero in the predictor step of the solution predicted a Mach number of zero at the second grid point. This problem was overcome by assuming the flow was incompressible for the first step away from the upstream wall. This gave a non-zero Mach number at the second grid point that was used successfully to continue the marching process with the compressible model.

One more aspect of the solution method needs to be discussed before presenting the results. A starting internal pressure needed to be guessed to be used in finding the amount of mass injected through the wall. From this pressure subsequent pressures were found. The total mass injected and removed in the evaporator and condenser were determined by the external manifold pressure boundary conditions specified by the problem statement and the internal pressure distribution calculated by the marching scheme. If the starting internal pressure was quessed high, a problem of more mass removal than mass injected resulted. The opposite occurred if the initial pressure was guessed low. An iterative method was used to refine the initial pressure guess until the mass injected equaled the mass removed. The computer code used is included as Appendix C.

Results

During all of the numerical simulations, a porous pipe system with mass injection and mass removal like the one used for the two-dimensional Navier-Stokes solution technique and for the experimental portion of the research was modeled.

The first simulation assumed that there was no friction ($f=0$). This result was compared to the exact integration of Eq (7.1) for the no friction assumption and to the experimental data for the case studied. The results are shown in Figure 7.1. The two frictionless solutions compare favorably with each other; however, both models do a poor

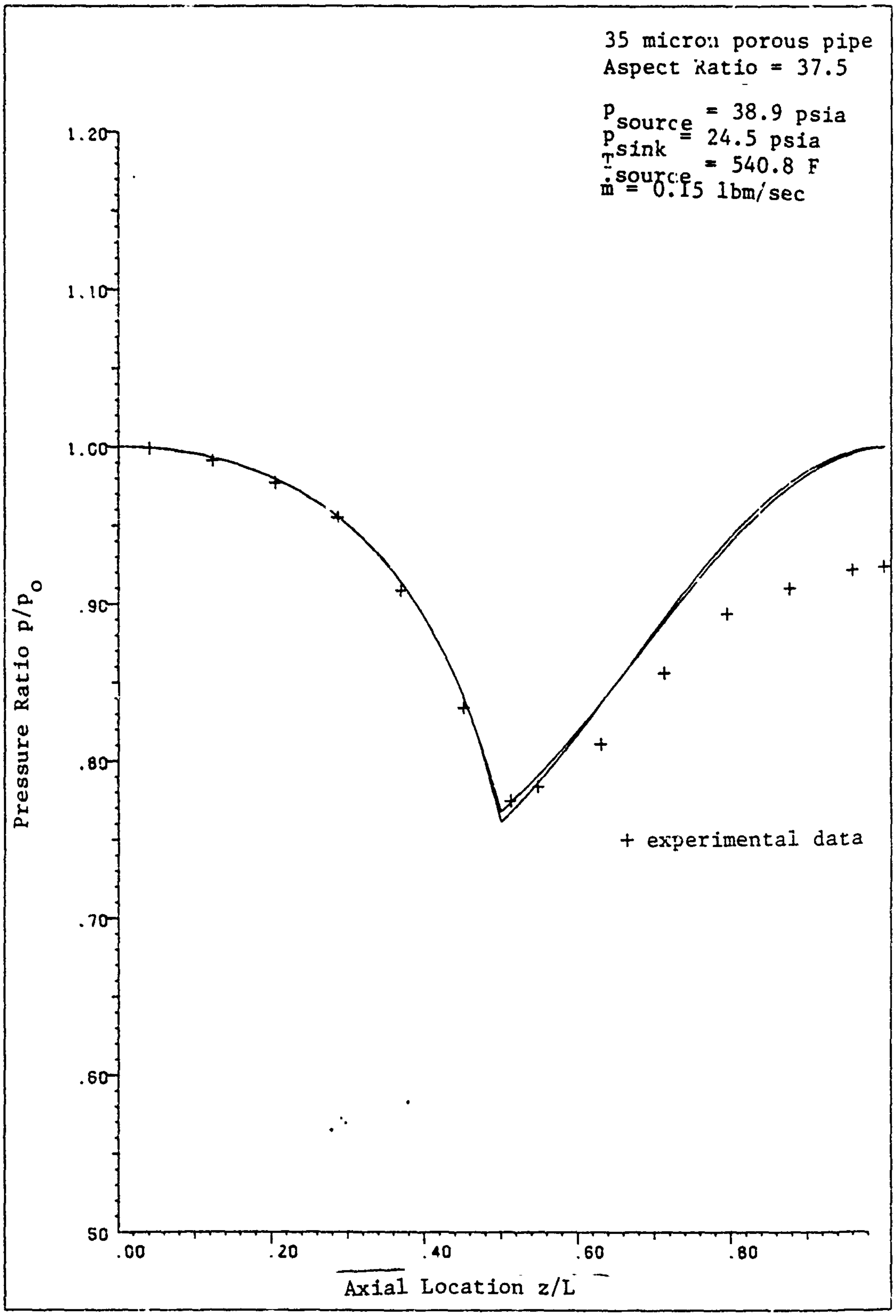

Figure 7.1 Comparison, 1-D Frictionless Models

job of matching the experimental results, especially in the condenser region.

The second study conducted assumed that the friction coefficient needed in Eq (7.1) was the same as that used for non-blowing smooth pipe calculations. In the evaporator, the flow was assumed to be laminar or

$$f_l = \frac{16}{Rey} \tag{7.17}$$

In most of the condenser the flow was assumed to be turbulent or

$$f_t = \frac{0.046}{Re^{1/5}} \tag{7.18}$$

A smooth transition from the laminar region to the turbulent region (Eq (6.15)) was used.

Figure 7.2 compares the experimental results to the smooth pipe friction solution. Adding the smooth pipe friction coefficients only slightly improved the results. It is clear that larger friction coefficient values are needed to match the experimental results.

The third simulation used the friction coefficient model developed using the two-dimensional computer code, reported in Chapter VI, Eqs (6.12), (6.13) and (6.15). Figure 7.3 compares the numerical results with the experimental data. Extremely good results were obtained.

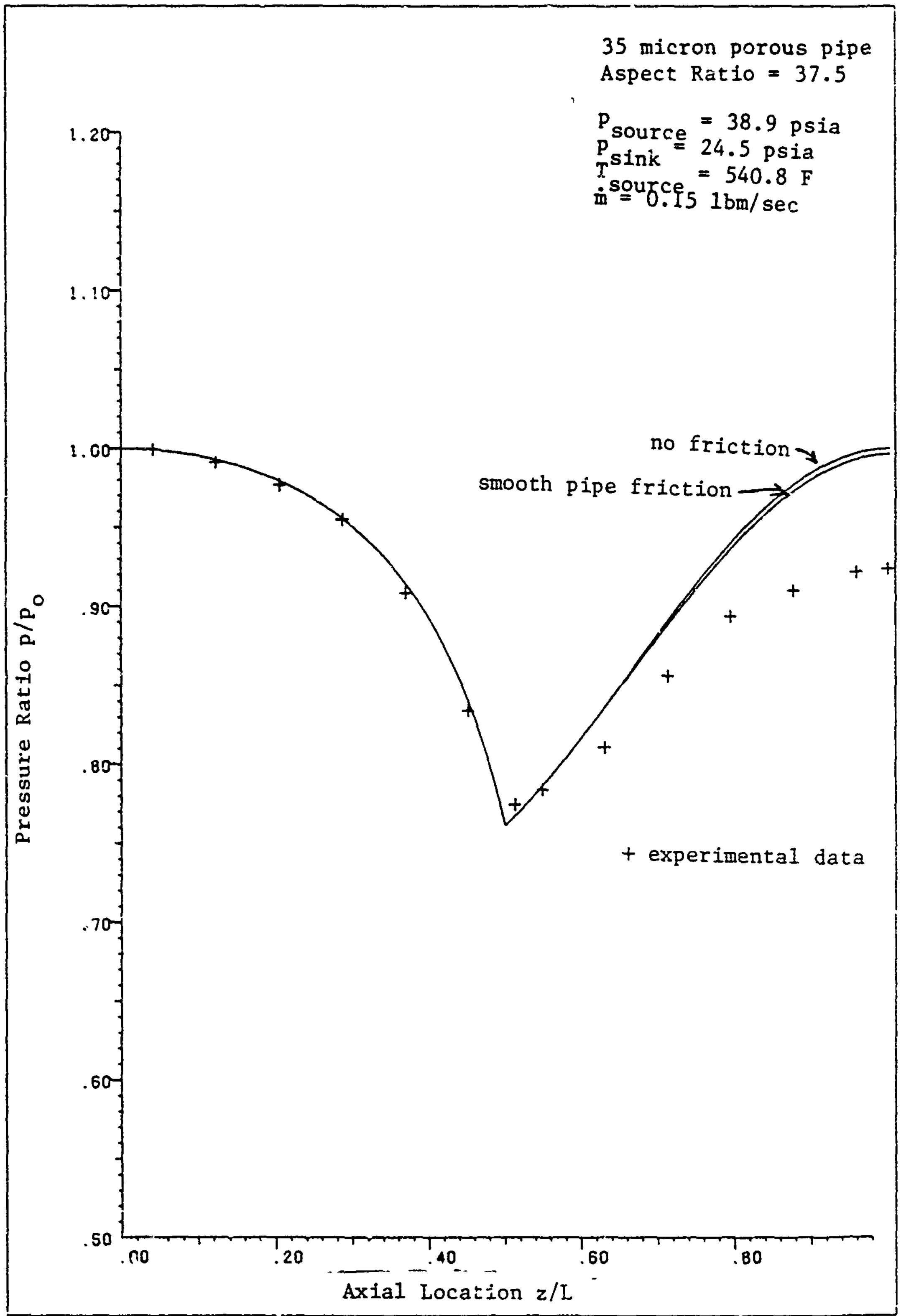

Figure 7.2 1-D Model with Smooth Pipe Friction

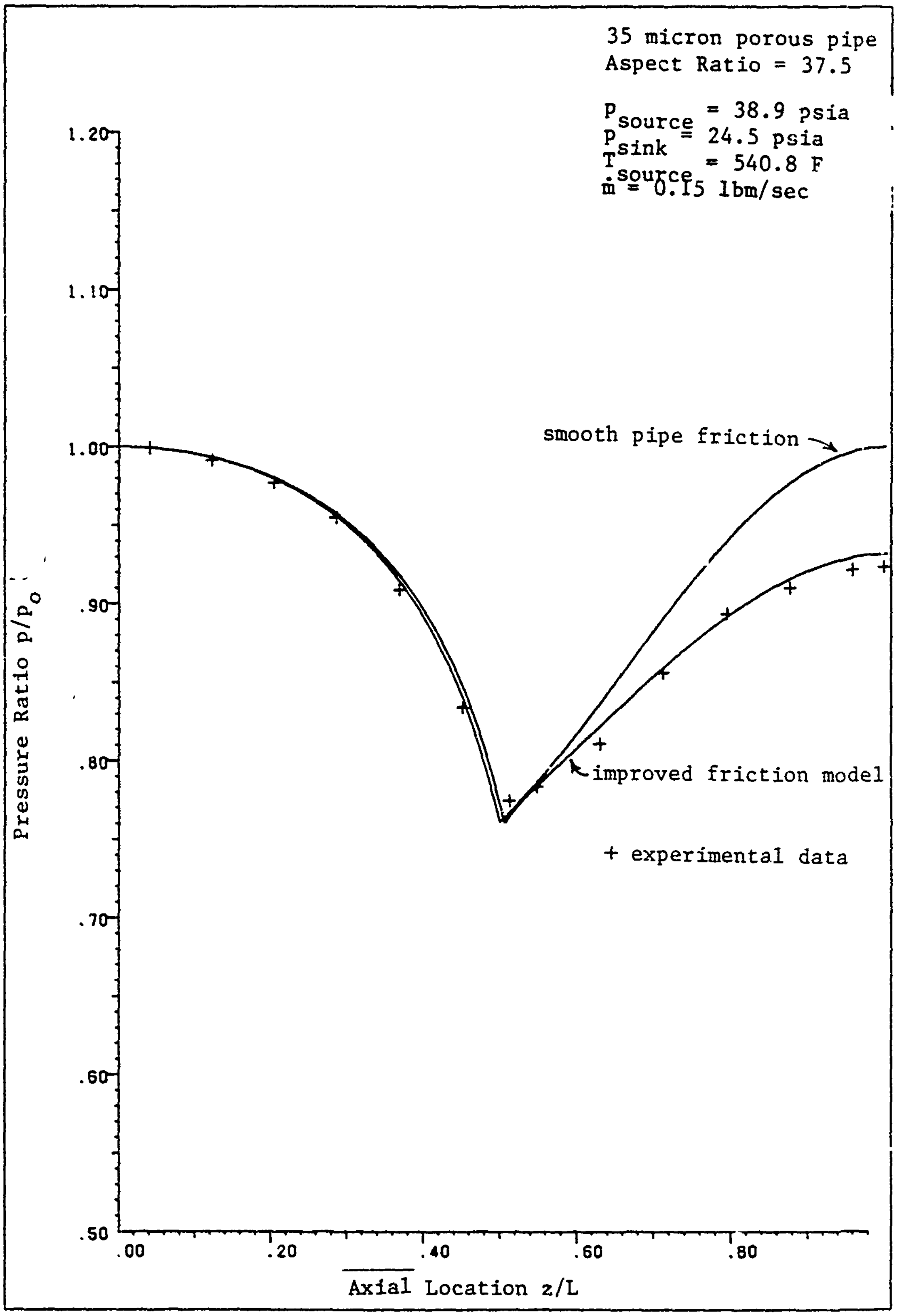

Figure 7.3 1-D Model with Improved Friction Model

VIII. Conclusions and Recommendations

Conclusions

As a result of the numerical and experimental studies conducted, expressions for friction coefficient as functions of local axial Reynolds number, Mach number, pipe aspect ratio, and radial Reynolds number were developed. The expressions were shown to give excellent results when pressures calculated using the friction coefficients in a one-dimensional model were compared with experimental data. The expressions are valid for Mach numbers up to one with maximum axial Reynolds numbers between 30,000 and 2,000,000; and for radial Reynolds numbers ranging from ±100 to ±20,000.

An interesting outcome of this research was a better understanding of the effect of mass injection and suction and/or axial pressure gradients on transition from laminar to turbulent flow. It was observed that mass injection/favorable pressure gradients caused flows to stay laminar. For all cases studied, the flow always remained laminar in the evaporator. Axial Reynolds numbers based on pipe diameters as high as 1,000,000 where tested. In the condenser region, a region with mass removal and an adverse pressure gradient, the flow was found to stay laminar at axial Reynolds numbers less than 12,000. For most cases studied, the flow entering the condenser was laminar with an axial Reynolds number much larger than 12,000. For all of these cases the flow was observed to transition from fully laminar to fully turbulent in the condenser entrance region.

An interesting experimental and numerical observation was that supersonic velocities could be obtained as a result of mass removal from a constant area pipe.

One goal of this research was to better understand the vapor dynamics of heat-pipe transients. It was found that the simulated vapor transient phenomena occur very quickly when compared to the slow thermal response of heat-pipe walls, wicks and liquids. It is felt that a steady-state vapor model can be used in conjuction with a transient wall model when studying most heat-pipe transients.

A numerical study was conducted to help understand when boundary-layer assumptions can be made and when the full Navier-Stokes equations need to be solved. It was found that for large blowing parameters (above 0.02) or for pipes with small aspect ratios (L/R < 24) the boundary-layer assumptions are invalid. However, for most heat-pipe applications, the boundary-layer assumptions will give good results because most heat pipes have larger aspect ratios than 24. For pipes with small aspect ratios the boundary-layer assumptions are only invalid in small regions near the pipe ends and near the evaporator/condenser junction.

Recommendations

There will always be more work that can be done to better understand heat-pipe vapor dynamics. Some ideas for further research are:

1) Intermediate radial Reynolds number, compressible flow experiments could be conducted to better verify the friction coefficient expressions presented in Chapter 6 (Equations (6.12) and (6.13)).

2) The turbulence studies could be refined to better determine how and where turbulence begins. This would require measuring the turbulence in the pipe as a function of both radial and axial position, not just along the center line of the pipe as was done with this research. It would also be interesting to study what happens to a [illegible] high-axial-Reynolds-number laminar flow leaving the evaporator when it enters an adiabatic region.

3) Perform experiments to measure the transient flow behavior. Such work could be used to validate the transient portion of the numerical results. A movie of the transient flow behavior predicted by the numerical study might also be made to help visualize what happens during the transient.

4) Ultimately, the experimental and numerical work should be extended from the simulated heat pipe with air to an actual heat pipe involving an evaporating liquid.

APPENDIX A: Experimental Data

This appendix contains much of the raw experimental data obtained during the experimental portion of this research. Each data file has a name made up of two parts. The name first tells the target mass flow rate for the data run. Next, the file name gives the location of the velocity rake when the data was taken. For examle, file M030A had a target mass flow rate of 0.030 lbm/sec of air and the velocity rake was in position A (at the upstream end of the evaporator).

Each data files contains the following information:

1) the actual system mass flow rate

2) 36 pressure measurements (psia).

3) for all data runs the supply air temperature was at 75 F +5 F.

Figure B.1 can be used to determine the velocity rake location, A through O, and locate where the 36 pressure measurements were made. In general, pressure measurements 1 - 2 where for the orifice plate, 3 - 8 for the evaporator manifold pressures, 9 - 23 were for the inside of the porous pipe, 24 - 30 were for the velocity rake stagnation pressures, and 31 - 36 were for the condenser manifold. Velocity rake locations A through O correspond to pressure taps 9 through 23, respectively. In Figure B.1, pressure taps 9 and 23 were at the ends of the test section. Taps 10 and 22 were 1 inch from the test secton ends. Taps 10-15 and 17-22 were 2 inches apart. Pressure tape 16 is 0.900

inches from tap 17. The total length of the test section was 24 3/8 inches.

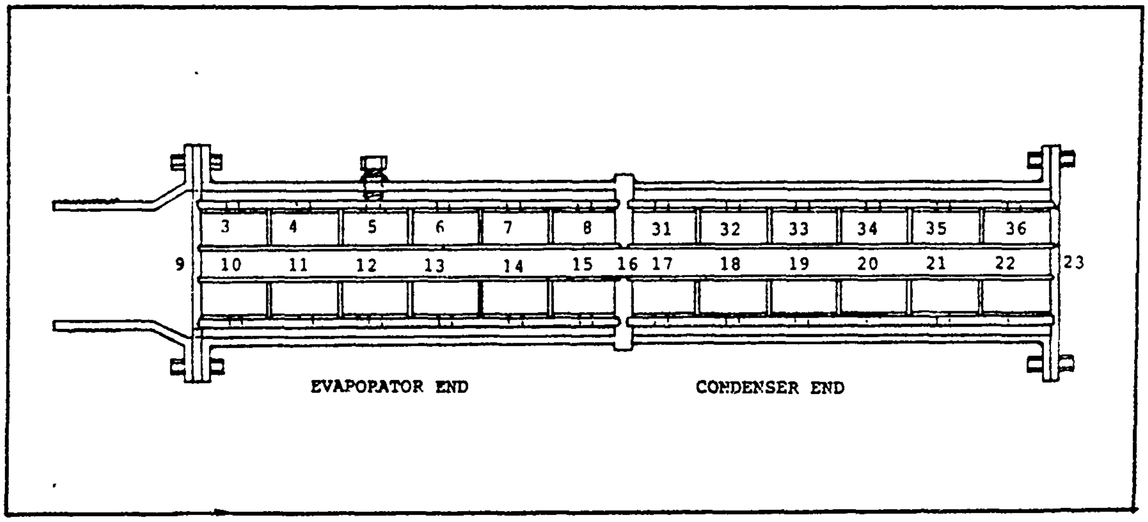

Figure A.1 Velocity Rake and Pressure Tap Locations

FILE: MO30A

MASS FLOW RATE (LBM/SEC) = 2.908601E-02

PORT	PRESSURE	PORT	PRESSURE
1	102.513	19	18.71117
2	98.16144	20	18.77452
3	20.37589	21	18.7915
4	20.37785	22	18.8137
5	20.3661	23	18.81501
6	20.36544	24	18.99265
7	20.40528	25	18.99722
8	20.55941	26	19.00114
9	19.02857	27	18.99265
10	19.04751	28	18.98938
11	19.00702	29	18.99592
12	18.95477	30	18.99004
13	18.89599	31	17.51354
14	18.77517	32	17.50557
15	18.62627	33	17.51079
16	18.55443	34	17.50753
17	18.56226	35	17.50557
18	18.60929	36	17.50753

FILE: MO30B

MASS FLOW RATE (LBM/SEC) = 2.859936E-02

PORT	PRESSURE	PORT	PRESSURE
1	100.4989	19	18.62235
2	96.20675	20	18.69354
3	20.25181	21	18.70594
4	20.24528	22	18.72031
5	20.23609	23	18.73076
6	20.24005	24	18.92734
7	20.23874	25	18.93257
8	20.2394	26	18.92865
9	18.9293	27	18.92799
10	18.92604	28	18.93322
11	18.89665	29	18.93583
12	18.86007	30	18.93583
13	18.79084	31	17.45724
14	18.69158	32	17.4814
15	18.55769	33	17.4592
16	18.48193	34	17.56043
17	18.49696	35	17.45462
18	18.54137	36	17.48336

FILE: MO3OC

MASS FLOW RATE (LBM/SEC) = 2.835925E-02

PORT	PRESSURE	PORT	PRESSURE
1	100.7013	19	18.59361
2	96.49411	20	18.66219
3	20.23613	21	18.68047
4	20.2407	22	18.68962
5	20.23287	23	18.69354
6	20.23679	24	18.86922
7	20.23417	25	18.89469
8	20.23548	26	18.89142
9	18.91297	27	18.88946
10	18.92016	28	18.89142
11	18.89665	29	18.90448
12	18.84897	30	18.88489
13	18.78301	31	17.42981
14	18.6746	32	17.43177
15	18.54006	33	17.42589
16	18.46561	34	17.42197
17	18.48063	35	17.42328
18	18.5283	36	17.41609

FILE: MO3OD

MASS FLOW RATE (LBM/SEC) = 2.845921E-02

PORT	PRESSURE	PORT	PRESSURE
1	100.8737	19	18.62431
2	96.64367	20	18.66676
3	20.24528	21	18.69223
4	20.25181	22	18.71313
5	20.24462	23	18.70529
6	20.23679	24	18.86203
7	20.24658	25	18.92995
8	20.24462	26	18.9195
9	18.92146	27	18.92408
10	18.93061	28	18.92995
11	18.9071	29	18.92995
12	18.86856	30	18.88554
13	18.79281	31	17.46573
14	18.69092	32	17.4592
15	18.55247	33	17.45854
16	18.47149	34	17.45332
17	18.50349	35	17.4592
18	18.55639	36	17.46638

FILE: M030E

MASS FLOW RATE (LBM/SEC) = 2.936515E-02

PORT	PRESSURE	PORT	PRESSURE
1	103.8218	19	18.78562
2	99.44542	20	18.84309
3	20.49149	21	18.8666
4	20.48692	22	18.88489
5	20.48627	23	18.88097
6	20.48235	24	19.00375
7	20.47125	25	19.07951
8	20.47582	26	19.09845
9	19.13568	27	19.12523
10	19.13306	28	19.11804
11	19.10106	29	19.11935
12	19.06057	30	19.02792
13	19.00637	31	17.57806
14	18.88685	32	17.59177
15	18.75166	33	17.59439
16	18.66088	34	17.58459
17	18.6759	35	17.58132
18	18.74056	36	17.57937

FILE: M030F

MASS FLOW RATE (LBM/SEC) = 2.911141E-02

PORT	PRESSURE	PORT	PRESSURE
1	103.055	19	18.75884
2	98.72311	20	18.80391
3	20.43598	21	18.81958
4	20.43663	22	18.83852
5	20.42945	23	18.85158
6	20.43206	24	18.89534
7	20.49149	25	19.06057
8	20.43663	26	19.04555
9	19.1089	27	19.10172
10	19.088	28	19.09976
11	19.08408	29	19.09323
12	19.0449	30	18.91167
13	18.97828	31	17.56108
14	18.85746	32	17.55128
15	18.6968	33	17.55193
16	18.61516	34	17.55585
17	18.64325	35	17.56043
18	18.70072	36	17.5454

FILE: M030G

MASS FLOW RATE (LBM/SEC) = 2.907956E-02

PORT	PRESSURE	PORT	PRESSURE
1	103.0459	19	18.76668
2	98.72245	20	18.79346
3	20.44773	21	18.83199
4	20.44316	22	18.84048
5	20.45426	23	18.83787
6	20.4412	24	18.78627
7	20.44316	25	19.00506
8	20.44969	26	19.01616
9	19.10629	27	19.09518
10	19.09845	28	19.09061
11	19.07298	29	19.09584
12	19.04163	30	18.83003
13	18.97306	31	17.56696
14	18.87705	32	17.57153
15	18.72292	33	17.54932
16	18.60276	34	17.55193
17	18.63149	35	17.55389
18	18.68962	36	17.55063

FILE: M030H

MASS FLOW RATE (LBM/SEC) = .029847

PORT	PRESSURE	PORT	PRESSURE
1	105.5838	19	18.89077
2	101.1382	20	18.94106
3	20.65542	21	18.96391
4	20.64301	22	18.97436
5	20.64627	23	18.97959
6	20.63386	24	18.86203
7	20.6417	25	19.05404
8	20.63452	26	19.12457
9	19.27087	27	19.2369
10	19.27152	28	19.22188
11	19.2369	29	19.21143
12	19.18205	30	18.91036
13	19.13241	31	17.66818
14	19.05208	32	17.66688
15	18.88881	33	17.67276
16	18.79607	34	17.65643
17	18.77321	35	17.66557
18	18.80913	36	17.65904

FILE: MO3OI

MASS FLOW RATE (LBM/SEC) = 2.954233E-02

PORT	PRESSURE	PORT	PRESSURE
1	104.5095	19	18.84048
2	100.1103	20	18.89469
3	20.54047	21	18.90971
4	20.53721	22	18.92799
5	20.53721	23	18.95804
6	20.52088	24	18.89338
7	20.52545	25	18.98612
8	20.53067	26	19.02792
9	19.17421	27	19.13502
10	19.19707	28	19.1409
11	19.14286	29	19.11608
12	19.09584	30	18.87575
13	19.04359	31	17.6179
14	18.91885	32	17.61202
15	18.79542	33	17.61724
16	18.72488	34	17.61267
17	18.72031	35	17.60745
18	18.75689	36	17.61137

FILE: MO3OJ

MASS FLOW RATE (LBM/SEC) = 2.927578E-02

PORT	PRESSURE	PORT	PRESSURE
1	103.6435	19	18.78431
2	99.28737	20	18.84766
3	20.51565	21	18.85615
4	20.42945	22	18.87836
5	20.43402	23	18.88162
6	20.4301	24	18.8444
7	20.42814	25	18.89273
8	20.42749	26	18.90644
9	19.07102	27	19.02204
10	19.07951	28	18.992
11	19.05339	29	18.97306
12	19.00375	30	18.84505
13	18.9404	31	17.59047
14	18.83591	32	17.58198
15	18.70333	33	17.5774
16	18.6341	34	17.5761
17	18.64129	35	17.58459
18	18.71509	36	17.57218

FILE: M030K

MASS FLOW RATE (LBM/SEC) = 2.921422E-02

PORT	PRESSURE	PORT	PRESSURE
1	103.3071	19	18.76995
2	98.95495	20	18.82285
3	20.40332	21	18.82872
4	20.39287	22	18.85942
5	20.38895	23	18.85942
6	20.38373	24	18.86007
7	20.39549	25	18.87248
8	20.39353	26	18.8666
9	19.03184	27	18.90579
10	19.03249	28	18.87509
11	19.01028	29	18.88554
12	18.97306	30	18.85028
13	18.90971	31	17.56369
14	18.79803	32	17.55651
15	18.65174	33	17.55781
16	18.59884	34	17.5552
17	18.61843	35	17.54279
18	18.70921	36	17.54671

FILE: M030M

MASS FLOW RATE (LBM/SEC) = 2.861617E-02

PORT	PRESSURE	PORT	PRESSURE
1	101.3929	19	18.65762
2	97.13871	20	18.72162
3	20.23483	21	18.74644
4	20.23809	22	18.79803
5	20.23613	23	18.75754
6	20.23679	24	18.81566
7	20.23809	25	18.78431
8	20.22438	26	18.77648
9	18.88685	27	18.80978
10	18.89926	28	18.8026
11	18.86791	29	18.78889
12	18.83003	30	18.74121
13	18.77582	31	17.46246
14	18.6759	32	17.4716
15	18.54006	33	17.4703
16	18.47932	34	17.4605
17	18.50087	35	17.47422
18	18.57794	36	17.46507

FILE: M0300

MASS FLOW RATE (LBM/SEC) = 2.993901E-02

PORT	PRESSURE	PORT	PRESSURE
1	101.3505	19	18.62888
2	96.67959	20	18.68831
3	20.24005	21	18.71901
4	20.2087	22	18.73207
5	20.21785	23	18.74121
6	20.19303	24	18.7288
7	20.19499	25	18.73729
8	20.20544	26	18.73142
9	18.86203	27	18.77648
10	18.85354	28	18.7608
11	18.82742	29	18.77909
12	18.80587	30	18.72684
13	18.75035	31	17.46311
14	18.6439	32	17.46311
15	18.51459	33	17.46116
16	18.45255	34	17.45985
17	18.46887	35	17.46116
18	18.55769	36	17.45201

FILE: M060A

MASS FLOW RATE (LBM/SEC) = 6.041523E-02

PORT	PRESSURE	PORT	PRESSURE
1	110.5963	19	23.08687
2	91.86436	20	23.31022
3	26.33011	21	23.40819
4	26.33011	22	23.4957
5	26.32684	23	23.52509
6	26.33991	24	24.15467
7	26.33664	25	24.1723
8	26.33795	26	24.17557
9	24.18732	27	24.16643
10	24.18994	28	24.15467
11	24.11418	29	24.14487
12	23.97768	30	24.14683
13	23.75563	31	21.01135
14	23.35855	32	20.90816
15	22.87266	33	20.8951
16	22.53697	34	20.8964
17	22.58268	35	20.88792
18	22.73224	36	20.87355

FILE: M090A

MASS FLOW RATE (LBM/SEC) = 8.913799E-02

PORT	PRESSURE	PORT	PRESSURE
1	108.7409	19	25.85793
2	58.76841	20	26.34513
3	30.8939	21	26.50448
4	30.87039	22	26.6978
5	30.86451	23	26.76703
6	30.83969	24	27.96937
7	30.83839	25	28.00202
8	30.82271	26	27.99941
9	28.06406	27	28.00267
10	28.07451	28	28.0079
11	27.94324	29	28.00463
12	27.72511	30	28.0079
13	27.34632	31	22.87592
14	26.62204	32	22.87853
15	25.59473	33	22.872
16	24.89005	34	22.86678
17	24.98083	35	22.86482
18	25.25055	36	22.84523

FILE: M090C

MASS FLOW RATE (LBM/SEC) = 8.821321E-02

PORT	PRESSURE	PORT	PRESSURE
1	107.6554	19	25.85401
2	58.23875	20	26.26807
3	30.69862	21	26.40456
4	30.70516	22	26.55085
5	30.70777	23	26.6129
6	30.69144	24	27.65392
7	30.6934	25	27.89361
8	30.68491	26	27.95892
9	27.96087	27	27.97524
10	27.96479	28	27.97198
11	27.83352	29	27.98243
12	27.60364	30	27.71988
13	27.23007	31	22.81322
14	26.54759	32	22.81518
15	25.54183	33	22.81127
16	24.82213	34	22.82106
17	24.96254	35	22.82237
18	25.30215	36	22.79167

FILE: M090E

MASS FLOW RATE (LBM/SEC) = 8.886908E-02

PORT	PRESSURE	PORT	PRESSURE
1	108.4372	19	25.97222
2	58.62604	20	26.37909
3	30.89063	21	26.53257
4	30.88802	22	26.63184
5	30.88541	23	26.74156
6	30.85471	24	27.54355
7	30.86059	25	27.95565
8	30.84753	26	27.96349
9	28.11435	27	28.12284
10	28.11631	28	28.10063
11	27.98569	29	28.11043
12	27.77083	30	27.59841
13	27.45212	31	22.89747
14	26.67429	32	22.90792
15	25.65351	33	22.90727
16	24.93315	34	22.89878
17	25.08336	35	22.8929
18	25.43668	36	22.87004

FILE: M090G

MASS FLOW RATE (LBM/SEC) = 8.907914E-02

PORT	PRESSURE	PORT	PRESSURE
1	108.6971	19	25.94609
2	58.78212	20	26.39215
3	31.07807	21	26.52604
4	31.0833	22	26.60776
5	31.05979	23	26.73045
6	31.15579	24	26.59657
7	31.04607	25	27.61017
8	31.03105	26	27.65196
9	28.26717	27	28.23648
10	28.25868	28	28.13264
11	28.15223	29	28.147
12	27.92887	30	26.82776
13	27.61212	31	22.92817
14	26.97667	32	22.92686
15	26.00161	33	22.9249
16	24.93119	34	22.93209
17	25.05005	35	22.93143
18	25.41448	36	22.89421

FILE: M090I

MASS FLOW RATE (LBM/SEC) = 8.897614E-02

PORT	PRESSURE	PORT	PRESSURE
1	108.5756	19	25.54636
2	58.72204	20	25.9585
3	30.99774	21	26.09565
4	30.99317	22	26.23476
5	30.98599	23	26.28962
6	30.90173	24	25.79066
7	30.77895	25	26.74025
8	30.68943	26	26.97406
9	27.84528	27	27.69833
10	27.80283	28	27.54028
11	27.65327	29	27.48543
12	27.39726	30	26.07606
13	27.10467	31	22.59966
14	26.44244	32	22.59509
15	25.54575	33	22.59575
16	24.97038	34	22.5964
17	24.92336	35	22.59052
18	25.02393	36	22.56505

FILE: M090K

MASS FLOW RATE (LBM/SEC) = 8.748751E-02

PORT	PRESSURE	PORT	PRESSURE
1	106.747	19	25.67637
2	57.71693	20	26.09369
3	30.37012	21	26.26154
4	30.36228	22	26.38823
5	30.36163	23	26.44636
6	30.35771	24	26.23411
7	30.3453	25	26.47183
8	30.34465	26	26.52016
9	27.5331	27	27.09227
10	27.52265	28	26.90352
11	27.4051	29	26.85585
12	27.18435	30	26.28701
13	26.86042	31	22.67346
14	26.21909	32	22.67216
15	25.30998	33	22.67216
16	24.69935	34	22.67738
17	24.81756	35	22.67412
18	25.1761	36	22.64864

FILE: M090M

MASS FLOW RATE (LBM/SEC) = 8.770174E-02

PORT	PRESSURE	PORT	PRESSURE
1	106.9821	19	25.67245
2	57.80902	20	26.13092
3	30.36033	21	26.31052
4	30.36751	22	26.43526
5	30.35314	23	26.46007
6	30.35053	24	26.5391
7	30.34596	25	26.48947
8	30.34987	26	26.47248
9	27.51743	27	26.51363
10	27.51873	28	26.50383
11	27.39334	29	26.51298
12	27.16606	30	26.44571
13	26.84866	31	22.66105
14	26.20602	32	22.6604
15	25.28256	33	22.65844
16	24.67453	34	22.6604
17	24.77184	35	22.65518
18	25.10034	36	22.63558

FILE: M0900

MASS FLOW RATE (LBM/SEC) = 8.761744E-02

PORT	PRESSURE	PORT	PRESSURE
1	106.9083	19	25.70315
2	57.79465	20	26.16357
3	30.33551	21	26.34578
4	30.34139	22	26.50253
5	30.34792	23	26.53126
6	30.32767	24	26.53322
7	30.32767	25	26.53257
8	30.31592	26	26.52604
9	27.5011	27	26.53126
10	27.50045	28	26.61551
11	27.36656	29	26.52995
12	27.14517	30	26.53322
13	26.82254	31	22.69109
14	26.18251	32	22.67803
15	25.27864	33	22.68195
16	24.66408	34	22.68065
17	24.79862	35	22.66955
18	25.11994	36	22.65648

FILE: M15A

MASS FLOW RATE (LBM/SEC) = .1544962

PORT	PRESSURE	PORT	PRESSURE
1	106.7326	19	29.92539
2	103.1276	20	31.22242
3	39.77136	21	31.64955
4	39.76418	22	32.25953
5	39.75696	23	32.4548
6	39.72826	24	35.69086
7	39.67797	25	35.74115
8	39.67993	26	35.73201
9	35.75552	27	35.7307
10	35.74899	28	35.72809
11	35.49037	29	35.72874
12	34.98553	30	35.73527
13	34.27627	31	24.57724
14	32.48158	32	24.6739
15	29.58448	33	24.70002
16	27.14911	34	24.7268
17	27.4652	35	24.73725
18	28.32271	36	24.63275

FILE: M15C

MASS FLOW RATE (LBM/SEC) = .1542165

PORT	PRESSURE	PORT	PRESSURE
1	106.651	19	30.05078
2	103.0564	20	31.25508
3	39.74067	21	31.62212
4	39.74067	22	32.11455
5	39.72826	23	32.49791
6	39.70213	24	35.43681
7	39.66034	25	35.78034
8	39.66361	26	35.69086
9	35.73593	27	35.7196
10	35.79209	28	35.72939
11	35.52432	29	35.70131
12	34.9274	30	35.52759
13	34.13912	31	24.59096
14	32.42019	32	24.64843
15	29.55117	33	24.67128
16	27.22094	34	24.72353
17	27.4972	35	24.72027
18	28.43438	36	24.59879

FILE: M15E

MASS FLOW RATE (LBM/SEC) = .1539294

PORT	PRESSURE	PORT	PRESSURE
1	106.5791	19	29.95282
2	102.995	20	31.13034
3	39.77789	21	31.53982
4	39.80467	22	31.97413
5	39.77529	23	32.16548
6	39.74394	24	34.48004
7	39.70736	25	35.35387
8	39.68581	26	35.41918
9	35.79013	27	35.75421
10	35.83062	28	35.73527
11	35.54457	29	35.71699
12	35.05737	30	34.66486
13	34.32068	31	24.50409
14	32.40321	32	24.60728
15	29.55509	33	24.63406
16	27.16413	34	24.65692
17	27.48545	35	24.6432
18	28.42132	36	24.54001

FILE: M15G

MASS FLOW RATE (LBM/SEC) = .1534545

PORT	PRESSURE	PORT	PRESSURE
1	106.5511	19	29.89535
2	102.9885	20	31.08136
3	40.318	21	31.50129
4	40.32453	22	31.87878
5	40.33302	23	32.02572
6	40.32192	24	32.12303
7	40.31082	25	34.90062
8	40.22918	26	34.95156
9	36.35505	27	36.2695
10	36.37269	28	36.12713
11	36.09186	29	36.14084
12	35.6347	30	32.60567
13	34.89213	31	24.47405
14	33.38741	32	24.56157
15	30.9429	33	24.56875
16	27.07465	34	24.59487
17	27.45998	35	24.59618
18	28.30899	36	24.4832

FILE: M15I

MASS FLOW RATE (LBM/SEC) = .153184

PORT	PRESSURE	PORT	PRESSURE
1	106.3708	19	29.74056
2	102.8141	20	30.87237
3	40.02411	21	31.24136
4	40.00321	22	31.60448
5	40.00582	23	31.86572
6	39.96599	24	31.03303
7	39.95031	25	33.62057
8	39.94117	26	33.75054
9	35.9521	27	35.81495
10	35.97822	28	35.39305
11	35.68433	29	35.43289
12	35.18472	30	31.3021
13	34.4944	31	24.44074
14	32.87539	32	24.54981
15	30.38712	33	24.52369
16	28.50688	34	24.54459
17	28.65905	35	24.56745
18	28.28418	36	24.44793

FILE: M15K

MASS FLOW RATE (LBM/SEC) = .1534468

PORT	PRESSURE	PORT	PRESSURE
1	106.4472	19	29.82285
2	102.8807	20	31.01148
3	39.24106	21	31.55942
4	39.1875	22	31.91862
5	39.1973	23	32.03291
6	39.17967	24	31.5137
7	39.12154	25	32.20532
8	39.0915	26	32.35684
9	35.03255	27	34.12737
10	35.02928	28	33.50432
11	34.76935	29	33.38938
12	34.24165	30	31.5666
13	33.46905	31	24.45315
14	31.87486	32	24.57006
15	29.29581	33	24.57659
16	27.24903	34	24.61447
17	27.61084	35	24.59422
18	28.60158	36	24.4845

FILE: M15M

MASS FLOW RATE (LBM/SEC) = .1534006

PORT	PRESSURE	PORT	PRESSURE
1	106.4786	19	29.8849
2	102.9147	20	31.17736
3	39.04643	21	31.68481
4	39.04121	22	32.08711
5	39.03794	23	32.15112
6	39.01901	24	32.09887
7	38.97982	25	32.15634
8	38.95631	26	32.15046
9	34.85621	27	32.27455
10	34.8856	28	32.23798
11	34.58975	29	32.22622
12	34.07512	30	32.03552
13	33.31754	31	24.37805
14	31.69526	32	24.47862
15	29.08095	33	24.50475
16	27.01457	34	24.56287
17	27.35548	35	24.53936
18	28.28809	36	24.43095

FILE: M150

MASS FLOW RATE (LBM/SEC) = .1536321

PORT	PRESSURE	PORT	PRESSURE
1	106.2892	19	29.78889
2	102.707	20	31.09703
3	38.94521	21	31.66587
4	38.92561	22	32.07862
5	38.96219	23	32.14198
6	38.9008	24	32.14067
7	38.88251	25	32.14198
8	38.86226	26	32.13414
9	34.79221	27	32.15242
10	34.76347	28	32.15438
11	34.48983	29	32.16418
12	33.99217	30	32.16091
13	33.22218	31	24.39764
14	31.61754	32	24.50475
15	29.01825	33	24.52695
16	26.95514	34	24.55895
17	27.2745	35	24.55504
18	28.2143	36	24.45511

FILE: M40A

MASS FLOW RATE (LBM/SEC) = .3818089

PORT	PRESSURE	PORT	PRESSURE
1	112.7265	19	35.68415
2	89.57382	20	46.33082
3	77.27223	21	48.8106
4	77.0763	22	54.02291
5	76.98096	23	55.67914
6	76.90846	24	71.3572
7	76.91826	25	71.22463
8	76.74323	26	71.20177
9	71.1332	27	71.02675
10	71.23376	28	15.37765
11	70.67146	29	69.73428
12	69.39728	30	70.78836
13	67.10167	31	15.37765
14	61.83516	32	15.57553
15	50.78946	33	16.26324
16	25.30265	34	18.29238
17	19.79841	35	19.30271
18	15.43838	36	19.41635

FILE: M40C

MASS FLOW RATE (LBM/SEC) = .3761953

PORT	PRESSURE	PORT	PRESSURE
1	112.127	19	34.94943
2	89.61106	20	46.00101
3	77.31925	21	48.96081
4	77.50016	22	53.19152
5	77.72548	23	54.84188
6	77.88418	24	70.40565
7	78.00892	25	70.97188
8	77.76531	26	71.32585
9	72.0018	27	71.57664
10	71.85225	28	15.37765
11	70.94641	29	70.71913
12	69.12233	30	71.27948
13	66.44466	31	15.37765
14	60.9241	32	15.6108
15	49.85358	33	16.2776
16	24.71421	34	18.43084
17	19.5535	35	19.48297
18	15.37765	36	19.417

FILE: M40E

MASS FLOW RATE (LBM/SEC) = .3843844

PORT	PRESSURE	PORT	PRESSURE
1	113.5938	19	35.26291
2	90.32814	20	46.60642
3	78.00826	21	50.40087
4	77.80255	22	53.57358
5	77.60923	23	55.2481
6	77.33885	24	68.66582
7	77.09395	25	71.1541
8	76.66682	26	71.14233
9	70.98886	27	71.82678
10	71.0261	28	15.37765
11	70.4899	29	70.33316
12	69.3163	30	68.20996
13	67.24666	31	15.37765
14	61.45375	32	15.57096
15	50.48447	33	16.22274
16	25.10411	34	18.26626
17	19.83825	35	19.31186
18	15.41683	36	19.23806

FILE: M40G

MASS FLOW RATE (LBM/SEC) = .370752

PORT	PRESSURE	PORT	PRESSURE
1	112.0871	19	34.73391
2	90.31116	20	45.08211
3	78.91214	21	49.09273
4	79.02316	22	52.06233
5	79.12831	23	52.82514
6	79.18578	24	60.7863
7	79.28897	25	68.86566
8	79.095	26	69.24446
9	73.89446	27	73.17018
10	74.08124	28	15.37765
11	73.6267	29	72.03772
12	72.57783	30	62.21787
13	70.67734	31	15.37765
14	66.41593	32	15.52524
15	58.00153	33	16.19205
16	23.72674	34	18.14609
17	18.86514	35	19.19626
18	15.37765	36	19.15577

FILE: M40H

MASS FLOW RATE (LBM/SEC) = .3715094

PORT	PRESSURE	PORT	PRESSURE
1	112.1955	19	34.51578
2	90.33598	20	44.73271
3	80.49197	21	49.50353
4	80.53246	22	51.53333
5	80.79565	23	51.99768
6	80.96023	24	56.89846
7	81.03468	25	68.51691
8	80.90472	26	69.91583
9	75.47428	27	74.74543
10	75.91838	28	69.61868
11	75.37501	29	73.60775
12	74.03944	30	60.41992
13	72.16769	31	15.37765
14	68.2165	32	15.38614
15	60.51004	33	16.07123
16	50.4159	34	18.02005
17	16.3501	35	19.08654
18	15.37765	36	19.05193

FILE: M40I

MASS FLOW RATE (LBM/SEC) = .3913754

PORT	PRESSURE	PORT	PRESSURE
1	114.0392	19	34.01616
2	89.95849	20	42.44886
3	78.7959	21	46.5594
4	78.54315	22	49.92673
5	78.37987	23	50.54194
6	78.34265	24	54.0647
7	78.17741	25	65.51728
8	77.72483	26	65.43564
9	71.69485	27	72.18205
10	71.49108	28	66.51911
11	70.75833	29	70.7433
12	69.43712	30	54.96401
13	67.26625	31	16.04968
14	62.53462	32	15.46255
15	53.2712	33	16.13458
16	42.78716	34	17.65432
17	45.94941	35	18.5497
18	15.37765	36	18.4746

FILE: M40J

MASS FLOW RATE (LBM/SEC) = .391389

PORT	PRESSURE	PORT	PRESSURE
1	112.127	19	31.47042
2	87.50418	20	41.1257
3	76.07446	21	44.66609
4	76.18418	22	47.7219
5	76.30631	23	48.34103
6	76.37881	24	49.22596
7	76.46436	25	59.68519
8	76.24884	26	58.87732
9	70.19863	27	66.74771
10	70.30573	28	66.26964
11	69.70555	29	67.08078
12	68.34123	30	49.88428
13	65.89672	31	15.7597
14	60.45649	32	16.58521
15	49.33764	33	16.51272
16	24.85659	34	17.79604
17	29.28192	35	18.59803
18	42.33914	36	18.49941

FILE: M40K

MASS FLOW RATE (LBM/SEC) = .3923856

PORT	PRESSURE	PORT	PRESSURE
1	112.2386	19	41.54563
2	87.51333	20	43.0079
3	76.20966	21	46.15383
4	76.3246	22	48.95951
5	76.45065	23	50.17164
6	76.51008	24	47.31568
7	76.59171	25	55.87572
8	76.4206	26	59.95883
9	70.35667	27	66.62036
10	70.46051	28	66.32515
11	69.83028	29	65.85166
12	68.43332	30	50.18666
13	65.89933	31	15.38548
14	60.39249	32	16.32789
15	49.23249	33	16.85363
16	24.76058	34	18.17352
17	19.30206	35	18.97421
18	29.45564	36	18.7613

FILE: M40M

MASS FLOW RATE (LBM/SEC) = .3950864

PORT	PRESSURE	PORT	PRESSURE
1	113.4299	19	34.95531
2	88.66081	20	46.57311
3	76.63025	21	52.95706
4	76.41603	22	56.22708
5	76.23578	23	57.0761
6	75.96215	24	54.79421
7	75.74139	25	56.41387
8	75.40113	26	56.99773
9	69.25035	27	60.82418
10	69.30585	28	59.46314
11	68.705	29	58.64547
12	67.38511	30	54.47876
13	65.04509	31	15.37765
14	59.8132	32	15.53439
15	48.96211	33	16.22666
16	24.73119	34	18.36161
17	19.29749	35	19.68281
18	15.37765	36	19.77816

FILE: M400

MASS FLOW RATE (LBM/SEC) = .3937804

PORT	PRESSURE	PORT	PRESSURE
1	113.601	19	34.63137
2	89.05919	20	46.33278
3	76.81441	21	52.96556
4	76.61131	22	57.03887
5	76.4304	23	57.51628
6	76.15415	24	57.45685
7	75.90532	25	57.31448
8	75.4338	26	57.26158
9	69.26406	27	57.1721
10	69.29801	28	57.04279
11	68.66191	29	56.87168
12	67.32699	30	56.66922
13	64.98762	31	15.37765
14	59.74985	32	15.52655
15	48.9164	33	16.19531
16	24.71552	34	18.327
17	19.28508	35	19.69
18	15.37765	36	19.85392

APPENDIX B: Navier-Stokes Computer Code

With the exception of the boundry conditions subroutine, the computer code contained in this appendix was written by Dr. Joe Shang of the Flight Dynamics Laboratory, Wright Patterson Air Force Base, Dayton, Ohio. It solves the compressible Navier-Stokes equations for axisymmetric flow situations. The main variables used in the program are defined below.

BETA	Program variable, Ø=time accurate solution 1=accelerated solution
CFL	time step safety factor
CINF	initial condition sonic velocity
CV	constant volume specific heat
CX	dampening factor (between Ø and 5)
CY	dampening factor (bewteen Ø and 5)
DETA	radial direction node spacing
DT	time step
DZETA	axial direction node spacing
EP	turbulent eddy viscosity
GAMMA	ratio of specific heats
GAMM1	GAMMA - 1
IG	1
ILE	1
ISMTHX	dampening parameter: Ø=no damping 1=damping
ISMTHY	dampening parameter (same values as above)

JL	number of radial nodes
JLM	JL - 1
KL	number of axial nodes
KLM	KL - 1
NEND	number of last iteration
NI	number of first iteration
PEX	porous pipe environment pressure
PHIGH	evaporator environment pressure
PINF	initial pressure
PLOW	condenser environment pressure
PR	Prandtl number
PRT	Turbulent Prandtl number
RC	Ideal gas constant
RCV	reciprocal of CV
REY	axial Reynolds number
RHO	density
RHOINF	initial density
RHOP	RHO for predictor step
RHOE	density times total energy
RHOEP	RHOE for predictor step
RHOU	density times axial velocity
RHOUP	RHOU for predictor step
RHOV	density times radial velocity
RHOVP	RHOV for predictor step
RL	reference length
RLMBD	combination of first and second coefficients of viscosity
RMU	first coefficient of viscosity

RMINF	initial value of RMU
TCH	reference time
TEX	porous pipe environment temperature
TINF	initial reference temperaature
TMS1	total time variable
TMS2	total time variable
UINF	initial axial velocity
VINF	initial radial velocity
X	axial coordinates of grid
XM	initial Mach number
Y	radial coordinates of grid

```
      PROGRAM MAIN
      COMMON / / DETA,DZETA,CV,RC,PR,PRT,GAMMA,EP(96,25,1),DTL(25),
     1 GAMM1,CFL,BETA,UINF,VINF,RHOINF,CINF,TINF,PINF,TW,DT,CX,CY,L,
     2 JL,KL,JLM,KLM,ILE,ISMTHX,ISMTHY,GAMM2,RL,TMS1
      COMMON /DEPP/ RHOP(96,25,1),RHOUP(96,25,1),RHOVP(96,25,1),
     1 RHOEP(96,25,1)
      COMMON /DEP/ RHO(96,25,1),RHOU(96,25,1),RHOV(96,25,1),
     1 RHOE(96,25,1)
      COMMON /DOF/ X(96,25,1),Y(96,25,1)
      COMMON /TV/ ETY(96,25,1),ZTX(96,25,1)
      COMMON /BV/ PEX(96),TEX(96)
C
C     CONSTANTS AND PARAMETER FOR AIR
C
      CV=4290.
      RC=1718.
      GAMMA=1.4
      GAMM1=GAMMA-1.0
      GAMM2=2
      PR=0.73
      PRT=0.90
      RCV=1.0/CV
C
  100 FORMAT(7E13.5)
  101  FORMAT(2E15.9)
  110 FORMAT(10I5)
  500 FORMAT('  REYNOLDS NO.=',E15.7,
     1 'REFERENCE LENGTH=',F10.4/)
  510 FORMAT('  RHOINF=',E15.7,'VINF=',F10.4,'CINF=',F10.4,'TINF=',
     1 F10.4,'PINF=',F10.2,'RMUINF=',E15.7/)
  520 FORMAT('  DETA=',E15.7,'DZETA=',E15.7/)
  530 FORMAT('  CFL=',F10.4,'CX=',F10.4,'CY=',F10.4,'BETA=',F10.4/)
  550 FORMAT('       NEND=',I5,'JL=',I5,'KL=',I5/)
  560 FORMAT('    LOCAL CFL TIME STEP CALCULATION (TIME-WARP)'/)
  580 FORMAT(' N=',I5,'DTCFL=',E15.7,'TMS2=',E15.7,'TMS1=',E15.7,
     1 'TMS2/TCH=',E15.7,'DTMAX=',E15.7)
  590 FORMAT('   J  K      X         Y        Y/YL          RHO
     1 U         V          W          T          P         EP'/)
  600 FORMAT(4X,2I3,11E11.4)
  610 FORMAT(7E15.7)
C     ***********************
C     READ IN THE INPUT DATA
C     ***********************
C
      OPEN (UNIT=1,FILE='TAPE1',FORM='UNFORMATTED')
      OPEN (UNIT=2,FILE='TAPE2',FORM='UNFORMATTED')
      OPEN (UNIT=3,FILE='TAPE3')
      OPEN (UNIT=4,FILE='TAPE4')
      OPEN (UNIT=8,FILE='TAPE8')
      OPEN (UNIT=9,FILE='TAPE9')
C
```

```
      READ(5,100) REY,RL,PHIGH,PLOW,TEX(1)
      READ(5,100) CX,CY,CFL,BETA
      READ(5,110) ISTART,ILE,IG
      READ(5,110) NEND,JL,KL,ISMTHX,ISMTHY
C
      NI=1
      TMS1=0.0
      TMS2=0.0
C
C     READ IN THE RESTART DATA FROM PREVIOUS RUNS
C     *******************************************
      IF(ISTART.NE.0) READ(1) NI,TMS1,TMS2,RHO,RHOU,RHOV,RHOE,
     1 X,Y,Z,EP,PEX,TEX
C
C
C     READ IN PIPE EXTERNAL ENVIRONMENT PRESSURE AND TEMP DATA
C     *********************************************************
C
      IF(ISTART.EQ.1) GO TO 30
      DO 25 K=1,KL
      PEX(K)=PHIGH*144.
      TEX(K)=TEX(1)
25    CONTINUE
      DO 26 K=KL/2+1,KL
      PEX(K)=PLOW*144
26    CONTINUE
30    CONTINUE
C
C     GENERATING THE FREESTREAM INFORMATION
C
      PINF=PEX(1)
      TINF=TEX(1)
      RHOINF=PINF/TINF/RC
      RMUINF=2.27E-08*SQRT(TINF**3)/(TINF+198.6)
      CINF=SQRT(GAMMA*RC*TINF)
      VINF=REY*RMUINF/RHOINF/RL
C
      JLM=JL-1
      KLM=KL-1
      DETA=1.0/JLM
      DZETA=1.0/KLM
C
C     WRITE OUT THE INPUT AND FLOW FIELD INFORMATION
C
      WRITE(4,500) REY,RL
      WRITE(4,510) RHOINF,VINF,CINF,TINF,PINF,RMUINF
      WRITE(4,520) DETA,DZETA
      WRITE(4,530) CFL,CX,CY,BETA
      WRITE(4,550) NEND,JL,KL
      IF(BETA.NE.0.0) WRITE(6,560)
C
```

```
C
C     INITILIZATION OF ALL DEPENDENT VARIABLES
C     ****************************************
      IF(ISTART.EQ.0) CALL PREAMB
C
C
C     READ IN THE GRID POINTS IN CARTESIAN FRAME
C     ******************************************
      IF(ISTART.EQ.1) GO TO 32
      DO 31 K=1,KL
      DO 31 J=1,JL
31    READ(3,101) X(K,J,1),Y(K,J,1)
32    CONTINUE
C
C
C     INITIALIZE THE PREDICTOR VARIABLES
C
      IF (ISTART .EQ. 0) GO TO 4
      DO 3 J=1,JL
      DO 3 K=1,KL
      RHOP (K,J,1)=RHO (K,J,1)
      RHOUP(K,J,1)=RHOU(K,J,1)
      RHOVP(K,J,1)=RHOV(K,J,1)
      RHOEP(K,J,1)=RHOE(K,J,1)
 3    CONTINUE
C
C
 4    CALL TRANS
      CALL TMSTEP
C
      DO 1 N=NI,NEND
C
C
      IF((N/10)*10.NE.N) GO TO 5
C
C     DETERMINE THE ALLOWABLE TIME STEP SIZE (DT CFL)
C     ***********************************************
      CALL TMSTEP
      CALL EDDY
C
C     CONTROL THE DATA FLOW AND DIFFERENCE OPERATORS
C     **********************************************
 5    CALL PAGE
C
      TMS2=TMS1+DTL(2)
      TMS1=TMS2
C
C
 1    CONTINUE
C
```

```
C     WRITE THE RESTART DATA INTO RESTART TAPE
C     ****************************************
      NEND=NEND+1
      WRITE(2) NEND,TMS1,TMS2,RHO,RHOU,RHOV,RHOE,X,Y,Z,EP
     1 ,PEX,TEX
C     ********************************
C     WRITE OUT THE COMPUTED FLOW DATA
C     ********************************
C
      WRITE(4,580) N,DTL(2),TMS2,TMS1,T,DTL(JLM)
C
C     GENERATING THE GRAPHICAL DATA FILE ON TAPE4
C
      RRL=1.0/RL
      RUINF=1.0/CINF
C
      DO 20 K=1,KL
C     WRITE(6,590)
      DO 20 J=1,JL
C
      RH=1.0/RHO(K,J,1)
      U=RHOU(K,J,1)*RH
      V=RHOV(K,J,1)*RH
      W=U*RUINF
      T=(RHOE(K,J,1)*RH-0.5*(U**2+V**2))*RCV
      P=RHO(K,J,1)*RC*T
      XB=X(K,J,1)*RRL
      YB=Y(K,J,1)*RRL
      XM=SQRT((U**2+V**2)/(GAMMA*RC*T))
C
C     WRITE(6,600) J,K,X(K,J,1),Y(K,J,1),YB,RHO(K,J,1),
C    1 U,V,W,T,P,EP(K,J,1)
C     WRITE(4,610) X(K,J,1),Y(K,J,1),U,V,P,T,RHO(K,J,1)
      WRITE(4,610) XB/4,YB,U,V
C
 20    CONTINUE
C
      STOP
      END
```

```
      SUBROUTINE PREAMB
      COMMON / / DETA,DZETA,CV,RC,PR,PRT,GAMMA,EP(96,25,1),DTL(25),
     1 GAMM1,CFL,BETA,UINF,VINF,RHOINF,CINF,TINF,PINF,TW,DT,CX,CY,L,
     2 JL,KL,JLM,KLM,ILE,ISMTHX,ISMTHY,GAMM2,RL,TMS1
      COMMON /FLUET/
     1 G21(96,2),G22(96,2),G23(96,2),G25(96,2),H(96)
      COMMON /FLUZT/ F31(96),F32(96),F33(96),F35(96)
      COMMON /TV/ ETY(96,25,1),ZTX(96,25,1)
      COMMON /DEP/ RHO(96,25,1),RHOU(96,25,1),RHOV(96,25,1),
     1 RHOE(96,25,1)
      COMMON /DEPP/ RHOP(96,25,1),RHOUP(96,25,1),RHOVP(96,25,1),
     1 RHOEP(96,25,1)
      COMMON /BV/ PEX(96),TEX(96)
C
C     SPECIFIED INITIAL CONDITIONS FOR THE FLOW FIELD
C
      REINF=RHOINF*(CV*TINF)
C
      DO 1 J=1,JL
      DO 1 K=1,KL
      RHO (K,J,1)=RHOINF
      RHOP(K,J,1)=RHOINF
      RHOU(K,J,1)=0.0
      RHOUP(K,J,1)=0.0
      RHOV(K,J,1)=0.0
      RHOVP(K,J,1)=0.0
      RHOE(K,J,1)=REINF
      RHOEP(K,J,1)=REINF
      EP(K,J,1)=0.0
 1    CONTINUE
C
C     SPECIFIED THE NOSLIP BOUNDARY CONDITION AND SURFACE TEMPERATURE
C
C
      RHOWL=RHOINF
C
      DO 2 K=ILE,KL
      RHOEW=RHOWL*CV*TEX(K)
      RHO (K,1,1)=RHOWL
      RHOU(K,1,1)=0.0
      RHOV(K,1,1)=0.0
      RHOE(K,1,1)=RHOEW
      RHOP (K,1,1)=RHOWL
      RHOUP(K,1,1)=0.0
      RHOVP(K,1,1)=0.0
      RHOEP(K,1,1)=RHOEW
 2    CONTINUE
C
```

```
C      INITIALIZE THE FLUX COMPONENTS
C
C
       DO 3 J=1,2
       DO 3 K=1,KL
C
C
       G21(K,J)=0.0
       G22(K,J)=0.0
       G23(K,J)=0.0
       G25(K,J)=0.0
C
  3    CONTINUE
C
       DO 4 K=1,KL
       F31(K)=0.0
       F32(K)=0.0
       F33(K)=0.0
       F35(K)=0.0
C
       H(K)=0.0
C
  4    CONTINUE
C
       RETURN
       END
       SUBROUTINE TMSTEP
       COMMON / / DETA,DZETA,CV,RC,PR,PRT,GAMMA,EP(96,25,1),DTL(25),
      1 GAMM1,CFL,BETA,UINF,VINF,RHOINF,CINF,TINF,PINF,TW,DT,CX,CY,L,
      2 JL,KL,JLM,KLM,ILE,ISMTHX,ISMTHY,GAMM2,RL,TMS1
       COMMON /TV/ ETY(96,25,1),ZTX(96,25,1)
       COMMON /DEP/ RHO(96,25,1),RHOU(96,25,1),RHOV(96,25,1),
      1 RHOE(96,25,1)
       DIMENSION UET(96),UZT(96),DTC(96),U(96),V(96),C(96)
C
C      SET UP INITIAL CFL TIME STEP VALUE
C
       DTC(1)=1.0
       GAMM3=GAMMA*GAMM1
       DTCFL=1.0
       RDET=1.0/DETA
       RDZT=1.0/DZETA
C
       DO 1 J=2,JLM
       DO 2 K=2,KLM
C
       RH=1.0/RHO(K,J,1)
       U(K)=RHOU(K,J,1)*RH
       V(K)=RHOV(K,J,1)*RH
       C(K)=SQRT(GAMM3*(RHOE(K,J,1)*RH-0.5*(U(K)**2+V(K)**2)))
C
```

```
      JET(K)=ETY(K,J,1)*V(K)
      UZT(K)=ZTX(K,J,1)*U(K)
C
      DTC(K)=1.0/(ABS(JET(K))*RDET+ABS(UZT(K))*RDZT+
     1 C(K)*SQRT((ZTX(K,J,1)*RDZT)**2+
     2           (ETY(K,J,1)*RDET)**2))
C
 2    CONTINUE
C
C     PERFORM THE COMPARISON AND MODIFIED THE CFL TIME STEP
C
      DTMIN=DTC(1)
      DO 3 K=2,KLM
      DTMIN=AMIN1(DTC(K),DTMIN)
 3    CONTINUE
C
      DTL(J)=DTMIN*CFL
C     COMPARING DTMIN BETWEEN ADJACENT PLANES
      DTCFL=AMIN1(DTCFL,DTMIN)
C
 1    CONTINUE
C
C     ADJUST DTCFL FOR VISCOUS EFFECT (TRAIL AND ERROR)
      DT=CFL*DTCFL
C
      RETURN
      END
      SUBROUTINE BC
      COMMON / / DETA,DZETA,CV,RC,PR,PRT,GAMMA,EP(96,25,1),DTL(25),
     1 GAMM1,CFL,BETA,UINF,VINF,RHOINF,CINF,TINF,PINF,TW,DT,CX,CY,L,
     2 JL,KL,JLM,KLM,ILE,ISMTHX,ISMTHY,GAMM2,RL,TMS1
      COMMON /TV/ ETY(96,25,1),ZTX(96,25,1)
      COMMON /DEP/ RHO(96,25,1),RHOU(96,25,1),RHOV(96,25,1),
     1 RHOE(96,25,1)
      COMMON /DEPP/ RHOP(96,25,1),RHOUP(96,25,1),RHOVP(96,25,1),
     1 RHOEP(96,25,1)
      COMMON /DV/ R(96,25,1),U(96,25,1),V(96,25,1),W(1,1,1),
     1 P(96,25,1),T(96,25,1)
      COMMON /BV/ PEX(96),TEX(96)
      COMMON /DOF/ X(96,25,1),Y(96,25,1)
      DIMENSION PET(96),PZETAE(25),PZETAC(25)
C
C
      RG=1.
      K2=KL/2+1
      CA=3.639E+9
      CB=1.7315E+8
      KM=48
      KN=49
      IF(L.EQ.2) GO TO 10
C
```

```
C                    ****************
C                    PREDICTOR SWEEP
C                    ****************
C
C     DECODE THE PROBLEM VARIABLES TO THE PRIMATIVE VARIABLES
C
      DO 4 JV=1,JL
      DO 4 K=1,KL
      R(K,JV,1)=RHOP(K,JV,1)
      U(K,JV,1)=RHOUP(K,JV,1)/R(K,JV,1)
      V(K,JV,1)=RHOVP(K,JV,1)/R(K,JV,1)
      T(K,JV,1)=(RHOEP(K,JV,1)/R(K,JV,1)-0.5*(V(K,JV,1)**2
     1  +U(K,JV,1)**2))/CV
      P(K,JV,1)=R(K,JV,1)*RC*T(K,JV,1)
    4 CONTINUE
C
C
C     SUCTION AND INJECTION BOUNDARY CONDITIONS
C
      RR=1.0/RC
      DO 1 K=1,KL
      FUDGE=1.07
      RHOUP(K,1,1)=0.0
      RHOP(K,1,1)=(P(K,2,1)+RHOVP(K,1,1)*(V(K,2,1)-V(K,1,1)))
     1  /(RC*T(K,1,1))
      C=P(K,1,1)**2-PEX(K)**2
      DI=1
      IF(C .LT. 0) DI=-1
      C=ABS(C)
      RHOVP(K,1,1)=DI*(-CB+SQRT(CB**2+4.*CA*C))/(2.*CA)*FUDGE
      RHOEP(K,1,1)=RHOP(K,1,1)*(CV*TEX(K)+0.5*(RHOVP(K,1,1)
     1  /RHOP(K,1,1))**2)
    1 CONTINUE
      DO 5 K=K2,KL
    5 RHOEP(K,1,1)=RHOP(K,1,1)*(CV*T(K,2,1)+0.5*(RHOVP(K,1,1)
     1  /RHOP(K,1,1))**2)
C
C      ELIMINATE THE SUCTION OF BLOWING AT THE CENTER OF THE PIPE
C
      RHOVP(KM,1,1)=0.5*RHOVP(KM,1,1)
      RHOVP(KN,1,1)=0.0*RHOVP(KN,1,1)
C
C     FAR FIELD BOUNDARY CONDITIONS
C
C
      DO 2 K=1,KL
      RHOP(K,JL,1)=RHOP(K,JLM,1)
      RHOUP(K,JL,1)=RHOUP(K,JLM,1)
      RHOVP(K,JL,1)=RHOVP(K,JLM,1)
C     RHOVP(K,JLM,1)=0.0
      RHOEP(K,JL,1)=RHOEP(K,JLM,1)
    2 CONTINUE
```

```
C
C     THE UPSTREAM AND DOWNSTREAM BOUNDARY CONDITIONS
C
      RR=1./RC
      DO 3 J=1,JLM
C     RHOP (1,J,1)=RHOP(2,J,1)*T(2,J,1)/T(1,J,1)
      RHOP (1,J,1)=(R(2,J,1)*U(2,J,1)**2+P(2,J,1))/RC/T(1,J,1)
      RHOUP(1,J,1)= 0.0
      RHOVP(1,J,1)=0.0
C     RHOEP(1,J,1)= RHOP(1,J,1)*CV*T(2,J,1)
      RHOEP(1,J,1)=RHOEP(2,J,1)*RHOP(1,J,1)/RHOP(2,J,1)
C
      RHOP (KL,J,1)=RHOP(KLM,J,1)*T(KLM,J,1)/T(KL,J,1)
C     RHOP(KL,J,1)=(R(KLM,J,1)*U(KLM,J,1)**2+P(KLM,J,1))/RC/T(KLM,J,1)
      RHOUP(KL,J,1)=0.0
      RHOVP(KL,J,1)=0.0
      RHOEP(KL,J,1)=RHOEP(KLM,J,1)*RHOP(KL,J,1)/RHOP(KLM,J,1)
 3    CONTINUE
C
C
      GO TO 100
C
C                   ****************
C                   CORRECTOR SWEEP
C                   ****************
C
C     DECODE THE PROBLEM VARIABLES TO THE PERIMATIVE VARIABLES
C
 10   DO 14 JV=1,JL
      DO 14 K=1,KL
      R(K,JV,1)=RHO(K,JV,1)
      U(K,JV,1)=RHOU(K,JV,1)/R(K,JV,1)
      V(K,JV,1)=RHOV(K,JV,1)/R(K,JV,1)
      T(K,JV,1)=(RHOE(K,JV,1)/R(K,JV,1)-0.5*(V(K,JV,1)**2
     1  +U(K,JV,1)**2))/CV
      P(K,JV,1)=R(K,JV,1)*RC*T(K,JV,1)
 14   CONTINUE
      WRITE(8,9) TMS1,P(2,JLM,1),P(48,JLM,1),P(KLM,JLM,1)
 9    FORMAT(6E15.7)
C
C
C     SUCTION AND INJECTION BOUNDARY CONDITION
C
      RR=1.0/RC
      DO 11 K=1,KL
      FUDGE=1.07
      RHOU(K,1,1)=0.0
      RHO (K,1,1)=(P(K,2,1)+RHOV(K,1,1)*(V(K,2,1)-V(K,1,1)))
     1  /(RC*T(K,1,1))
      C=P(K,1,1)**2-PEX(K)**2
```

```
      DI=1
      IF(C .LT. 0) DI=-1
      C=ABS(C)
      RHOV(K,1,1)=DI*(-CB+SQRT(CB**2+4.*CA*C))/(2.*CA)*FUDGE
      RHOE(K,1,1)=RHO(K,1,1)*(CV*TEX(K)+0.5*(RHOV(K,1,1)
     1  /RHO(K,1,1))**2)
 11   CONTINUE
      DO 15 K=K2,KL
 15   RHOE(K,1,1)=RHO(K,1,1)*(CV*T(K,2,1)+0.5*(RHOV(K,1,1)
     1  /RHO(K,1,1))**2)
C
C     ELIMINATE THE SUCTION OF BLOWING IN THE MIDDLE OF THE PIPE
C
      RHOV(KM,1,1)=0.5*RHOV(KM,1,1)
      RHOV(KN,1,1)=0.0*RHOV(KN,1,1)
C     DO 17 K=KM,KM
C17   RHOV(K,1,1)=2.0*RHOV(K,1,1)
C
C
C     FAR FIELD BOUNDARY CONDITIONS
C
C
      DO 12 K=1,KL
      RHO (K,JL,1)=RHO(K,JLM,1)
      RHOU(K,JL,1)=RHOU(K,JLM,1)
      RHOV(K,JL,1)=RHOV(K,JLM,1)
C     RHOV(K,JLM,1)=0.0
      RHOE(K,JL,1)=RHOE(K,JLM,1)
 12   CONTINUE
C
C     THE UPSTREAM AND DOWNSTREAM BOUNDARY CONDITIONS
C
      RR=1./RC
      DO 13 J=1,JLM
C     RHO (1,J,1)=RHO(2,J,1)*T(2,J,1)/T(1,J,1)
      RHO (1,J,1)=(RHO(2,J,1)*U(2,J,1)**2+P(2,J,1))/RC/T(1,J,1)
      RHOU(1,J,1)= 0.0
      RHOV(1,J,1)=0.0
C     RHOE(1,J,1)= RHO(1,J,1)*CV*T(2,J,1)
      RHOE(1,J,1)=RHOE(2,J,1)*RHO(1,J,1)/RHO(2,J,1)
C
      RHO (KL,J,1)=RHO(KLM,J,1)*T(KLM,J,1)/T(KL,J,1)
C     RHO (KL,J,1)=(RHO(KLM,J,1)*U(KLM,J,1)**2+P(KLM,J,1))/RC/T(KLM,J,1)
      RHOU(KL,J,1)=0.0
      RHOV(KL,J,1)=0.0
      RHOE(KL,J,1)=RHOE(KLM,J,1)*RHO(KL,J,1)/RHO(KLM,J,1)
 13   CONTINUE
C
C
 100  RETURN
      END
```

```
      SUBROUTINE TRANS
      COMMON / / DETA,DZETA,CV,RC,PR,PRT,GAMMA,EP(96,25,1),DTL(25),
     1 GAMM1,CFL,BETA,UINF,VINF,RHOINF,CINF,TINF,PINF,TW,DT,CX,CY,L,
     2 JL,KL,JLM,KLM,ILE,ISMTHX,ISMTHY,GAMM2,RL,TMS1
      COMMON /TV/ ETY(96,25,1),ZTX(96,25,1)
      COMMON /DOF/ X(96,25,1),Y(96,25,1)
      DIMENSION YET(96,30),DJ(96,30),
     1 XZT(96,30),RDJ(96,30)
C
      RDET=1.0/(2.0*DETA)
      RDZT=1.0/(2.0*DZETA)
      JLM2=JLM-1
      KLM2=KLM-1
C
C
C     GENERATING DX/DTEA AND DY/DTEA
C
C
C     ONE-SIDE DIFFERENCING FOR J=1
C
      DO 101 KV=1,KL
      YET(KV,1)=(4.0*Y(KV,2,1)-Y(KV,3,1)-3.0*Y(KV,1,1))*RDET
 101   CONTINUE
C
C     ONE-SIDE DIFFERENCING FOR J=JL
C
      DO 102 KV=1,KL
      YET(KV,JL)=-(4.0*Y(KV,JLM,1)-Y(KV,JLM2,1)-3.0*Y(KV,JL,1))*RDET
 102  CONTINUE
C
C     CENTRAL DIFFERENCING FOR FIELD POINTS
C
      DO 103 JV=2,JLM
      JP=JV+1
      JM=JV-1
      DO 104 KV=1,KL
      YET(KV,JV)=(Y(KV,JP,1)-Y(KV,JM,1))*RDET
 104  CONTINUE
 103  CONTINUE
C
C     GENERATING DX/DZETA AND DY/DZETA
C
C
C     ONE-SIDE DIFFERENCING FOR K=1
C
      DO 201 JV=1,JL
      XZT(1,JV)=(4.0*X(2,JV,1)-X(3,JV,1)-3.0*X(1,JV,1))*RDZT
 201  CONTINUE
```

```
C
C     ONE-SIDE DIFFERENCING FOR K=KL
C
      DO 202 JV=1,JL
      XZT(KL,JV)=-(4.0*X(KLM,JV,1)-X(KLM2,JV,1)-3.0*X(KL,JV,1))*RDZT
  202 CONTINUE
C
C     CENTRAL DIFFERENCING FOR FIELD POINTS
C
      DO 203 JV=1,JL
      DO 204 KV=2,KLM
      KP=KV+1
      KM=KV-1
      XZT(KV,JV)=(X(KP,JV,1)-X(KM,JV,1))*RDZT
  204 CONTINUE
  203 CONTINUE
C
C
C     GENERATING THE METRICS OF COORDINATES TRANSFORMATION
C
      DO 305 JV=1,JL
      DO 306 KV=1,KL
C
      ZTX(KV,JV,1)=1.0/XZT(KV,JV)
      ETY(KV,JV,1)=1.0/YET(KV,JV)
C
  306 CONTINUE
  305 CONTINUE
C
      RETURN
      END
```

```
      SUBROUTINE PAGE
      COMMON / / DETA,DZETA,CV,RC,PR,PRT,GAMMA,EP(96,25,1),DTL(25),
     1 GAMM1,CFL,BETA,JINF,VINF,RHOINF,CINF,TINF,PINF,TW,DT,CX,CY,L,
     2 JL,KL,JLM,KLM,ILE,ISMTHX,ISMTHY,GAMM2,RL,TMS1
      COMMON /DV/ R(96,25,1),U(96,25,1),V(96,25,1),W(1,1,1),
     1 P(96,25,1),T(96,25,1)
      COMMON /TV/ ETY(96,25,1),ZTX(96,25,1)
      COMMON /DEP/ RHO(96,25,1),RHOU(96,25,1),RHOV(96,25,1),
     1 RHOE(96,25,1)
      COMMON /DEPP/ RHOP(96,25,1),RHOUP(96,25,1),RHOVP(96,25,1),
     1 RHOEP(96,25,1)
C
C
C                         ***************
C                         PREDICTOR SWEEP
C                         ***************
C
                              L=1
C
C     GENERATING THREE PAGES TEMPORAL VECTOR ARRAYS
C
      DO 1 JV=1,JL
      DO 1 KV=1,KL
C
      R(KV,JV,1)=RHO (KV,JV,1)
      U(KV,JV,1)=RHOU(KV,JV,1)/R(KV,JV,1)
      V(KV,JV,1)=RHOV(KV,JV,1)/R(KV,JV,1)
      T(KV,JV,1)=(RHOE(KV,JV,1)/R(KV,JV,1)-0.5*(U(KV,JV,1)**2
     1 +V(KV,JV,1)**2))/CV
      P(KV,JV,1)=R(KV,JV,1)*RC*T(KV,JV,1)
C
 1    CONTINUE
C
C
C
      DO 2 J=2,JLM
      CALL LETA(J)
      CALL LZETA(J)
      CALL SUM(J)
 2    CONTINUE
C
      CALL BC
C
```

```
C
C                     *****************
C                     CORRECTCR SWEEPS
C                     *****************
C
                       L=2
C
C
C     GENERATING THREE PAGES TEMPORAL VECTOR ARRAYS
C
      DO 10 JV=1,JL
      DO 10 KV=1,KL
C
      R(KV,JV,1)=RHOP (KV,JV,1)
      U(KV,JV,1)=RHOUP(KV,JV,1)/R(KV,JV,1)
      V(KV,JV,1)=RHOVP(KV,JV,1)/R(KV,JV,1)
      T(KV,JV,1)=(RHOEP(KV,JV,1)/R(KV,JV,1)-0.5*(U(KV,JV,1)**2
     1 +V(KV,JV,1)**2))/CV
      P(KV,JV,1)=R(KV,JV,1)*RC*T(KV,JV,1)
C
 10   CONTINUE
C
C
C
      DO 11 J=2,JLM
      CALL LETA(J)
      CALL LZETA(J)
      CALL SUM(J)
 11   CONTINUE
C
      CALL BC
C
      RETURN
      END
```

```
      SUBROUTINE LETA(J)
      COMMON / / DETA,DZETA,CV,RC,PR,PRT,GAMMA,EP(96,25,1),DTL(25),
     1 GAMM1,CFL,BETA,UINF,VINF,RHOINF,CINF,TINF,PINF,T*,DT,CX,CY,L,
     2 JL,KL,JLM,KLM,ILE,ISMTHX,ISMTHY,GAMM2,RL,TMS1
      COMMON /FLUET/
     1 G21(96,2),G22(96,2),G23(96,2),G25(96,2),H(96)
      COMMON /DV/ R(96,25,1),U(96,25,1),V(96,25,1),W(1,1,1),
     1 P(96,25,1),T(96,25,1)
      COMMON /TV/ ETY(96,25,1),ZTX(96,25,1)
      COMMON /DOF/ X(96,25,1),Y(96,25,1)
      DIMENSION UET(96),UZT(96),VET(96),VZT(96),RMU(96),
     1 RLMBD(96),SMU(96),RK(96),TAUXX(96),TAUXR(96),
     2 TAURR(96),TX(96),TY(96),TET(96),TZT(96),DUDX(96),
     3 DVDR(96)
C
      RDET=1.0/DETA
      RDZT=1.0/(2.0*DZETA)
C
      DO 1 M=1,2
C
C
C     FORWARD & BACKWARD DIFFERENCING FOR PREDICTOR & CORRECTOR
C
C
C     **********
      JV=L+M+J-3
      JM=J+M-2
      JP=JM+1
C     **********
C
C
      DO 2 KV=2,KLM
C
      KP=KV+1
      KM=KV-1
C     GENERATING THE SHEAR STRESS & HEAT FLUX TERMS
C
      UET(KV)=(U(KV,JP,1)-U(KV,JM,1))*RDET
      VET(KV)=(V(KV,JP,1)-V(KV,JM,1))*RDET
      TET(KV)=(T(KV,JP,1)-T(KV,JM,1))*RDET
C
      UZT(KV)=(U(KP,JV,1)-U(KM,JV,1))*RDZT
      VZT(KV)=(V(KP,JV,1)-V(KM,JV,1))*RDZT
      TZT(KV)=(T(KP,JV,1)-T(KM,JV,1))*RDZT
C
C     GENERATING THE VISCOSITY COEFFS & HEAT CONDUCTIVITY
C
      RMU(KV)=2.27E-08*SQRT(T(KV,JV,1)**3)/(T(KV,JV,1)+198.6)
      RK(KV)=GAMMA*CV*(RMU(KV)/PR+EP(KV,JV,1)/PRT)
      RMU(KV)=RMU(KV)+EP(KV,JV,1)
      RLMBD(KV)=-(2.0/3.0)*RMU(KV)
      SMU(KV)=2.0*RMU(KV)+RLMBD(KV)
C
  2   CONTINUE
```

```
C
      DO 3 KV=2,KLM
C
      RY=1.0/Y(KV,JV,1)
C
      DUDX(KV)=ZTX(KV,JV,1)*UZT(KV)
      DVDR(KV)=ETY(KV,JV,1)*VET(KV)
C
      TAUXX(KV)=SMU(KV)*DUDX(KV)+RLMBD(KV)*(V(KV,JV,1)*RY
     1 +DVDR(KV))-P(KV,JV,1)
      TAURR(KV)=SMU(KV)*DVDR(KV)+RLMBD(KV)*(V(KV,JV,1)*RY
     1 +DUDX(KV))-P(KV,JV,1)
      TAUXR(KV)=RMU(KV)*(ETY(KV,JV,1)*UET(KV)+
     1 ZTX(KV,JV,1)*VZT(KV))
C
 3    CONTINUE
C
      IF(JV.NE.J) GO TO 20
C
      DO 10 KV=2,KLM
C
      RY=1.0/Y(KV,J,1)
C
      DUDX(KV)=ZTX(KV,J,1)*(U(KV+1,J,1)-U(KV-1,J,1))*RDZT
      DVDR(KV)=ETY(KV,J,1)*(V(KV,J+1,1)-V(KV,J-1,1))*(0.5*RDET)
C
      H(KV)=(SMU(KV)*V(KV,J,1)*RY+RLMBD(KV)*(DUDX(KV)
     1 +DVDR(KV))-P(KV,J,1))*RY
C
 10   CONTINUE
C
C
C     GENERATING THE HEAT FLUX TERMS
C
 20   DO 4 KV=2,KLM
C
      TX(KV)=ZTX(KV,JV,1)*TZT(KV)
      TY(KV)=ETY(KV,JV,1)*TET(KV)
C
 4    CONTINUE
C
C     GENERATING THE FLUX TERMS
C
      DO 5 KV=2,KLM
C
C
      G21(KV,M)=R(KV,JV,1)*V(KV,JV,1)*Y(KV,JV,1)
      G22(KV,M)=G21(KV,M)*U(KV,JV,1)-TAUXR(KV)*Y(KV,JV,1)
      G23(KV,M)=G21(KV,M)*V(KV,JV,1)-TAURR(KV)*Y(KV,JV,1)
      G25(KV,M)=G21(KV,M)*(CV*T(KV,JV,1)+0.5*(U(KV,JV,1)**2+
     1 V(KV,JV,1)**2))-(RK(KV)*TY(KV)
     2 +(U(KV,JV,1)*TAUXR(KV)+V(KV,JV,1)*TAURR(KV)))*Y(KV,JV,1)
C
 5    CONTINUE
```

```
C
 1     CONTINUE
       RETURN
       END
       SUBROUTINE LZETA(J)
       COMMON / / DETA,DZETA,CV,RC,PR,PRT,GAMMA,EP(96,25,1),DTL(25),
      1 GAMM1,CFL,BETA,UINF,VINF,RHOINF,CINF,TINF,PINF,TW,DT,CX,CY,L,
      2 JL,KL,JLM,KLM,ILE,ISMTHX,ISMTHY,GAMM2,RL,TMS1
       COMMON /FLUZT/ F31(96),F32(96),F33(96),F35(96)
       COMMON /DV/ R(96,25,1),U(96,25,1),V(96,25,1),W(1,1,1),
      1 P(96,25,1),T(96,25,1)
       COMMON /TV/ ETY(96,25,1),ZTX(96,25,1)
       COMMON /DOF/ X(96,25,1),Y(96,25,1)
       DIMENSION UET(96),UZT(96),VET(96),VZT(96),RMU(96),
      1 RLMBD(96),SMU(96),RK(96),TAUXX(96),TAUXR(96),
      2 TAURR(96),TX(96),TY(96),TET(96),TZT(96),DUDX(96),
      3 DVDR(96)
C
       RDET=1.0/(2.0*DETA)
       RDZT=1.0/DZETA
       JP=J+1
       JM=J-1
C
       DO 1 KK=1,KLM
C
C
C      FORWARD & BACKWARD DIFFERENCING FOR PREDICTOR & CORRECTOR
C
C      *********
       KV=KK+L-1
       KM=KK
       KP=KM+1
C      *********
C
C      GENERATING THE SHEAR STRESS & HEAT FLUX TERMS
C
       UET(KK)=(U(KV,JP,1)-U(KV,JM,1))*RDET
       VET(KK)=(V(KV,JP,1)-V(KV,JM,1))*RDET
       TET(KK)=(T(KV,JP,1)-T(KV,JM,1))*RDET
C
       UZT(KK)=(U(KP,J,1)-U(KM,J,1))*RDZT
       VZT(KK)=(V(KP,J,1)-V(KM,J,1))*RDZT
       TZT(KK)=(T(KP,J,1)-T(KM,J,1))*RDZT
C
C      GENERATING THE VISCOSITY COEFFS & HEAT CONDUCTIVITY
C
       RMU(KK)=2.27E-08*SQRT(T(KV,J,1)**3)/(T(KV,J,1)+198.6)
       RK(KK)=GAMMA*CV*(RMU(KK)/PR+EP(KV,J,1)/PRT)
       RMU(KK)=RMU(KK)+EP(KV,J,1)
       RLMBD(KK)=-(2.0/3.0)*RMU(KK)
       SMU(KK)=2.0*RMU(KK)+RLMBD(KK)
C
 1     CONTINUE
```

```
C
      DO 2 KK=1,KLM
C
      KV=KK+L-1
C
      RY=1.0/Y(KV,J,1)
C
      DUDX(KK)=ZTX(KV,J,1)*UZT(KK)
      DVDR(KK)=ETY(KV,J,1)*VET(KK)
C
      TAUXX(KK)=SMU(KK)*DUDX(KK)+RLMBD(KK)*(V(KV,J,1)*RY
     1 +DVDR(KK))-P(KV,J,1)
      TAURR(KK)=SMU(KK)*DVDR(KK)+RLMBD(KK)*(V(KV,J,1)*RY
     1 +DUDX(KK))-P(KV,J,1)
      TAUXR(KK)=RMU(KK)*(ETY(KV,J,1)*UET(KK)+
     1 ZTX(KV,J,1)*VZT(KK))
C
C     GENERATING THE HEAT FLUX TERMS
C
      TX(KK)=ZTX(KV,J,1)*TZT(KK)
      TY(KK)=ETY(KV,J,1)*TET(KK)
C
    2 CONTINUE
C
C
C     GENERATING THE FLUX TERMS
C
      DO 3 KK=1,KLM
C
      KV=KK+L-1
C
      F31(KK)=R(KV,J,1)*U(KV,J,1)
      F32(KK)=F31(KK)*U(KV,J,1)-TAUXX(KK)
      F33(KK)=F31(KK)*V(KV,J,1)-TAUXR(KK)
      F35(KK)=F31(KK)*(CV*T(KV,J,1)+0.5*(U(KV,J,1)**2+
     1 V(KV,J,1)**2))-RK(KK)*TX(KK)
     2 -(U(KV,J,1)*TAUXX(KK)+V(KV,J,1)*TAUXR(KK))
C
C
    3 CONTINUE
      RETURN
      END
```

```
      SUBROUTINE SUM(J)
      COMMON / / DETA,DZETA,CV,RC,PR,PRT,GAMMA,EP(96,25,1),DTL(25),
     1 GAMM1,CFL,BETA,JINF,VINF,RHOINF,CINF,TINF,PINF,TW,DT,CX,CY,L,
     2 JL,KL,JLM,KLM,ILE,ISMTHX,ISMTHY,GAMM2,RL,TMS1
      COMMON /FLUET/
     1 G21(96,2),G22(96,2),G23(96,2),G25(96,2),H(96)
      COMMON /FLUZT/ F31(96),F32(96),F33(96),F35(96)
      COMMON /TV/ ETY(96,25,1),ZTX(96,25,1)
      COMMON /DEP/ RHO(96,25,1),RHOU(96,25,1),RHOV(96,25,1),
     1 RHOE(96,25,1)
      COMMON /DEPP/ RHOP(96,25,1),RHOUP(96,25,1),RHOVP(96,25,1),
     1 RHOEP(96,25,1)
      COMMON /DAMP/ ADD1(96),ADD2(96),ADD3(96),ADD5(96)
      COMMON /DOF/ X(96,25,1),Y(96,25,1)
C
      IF(BETA.NE.0.0) DT=DTL(J)
      RDET=1.0/DETA
      RDZT=1.0/DZETA
C
      IF(L.EQ.2) GO TO 100
C
C                         ****************
C                         PREDICTOR SWEEPS
C                         ****************
C
      DO 1 KV=2,KLM
C
      KM=KV-1
      RY=1.0/Y(KV,J,1)
C
      RHOP(KV,J,1)=RHO(KV,J,1)-DT*((
     1 +ETY(KV,J,1)*RY*(G21(KV,2)-G21(KV,1)))*RDET+(ZTX(KV,J,1)*
     2 (F31(KV)-F31(KM)))*RDZT)
C
      RHOUP(KV,J,1)=RHOU(KV,J,1)-DT*((
     1 +ETY(KV,J,1)*RY*(G22(KV,2)-G22(KV,1)))*RDET+(ZTX(KV,J,1)*
     2 (F32(KV)-F32(KM)))*RDZT)
C
    1 CONTINUE
C
      DO 2 KV=2,KLM
C
      KM=KV-1
      RY=1.0/Y(KV,J,1)
C
      RHOVP(KV,J,1)=RHOV(KV,J,1)-DT*((
     1 +ETY(KV,J,1)*RY*(G23(KV,2)-G23(KV,1)))*RDET+(ZTX(KV,J,1)*
     2 (F33(KV)-F33(KM)))*RDZT+H(KV))
C
      RHOEP(KV,J,1)=RHOE(KV,J,1)-DT*((
     1 +ETY(KV,J,1)*RY*(G25(KV,2)-G25(KV,1)))*RDET+(ZTX(KV,J,1)*
     2 (F35(KV)-F35(KM)))*RDZT)
C
    2 CONTINUE
```

```
C
      IF((ISMTHX.EQ.0).AND.(ISMTHY.EQ.0)) GO TO 200
C
      CALL DAMPING(J)
C
      DO 10 KV=2,KLM
C
      RHOP (KV,J,1)=RHOP (KV,J,1)+ADD1(KV)
      RHOUP(KV,J,1)=RHOUP(KV,J,1)+ADD2(KV)
      RHOVP(KV,J,1)=RHOVP(KV,J,1)+ADD3(KV)
      RHOEP(KV,J,1)=RHOEP(KV,J,1)+ADD5(KV)
 10   CONTINUE
C
      GO TO 200
C
C                          ****************
C                          CORRECTOR SWEEPS
C                          ****************
 100  DO 3 KV=2,KLM
C
      KM=KV-1
      RY=1.0/Y(KV,J,1)
C
      RHO(KV,J,1)=0.5*(RHO(KV,J,1)+RHOP(KV,J,1)-DT*((
     1 ETY(KV,J,1)*RY*(G21(KV,2)-G21(KV,1)))*RDET
     2 +(ZTX(KV,J,1)*(F31(KV)-F31(KM)))
     3 *RDZT))
C
      RHOU(KV,J,1)=0.5*(RHOU(KV,J,1)+RHOUP(KV,J,1)-DT*((
     1 ETY(KV,J,1)*RY*(G22(KV,2)-G22(KV,1)))*RDET
     2 +(ZTX(KV,J,1)*(F32(KV)-F32(KM)))
     3 *RDZT))
C
 3    CONTINUE
C
      DO 4 KV=2,KLM
C
      KM=KV-1
      RY=1.0/Y(KV,J,1)
C
      RHOV(KV,J,1)=0.5*(RHOV(KV,J,1)+RHOVP(KV,J,1)-DT*((
     1 ETY(KV,J,1)*RY*(G23(KV,2)-G23(KV,1)))*RDET
     2 +(ZTX(KV,J,1)*(F33(KV)-F33(KM)))
     3 *RDZT+H(KV)))
C
      RHOE(KV,J,1)=0.5*(RHOE(KV,J,1)+RHOEP(KV,J,1)-DT*((
     1 ETY(KV,J,1)*RY*(G25(KV,2)-G25(KV,1)))*RDET
     2 +(ZTX(KV,J,1)*(F35(KV)-F35(KM)))
     3 *RDZT))
C
 4    CONTINUE
```

```
C
      IF((ISMTHX.EQ.0).AND.(ISMTHY.EQ.0)) GO TO 200
C
      CALL DAMPING(J)
C
      DO 20 KV=2,KLM
C
      RHO (KV,J,1)=RHO (KV,J,1)+ADD1(KV)
      RHOU(KV,J,1)=RHOU(KV,J,1)+ADD2(KV)
      RHOV(KV,J,1)=RHOV(KV,J,1)+ADD3(KV)
      RHOE(KV,J,1)=RHOE(KV,J,1)+ADD5(KV)
C
 20   CONTINUE
C
 200  RETURN
      END
      SUBROUTINE DAMPING(J)
      COMMON / / DETA,DZETA,CV,RC,PR,PRT,GAMMA,EP(96,25,1),DTL(25),
     1 GAMM1,CFL,BETA,UINF,VINF,RHOINF,CINF,TINF,PINF,TW,DT,CX,CY,L,
     2 JL,KL,JLM,KLM,ILE,ISMTHX,ISMTHY,GAMM2,RL,TMS1
      COMMON /DEP/ RHO(96,25,1),RHOU(96,25,1),RHOV(96,25,1),
     1 RHOE(96,25,1)
      COMMON /DEPP/ RHOP(96,25,1),RHOUP(96,25,1),RHOVP(96,25,1),
     1 RHOEP(96,25,1)
      COMMON /DAMP/ ADD1(96),ADD2(96),ADD3(96),ADD5(96)
      COMMON /DV/ R(96,25,1),U(96,25,1),V(96,25,1),W(1,1,1),
     1 P(96,25,1),T(96,25,1)
      COMMON /TV/ ETY(96,25,1),ZTX(96,25,1)
      DIMENSION ADDG1(96),ADDG2(96),ADDG3(96),
     2 ADDG5(96),ADDH1(96),ADDH2(96),ADDH3(96),
     3 ADDH5(96),PD(96,2)
C
      KLM2=KLM-1
      GAMMR=GAMMA*RC
      RDET=1.0/DETA
      RDZT=1.0/DZETA
C
C     SET DAMPING TERMS TO ZERO FOR END POINTS
C
      DO 1 KV=1,KL
C
      ADDG1(KV)=0.0
      ADDG2(KV)=0.0
      ADDG3(KV)=0.0
      ADDG5(KV)=0.0
C
      ADDH1(KV)=0.0
      ADDH2(KV)=0.0
      ADDH3(KV)=0.0
      ADDH5(KV)=0.0
C
 1    CONTINUE
```

```
C
C           *** GENERATING ADDG ***
C
       IF((J.LE.2).OR.(J.GE.JLM)) GO TO 200
C
      DO 110 M=1,2
C
      JV=J+M+L-3
      JP=JV+1
      JM=JV-1
C
      DO 120 KV=1,KL
      PD(KV,M)=CY*(ABS(P(KV,JP,1)-2.0*P(KV,JV,1)+
     1 P(KV,JM,1))/(P(KV,JP,1)+2.0*P(KV,JV,1)+P(KV,JM,1)))*
     2 (ABS(+ETY(KV,JV,1)*V(KV,JV,1))+
     3 SQRT(GAMMR*T(KV,JV,1)*(ETY(KV,JV,1)**2)))
 120  CONTINUE
 110  CONTINUE
C
      IF(L.EQ.2) GO TO 140
C
C                 PREDICTOR
C
      JP=J+1
      JM=J-1
C
      DO 130 KV=1,KL
C
      ADDG1(KV)=DT*(PD(KV,2)*(RHO (KV,JP,1)-RHO (KV,J,1))-
     1 PD(KV,1)*(RHO (KV,J,1)-RHO (KV,JM,1)))*RDET
      ADDG2(KV)=DT*(PD(KV,2)*(RHOU(KV,JP,1)-RHOU(KV,J,1))-
     1 PD(KV,1)*(RHOU(KV,J,1)-RHOU(KV,JM,1)))*RDET
      ADDG3(KV)=DT*(PD(KV,2)*(RHOV(KV,JP,1)-RHOV(KV,J,1))-
     1 PD(KV,1)*(RHOV(KV,J,1)-RHOV(KV,JM,1)))*RDET
      ADDG5(KV)=DT*(PD(KV,2)*(RHOE(KV,JP,1)-RHOE(KV,J,1))-
     1 PD(KV,1)*(RHOE(KV,J,1)-RHOE(KV,JM,1)))*RDET
C
 130  CONTINUE
C
      GO TO 200
C
```

```
C                  CORRECTOR
 140   JP=J+1
       JM=J-1
C
       DO 150 KV=1,KL
C
       ADDG1(KV)=DT*(PD(KV,2)*(RHOP (KV,JP,1)-RHOP (KV,J,1))-
     1 PD(KV,1)*(RHOP (KV,J,1)-RHOP (KV,JM,1)))*RDET
       ADDG2(KV)=DT*(PD(KV,2)*(RHOUP(KV,JP,1)-RHOUP(KV,J,1))-
     1 PD(KV,1)*(RHOUP(KV,J,1)-RHOUP(KV,JM,1)))*RDET
       ADDG3(KV)=DT*(PD(KV,2)*(RHOVP(KV,JP,1)-RHOVP(KV,J,1))-
     1 PD(KV,1)*(RHOVP(KV,J,1)-RHOVP(KV,JM,1)))*RDET
       ADDG5(KV)=DT*(PD(KV,2)*(RHOEP(KV,JP,1)-RHOEP(KV,J,1))-
     1 PD(KV,1)*(RHOEP(KV,J,1)-RHOEP(KV,JM,1)))*RDET
C
 150   CONTINUE
C
C
C                  *** GENERATING ADDH ***
C
 200   DO 210 M=1,2
       DO 220 K=3,KLM2
C
       KV=K+M+L-3
       KP=KV+1
       KM=KV-1
C
       PD(K,M)=CX*(ABS(P(KP,J,1)-2.0*P(KV,J,1)+
     1 P(KM,J,1))/(P(KP,J,1)+2.0*P(KV,J,1)+P(KM,J,1)))*
     2 (ABS(ZTX(KV,J,1)*U(KV,J,1))+
     3 SQRT(GAMMR*T(KV,J,1)*(ZTX(KV,J,1)**2)))
C
 220   CONTINUE
 210   CONTINUE
C
       IF(L.EQ.2) GO TO 240
C
C                  PREDICTOR
C
       DO 230 KV=3,KLM2
C
       KP=KV+1
       KM=KV-1
C
       ADDH1(KV)=DT*(PD(KV,2)*(RHO (KP,J,1)-RHO (KV,J,1))-
     1 PD(KV,1)*(RHO (KV,J,1)-RHO (KM,J,1)))*RDZT
       ADDH2(KV)=DT*(PD(KV,2)*(RHOU(KP,J,1)-RHOU(KV,J,1))-
     1 PD(KV,1)*(RHOU(KV,J,1)-RHOU(KM,J,1)))*RDZT
       ADDH3(KV)=DT*(PD(KV,2)*(RHOV(KP,J,1)-RHOV(KV,J,1))-
     1 PD(KV,1)*(RHOV(KV,J,1)-RHOV(KM,J,1)))*RDZT
       ADDH5(KV)=DT*(PD(KV,2)*(RHOE(KP,J,1)-RHOE(KV,J,1))-
     1 PD(KV,1)*(RHOE(KV,J,1)-RHOE(KM,J,1)))*RDZT
C
 230   CONTINUE
```

```
C
      GO TO 300
C
C                CORRECTOR
C
 240  DO 250 KV=3,KLM2
C
      KP=KV+1
      KM=KV-1
C
      ADDH1(KV)=DT*(PD(KV,2)*(RHOP (KP,J,1)-RHOP (KV,J,1))-
     1 PD(KV,1)*(RHOP (KV,J,1)-RHOP (KM,J,1)))*RDZT
      ADDH2(KV)=DT*(PD(KV,2)*(RHOUP(KP,J,1)-RHOUP(KV,J,1))-
     1 PD(KV,1)*(RHOUP(KV,J,1)-RHOUP(KM,J,1)))*RDZT
      ADDH3(KV)=DT*(PD(KV,2)*(RHOVP(KP,J,1)-RHOVP(KV,J,1))-
     1 PD(KV,1)*(RHOVP(KV,J,1)-RHOVP(KM,J,1)))*RDZT
      ADDH5(KV)=DT*(PD(KV,2)*(RHOEP(KP,J,1)-RHOEP(KV,J,1))-
     1 PD(KV,1)*(RHOEP(KV,J,1)-RHOEP(KM,J,1)))*RDZT
C
 250  CONTINUE
C
C
C     SUMMING THE ARTIFICIAL VISCOSITY-LIKE TERMS
C
 300  DO 310 KV=1,KL
C
      ADD1(KV)=ISMTHX*ADDG1(KV)+ISMTHY*ADDH1(KV)
      ADD2(KV)=ISMTHX*ADDG2(KV)+ISMTHY*ADDH2(KV)
      ADD3(KV)=ISMTHX*ADDG3(KV)+ISMTHY*ADDH3(KV)
      ADD5(KV)=ISMTHX*ADDG5(KV)+ISMTHY*ADDH5(KV)
C
 310  CONTINUE
C
      RETURN
      END
      SUBROUTINE EDDY
      COMMON / / DETA,DZETA,CV,RC,PR,PRT,GAMMA,EP(96,25,1),DTL(25),
     1 GAMM1,CFL,BETA,UINF,VINF,RHOINF,CINF,TINF,PINF,TW,DT,CX,CY,L,
     2 JL,KL,JLM,KLM,ILE,ISMTHX,ISMTHY,GAMM2,RL,TMS1
      COMMON /DEP/ RHO(96,25,1),RHOU(96,25,1),RHOV(96,25,1),
     1 RHOE(96,25,1)
      COMMON /DOF/ X(96,25,1),Y(96,25,1)
      COMMON /TV/ ETY(96,25,1),ZTX(96,25,1)
      COMMON /DV/ R(96,25,1),U(96,25,1),V(96,25,1),W(1,1,1),
     1 P(96,25,1),T(96,25,1)
      DIMENSION F(96,30),JMAX(96),OMEGA(96,30),SL(96,30),
     1 EPMAX(96),UET(96,30),VET(96,30),UZT(96,30),VZT(96,30),
     2 APLUS(96)
C
      RMU=2.270E-08*SQRT(TINF**3)/(TINF+198.6)
      K3=KL/2
```

```
C
      DO 3 J=1,JL
      DO 3 K=1,KL
      RR=1.0/RHO(K,J,1)
      U(K,J,1)=RHOU(K,J,1 )*RR
      V(K,J,1)=RHOV(K,J,1 )*RR
  3   CONTINUE
C
C     GENERATING THE DERIVATIVES OF VELOCITY
C
      RDET=1.0/(2.0*DETA)
      RDZT=1.0/(2.0*DZETA)
C
      DO 4 J=2,JLM
      DO 4 K=2,KLM
      UET(K,J)=(U(K,J+1,1 )-U(K,J-1,1 ))*RDET
      VET(K,J)=(V(K,J+1,1 )-V(K,J-1,1 ))*RDET
      UZT(K,J)=(U(K+1,J,1 )-U(K-1,J,1 ))*RDZT
      VZT(K,J)=(V(K+1,J,1 )-V(K-1,J,1 ))*RDZT
  4   CONTINUE
C
C     GENERATING THE VORTICITY DISTRIBUTION
C
      DO 5 J=2,JLM
      DO 5 K=2,KLM
      OMEGA(K,J)=SQRT(
     1 (ZTX(K,J,1)*VZT(K,J)
     2 -ETY(K,J,1)*UET(K,J))**2)
  5   CONTINUE
C
C     GENERATING THE SCALING LEAGTH
C
      DO 6 J=1,JL
      DO 6 K=1,KL
      SL(K,J)=SQRT((Y(K,J,1)-Y(K,1,1))**2+(X(K,J,1)-X(K,1,1))**2)
  6   CONTINUE
C
C     GENERATING THE SURFACE VORTICITY AND THE INJECTION/SUCTION A+
C
      RDET=1.0/DETA
C
      DO 7 K=2,KLM
      OMEGA(K,1)=SQRT((-ETY(K,1,1)*
     1 (U(K,2,1)-U(K,1,1)))**2)*RDET
C     TAU = RMU*OMEGA(K,1 )
C     UTAU=SQRT(TAU/RHO(K,1,1))
C     DPDX=(P(K+1,1,1)-P(K-1,1,1))*RDZT*ZTX(K,1,1)
C     PPLUS=RMU/RHO(K,1,1 )**2/UTAU**3*DPDX
C     VPLUS=-V(K,1,1)/UTAU
      APLUS(K)=26.0
  7   CONTINUE
```

```
C
C     GENERATING THE INNER VISCOSITY COEFFICIENT
C
      DO 8 J=2,JLM
      DO 8 K=2,KLM
C
C     SUPRESS THE UNDERFLOW MESSAGE FROM EXPONENTIAL CALCULATIONS
C
      YPB=SQRT(RHO(K,1,1)*OMEGA(K,1)/RMU)*SL(K,J)/APLUS(K)
      YPB=AMIN1(YPB,50.0)
      EP(K,J,1)=RHO(K,J,1)*(0.40*SL(K,J)*(1.0-EXP(-YPB)))**2*OMEGA(K,J)
      F(K,J)=SL(K,J)*(1.0-EXP(-YPB))*OMEGA(K,J)
C
    8 CONTINUE
C
C     THE BALDWIN-LOMAX MODEL WITH INTERMITTENCY CORRECTION
C
C     SEARCH THE MAX. EDDY VISCOSITY COEFF. FOR A J ARRAY
C
      DO 9 K=2,KLM
C
      DU2MAX=0.0
      FMAX=0.0
C
      DO 10 J=2,JLM
C
      DU2=U(K,J,1)**2+V(K,J,1)**2
      DU2MAX=AMAX1(DU2,DU2MAX)
      FMAX=AMAX1(F(K,J),FMAX)
C
   10 CONTINUE
C
      JMAX(K)=0
      DO 40 J=2,JLM
      IF(JMAX(K).NE.0) GO TO 40
      IF(F(K,J).EQ.FMAX) JMAX(K)=J
   40 CONTINUE
C
      F1=1.0E+20
      FWAKE=SL(K,JMAX(K))*F(K,JMAX(K))
      IF (F(K,JMAX(K)) .EQ. 0.0) GO TO 41
      F1=0.25*SL(K,JMAX(K))*DU2MAX/F(K,JMAX(K))
   41 FWAKE=AMIN1(FWAKE,F1)
      EPMAX(K)=0.0336*RHO(K,JMAX(K),1)*FWAKE
C
    9 CONTINUE
```

```
C
C     SET THE MAX EDDY VISCOSITY FOR THE OUTER REGION
C
      DO 11 K=2,KLM
C
      ISWTH=0
C
      XXTT=1.00
      XBAR2=((X(K,1,1)-XXTT)/0.10)**2
      DO 12 J=2,JLM
C
      IF(EPMAX(K).LE.EP(K,J,1)) ISWTH=1
      IF(ISWTH.EQ.1) EP(K,J,1)=EPMAX(K)*RHO(K,J,1)/RHO(K,JMAX(K),1)
      EP(K,J,1)=EP(K,J,1)/(1.0+5.5*(0.3*SL(K,J)/SL(K,JMAX(K)))**6)
C
C     ACCOUNT FOR THE TRANSITION FROM LAMINAR TO TURBULENT FLOW
C
      EP(K,J,1)=EP(K,J,1)*(1.0-EXP(-0.412*XBAR2))
      IF (X(K,J,1) .LT. XXTT) EP(K,J,1)=0.0
C
 12   CONTINUE
 11   CONTINUE
C
C     COMPLETE THE EDDY VISCOSITY MATRIX
C
      EP(1,JLM,1)=EP(2,JLM,1)
      EP(KL,JLM,1)=EP(KLM,JLM,1)
C
      DO 20 K=1,KL
      EP(K,1,1)=0.0
 20   EP(K,JL,1)=EP(K,JLM,1)
C
      DO 30 J=1,JL
      EP(KL,J,1)=EP(KLM,J,1)
 30   EP(1,J,1)=EP(2,J,1)
C
      RETURN
      END
```

APPENDIX C: Raw Numerical Friction Coefficient Data

This Appendix contains the raw friction coefficient data discussed in Chapter VI. The table of data contains the following information 1) axial location (Z/L), 2) local axial Reynolds number (RE), 3) friction coefficient (F), 4) Mach number squared (MA2), 5) blowing parameter (V/U), and 6) the momentum flux factor (PHI). The pipe size and external manifold pressures can be determined from the table headings. The radial Reynolds number at any location can be found by multiplying the location's axial Reynolds number times the location's blowing parameter.

PIPE LENGTH = 2 FEET, INSIDE DIAMETER = 2 INCHES
SOURCE PRESSURE = 30 PSIA, SINK PRESSURE = 15 PSIA

Z/L	RE	F	MA2	V/U	PHI
.1053E-01	.2700E+04	.1047E-01	.2119E-05	-.4319E+01	.1271E+01
.2105E-01	.5541E+04	.6954E-02	.9101E-05	-.2077E+01	.1232E+01
.3158E-01	.8776E+04	.2340E-02	.2254E-04	-.1323E+01	.1235E+01
.4211E-01	.1227E+05	.1832E-02	.4405E-04	-.9466E+00	.1230E+01
.5263E-01	.1604E+05	.1381E-02	.7519E-04	-.7248E+00	.1229E+01
.6316E-01	.2016E+05	.9528E-03	.1191E-03	-.5757E+00	.1229E+01
.7368E-01	.2464E+05	.8583E-03	.1779E-03	-.4713E+00	.1228E+01
.8421E-01	.2953E+05	.6903E-03	.2558E-03	-.3932E+00	.1229E+01
.9474E-01	.3488E+05	.5735E-03	.3567E-03	-.3332E+00	.1229E+01
.1053E+00	.4072E+05	.4965E-03	.4864E-03	-.2856E+00	.1230E+01
.1158E+00	.4717E+05	.4294E-03	.6527E-03	-.2468E+00	.1230E+01
.1263E+00	.5367E+05	.3748E-03	.8450E-03	-.2172E+00	.1230E+01
.1368E+00	.6014E+05	.3342E-03	.1061E-02	-.1941E+00	.1231E+01
.1474E+00	.6663E+05	.3011E-03	.1304E-02	-.1754E+00	.1231E+01
.1579E+00	.7309E+05	.2744E-03	.1570E-02	-.1601E+00	.1231E+01
.1684E+00	.7960E+05	.2520E-03	.1864E-02	-.1472E+00	.1231E+01
.1789E+00	.8606E+05	.2333E-03	.2182E-02	-.1364E+00	.1231E+01
.1895E+00	.9261E+05	.2169E-03	.2529E-02	-.1269E+00	.1231E+01
.2000E+00	.9912E+05	.2026E-03	.2893E-02	-.1188E+00	.1231E+01
.2105E+00	.1057E+06	.1903E-03	.3300E-02	-.1117E+00	.1231E+01
.2211E+00	.1122E+06	.1792E-03	.3725E-02	-.1054E+00	.1231E+01
.2316E+00	.1189E+06	.1693E-03	.4182E-02	-.9976E-01	.1230E+01
.2421E+00	.1254E+06	.1604E-03	.4661E-02	-.9480E-01	.1230E+01
.2526E+00	.1321E+06	.1525E-03	.5177E-02	-.9023E-01	.1230E+01
.2632E+00	.1387E+06	.1452E-03	.5713E-02	-.8621E-01	.1230E+01
.2737E+00	.1454E+06	.1387E-03	.6290E-02	-.8243E-01	.1230E+01
.2842E+00	.1520E+06	.1326E-03	.6883E-02	-.7912E-01	.1230E+01
.2947E+00	.1588E+06	.1273E-03	.7525E-02	-.7594E-01	.1229E+01
.3053E+00	.1654E+06	.1221E-03	.8176E-02	-.7318E-01	.1230E+01
.3158E+00	.1723E+06	.1175E-03	.8886E-02	-.7046E-01	.1229E+01
.3263E+00	.1788E+06	.1130E-03	.9596E-02	-.6814E-01	.1229E+01
.3368E+00	.1858E+06	.1091E-03	.1038E-01	-.6578E-01	.1229E+01
.3474E+00	.1923E+06	.1052E-03	.1115E-01	-.6381E-01	.1229E+01
.3579E+00	.1995E+06	.1018E-03	.1201E-01	-.6173E-01	.1228E+01
.3684E+00	.2060E+06	.9829E-04	.1285E-01	-.6006E-01	.1229E+01
.3789E+00	.2133E+06	.9550E-04	.1380E-01	-.5820E-01	.1228E+01
.3895E+00	.2197E+06	.9223E-04	.1469E-01	-.5679E-01	.1228E+01
.4000E+00	.2272E+06	.8989E-04	.1574E-01	-.5509E-01	.1227E+01
.4105E+00	.2336E+06	.8684E-04	.1669E-01	-.5391E-01	.1228E+01
.4211E+00	.2414E+06	.8492E-04	.1785E-01	-.5234E-01	.1227E+01
.4316E+00	.2476E+06	.8208E-04	.1884E-01	-.5137E-01	.1227E+01
.4421E+00	.2557E+06	.8051E-04	.2014E-01	-.4989E-01	.1226E+01
.4526E+00	.2616E+06	.7799E-04	.2117E-01	-.4912E-01	.1226E+01
.4632E+00	.2702E+06	.7670E-04	.2261E-01	-.4770E-01	.1225E+01
.4737E+00	.2757E+06	.7570E-04	.2366E-01	-.4714E-01	.1224E+01
.4842E+00	.2848E+06	.7690E-04	.2526E-01	-.4576E-01	.1218E+01
.4947E+00	.2898E+06	.7839E-04	.2625E-01	-.2271E-01	.1214E+01

.5158E+00	.2893E+06	.9424E-04	.2614E-01	.4009E-01	.1208E+01
.5263E+00	.2798E+06	.3015E-02	.2431E-01	.4191E-01	.1212E+01
.5368E+00	.2754E+06	.4937E-02	.2357E-01	.4255E-01	.1201E+01
.5474E+00	.2664E+06	.8117E-02	.2192E-01	.4441E-01	.1197E+01
.5579E+00	.2614E+06	.1209E-01	.2109E-01	.4527E-01	.1185E+01
.5684E+00	.2530E+06	.1647E-01	.1965E-01	.4714E-01	.1178E+01
.5789E+00	.2475E+06	.2086E-01	.1880E-01	.4822E-01	.1169E+01
.5895E+00	.2395E+06	.2499E-01	.1753E-01	.5013E-01	.1163E+01
.6000E+00	.2338E+06	.2873E-01	.1668E-01	.5143E-01	.1155E+01
.6105E+00	.2261E+06	.3234E-01	.1555E-01	.5344E-01	.1151E+01
.6211E+00	.2201E+06	.3550E-01	.1472E-01	.5497E-01	.1145E+01
.6316E+00	.2127E+06	.3843E-01	.1370E-01	.5713E-01	.1142E+01
.6421E+00	.2064E+06	.4155E-01	.1289E-01	.5894E-01	.1138E+01
.6526E+00	.1991E+06	.4486E-01	.1197E-01	.6132E-01	.1136E+01
.6632E+00	.1927E+06	.4777E-01	.1120E-01	.6345E-01	.1133E+01
.6737E+00	.1856E+06	.5051E-01	.1036E-01	.6609E-01	.1131E+01
.6842E+00	.1790E+06	.5342E-01	.9632E-02	.6861E-01	.1129E+01
.6947E+00	.1720E+06	.5645E-01	.8868E-02	.7162E-01	.1129E+01
.7053E+00	.1654E+06	.5952E-01	.8189E-02	.7460E-01	.1128E+01
.7158E+00	.1584E+06	.6263E-01	.7495E-02	.7809E-01	.1128E+01
.7263E+00	.1516E+06	.6544E-01	.6863E-02	.8168E-01	.1128E+01
.7368E+00	.1446E+06	.6921E-01	.6232E-02	.8583E-01	.1130E+01
.7474E+00	.1379E+06	.7416E-01	.5659E-02	.9014E-01	.1131E+01
.7579E+00	.1309E+06	.7889E-01	.5095E-02	.9510E-01	.1134E+01
.7684E+00	.1242E+06	.8201E-01	.4580E-02	.1004E+00	.1137E+01
.7789E+00	.1173E+06	.8498E-01	.4079E-02	.1065E+00	.1142E+01
.7895E+00	.1106E+06	.8852E-01	.3622E-02	.1131E+00	.1148E+01
.8000E+00	.1038E+06	.9330E-01	.3179E-02	.1208E+00	.1157E+01
.8105E+00	.9716E+05	.9583E-01	.2776E-02	.1293E+00	.1170E+01
.8211E+00	.9022E+05	.8680E-01	.2400E-02	.1390E+00	.1203E+01
.8316E+00	.8328E+05	.8305E-01	.2039E-02	.1509E+00	.1254E+01
.8421E+00	.7651E+05	.9089E-01	.1715E-02	.1645E+00	.1283E+01
.8526E+00	.6992E+05	.7023E-01	.1430E-02	.1801E+00	.1330E+01
.8632E+00	.6302E+05	.7708E-02	.1159E-02	.2000E+00	.1389E+01
.8737E+00	.5678E+05	.5983E-02	.9405E-03	.2211E+00	.1535E+01
.8842E+00	.5143E+05	.6312E-01	.7732E-03	.2421E+00	.1818E+01
.8947E+00	.4543E+05	-.1635E-01	.6054E-03	.2733E+00	.2180E+01
.9053E+00	.3919E+05	-.1629E+00	.4513E-03	.3161E+00	.2611E+01
.9158E+00	.3363E+05	-.2232E+00	.3333E-03	.3671E+00	.3182E+01
.9263E+00	.2814E+05	-.3284E+00	.2346E-03	.4369E+00	.3850E+01
.9368E+00	.2279E+05	-.3352E+00	.1551E-03	.5391E+00	.4310E+01
.9474E+00	.1748E+05	.6153E+00	.9218E-04	.7031E+00	.4914E+01
.9579E+00	.1245E+05	.3298E+01	.4715E-04	.9816E+00	.6945E+01
.9684E+00	.7805E+04	-.3369E+02	.1842E-04	.1558E+01	.1566E+02
.9789E+00	.3591E+04	-.2342E+03	.3983E-05	.3295E+01	.7427E+02
.9895E+00	.8592E+03	-.6394E+03	.2823E-06	.1187E+02	.5683E+03

PIPE LENGTH = 2 FEET, INSIDE DIAMETER = 2 INCHES
SOURCE PRESSURE = 45 PSIA, SINK PRESSURE = 15 PSIA

Z/L	RE	F	MA2	V/U	PHI
.1053E-01	.5252E+04	-.3415E-02	.3884E-05	-.4295E+01	.1344E+01
.2105E-01	.1088E+05	.3582E-03	.1682E-04	-.2061E+01	.1271E+01
.3158E-01	.1717E+05	.9966E-03	.4133E-04	-.1318E+01	.1243E+01
.4211E-01	.2385E+05	.7347E-03	.8020E-04	-.9453E+00	.1236E+01
.5263E-01	.3129E+05	.5672E-03	.1376E-03	-.7225E+00	.1233E+01
.6316E-01	.3922E+05	.4973E-03	.2171E-03	-.5749E+00	.1230E+01
.7368E-01	.4798E+05	.4061E-03	.3247E-03	-.4705E+00	.1230E+01
.8421E-01	.5759E+05	.3440E-03	.4675E-03	-.3924E+00	.1229E+01
.9474E-01	.6805E+05	.2942E-03	.6520E-03	-.3328E+00	.1229E+01
.1053E+00	.7937E+05	.2509E-03	.8889E-03	-.2852E+00	.1230E+01
.1158E+00	.9192E+05	.2193E-03	.1193E-02	-.2466E+00	.1229E+01
.1263E+00	.1045E+06	.1924E-03	.1545E-02	-.2171E+00	.1229E+01
.1368E+00	.1172E+06	.1712E-03	.1942E-02	-.1940E+00	.1230E+01
.1474E+00	.1298E+06	.1546E-03	.2388E-02	-.1754E+00	.1230E+01
.1579E+00	.1425E+06	.1411E-03	.2880E-02	-.1601E+00	.1230E+01
.1684E+00	.1553E+06	.1295E-03	.3423E-02	-.1473E+00	.1230E+01
.1789E+00	.1680E+06	.1199E-03	.4012E-02	-.1365E+00	.1230E+01
.1895E+00	.1807E+06	.1116E-03	.4653E-02	-.1271E+00	.1229E+01
.2000E+00	.1935E+06	.1042E-03	.5343E-02	-.1190E+00	.1229E+01
.2105E+00	.2063E+06	.9782E-04	.6088E-02	-.1119E+00	.1229E+01
.2211E+00	.2192E+06	.9217E-04	.6883E-02	-.1057E+00	.1229E+01
.2316E+00	.2320E+06	.8716E-04	.7736E-02	-.1001E+00	.1229E+01
.2421E+00	.2450E+06	.8260E-04	.8641E-02	-.9516E-01	.1229E+01
.2526E+00	.2580E+06	.7853E-04	.9610E-02	-.9065E-01	.1228E+01
.2632E+00	.2710E+06	.7483E-04	.1063E-01	-.8664E-01	.1228E+01
.2737E+00	.2842E+06	.7146E-04	.1172E-01	-.8293E-01	.1228E+01
.2842E+00	.2973E+06	.6828E-04	.1286E-01	-.7963E-01	.1228E+01
.2947E+00	.3106E+06	.6550E-04	.1408E-01	-.7652E-01	.1227E+01
.3053E+00	.3237E+06	.6289E-04	.1535E-01	-.7376E-01	.1227E+01
.3158E+00	.3372E+06	.6054E-04	.1671E-01	-.7111E-01	.1226E+01
.3263E+00	.3505E+06	.5827E-04	.1811E-01	-.6879E-01	.1226E+01
.3368E+00	.3642E+06	.5627E-04	.1962E-01	-.6650E-01	.1226E+01
.3474E+00	.3774E+06	.5431E-04	.2116E-01	-.6453E-01	.1226E+01
.3579E+00	.3914E+06	.5256E-04	.2285E-01	-.6253E-01	.1225E+01
.3684E+00	.4047E+06	.5082E-04	.2454E-01	-.6084E-01	.1225E+01
.3789E+00	.4189E+06	.4931E-04	.2641E-01	-.5907E-01	.1224E+01
.3895E+00	.4322E+06	.4772E-04	.2825E-01	-.5764E-01	.1224E+01
.4000E+00	.4468E+06	.4642E-04	.3034E-01	-.5604E-01	.1223E+01
.4105E+00	.4600E+06	.4497E-04	.3233E-01	-.5484E-01	.1223E+01
.4211E+00	.4752E+06	.4383E-04	.3467E-01	-.5337E-01	.1222E+01
.4316E+00	.4882E+06	.4254E-04	.3682E-01	-.5237E-01	.1222E+01
.4421E+00	.5041E+06	.4157E-04	.3944E-01	-.5100E-01	.1221E+01
.4526E+00	.5167E+06	.4050E-04	.4173E-01	-.5020E-01	.1221E+01
.4632E+00	.5335E+06	.3964E-04	.4469E-01	-.4890E-01	.1219E+01
.4737E+00	.5454E+06	.3941E-04	.4707E-01	-.4832E-01	.1218E+01
.4842E+00	.5633E+06	.3978E-04	.5036E-01	-.4707E-01	.1213E+01
.4947E+00	.5740E+06	.4087E-04	.5265E-01	-.2338E-01	.1209E+01

.5158E+00	.5726E+06	.4986E-04	.5239E-01	.3991E-01	.1202E+01
.5263E+00	.5540E+06	.3431E-02	.4850E-01	.4174E-01	.1206E+01
.5368E+00	.5452E+06	.5808E-02	.4696E-01	.4241E-01	.1196E+01
.5474E+00	.5275E+06	.9483E-02	.4350E-01	.4428E-01	.1192E+01
.5579E+00	.5174E+06	.1372E-01	.4177E-01	.4519E-01	.1182E+01
.5684E+00	.5010E+06	.1808E-01	.3882E-01	.4706E-01	.1176E+01
.5789E+00	.4901E+06	.2213E-01	.3705E-01	.4819E-01	.1168E+01
.5895E+00	.4745E+06	.2596E-01	.3447E-01	.5010E-01	.1164E+01
.6000E+00	.4629E+06	.2929E-01	.3272E-01	.5146E-01	.1157E+01
.6105E+00	.4481E+06	.3246E-01	.3046E-01	.5346E-01	.1153E+01
.6211E+00	.4360E+06	.3579E-01	.2876E-01	.5506E-01	.1149E+01
.6316E+00	.4216E+06	.3893E-01	.2674E-01	.5721E-01	.1146E+01
.6421E+00	.4092E+06	.4173E-01	.2511E-01	.5909E-01	.1142E+01
.6526E+00	.3950E+06	.4450E-01	.2329E-01	.6146E-01	.1140E+01
.6632E+00	.3823E+06	.4704E-01	.2174E-01	.6366E-01	.1138E+01
.6737E+00	.3682E+06	.4964E-01	.2009E-01	.6632E-01	.1137E+01
.6842E+00	.3552E+06	.5284E-01	.1864E-01	.6891E-01	.1135E+01
.6947E+00	.3412E+06	.5647E-01	.1714E-01	.7195E-01	.1135E+01
.7053E+00	.3279E+06	.5972E-01	.1580E-01	.7502E-01	.1134E+01
.7158E+00	.3140E+06	.6266E-01	.1444E-01	.7853E-01	.1134E+01
.7263E+00	.3006E+06	.6575E-01	.1320E-01	.8218E-01	.1134E+01
.7368E+00	.2868E+06	.6834E-01	.1198E-01	.8634E-01	.1135E+01
.7474E+00	.2734E+06	.6990E-01	.1086E-01	.9077E-01	.1137E+01
.7579E+00	.2598E+06	.7173E-01	.9762E-02	.9581E-01	.1140E+01
.7684E+00	.2465E+06	.7525E-01	.8754E-02	.1012E+00	.1143E+01
.7789E+00	.2329E+06	.8016E-01	.7790E-02	.1074E+00	.1148E+01
.7895E+00	.2194E+06	.8556E-01	.6897E-02	.1142E+00	.1154E+01
.8000E+00	.2058E+06	.9053E-01	.6050E-02	.1219E+00	.1162E+01
.8105E+00	.1924E+06	.9416E-01	.5270E-02	.1306E+00	.1172E+01
.8211E+00	.1789E+06	.9615E-01	.4542E-02	.1406E+00	.1187E+01
.8316E+00	.1656E+06	.9734E-01	.3875E-02	.1522E+00	.1208E+01
.8421E+00	.1524E+06	.9579E-01	.3264E-02	.1656E+00	.1235E+01
.8526E+00	.1391E+06	.7160E-01	.2706E-02	.1816E+00	.1276E+01
.8632E+00	.1258E+06	.5366E-02	.2196E-02	.2012E+00	.1332E+01
.8737E+00	.1132E+06	-.3256E-01	.1777E-02	.2222E+00	.1432E+01
.8842E+00	.1025E+06	.7918E-02	.1449E-02	.2435E+00	.1681E+01
.8947E+00	.9129E+05	-.5783E-01	.1142E-02	.2728E+00	.1941E+01
.9053E+00	.7933E+05	-.2661E+00	.8582E-03	.3142E+00	.2201E+01
.9158E+00	.6843E+05	-.4137E+00	.6386E-03	.3629E+00	.2644E+01
.9263E+00	.5813E+05	-.5706E+00	.4614E-03	.4273E+00	.3319E+01
.9368E+00	.4826E+05	-.8551E+00	.3161E-03	.5202E+00	.4078E+01
.9474E+00	.3820E+05	-.9910E+00	.1975E-03	.6637E+00	.4267E+01
.9579E+00	.2808E+05	-.2723E+00	.1057E-03	.9084E+00	.3374E+01
.9684E+00	.1843E+05	-.2386E+02	.4372E-04	.1400E+01	.3268E+01
.9789E+00	.8989E+04	-.9828E+02	.1004E-04	.2903E+01	.2496E+02
.9895E+00	.2486E+04	-.1990E+03	.8294E-06	.9941E+01	.2581E+03

PIPE LENGTH = 2 FEET, INSIDE DIAMETER = 2 INCHES
SOURCE PRESSURE = 75 PSIA, SINK PRESSURE = 15 PSIA

Z/L	RE	F	MA2	V/U	PHI
.1053E-01	.1054E+05	-.6353E-02	.5744E-05	-.4233E+01	.1343E+01
.2105E-01	.2134E+05	.6166E-03	.2419E-04	-.2052E+01	.1227E+01
.3158E-01	.3342E+05	.5681E-03	.5873E-04	-.1320E+01	.1230E+01
.4211E-01	.4669E+05	.2778E-03	.1149E-03	-.9431E+00	.1233E+01
.5263E-01	.6112E+05	.3243E-03	.1963E-03	-.7225E+00	.1227E+01
.6316E-01	.7682E+05	.2398E-03	.3103E-03	-.5748E+00	.1229E+01
.7368E-01	.9406E+05	.2024E-03	.4645E-03	-.4703E+00	.1229E+01
.8421E-01	.1126E+06	.1783E-03	.6675E-03	-.3926E+00	.1228E+01
.9474E-01	.1330E+06	.1486E-03	.9314E-03	-.3328E+00	.1229E+01
.1053E+00	.1552E+06	.1291E-03	.1270E-02	-.2853E+00	.1229E+01
.1158E+00	.1799E+06	.1123E-03	.1707E-02	-.2467E+00	.1229E+01
.1263E+00	.2046E+06	.9853E-04	.2212E-02	-.2172E+00	.1229E+01
.1368E+00	.2294E+06	.8805E-04	.2783E-02	-.1942E+00	.1230E+01
.1474E+00	.2542E+06	.7950E-04	.3424E-02	-.1756E+00	.1229E+01
.1579E+00	.2791E+06	.7242E-04	.4133E-02	-.1604E+00	.1230E+01
.1684E+00	.3040E+06	.6659E-04	.4916E-02	-.1475E+00	.1229E+01
.1789E+00	.3290E+06	.6167E-04	.5768E-02	-.1368E+00	.1229E+01
.1895E+00	.3541E+06	.5740E-04	.6699E-02	-.1274E+00	.1229E+01
.2000E+00	.3792E+06	.5361E-04	.7702E-02	-.1194E+00	.1229E+01
.2105E+00	.4044E+06	.5038E-04	.8790E-02	-.1123E+00	.1228E+01
.2211E+00	.4298E+06	.4743E-04	.9952E-02	-.1061E+00	.1228E+01
.2316E+00	.4553E+06	.4483E-04	.1121E-01	-.1005E+00	.1228E+01
.2421E+00	.4808E+06	.4250E-04	.1254E-01	-.9560E-01	.1228E+01
.2526E+00	.5061E+06	.4045E-04	.1397E-01	-.9110E-01	.1227E+01
.2632E+00	.5322E+06	.3854E-04	.1548E-01	-.8713E-01	.1227E+01
.2737E+00	.5583E+06	.3683E-04	.1710E-01	-.8344E-01	.1226E+01
.2842E+00	.5842E+06	.3519E-04	.1880E-01	-.8019E-01	.1226E+01
.2947E+00	.6106E+06	.3377E-04	.2064E-01	-.7708E-01	.1225E+01
.3053E+00	.6366E+06	.3241E-04	.2254E-01	-.7437E-01	.1225E+01
.3158E+00	.6635E+06	.3120E-04	.2461E-01	-.7173E-01	.1224E+01
.3263E+00	.6897E+06	.3002E-04	.2673E-01	-.6945E-01	.1224E+01
.3368E+00	.7171E+06	.2901E-04	.2906E-01	-.6718E-01	.1223E+01
.3474E+00	.7435E+06	.2799E-04	.3142E-01	-.6525E-01	.1223E+01
.3579E+00	.7714E+06	.2708E-04	.3404E-01	-.6327E-01	.1222E+01
.3684E+00	.7979E+06	.2618E-04	.3666E-01	-.6164E-01	.1222E+01
.3789E+00	.8266E+06	.2541E-04	.3960E-01	-.5988E-01	.1221E+01
.3895E+00	.8531E+06	.2460E-04	.4251E-01	-.5850E-01	.1221E+01
.4000E+00	.8827E+06	.2396E-04	.4584E-01	-.5692E-01	.1219E+01
.4105E+00	.9093E+06	.2325E-04	.4905E-01	-.5576E-01	.1219E+01
.4211E+00	.9400E+06	.2266E-04	.5283E-01	-.5431E-01	.1218E+01
.4316E+00	.9663E+06	.2206E-04	.5636E-01	-.5336E-01	.1217E+01
.4421E+00	.9985E+06	.2152E-04	.6067E-01	-.5202E-01	.1216E+01
.4526E+00	.1024E+07	.2106E-04	.6454E-01	-.5126E-01	.1215E+01
.4632E+00	.1058E+07	.2056E-04	.6946E-01	-.5000E-01	.1213E+01
.4737E+00	.1083E+07	.2058E-04	.7361E-01	-.4946E-01	.1211E+01
.4842E+00	.1119E+07	.2067E-04	.7908E-01	-.4832E-01	.1207E+01
.4947E+00	.1142E+07	.2148E-04	.8317E-01	-.2403E-01	.1202E+01

.5158E+00	.1140E+07	.2643E-04	.8279E-01	.3948E-01	.1196E+01
.5263E+00	.1102E+07	.4483E-02	.7626E-01	.4132E-01	.1201E+01
.5368E+00	.1086E+07	.7084E-02	.7383E-01	.4195E-01	.1190E+01
.5474E+00	.1050E+07	.1069E-01	.6804E-01	.4384E-01	.1188E+01
.5579E+00	.1031E+07	.1483E-01	.6531E-01	.4472E-01	.1178E+01
.5684E+00	.9979E+06	.1927E-01	.6040E-01	.4660E-01	.1176E+01
.5789E+00	.9766E+06	.2340E-01	.5764E-01	.4770E-01	.1168E+01
.5895E+00	.9456E+06	.2724E-01	.5346E-01	.4960E-01	.1164E+01
.6000E+00	.9228E+06	.3086E-01	.5070E-01	.5094E-01	.1159E+01
.6105E+00	.8931E+06	.3405E-01	.4706E-01	.5294E-01	.1156E+01
.6211E+00	.8693E+06	.3689E-01	.4440E-01	.5451E-01	.1151E+01
.6316E+00	.8404E+06	.3979E-01	.4117E-01	.5666E-01	.1149E+01
.6421E+00	.8158E+06	.4234E-01	.3864E-01	.5851E-01	.1146E+01
.6526E+00	.7874E+06	.4474E-01	.3576E-01	.6088E-01	.1144E+01
.6632E+00	.7622E+06	.4737E-01	.3336E-01	.6305E-01	.1142E+01
.6737E+00	.7342E+06	.4991E-01	.3078E-01	.6570E-01	.1141E+01
.6842E+00	.7085E+06	.5244E-01	.2855E-01	.6824E-01	.1140E+01
.6947E+00	.6808E+06	.5536E-01	.2622E-01	.7127E-01	.1140E+01
.7053E+00	.6548E+06	.5831E-01	.2416E-01	.7427E-01	.1139E+01
.7158E+00	.6273E+06	.6130E-01	.2207E-01	.7776E-01	.1139E+01
.7263E+00	.6010E+06	.6485E-01	.2019E-01	.8135E-01	.1139E+01
.7368E+00	.5736E+06	.6875E-01	.1831E-01	.8548E-01	.1141E+01
.7474E+00	.5471E+06	.7229E-01	.1660E-01	.8981E-01	.1142E+01
.7579E+00	.5198E+06	.7539E-01	.1492E-01	.9477E-01	.1145E+01
.7684E+00	.4931E+06	.7842E-01	.1338E-01	.1001E+00	.1148E+01
.7789E+00	.4656E+06	.8156E-01	.1189E-01	.1062E+00	.1152E+01
.7895E+00	.4387E+06	.8586E-01	.1052E-01	.1129E+00	.1158E+01
.8000E+00	.4115E+06	.9059E-01	.9230E-02	.1206E+00	.1167E+01
.8105E+00	.3846E+06	.9429E-01	.8038E-02	.1292E+00	.1178E+01
.8211E+00	.3577E+06	.9739E-01	.6928E-02	.1392E+00	.1193E+01
.8316E+00	.3310E+06	.9901E-01	.5905E-02	.1508E+00	.1215E+01
.8421E+00	.3045E+06	.8624E-01	.4956E-02	.1645E+00	.1248E+01
.8526E+00	.2771E+06	.4146E-01	.4119E-02	.1804E+00	.1306E+01
.8632E+00	.2499E+06	.1186E-01	.3341E-02	.2000E+00	.1395E+01
.8737E+00	.2271E+06	.3338E-01	.2733E-02	.2198E+00	.1515E+01
.8842E+00	.2069E+06	-.1845E-01	.2266E-02	.2400E+00	.1737E+01
.8947E+00	.1811E+06	-.1934E+00	.1734E-02	.2738E+00	.2028E+01
.9053E+00	.1576E+06	-.3933E+00	.1319E-02	.3126E+00	.2534E+01
.9158E+00	.1358E+06	-.6231E+00	.9855E-03	.3603E+00	.3265E+01
.9263E+00	.1160E+06	-.9594E+00	.7200E-03	.4211E+00	.4207E+01
.9368E+00	.9705E+05	-.1279E+01	.5035E-03	.5033E+00	.5469E+01
.9474E+00	.8035E+05	-.2028E+01	.3442E-03	.6097E+00	.7003E+01
.9579E+00	.6287E+05	-.3415E+01	.2103E-03	.7811E+00	.9518E+01
.9634E+00	.4755E+05	-.7710E+01	.1197E-03	.1038E+01	.1286E+02
.9789E+00	.3091E+05	-.1939E+02	.5052E-04	.1600E+01	.1817E+02
.9895E+00	.1686E+05	-.3697E+02	.1485E-04	.2951E+01	.1917E+02

PIPE LENGTH = 2 FEET, INSIDE DIAMETER = 2 INCHES
SOURCE PRESSURE = 135 PSIA, SINK PRESSURE = 15 PSIA

Z/L	RE	F	MA2	V/U	PHI
.1053E-01	.1992E+05	.5203E-02	.6332E-05	-.4445E+01	.1344E+01
.2105E-01	.4176E+05	.4077E-03	.2858E-04	-.2081E+01	.1279E+01
.3158E-01	.6605E+05	.3582E-03	.7121E-04	-.1320E+01	.1236E+01
.4211E-01	.9172E+05	.2736E-03	.1379E-03	-.9477E+00	.1228E+01
.5263E-01	.1206E+06	.1725E-03	.2377E-03	-.7226E+00	.1230E+01
.6316E-01	.1515E+06	.1520E-03	.3758E-03	-.5750E+00	.1227E+01
.7368E-01	.1857E+06	.1136E-03	.5633E-03	-.4704E+00	.1228E+01
.8421E-01	.2227E+06	.9372E-04	.8112E-03	-.3923E+00	.1228E+01
.9474E-01	.2631E+06	.7960E-04	.1132E-02	-.3326E+00	.1228E+01
.1053E+00	.3071E+06	.6683E-04	.1545E-02	-.2852E+00	.1228E+01
.1158E+00	.3559E+06	.5790E-04	.2077E-02	-.2466E+00	.1228E+01
.1263E+00	.4047E+06	.5057E-04	.2692E-02	-.2171E+00	.1228E+01
.1368E+00	.4538E+06	.4484E-04	.3388E-02	-.1942E+00	.1229E+01
.1474E+00	.5029E+06	.4045E-04	.4171E-02	-.1756E+00	.1229E+01
.1579E+00	.5522E+06	.3683E-04	.5037E-02	-.1604E+00	.1229E+01
.1684E+00	.6014E+06	.3381E-04	.5994E-02	-.1476E+00	.1228E+01
.1789E+00	.6510E+06	.3124E-04	.7038E-02	-.1369E+00	.1228E+01
.1895E+00	.7006E+06	.2906E-04	.8179E-02	-.1276E+00	.1228E+01
.2000E+00	.7505E+06	.2710E-04	.9410E-02	-.1196E+00	.1228E+01
.2105E+00	.8004E+06	.2544E-04	.1075E-01	-.1125E+00	.1228E+01
.2211E+00	.8506E+06	.2391E-04	.1217E-01	-.1063E+00	.1227E+01
.2316E+00	.9010E+06	.2257E-04	.1372E-01	-.1008E+00	.1227E+01
.2421E+00	.9515E+06	.2139E-04	.1536E-01	-.9590E-01	.1227E+01
.2526E+00	.1002E+07	.2034E-04	.1713E-01	-.9143E-01	.1226E+01
.2632E+00	.1053E+07	.1937E-04	.1900E-01	-.8748E-01	.1226E+01
.2737E+00	.1105E+07	.1851E-04	.2102E-01	-.8380E-01	.1225E+01
.2842E+00	.1157E+07	.1769E-04	.2314E-01	-.8056E-01	.1225E+01
.2947E+00	.1209E+07	.1699E-04	.2544E-01	-.7748E-01	.1224E+01
.3053E+00	.1261E+07	.1632E-04	.2784E-01	-.7478E-01	.1224E+01
.3158E+00	.1315E+07	.1572E-04	.3045E-01	-.7216E-01	.1223E+01
.3263E+00	.1367E+07	.1514E-04	.3315E-01	-.6990E-01	.1223E+01
.3368E+00	.1422E+07	.1465E-04	.3611E-01	-.6764E-01	.1222E+01
.3474E+00	.1475E+07	.1416E-04	.3914E-01	-.6573E-01	.1221E+01
.3579E+00	.1531E+07	.1372E-04	.4250E-01	-.6376E-01	.1220E+01
.3684E+00	.1585E+07	.1329E-04	.4590E-01	-.6215E-01	.1220E+01
.3789E+00	.1642E+07	.1291E-04	.4971E-01	-.6041E-01	.1218E+01
.3895E+00	.1696E+07	.1251E-04	.5351E-01	-.5905E-01	.1218E+01
.4000E+00	.1755E+07	.1218E-04	.5786E-01	-.5749E-01	.1216E+01
.4105E+00	.1809E+07	.1183E-04	.6211E-01	-.5636E-01	.1216E+01
.4211E+00	.1871E+07	.1153E-04	.6709E-01	-.5495E-01	.1214E+01
.4316E+00	.1924E+07	.1124E-04	.7185E-01	-.5402E-01	.1214E+01
.4421E+00	.1989E+07	.1095E-04	.7759E-01	-.5271E-01	.1212E+01
.4526E+00	.2041E+07	.1074E-04	.8287E-01	-.5198E-01	.1211E+01
.4632E+00	.2110E+07	.1047E-04	.8948E-01	-.5078E-01	.1209E+01
.4737E+00	.2161E+07	.1052E-04	.9526E-01	-.5026E-01	.1207E+01
.4842E+00	.2233E+07	.1052E-04	.1026E+00	-.4920E-01	.1203E+01
.4947E+00	.2281E+07	.1106E-04	.1084E+00	-.2450E-01	.1198E+01

.5158E+00	.2278E+07	.1338E-04	.1080E+00	.3915E-01	.1192E+01
.5263E+00	.2202E+07	.4645E-02	.9914E-01	.4098E-01	.1197E+01
.5368E+00	.2169E+07	.7163E-02	.9583E-01	.4161E-01	.1187E+01
.5474E+00	.2098E+07	.1091E-01	.8797E-01	.4349E-01	.1185E+01
.5579E+00	.2059E+07	.1540E-01	.8428E-01	.4437E-01	.1175E+01
.5684E+00	.1993E+07	.2019E-01	.7774E-01	.4624E-01	.1173E+01
.5789E+00	.1951E+07	.2451E-01	.7407E-01	.4733E-01	.1165E+01
.5895E+00	.1889E+07	.2846E-01	.6856E-01	.4922E-01	.1162E+01
.6000E+00	.1844E+07	.3211E-01	.6493E-01	.5055E-01	.1157E+01
.6105E+00	.1785E+07	.3506E-01	.6017E-01	.5253E-01	.1155E+01
.6211E+00	.1737E+07	.3721E-01	.5671E-01	.5409E-01	.1150E+01
.6316E+00	.1679E+07	.3911E-01	.5251E-01	.5624E-01	.1149E+01
.6421E+00	.1630E+07	.4078E-01	.4920E-01	.5809E-01	.1146E+01
.6526E+00	.1573E+07	.4268E-01	.4547E-01	.6045E-01	.1145E+01
.6632E+00	.1523E+07	.4503E-01	.4236E-01	.6263E-01	.1143E+01
.6737E+00	.1467E+07	.4721E-01	.3903E-01	.6527E-01	.1142E+01
.6842E+00	.1415E+07	.4919E-01	.3616E-01	.6782E-01	.1141E+01
.6947E+00	.1360E+07	.5190E-01	.3317E-01	.7083E-01	.1141E+01
.7053E+00	.1308E+07	.5530E-01	.3053E-01	.7384E-01	.1141E+01
.7158E+00	.1253E+07	.5841E-01	.2786E-01	.7732E-01	.1142E+01
.7263E+00	.1201E+07	.6102E-01	.2546E-01	.8089E-01	.1142E+01
.7368E+00	.1146E+07	.6395E-01	.2308E-01	.8500E-01	.1144E+01
.7474E+00	.1093E+07	.6740E-01	.2090E-01	.8933E-01	.1145E+01
.7579E+00	.1039E+07	.7133E-01	.1879E-01	.9424E-01	.1148E+01
.7684E+00	.9853E+06	.7489E-01	.1685E-01	.9954E-01	.1151E+01
.7789E+00	.9310E+06	.7690E-01	.1497E-01	.1056E+00	.1156E+01
.7895E+00	.8773E+06	.7775E-01	.1324E-01	.1123E+00	.1162E+01
.8000E+00	.8226E+06	.8046E-01	.1160E-01	.1200E+00	.1170E+01
.8105E+00	.7692E+06	.8576E-01	.1011E-01	.1285E+00	.1181E+01
.8211E+00	.7149E+06	.9284E-01	.8698E-02	.1385E+00	.1197E+01
.8316E+00	.6620E+06	.9836E-01	.7433E-02	.1498E+00	.1217E+01
.8421E+00	.6080E+06	.9769E-01	.6249E-02	.1634E+00	.1245E+01
.8526E+00	.5557E+06	.7733E-01	.5203E-02	.1790E+00	.1283E+01
.8632E+00	.5014E+06	.3016E-01	.4217E-02	.1987E+00	.1340E+01
.8737E+00	.4527E+06	.1698E-01	.3409E-02	.2205E+00	.1425E+01
.8842E+00	.4104E+06	.3724E-03	.2821E-02	.2407E+00	.1718E+01
.8947E+00	.3680E+06	-.1578E+00	.2269E-02	.2670E+00	.2114E+01
.9053E+00	.3176E+06	-.3759E+00	.1675E-02	.3109E+00	.2351E+01
.9158E+00	.2726E+06	-.5392E+00	.1238E-02	.3601E+00	.2908E+01
.9263E+00	.2351E+06	-.8040E+00	.9208E-03	.4166E+00	.3613E+01
.9368E+00	.1965E+06	-.1152E+01	.6420E-03	.4992E+00	.4636E+01
.9474E+00	.1636E+06	-.2008E+01	.4456E-03	.5996E+00	.6033E+01
.9579E+00	.1272E+06	-.3144E+01	.2700E-03	.7719E+00	.8772E+01
.9684E+00	.9854E+05	-.8117E+01	.1614E-03	.1001E+01	.1172E+02
.9789E+00	.6297E+05	-.2024E+02	.6587E-04	.1568E+01	.1783E+02
.9895E+00	.3682E+05	-.3341E+02	.2231E-04	.2699E+01	.1695E+02

PIPE LENGTH = 2 FEET, INSIDE DIAMETER = 1 INCH
SOURCE PRESSURE = 30 PSIA, SINK PRESSURE = 15 PSIA

Z/L	RE	F	MA2	V/U	PHI
.1053E-01	.2318E+04	.9045E-02	.5703E-05	-.2184E+01	.1295E+01
.2105E-01	.4884E+04	.4220E-02	.2531E-04	-.1037E+01	.1250E+01
.3158E-01	.7650E+04	.2668E-02	.6203E-04	-.6626E+00	.1236E+01
.4211E-01	.1069E+05	.1909E-02	.1213E-03	-.4739E+00	.1230E+01
.5263E-01	.1402E+05	.1451E-02	.2077E-03	-.3628E+00	.1230E+01
.6316E-01	.1752E+05	.1161E-02	.3281E-03	-.2883E+00	.1227E+01
.7368E-01	.2161E+05	.9351E-03	.4926E-03	-.2363E+00	.1230E+01
.8421E-01	.2577E+05	.7864E-03	.7079E-03	-.1970E+00	.1228E+01
.9474E-01	.3048E+05	.6636E-03	.9880E-03	-.1673E+00	.1229E+01
.1053E+00	.3559E+05	.5674E-03	.1351E-02	-.1434E+00	.1229E+01
.1158E+00	.4132E+05	.4902E-03	.1817E-02	-.1242E+00	.1230E+01
.1263E+00	.4699E+05	.4301E-03	.2359E-02	-.1094E+00	.1230E+01
.1368E+00	.5271E+05	.3826E-03	.2971E-02	-.9805E-01	.1230E+01
.1474E+00	.5843E+05	.3458E-03	.3664E-02	-.8871E-01	.1230E+01
.1579E+00	.6420E+05	.3151E-03	.4428E-02	-.8122E-01	.1230E+01
.1684E+00	.7005E+05	.2889E-03	.5285E-02	-.7482E-01	.1229E+01
.1789E+00	.7591E+05	.2668E-03	.6212E-02	-.6955E-01	.1230E+01
.1895E+00	.8182E+05	.2480E-03	.7239E-02	-.6490E-01	.1229E+01
.2000E+00	.8770E+05	.2307E-03	.8337E-02	-.6102E-01	.1229E+01
.2105E+00	.9365E+05	.2171E-03	.9548E-02	-.5748E-01	.1229E+01
.2211E+00	.9960E+05	.2036E-03	.1083E-01	-.5452E-01	.1229E+01
.2316E+00	.1057E+06	.1924E-03	.1225E-01	-.5175E-01	.1228E+01
.2421E+00	.1118E+06	.1822E-03	.1374E-01	-.4943E-01	.1228E+01
.2526E+00	.1180E+06	.1728E-03	.1539E-01	-.4721E-01	.1227E+01
.2632E+00	.1242E+06	.1646E-03	.1711E-01	-.4536E-01	.1227E+01
.2737E+00	.1306E+06	.1573E-03	.1902E-01	-.4354E-01	.1226E+01
.2842E+00	.1369E+06	.1500E-03	.2098E-01	-.4205E-01	.1226E+01
.2947E+00	.1434E+06	.1439E-03	.2318E-01	-.4053E-01	.1225E+01
.3053E+00	.1498E+06	.1377E-03	.2542E-01	-.3932E-01	.1225E+01
.3158E+00	.1566E+06	.1323E-03	.2795E-01	-.3804E-01	.1224E+01
.3263E+00	.1631E+06	.1271E-03	.3051E-01	-.3704E-01	.1224E+01
.3368E+00	.1701E+06	.1226E-03	.3342E-01	-.3595E-01	.1223E+01
.3474E+00	.1767E+06	.1181E-03	.3634E-01	-.3514E-01	.1222E+01
.3579E+00	.1840E+06	.1140E-03	.3970E-01	-.3418E-01	.1221E+01
.3684E+00	.1907E+06	.1102E-03	.4303E-01	-.3353E-01	.1221E+01
.3789E+00	.1983E+06	.1066E-03	.4693E-01	-.3269E-01	.1219E+01
.3895E+00	.2052E+06	.1031E-03	.5074E-01	-.3216E-01	.1219E+01
.4000E+00	.2131E+06	.1002E-03	.5527E-01	-.3142E-01	.1218E+01
.4105E+00	.2201E+06	.9703E-04	.5964E-01	-.3101E-01	.1217E+01
.4211E+00	.2285E+06	.9432E-04	.6495E-01	-.3035E-01	.1215E+01
.4316E+00	.2357E+06	.9176E-04	.6999E-01	-.3005E-01	.1214E+01
.4421E+00	.2446E+06	.8903E-04	.7629E-01	-.2945E-01	.1213E+01
.4526E+00	.2519E+06	.8701E-04	.8215E-01	-.2924E-01	.1211E+01
.4632E+00	.2614E+06	.8447E-04	.8967E-01	-.2869E-01	.1210E+01
.4737E+00	.2688E+06	.8385E-04	.9649E-01	-.2858E-01	.1207E+01
.4842E+00	.2790E+06	.8108E-04	.1055E+00	-.2811E-01	.1206E+01
.4947E+00	.2863E+06	.8338E-04	.1130E+00	-.1406E-01	.1202E+01

.5158E+00	.2[illegible]59E+06	.1056E-03	.1125E+00	.1677E-01	.1194E+01
.5263E+00	.2773E+06	.2505E-02	.1036E+00	.1805E-01	.1193E+01
.5368E+00	.2733E+06	.4674E-02	.1001E+00	.1846E-01	.1177E+01
.5474E+00	.2651E+06	.8034E-02	.9240E-01	.1971E-01	.1172E+01
.5579E+00	.2605E+06	.1155E-01	.8873E-01	.2023E-01	.1158E+01
.5684E+00	.2528E+06	.1519E-01	.8225E-01	.2139E-01	.1152E+01
.5789E+00	.2478E+06	.1870E-01	.7859E-01	.2200E-01	.1142E+01
.5895E+00	.2404E+06	.2190E-01	.7306E-01	.2313E-01	.1137E+01
.6000E+00	.2351E+06	.2470E-01	.6949E-01	.2382E-01	.1129E+01
.6105E+00	.2280E+06	.2720E-01	.6465E-01	.2497E-01	.1126E+01
.6211E+00	.2223E+06	.2947E-01	.6118E-01	.2579E-01	.1120E+01
.6316E+00	.2153E+06	.3160E-01	.5685E-01	.2699E-01	.1118E+01
.6421E+00	.2094E+06	.3356E-01	.5350E-01	.2795E-01	.1113E+01
.6526E+00	.2024E+06	.3533E-01	.4959E-01	.2925E-01	.1111E+01
.6632E+00	.1963E+06	.3688E-01	.4641E-01	.3036E-01	.1107E+01
.6737E+00	.1894E+06	.3829E-01	.4287E-01	.3179E-01	.1105E+01
.6842E+00	.1831E+06	.3972E-01	.3988E-01	.3309E-01	.1101E+01
.6947E+00	.1762E+06	.4137E-01	.3667E-01	.3470E-01	.1099E+01
.7053E+00	.1698E+06	.4317E-01	.3387E-01	.3623E-01	.1096E+01
.7158E+00	.1629E+06	.4499E-01	.3096E-01	.3807E-01	.1094E+01
.7263E+00	.1564E+06	.4702E-01	.2838E-01	.3988E-01	.1091E+01
.7368E+00	.1494E+06	.4936E-01	.2576E-01	.4202E-01	.1089E+01
.7474E+00	.1428E+06	.5173E-01	.2340E-01	.4420E-01	.1086E+01
.7579E+00	.1358E+06	.5388E-01	.2104E-01	.4676E-01	.1084E+01
.7684E+00	.1291E+06	.5616E-01	.1891E-01	.4943E-01	.1082E+01
.7789E+00	.1221E+06	.5927E-01	.1681E-01	.5257E-01	.1080E+01
.7895E+00	.1153E+06	.6348E-01	.1491E-01	.5592E-01	.1078E+01
.8000E+00	.1082E+06	.6843E-01	.1306E-01	.5986E-01	.1077E+01
.8105E+00	.1013E+06	.7345E-01	.1139E-01	.6418E-01	.1076E+01
.8211E+00	.9425E+05	.7874E-01	.9790E-02	.6932E-01	.1076E+01
.8316E+00	.8737E+05	.8495E-01	.8364E-02	.7505E-01	.1076E+01
.8421E+00	.8030E+05	.9269E-01	.7017E-02	.8199E-01	.1078E+01
.8526E+00	.7345E+05	.1011E+00	.5831E-02	.8997E-01	.1081E+01
.8632E+00	.6636E+05	.1107E+00	.4725E-02	.9996E-01	.1085E+01
.8737E+00	.5949E+05	.1255E+00	.3769E-02	.1119E+00	.1091E+01
.8842E+00	.5239E+05	.1475E+00	.2898E-02	.1275E+00	.1101E+01
.8947E+00	.4564E+05	.1638E+00	.2177E-02	.1467E+00	.1121E+01
.9053E+00	.3930E+05	.1751E+00	.1597E-02	.1707E+00	.1150E+01
.9158E+00	.3376E+05	.2168E+00	.1163E-02	.1996E+00	.1170E+01
.9263E+00	.2834E+05	.3353E+00	.808[illegible]E-03	.2394E+00	.1167E+01
.9368E+00	.2350E+05	.4383E+00	.5492E-03	.2907E+00	.1146E+01
.9474E+00	.1867E+05	.5631E+00	.3444E-03	.3675E+00	.1174E+01
.9579E+00	.1411E+05	.1555E+01	.1962E-03	.4874E+00	.1116E+01
.9684E+00	.1057E+05	.5780E+00	.1101E-03	.6500E+00	.1260E+01
.9789E+00	.5868E+04	-.1707E+01	.3394E-04	.1172E+01	.3289E+01
.9895E+00	.2853E+04	.2220E+01	.8018E-05	.2414E+01	.1213E+02

PIPE LENGTH = 2 FEET, INSIDE DIAMETER = 1 INCHE
SOURCE PRESSURE = 45 PSIA, SINK PRESSURE = 15 PSIA

Z/L	RE	F	MA2	V/U	PHI
.1053E-01	.4279E+04	.4637E-02	.8821E-05	-.2182E+01	.1288E+01
.2105E-01	.8932E+04	.2260E-02	.3880E-04	-.1039E+01	.1246E+01
.3158E-01	.1423E+05	.1413E-02	.9614E-04	-.6634E+00	.1238E+01
.4211E-01	.1943E+05	.1036E-02	.1854E-03	-.4748E+00	.1228E+01
.5263E-01	.2591E+05	.7760E-03	.3207E-03	-.3634E+00	.1231E+01
.6316E-01	.3235E+05	.6210E-03	.5062E-03	-.2889E+00	.1229E+01
.7368E-01	.3971E+05	.5040E-03	.7589E-03	-.2367E+00	.1230E+01
.8421E-01	.4736E+05	.4246E-03	.1091E-02	-.1975E+00	.1229E+01
.9474E-01	.5626E+05	.3558E-03	.1528E-02	-.1677E+00	.1230E+01
.1053E+00	.6557E+05	.3058E-03	.2087E-02	-.1439E+00	.1229E+01
.1158E+00	.7625E+05	.2644E-03	.2816E-02	-.1247E+00	.1230E+01
.1263E+00	.8662E+05	.2315E-03	.3657E-02	-.1100E+00	.1230E+01
.1368E+00	.9735E+05	.2058E-03	.4619E-02	-.9857E-01	.1231E+01
.1474E+00	.1078E+06	.1867E-03	.5702E-02	-.8930E-01	.1230E+01
.1579E+00	.1187E+06	.1695E-03	.6917E-02	-.8182E-01	.1230E+01
.1684E+00	.1294E+06	.1556E-03	.8266E-02	-.7548E-01	.1229E+01
.1789E+00	.1405E+06	.1439E-03	.9756E-02	-.7022E-01	.1229E+01
.1895E+00	.1514E+06	.1343E-03	.1140E-01	-.6563E-01	.1228E+01
.2000E+00	.1627E+06	.1249E-03	.1319E-01	-.6176E-01	.1228E+01
.2105E+00	.1738E+06	.1175E-03	.1515E-01	-.5830E-01	.1227E+01
.2211E+00	.1852E+06	.1103E-03	.1728E-01	-.5536E-01	.1227E+01
.2316E+00	.1965E+06	.1043E-03	.1961E-01	-.5266E-01	.1226E+01
.2421E+00	.2083E+06	.9868E-04	.2212E-01	-.5037E-01	.1226E+01
.2526E+00	.2199E+06	.9371E-04	.2487E-01	-.4822E-01	.1225E+01
.2632E+00	.2319E+06	.8927E-04	.2782E-01	-.4640E-01	.1225E+01
.2737E+00	.2438E+06	.8521E-04	.3106E-01	-.4465E-01	.1224E+01
.2842E+00	.2562E+06	.8119E-04	.3453E-01	-.4319E-01	.1223E+01
.2947E+00	.2685E+06	.7817E-04	.3835E-01	-.4175E-01	.1222E+01
.3053E+00	.2813E+06	.7478E-04	.4244E-01	-.4058E-01	.1221E+01
.3158E+00	.2941E+06	.7198E-04	.4695E-01	-.3938E-01	.1220E+01
.3263E+00	.3073E+06	.6915E-04	.5177E-01	-.3842E-01	.1219E+01
.3368E+00	.3207E+06	.6683E-04	.5714E-01	-.3741E-01	.1217E+01
.3474E+00	.3343E+06	.6440E-04	.6284E-01	-.3664E-01	.1216E+01
.3579E+00	.3483E+06	.6210E-04	.6927E-01	-.3579E-01	.1214E+01
.3684E+00	.3624E+06	.6021E-04	.7609E-01	-.3518E-01	.1213E+01
.3789E+00	.3772E+06	.5836E-04	.8386E-01	-.3446E-01	.1211E+01
.3895E+00	.3919E+06	.5655E-04	.9212E-01	-.3398E-01	.1209E+01
.4000E+00	.4074E+06	.5522E-04	.1016E+00	-.3337E-01	.1207E+01
.4105E+00	.4228E+06	.5365E-04	.1118E+00	-.3301E-01	.1204E+01
.4211E+00	.4394E+06	.5240E-04	.1237E+00	-.3251E-01	.1203E+01
.4316E+00	.4555E+06	.5145E-04	.1363E+00	-.3226E-01	.1198E+01
.4421E+00	.4735E+06	.5006E-04	.1517E+00	-.3186E-01	.1197E+01
.4526E+00	.4905E+06	.4963E-04	.1679E+00	-.3172E-01	.1191E+01
.4632E+00	.5101E+06	.4836E-04	.1883E+00	-.3142E-01	.1190E+01
.4737E+00	.5281E+06	.4948E-04	.2097E+00	-.3139E-01	.1182E+01
.4842E+00	.5500E+06	.4735E-04	.2377E+00	-.3129E-01	.1181E+01
.4947E+00	.5682E+06	.4996E-04	.2650E+00	-.1575E-01	.1173E+01

.5158E+00	.5680E+06	.5962E-04	.2647E+00	.1525E-01	.1167E+01
.5263E+00	.5516E+06	.2886E-02	.2394E+00	.1657E-01	.1169E+01
.5368E+00	.5424E+06	.5323E-02	.2272E+00	.1717E-01	.1159E+01
.5474E+00	.5271E+06	.8450E-02	.2071E+00	.1838E-01	.1159E+01
.5579E+00	.5172E+06	.1188E-01	.1961E+00	.1903E-01	.1151E+01
.5684E+00	.5029E+06	.1549E-01	.1803E+00	.2014E-01	.1148E+01
.5789E+00	.4922E+06	.1891E-01	.1702E+00	.2086E-01	.1143E+01
.5895E+00	.4784E+06	.2202E-01	.1573E+00	.2194E-01	.1138E+01
.6000E+00	.4671E+06	.2477E-01	.1480E+00	.2274E-01	.1134E+01
.6105E+00	.4535E+06	.2722E-01	.1370E+00	.2384E-01	.1130E+01
.6211E+00	.4417E+06	.2937E-01	.1284E+00	.2475E-01	.1127E+01
.6316E+00	.4284E+06	.3126E-01	.1189E+00	.2591E-01	.1124E+01
.6421E+00	.4162E+06	.3290E-01	.1110E+00	.2695E-01	.1122E+01
.6526E+00	.4029E+06	.3439E-01	.1026E+00	.2821E-01	.1120E+01
.6632E+00	.3904E+06	.3584E-01	.9534E-01	.2940E-01	.1117E+01
.6737E+00	.3771E+06	.3725E-01	.8781E-01	.3080E-01	.1115E+01
.6842E+00	.3642E+06	.3870E-01	.8114E-01	.3218E-01	.1113E+01
.6947E+00	.3508E+06	.4023E-01	.7443E-01	.3376E-01	.1112E+01
.7053E+00	.3378E+06	.4179E-01	.6835E-01	.3537E-01	.1109E+01
.7158E+00	.3242E+06	.4345E-01	.6233E-01	.3719E-01	.1108E+01
.7263E+00	.3109E+06	.4520E-01	.5682E-01	.3909E-01	.1105E+01
.7368E+00	.2972E+06	.4710E-01	.5145E-01	.4122E-01	.1103E+01
.7474E+00	.2837E+06	.4928E-01	.4650E-01	.4349E-01	.1100E+01
.7579E+00	.2699E+06	.5168E-01	.4173E-01	.4604E-01	.1098E+01
.7684E+00	.2563E+06	.5419E-01	.3733E-01	.4880E-01	.1096E+01
.7789E+00	.2425E+06	.5700E-01	.3315E-01	.5193E-01	.1094E+01
.7895E+00	.2287E+06	.6036E-01	.2927E-01	.5538E-01	.1092E+01
.8000E+00	.2148E+06	.6429E-01	.2563E-01	.5931E-01	.1090E+01
.8105E+00	.2008E+06	.6894E-01	.2225E-01	.6375E-01	.1089E+01
.8211E+00	.1868E+06	.7418E-01	.1912E-01	.6888E-01	.1088E+01
.8316E+00	.1727E+06	.8043E-01	.1625E-01	.7483E-01	.1088E+01
.8421E+00	.1586E+06	.8775E-01	.1360E-01	.8187E-01	.1089E+01
.8526E+00	.1445E+06	.9617E-01	.1123E-01	.9018E-01	.1092E+01
.8632E+00	.1304E+06	.1055E+00	.9084E-02	.1003E+00	.1097E+01
.8737E+00	.1164E+06	.1172E+00	.7188E-02	.1128E+00	.1103E+01
.8842E+00	.1024E+06	.1316E+00	.5521E-02	.1287E+00	.1115E+01
.8947E+00	.8835E+05	.1467E+00	.4084E-02	.1495E+00	.1135E+01
.9053E+00	.7579E+05	.1562E+00	.2982E-02	.1748E+00	.1169E+01
.9158E+00	.6417E+05	.1412E+00	.2122E-02	.2067E+00	.1223E+01
.9263E+00	.5375E+05	.7814E-01	.1477E-02	.2469E+00	.1307E+01
.9368E+00	.4459E+05	.2233E-01	.1009E-02	.2965E+00	.1472E+01
.9474E+00	.3682E+05	-.9376E-01	.6843E-03	.3577E+00	.1854E+01
.9579E+00	.2878E+05	-.4249E+00	.4172E-03	.4562E+00	.2551E+01
.9684E+00	.2117E+05	-.1104E+01	.2265E-03	.6158E+00	.3903E+01
.9789E+00	.1365E+05	-.3042E+01	.9580E-04	.9395E+00	.6277E+01
.9895E+00	.6948E+04	-.6779E+01	.2461E-04	.1853E+01	.8795E+01

PIPE LENGTH = 2 FEET, INSIDE DIAMETER = 1 INCH
SOURCE PRESSURE = 75 PSIA, SINK PRESSURE = 15 PSIA

Z/L	RE	F	MA2	V/U	PHI
.1053E-01	.7997E+04	.2240E-02	.1080E-04	-.2171E+01	.1287E+01
.2105E-01	.1652E+05	.1271E-02	.4700E-04	-.1037E+01	.1243E+01
.3158E-01	.2663E+05	.7606E-03	.1173E-03	-.6620E+00	.1238E+01
.4211E-01	.3617E+05	.5610E-03	.2254E-03	-.4743E+00	.1227E+01
.5263E-01	.4816E+05	.4197E-03	.3898E-03	-.3629E+00	.1230E+01
.6316E-01	.5995E+05	.3354E-03	.6138E-03	-.2887E+00	.1227E+01
.7368E-01	.7411E+05	.2735E-03	.9247E-03	-.2365E+00	.1230E+01
.8421E-01	.8823E+05	.2298E-03	.1327E-02	-.1975E+00	.1228E+01
.9474E-01	.1048E+06	.1917E-03	.1861E-02	-.1677E+00	.1230E+01
.1053E+00	.1218E+06	.1657E-03	.2538E-02	-.1440E+00	.1228E+01
.1158E+00	.1420E+06	.1427E-03	.3432E-02	-.1248E+00	.1230E+01
.1263E+00	.1611E+06	.1256E-03	.4458E-02	-.1102E+00	.1229E+01
.1368E+00	.1816E+06	.1107E-03	.5647E-02	-.9883E-01	.1230E+01
.1474E+00	.2010E+06	.1006E-03	.6975E-02	-.8964E-01	.1229E+01
.1579E+00	.2217E+06	.9127E-04	.8482E-02	-.8219E-01	.1230E+01
.1684E+00	.2414E+06	.8351E-04	.1014E-01	-.7591E-01	.1229E+01
.1789E+00	.2624E+06	.7729E-04	.1200E-01	-.7068E-01	.1229E+01
.1895E+00	.2825E+06	.7239E-04	.1403E-01	-.6616E-01	.1227E+01
.2000E+00	.3040E+06	.6703E-04	.1629E-01	-.6231E-01	.1228E+01
.2105E+00	.3245E+06	.6319E-04	.1874E-01	-.5891E-01	.1226E+01
.2211E+00	.3466E+06	.5924E-04	.2146E-01	-.5599E-01	.1226E+01
.2316E+00	.3677E+06	.5576E-04	.2440E-01	-.5335E-01	.1225E+01
.2421E+00	.3904E+06	.5289E-04	.2765E-01	-.5109E-01	.1225E+01
.2526E+00	.4123E+06	.5031E-04	.3117E-01	-.4900E-01	.1224E+01
.2632E+00	.4357E+06	.4778E-04	.3505E-01	-.4720E-01	.1223E+01
.2737E+00	.4583E+06	.4569E-04	.3927E-01	-.4553E-01	.1222E+01
.2842E+00	.4825E+06	.4338E-04	.4390E-01	-.4409E-01	.1220E+01
.2947E+00	.5059E+06	.4181E-04	.4896E-01	-.4273E-01	.1220E+01
.3053E+00	.5310E+06	.4005E-04	.5451E-01	-.4157E-01	.1218E+01
.3158E+00	.5554E+06	.3851E-04	.6063E-01	-.4045E-01	.1217E+01
.3263E+00	.5815E+06	.3715E-04	.6733E-01	-.3951E-01	.1214E+01
.3368E+00	.6071E+06	.3575E-04	.7480E-01	-.3860E-01	.1214E+01
.3474E+00	.6344E+06	.3471E-04	.8298E-01	-.3784E-01	.1210E+01
.3579E+00	.6614E+06	.3349E-04	.9222E-01	-.3710E-01	.1210E+01
.3684E+00	.6901E+06	.3250E-04	.1024E+00	-.3650E-01	.1205E+01
.3789E+00	.7188E+06	.3167E-04	.1140E+00	-.3591E-01	.1206E+01
.38[illegible]5E+00	.7491E+06	.3068E-04	.1268E+00	-.3545E-01	.1200E+01
.4000E+00	.7801E+06	.2989E-04	.1420E+00	-.3500E-01	.1200E+01
.4105E+00	.8119E+06	.2985E-04	.1584E+00	-.3466E-01	.1192E+01
.4211E+00	.8460E+06	.2855E-04	.1790E+00	-.3436E-01	.1193E+01
.4316E+00	.8801E+06	.2892E-04	.2011E+00	-.3415E-01	.1183E+01
.4421E+00	.9179E+06	.2833E-04	.2303E+00	-.3402E-01	.1183E+01
.4526E+00	.9546E+06	.2901E-04	.2615E+00	-.3395E-01	.1171E+01
.4632E+00	.9987E+06	.2789E-04	.3075E+00	-.3408E-01	.1170E+01
.4737E+00	.1039E+07	.3109E-04	.3554E+00	-.3423E-01	.1155E+01
.4842E+00	.1093E+07	.3092E-04	.4386E+00	-.3482E-01	.1147E+01
.4947E+00	.1140E+07	.3445E-04	.5292E+00	-.1784E-01	.1134E+01

.5158E+00	.1147E+07	.4124E-04	.5465E+00	.1345E-01	.1120E+01
.5263E+00	.1113E+07	.3482E-02	.4750E+00	.1491E-01	.1134E+01
.5368E+00	.1091E+07	.5849E-02	.4359E+00	.1574E-01	.1134E+01
.5474E+00	.1061E+07	.8868E-02	.3895E+00	.1694E-01	.1140E+01
.5579E+00	.1038E+07	.1219E-01	.3575E+00	.1781E-01	.1137E+01
.5684E+00	.1010E+07	.1546E-01	.3240E+00	.1889E-01	.1139E+01
.5789E+00	.9867E+06	.1853E-01	.3001E+00	.1973E-01	.1138E+01
.5895E+00	.9598E+06	.2149E-01	.2742E+00	.2078E-01	.1136E+01
.6000E+00	.9358E+06	.2419E-01	.2540E+00	.2169E-01	.1135E+01
.6105E+00	.9096E+06	.2646E-01	.2333E+00	.2275E-01	.1133E+01
.6211E+00	.8851E+06	.2833E-01	.2159E+00	.2374E-01	.1133E+01
.6316E+00	.8591E+06	.2998E-01	.1986E+00	.2486E-01	.1131E+01
.6421E+00	.8340E+06	.3150E-01	.1834E+00	.2597E-01	.1130E+01
.6526E+00	.8079E+06	.3291E-01	.1685E+00	.2720E-01	.1128E+01
.6632E+00	.7824E+06	.3426E-01	.1551E+00	.2845E-01	.1128E+01
.6737E+00	.7561E+06	.3560E-01	.1422E+00	.2983E-01	.1126E+01
.6842E+00	.7300E+06	.3693E-01	.1303E+00	.3125E-01	.1125E+01
.6947E+00	.7036E+06	.3832E-01	.1190E+00	.3281E-01	.1123E+01
.7053E+00	.6771E+06	.3979E-01	.1085E+00	.3446E-01	.1122E+01
.7158E+00	.6503E+06	.4131E-01	.9862E-01	.3626E-01	.1120E+01
.7263E+00	.6234E+06	.4299E-01	.8940E-01	.3818E-01	.1117E+01
.7368E+00	.5964E+06	.4490E-01	.8068E-01	.4029E-01	.1116E+01
.7474E+00	.5692E+06	.4687E-01	.7256E-01	.4258E-01	.1114E+01
.7579E+00	.5418E+06	.4893E-01	.6497E-01	.4510E-01	.1112E+01
.7684E+00	.5143E+06	.5124E-01	.5787E-01	.4787E-01	.1110E+01
.7789E+00	.4868E+06	.5374E-01	.5127E-01	.5095E-01	.1108E+01
.7895E+00	.4591E+06	.5648E-01	.4513E-01	.5439E-01	.1106E+01
.8000E+00	.4315E+06	.5968E-01	.3946E-01	.5825E-01	.1105E+01
.8105E+00	.4036E+06	.6354E-01	.3419E-01	.6266E-01	.1103E+01
.8211E+00	.3758E+06	.6818E-01	.2937E-01	.6770E-01	.1102E+01
.8316E+00	.3476E+06	.7361E-01	.2492E-01	.7358E-01	.1102E+01
.8421E+00	.3195E+06	.7990E-01	.2089E-01	.8043E-01	.1102E+01
.8526E+00	.2910E+06	.8721E-01	.1720E-01	.8867E-01	.1104E+01
.8632E+00	.2627E+06	.9573E-01	.1392E-01	.9863E-01	.1107E+01
.8737E+00	.2344E+06	.1064E+00	.1101E-01	.1109E+00	.1115E+01
.8842E+00	.2063E+06	.1193E+00	.8467E-02	.1265E+00	.1127E+01
.8947E+00	.1780E+06	.1320E+00	.6269E-02	.1470E+00	.1150E+01
.9053E+00	.1529E+06	.1366E+00	.4592E-02	.1716E+00	.1186E+01
.9158E+00	.1295E+06	.1141E+00	.3276E-02	.2029E+00	.1247E+01
.9263E+00	.1088E+06	.5480E-01	.2300E-02	.2417E+00	.1340E+01
.9368E+00	.9072E+05	-.1560E-01	.1591E-02	.2891E+00	.1543E+01
.9474E+00	.7530E+05	-.2485E+00	.1091E-02	.3474E+00	.1917E+01
.9579E+00	.5839E+05	-.6668E+00	.6565E-03	.4458E+00	.2722E+01
.9684E+00	.4450E+05	-.1759E+01	.3807E-03	.5852E+00	.4123E+01
.9789E+00	.2876E+05	-.4548E+01	.1594E-03	.9065E+00	.6946E+01
.9895E+00	.1582E+05	-.8605E+01	.4773E-04	.1664E+01	.8404E+01

PIPE LENGTH = 2 FEET, INSIDE DIAMETER = 1/2 INCH
SOURCE PRESSURE = 20 PSIA, SINK PRESSURE = 15 PSIA

Z/L	RE	F	MAZ	V/U	PHI
.1053E-01	.1422E+04	.1173E-01	.1593E-04	-.5097E+00	.1416E+01
.2105E-01	.2918E+04	.6787E-02	.6713E-04	-.2485E+00	.1263E+01
.3158E-01	.4242E+04	.4582E-02	.1488E-03	-.1672E+00	.1239E+01
.4211E-01	.5841E+04	.3437E-02	.2694E-03	-.1245E+00	.1233E+01
.5263E-01	.7268E+04	.2755E-02	.4176E-03	-.1003E+00	.1232E+01
.6316E-01	.8777E+04	.2292E-02	.6094E-03	-.8334E-01	.1231E+01
.7368E-01	.1023E+05	.1959E-02	.8267E-03	-.7172E-01	.1232E+01
.8421E-01	.1170E+05	.1721E-02	.1089E-02	-.6288E-01	.1230E+01
.9474E-01	.1323E+05	.1516E-02	.1382E-02	-.5628E-01	.1233E+01
.1053E+00	.1471E+05	.1367E-02	.1720E-02	-.5067E-01	.1231E+01
.1158E+00	.1617E+05	.1241E-02	.2082E-02	-.4642E-01	.1231E+01
.1263E+00	.1776E+05	.1133E-02	.2507E-02	-.4262E-01	.1231E+01
.1368E+00	.1926E+05	.1041E-02	.2952E-02	-.3967E-01	.1232E+01
.1474E+00	.2082E+05	.9675E-03	.3460E-02	-.3693E-01	.1231E+01
.1579E+00	.2232E+05	.9015E-03	.3984E-02	-.3479E-01	.1231E+01
.1684E+00	.2395E+05	.8427E-03	.4593E-02	-.3272E-01	.1230E+01
.1789E+00	.2555E+05	.7890E-03	.5219E-02	-.3112E-01	.1231E+01
.1895E+00	.2718E+05	.7441E-03	.5928E-02	-.2951E-01	.1230E+01
.2000E+00	.2873E+05	.7031E-03	.6643E-02	-.2827E-01	.1230E+01
.2105E+00	.3040E+05	.6657E-03	.7467E-02	-.2699E-01	.1230E+01
.2211E+00	.3203E+05	.6316E-03	.8236E-02	-.2602E-01	.1230E+01
.2316E+00	.3383E+05	.5995E-03	.9260E-02	-.2497E-01	.1229E+01
.2421E+00	.3547E+05	.5714E-03	.1021E-01	-.2421E-01	.1230E+01
.2526E+00	.3728E+05	.5451E-03	.1131E-01	-.2335E-01	.1229E+01
.2632E+00	.3894E+05	.5215E-03	.1239E-01	-.2274E-01	.1229E+01
.2737E+00	.4080E+05	.4994E-03	.1366E-01	-.2201E-01	.1228E+01
.2842E+00	.4255E+05	.4788E-03	.1490E-01	-.2153E-01	.1228E+01
.2947E+00	.4454E+05	.4597E-03	.1637E-01	-.2092E-01	.1228E+01
.3053E+00	.4636E+05	.4416E-03	.1779E-01	-.2054E-01	.1228E+01
.3158E+00	.4840E+05	.4247E-03	.1948E-01	-.2002E-01	.1227E+01
.3263E+00	.5025E+05	.4086E-03	.2110E-01	-.1973E-01	.1227E+01
.3368E+00	.5239E+05	.3935E-03	.2304E-01	-.1928E-01	.1226E+01
.3474E+00	.5431E+05	.3798E-03	.2490E-01	-.1906E-01	.1226E+01
.3579E+00	.5655E+05	.3668E-03	.2715E-01	-.1867E-01	.1225E+01
.3684E+00	.5858E+05	.3542E-03	.2929E-01	-.1831E-01	.1224E+01
.3789E+00	.6096E+05	.3411E-03	.3191E-01	-.1813E-01	.1224E+01
.3895E+00	.6307E+05	.3300E-03	.3438E-01	-.1808E-01	.1223E+01
.4000E+00	.6559E+05	.3187E-03	.3744E-01	-.1780E-01	.1223E+01
.4105E+00	.6779E+05	.3089E-03	.4030E-01	-.1774E-01	.1222E+01
.4211E+00	.7047E+05	.2989E-03	.4389E-01	-.1750E-01	.1221E+01
.4316E+00	.7277E+05	.2906E-03	.4724E-01	-.1749E-01	.1220E+01
.4421E+00	.7564E+05	.2800E-03	.5150E-01	-.1729E-01	.1220E+01
.4526E+00	.7807E+05	.2721E-03	.5545E-01	-.1732E-01	.1218E+01
.4632E+00	.8115E+05	.2636E-03	.6054E-01	-.1716E-01	.1218E+01
.4737E+00	.8373E+05	.2565E-03	.6525E-01	-.1722E-01	.1215E+01
.4842E+00	.8705E+05	.2468E-03	.7140E-01	-.1711E-01	.1215E+01
.4947E+00	.8974E+05	.2482E-03	.7692E-01	-.8604E-02	.1212E+01

.5158E+00	.8974E+05	.2575E-03	.7689E-01	.6357E-02	.1210E+01
.5263E+00	.8789E+05	.6836E-03	.7293E-01	.7051E-02	.1203E+01
.5368E+00	.8692E+05	.1593E-02	.7102E-01	.7359E-02	.1187E+01
.5474E+00	.8493E+05	.3230E-02	.6702E-01	.8138E-02	.1172E+01
.5579E+00	.8374E+05	.5464E-02	.6485E-01	.8505E-02	.1155E+01
.5684E+00	.8177E+05	.8059E-02	.6126E-01	.9211E-02	.1142E+01
.5789E+00	.8046E+05	.1083E-01	.5911E-01	.9569E-02	.1128E+01
.5895E+00	.7852E+05	.1355E-01	.5587E-01	.1022E-01	.1118E+01
.6000E+00	.7710E+05	.1601E-01	.5373E-01	.1057E-01	.1109E+01
.6105E+00	.7518E+05	.1809E-01	.5079E-01	.1117E-01	.1103E+01
.6211E+00	.7368E+05	.1988E-01	.4866E-01	.1154E-01	.1096E+01
.6316E+00	.7177E+05	.2143E-01	.4593E-01	.1213E-01	.1091E+01
.6421E+00	.7019E+05	.2278E-01	.4383E-01	.1255E-01	.1086E+01
.6526E+00	.6827E+05	.2394E-01	.4128E-01	.1316E-01	.1083E+01
.6632E+00	.6661E+05	.2496E-01	.3920E-01	.1363E-01	.1079E+01
.6737E+00	.6467E+05	.2585E-01	.3681E-01	.1429E-01	.1076E+01
.6842E+00	.6294E+05	.2664E-01	.3478E-01	.1482E-01	.1074E+01
.6947E+00	.6099E+05	.2739E-01	.3254E-01	.1554E-01	.1071E+01
.7053E+00	.5919E+05	.2809E-01	.3057E-01	.1617E-01	.1069E+01
.7158E+00	.5721E+05	.2882E-01	.2846E-01	.1697E-01	.1067E+01
.7263E+00	.5535E+05	.2966E-01	.2658E-01	.1770E-01	.1065E+01
.7368E+00	.5335E+05	.3053E-01	.2460E-01	.1861E-01	.1064E+01
.7474E+00	.5144E+05	.3133E-01	.2281E-01	.1947E-01	.1062E+01
.7579E+00	.4942E+05	.3218E-01	.2098E-01	.2052E-01	.1060E+01
.7684E+00	.4745E+05	.3322E-01	.1929E-01	.2156E-01	.1059E+01
.7789E+00	.4541E+05	.3450E-01	.1760E-01	.2279E-01	.1057E+01
.7895E+00	.4340E+05	.3585E-01	.1603E-01	.2404E-01	.1055E+01
.8000E+00	.4133E+05	.3711E-01	.1449E-01	.2551E-01	.1054E+01
.8105E+00	.3927E+05	.3839E-01	.1304E-01	.2706E-01	.1052E+01
.8211E+00	.3717E+05	.4008E-01	.1164E-01	.2888E-01	.1050E+01
.8316E+00	.3507E+05	.4247E-01	.1033E-01	.3083E-01	.1049E+01
.8421E+00	.3294E+05	.4526E-01	.9084E-02	.3312E-01	.1047E+01
.8526E+00	.3080E+05	.4847E-01	.7917E-02	.3566E-01	.1046E+01
.8632E+00	.2866E+05	.5266E-01	.6822E-02	.3867E-01	.1045E+01
.8737E+00	.2650E+05	.5816E-01	.5808E-02	.4210E-01	.1044E+01
.8842E+00	.2432E+05	.6432E-01	.4876E-02	.4620E-01	.1044E+01
.8947E+00	.2212E+05	.6993E-01	.4021E-02	.5106E-01	.1045E+01
.9053E+00	.2001E+05	.7574E-01	.3263E-02	.5698E-01	.1047E+01
.9158E+00	.1789E+05	.8123E-01	.2581E-02	.6438E-01	.1049E+01
.9263E+00	.1577E+05	.1055E+00	.1981E-02	.7388E-01	.1048E+01
.9368E+00	.1356E+05	.1621E+00	.1451E-02	.8660E-01	.1053E+01
.9474E+00	.1124E+05	.2116E+00	.9925E-03	.1050E+00	.1074E+01
.9579E+00	.8975E+04	.2736E+00	.6300E-03	.1320E+00	.1116E+01
.9684E+00	.6657E+04	.4248E+00	.3443E-03	.1790E+00	.1190E+01
.9789E+00	.4414E+04	.8755E+00	.1512E-03	.2704E+00	.1372E+01
.9895E+00	.2117E+04	.1797E+01	.3293E-04	.5865E+00	.2381E+01

PIPE LENGTH = 2 FEET, INSIDE DIAMETER = 1/2 INCH
SOURCE PRESSURE = 30 PSIA, SINK PRESSURE = 15 PSIA

Z/L	RE	F	MA2	V/U	PHI
.1053E-01	.2962E+04	.5636E-02	.3059E-04	-.5027E+00	.1422E+01
.2105E-01	.5991E+04	.3334E-02	.1254E-03	-.2486E+00	.1259E+01
.3158E-01	.8952E+04	.2259E-02	.2805E-03	-.1667E+00	.1236E+01
.4211E-01	.1200E+05	.1689E-02	.5042E-03	-.1248E+00	.1232E+01
.5263E-01	.1497E+05	.1358E-02	.7866E-03	-.1004E+00	.1231E+01
.6316E-01	.1806E+05	.1125E-02	.1144E-02	-.8378E-01	.1231E+01
.7368E-01	.2111E+05	.9616E-03	.1563E-02	-.7228E-01	.1232E+01
.8421E-01	.2404E+05	.8473E-03	.2053E-02	-.6346E-01	.1230E+01
.9474E-01	.2750E+05	.7366E-03	.2633E-02	-.5685E-01	.1233E+01
.1053E+00	.3024E+05	.6730E-03	.3259E-02	-.5141E-01	.1229E+01
.1158E+00	.3363E+05	.6026E-03	.3991E-02	-.4717E-01	.1231E+01
.1263E+00	.3671E+05	.5540E-03	.4799E-02	-.4351E-01	.1230E+01
.1368E+00	.4025E+05	.5031E-03	.5712E-02	-.4059E-01	.1231E+01
.1474E+00	.4318E+05	.4699E-03	.6686E-02	-.3798E-01	.1229E+01
.1579E+00	.4669E+05	.4343E-03	.7787E-02	-.3588E-01	.1230E+01
.1684E+00	.4995E+05	.4057E-03	.8989E-02	-.3394E-01	.1229E+01
.1789E+00	.5370E+05	.3770E-03	.1033E-01	-.3238E-01	.1229E+01
.1895E+00	.5702E+05	.3564E-03	.1177E-01	-.3090E-01	.1229E+01
.2000E+00	.6075E+05	.3327E-03	.1335E-01	-.2971E-01	.1228E+01
.2105E+00	.6413E+05	.3174E-03	.1507E-01	-.2855E-01	.1228E+01
.2211E+00	.6807E+05	.2984E-03	.1696E-01	-.2765E-01	.1227E+01
.2316E+00	.7175E+05	.2835E-03	.1904E-01	-.2673E-01	.1227E+01
.2421E+00	.7597E+05	.2692E-03	.2131E-01	-.2603E-01	.1226E+01
.2526E+00	.7981E+05	.2567E-03	.2379E-01	-.2530E-01	.1227E+01
.2632E+00	.8415E+05	.2451E-03	.2649E-01	-.2476E-01	.1224E+01
.2737E+00	.8809E+05	.2349E-03	.2945E-01	-.2419E-01	.1225E+01
.2842E+00	.9262E+05	.2250E-03	.3269E-01	-.2377E-01	.1222E+01
.2947E+00	.9689E+05	.2161E-03	.3629E-01	-.2332E-01	.1224E+01
.3053E+00	.1018E+06	.2059E-03	.4022E-01	-.2301E-01	.1220E+01
.3158E+00	.1065E+06	.1990E-03	.4464E-01	-.2266E-01	.1222E+01
.3263E+00	.1117E+06	.1913E-03	.4944E-01	-.2243E-01	.1217E+01
.3368E+00	.1167E+06	.1840E-03	.5490E-01	-.2218E-01	.1220E+01
.3474E+00	.1222E+06	.1774E-03	.6080E-01	-.2203E-01	.1214E+01
.3579E+00	.1276E+06	.1679E-03	.6765E-01	-.2186E-01	.1218E+01
.3684E+00	.1335E+06	.1638E-03	.7505E-01	-.2178E-01	.1211E+01
.3789E+00	.1394E+06	.1565E-03	.8378E-01	-.2169E-01	.1214E+01
.3895E+00	.1458E+06	.1526E-03	.9330E-01	-.2166E-01	.1206E+01
.4000E+00	.1524E+06	.1479E-03	.1047E+00	-.2166E-01	.1210E+01
.4105E+00	.1594E+06	.1414E-03	.1173E+00	-.2170E-01	.1200E+01
.4211E+00	.1668E+06	.1367E-03	.1330E+00	-.2180E-01	.1204E+01
.4316E+00	.1745E+06	.1382E-03	.1499E+00	-.2189E-01	.1193E+01
.4421E+00	.1830E+06	.1285E-03	.1726E+00	-.2210E-01	.1196E+01
.4526E+00	.1917E+06	.1324E-03	.1973E+00	-.2228E-01	.1183E+01
.4632E+00	.2014E+06	.1277E-03	.2321E+00	-.2265E-01	.1184E+01
.4737E+00	.2113E+06	.1354E-03	.2709E+00	-.2295E-01	.1169E+01
.4842E+00	.2235E+06	.1294E-03	.3334E+00	-.2361E-01	.1164E+01
.4947E+00	.2349E+06	.1371E-03	.4051E+00	-.1215E-01	.1152E+01

.5158E+00	.2357E+06	.1468E-03	.4111E+00	.3459E-02	.1147E+01
.5263E+00	.2335E+06	.1214E-02	.3954E+00	.3981E-02	.1144E+01
.5368E+00	.2301E+06	.2506E-02	.3716E+00	.4767E-02	.1144E+01
.5474E+00	.2268E+06	.4485E-02	.3513E+00	.5510E-02	.1136E+01
.5579E+00	.2228E+06	.6879E-02	.3289E+00	.6318E-02	.1133E+01
.5684E+00	.2195E+06	.9527E-02	.3129E+00	.6886E-02	.1129E+01
.5789E+00	.2154E+06	.1234E-01	.2944E+00	.7593E-02	.1123E+01
.5895E+00	.2116E+06	.1502E-01	.2800E+00	.8116E-02	.1120E+01
.6000E+00	.2077E+06	.1737E-01	.2652E+00	.8673E-02	.1117E+01
.6105E+00	.2036E+06	.1942E-01	.2519E+00	.9192E-02	.1112E+01
.6211E+00	.1995E+06	.2117E-01	.2388E+00	.9709E-02	.1111E+01
.6316E+00	.1954E+06	.2262E-01	.2265E+00	.1022E-01	.1107E+01
.6421E+00	.1911E+06	.2381E-01	.2144E+00	.1074E-01	.1106E+01
.6526E+00	.1868E+06	.2479E-01	.2028E+00	.1128E-01	.1103E+01
.6632E+00	.1824E+06	.2562E-01	.1912E+00	.1186E-01	.1102E+01
.6737E+00	.1778E+06	.2639E-01	.1799E+00	.1246E-01	.1099E+01
.6842E+00	.1731E+06	.2713E-01	.1688E+00	.1311E-01	.1098E+01
.6947E+00	.1684E+06	.2786E-01	.1580E+00	.1379E-01	.1095E+01
.7053E+00	.1635E+06	.2857E-01	.1474E+00	.1453E-01	.1093E+01
.7158E+00	.1585E+06	.2925E-01	.1373E+00	.1531E-01	.1091E+01
.7263E+00	.1535E+06	.2993E-01	.1273E+00	.1615E-01	.1088E+01
.7368E+00	.1484E+06	.3065E-01	.1178E+00	.1705E-01	.1086E+01
.7474E+00	.1432E+06	.3146E-01	.1085E+00	.1802E-01	.1084E+01
.7579E+00	.1380E+06	.3236E-01	.9967E-01	.1906E-01	.1083E+01
.7684E+00	.1326E+06	.3341E-01	.9113E-01	.2019E-01	.1081E+01
.7789E+00	.1272E+06	.3459E-01	.8299E-01	.2142E-01	.1079E+01
.7895E+00	.1217E+06	.3577E-01	.7519E-01	.2276E-01	.1077E+01
.8000E+00	.1161E+06	.3695E-01	.6782E-01	.2423E-01	.1076E+01
.8105E+00	.1104E+06	.3832E-01	.6077E-01	.2586E-01	.1074E+01
.8211E+00	.1047E+06	.4015E-01	.5416E-01	.2767E-01	.1072E+01
.8316E+00	.9893E+05	.4235E-01	.4789E-01	.2969E-01	.1070E+01
.8421E+00	.9313E+05	.4448E-01	.4206E-01	.3195E-01	.1067E+01
.8526E+00	.8718E+05	.4645E-01	.3656E-01	.3454E-01	.1065E+01
.8632E+00	.8120E+05	.4883E-01	.3145E-01	.3752E-01	.1063E+01
.8737E+00	.7512E+05	.5254E-01	.2670E-01	.4101E-01	.1061E+01
.8842E+00	.6901E+05	.5772E-01	.2237E-01	.4508E-01	.1059E+01
.8947E+00	.6286E+05	.6412E-01	.1841E-01	.4998E-01	.1057E+01
.9053E+00	.5668E+05	.7187E-01	.1485E-01	.5594E-01	.1056E+01
.9158E+00	.5033E+05	.8085E-01	.1166E-01	.6342E-01	.1057E+01
.9263E+00	.4422E+05	.9317E-01	.8906E-02	.7291E-01	.1059E+01
.9368E+00	.3797E+05	.1123E+00	.6513E-02	.8561E-01	.1063E+01
.9474E+00	.3158E+05	.1370E+00	.4499E-02	.1032E+00	.1071E+01
.9579E+00	.2545E+05	.1694E+00	.2875E-02	.1297E+00	.1087E+01
.9684E+00	.1971E+05	.2253E+00	.1649E-02	.1731E+00	.1108E+01
.9789E+00	.1355E+05	.4262E+00	.7462E-03	.2597E+00	.1133E+01
.9895E+00	.7093E+04	.8718E+00	.1924E-03	.5180E+00	.1267E+01

PIPE LENGTH = 2 FEET, INSIDE DIAMETER = 1/2 INCH

SOURCE PRESSURE = 45 PSIA, SINK PRESSURE = 15 PSIA

Z/L	RE	F	MA2	V/U	PHI
.1053E-01	.2043E+04	.9997E-02	.6181E-05	-.1065E+01	.1259E+01
.2105E-01	.4194E+04	.4808E-02	.2605E-04	-.5191E+00	.1234E+01
.3158E-01	.6616E+04	.3095E-02	.6486E-04	-.3292E+00	.1224E+01
.4211E-01	.9181E+04	.2145E-02	.1249E-03	-.2376E+00	.1225E+01
.5263E-01	.1207E+05	.1644E-02	.2158E-03	-.1812E+00	.1225E+01
.6316E-01	.1513E+05	.1299E-02	.3394E-03	-.1449E+00	.1227E+01
.7368E-01	.1857E+05	.1063E-02	.5116E-03	-.1185E+00	.1227E+01
.8421E-01	.2225E+05	.8823E-03	.7346E-03	-.9948E-01	.1228E+01
.9474E-01	.2636E+05	.7469E-03	.1033E-02	-.8442E-01	.1227E+01
.1053E+00	.3083E+05	.6365E-03	.1412E-02	-.7296E-01	.1229E+01
.1158E+00	.3578E+05	.5492E-03	.1913E-02	-.6329E-01	.1228E+01
.1263E+00	.4100E+05	.4777E-03	.2496E-02	-.5630E-01	.1230E+01
.1368E+00	.4598E+05	.4274E-03	.3169E-02	-.5060E-01	.1229E+01
.1474E+00	.5106E+05	.3872E-03	.3920E-02	-.4630E-01	.1229E+01
.1579E+00	.5707E+05	.3459E-03	.4831E-02	-.4258E-01	.1231E+01
.1684E+00	.6134E+05	.3244E-03	.5735E-02	-.3972E-01	.1228E+01
.1789E+00	.6770E+05	.2957E-03	.6889E-02	-.3713E-01	.1230E+01
.1895E+00	.7296E+05	.2759E-03	.8069E-02	-.3514E-01	.1229E+01
.2000E+00	.7917E+05	.2577E-03	.9477E-02	-.3326E-01	.1229E+01
.2105E+00	.8413E+05	.2435E-03	.1089E-01	-.3183E-01	.1228E+01
.2211E+00	.9094E+05	.2272E-03	.1265E-01	-.3043E-01	.1228E+01
.2316E+00	.9663E+05	.2163E-03	.1444E-01	-.2937E-01	.1227E+01
.2421E+00	.1039E+06	.2007E-03	.1662E-01	-.2831E-01	.1228E+01
.2526E+00	.1096E+06	.1929E-03	.1879E-01	-.2752E-01	.1225E+01
.2632E+00	.1169E+06	.1773E-03	.2142E-01	-.2675E-01	.1229E+01
.2737E+00	.1234E+06	.1696E-03	.2416E-01	-.2613E-01	.1222E+01
.2842E+00	.1312E+06	.1590E-03	.2743E-01	-.2555E-01	.1226E+01
.2947E+00	.1386E+06	.1497E-03	.3091E-01	-.2510E-01	.1221E+01
.3053E+00	.1469E+06	.1406E-03	.3498E-01	-.2469E-01	.1225E+01
.3158E+00	.1548E+06	.1314E-03	.3933E-01	-.2437E-01	.1220E+01
.3263E+00	.1637E+06	.1269E-03	.4449E-01	-.2407E-01	.1222E+01
.3368E+00	.1720E+06	.1221E-03	.4994E-01	-.2386E-01	.1216E+01
.3474E+00	.1818E+06	.1109E-03	.5665E-01	-.2371E-01	.1221E+01
.3579E+00	.1912E+06	.1141E-03	.6380E-01	-.2355E-01	.1213E+01
.3684E+00	.2020E+06	.1020E-03	.7253E-01	-.2350E-01	.1217E+01
.3789E+00	.2127E+06	.1071E-03	.8224E-01	-.2343E-01	.1207E+01
.3895E+00	.2244E+06	.1051E-03	.9363E-01	-.2346E-01	.1211E+01
.4000E+00	.2368E+06	.8613E-04	.1074E+00	-.2350E-01	.1203E+01
.4105E+00	.2503E+06	.9176E-04	.1242E+00	-.2369E-01	.1207E+01
.4211E+00	.2630E+06	.9688E-04	.1422E+00	-.2372E-01	.1193E+01
.4316E+00	.2793E+06	.7209E-04	.1687E+00	-.2412E-01	.1199E+01
.4421E+00	.2947E+06	.8621E-04	.1984E+00	-.2430E-01	.1183E+01
.4526E+00	.3125E+06	.8803E-04	.2392E+00	-.2481E-01	.1182E+01
.4632E+00	.3306E+06	.8399E-04	.2911E+00	-.2521E-01	.1167E+01
.4737E+00	.3559E+06	.8183E-04	.3840E+00	-.2628E-01	.1155E+01
.4842E+00	.3755E+06	.9598E-04	.4933E+00	-.2739E-01	.1146E+01
.4947E+00	.4080E+06	.1145E-03	.7647E+00	-.1495E-01	.1113E+01

.5158E+00	.4310E+06	.1932E-03	.1083E+01	.1730E-02	.1059E+01
.5263E+00	.4264E+06	.2244E-02	.9934E+00	.2607E-02	.1067E+01
.5368E+00	.4165E+06	.5120E-02	.8566E+00	.4093E-02	.1082E+01
.5474E+00	.4094E+06	.8486E-02	.7894E+00	.4828E-02	.1090E+01
.5579E+00	.4041E+06	.1155E-01	.7474E+00	.5280E-02	.1098E+01
.5684E+00	.3980E+06	.1418E-01	.7090E+00	.5669E-02	.1102E+01
.5789E+00	.3924E+06	.1605E-01	.6775E+00	.5983E-02	.1108E+01
.5895E+00	.3853E+06	.1766E-01	.6361E+00	.6491E-02	.1110E+01
.6000E+00	.3782E+06	.1914E-01	.5989E+00	.6958E-02	.1114E+01
.6105E+00	.3712E+06	.2046E-01	.5655E+00	.7395E-02	.1116E+01
.6211E+00	.3631E+06	.2167E-01	.5273E+00	.7991E-02	.1116E+01
.6316E+00	.3553E+06	.2263E-01	.4948E+00	.8496E-02	.1117E+01
.6421E+00	.3472E+06	.2348E-01	.4611E+00	.9096E-02	.1119E+01
.6526E+00	.3384E+06	.2431E-01	.4274E+00	.9769E-02	.1117E+01
.6632E+00	.3296E+06	.2505E-01	.3957E+00	.1046E-01	.1118E+01
.6737E+00	.3204E+06	.2577E-01	.3645E+00	.1121E-01	.1117E+01
.6842E+00	.3109E+06	.2653E-01	.3348E+00	.1203E-01	.1116E+01
.6947E+00	.3011E+06	.2735E-01	.3059E+00	.1292E-01	.1112E+01
.7053E+00	.2913E+06	.2819E-01	.2790E+00	.1386E-01	.1111E+01
.7158E+00	.2812E+06	.2900E-01	.2535E+00	.1487E-01	.1107E+01
.7263E+00	.2709E+06	.2983E-01	.2295E+00	.1595E-01	.1105E+01
.7368E+00	.2604E+06	.3079E-01	.2069E+00	.1712E-01	.1102E+01
.7474E+00	.2496E+06	.3197E-01	.1857E+00	.1841E-01	.1099E+01
.7579E+00	.2386E+06	.3343E-01	.1659E+00	.1930E-01	.1096E+01
.7684E+00	.2274E+06	.3504E-01	.1475E+00	.2132E-01	.1094E+01
.7789E+00	.2160E+06	.3668E-01	.1304E+00	.2298E-01	.1091E+01
.7895E+00	.2044E+06	.3832E-01	.1146E+00	.2482E-01	.1088E+01
.8000E+00	.1927E+06	.4001E-01	.9999E-01	.2688E-01	.1085E+01
.8105E+00	.1809E+06	.4182E-01	.8655E-01	.2920E-01	.1082E+01
.8211E+00	.1688E+06	.4372E-01	.7417E-01	.3186E-01	.1080E+01
.8316E+00	.1566E+06	.4587E-01	.6277E-01	.3495E-01	.1077E+01
.8421E+00	.1441E+06	.4902E-01	.5239E-01	.3859E-01	.1075E+01
.8526E+00	.1314E+06	.5350E-01	.4302E-01	.4291E-01	.1072E+01
.8632E+00	.1188E+06	.5908E-01	.3468E-01	.4808E-01	.1069E+01
.8737E+00	.1060E+06	.6716E-01	.2730E-01	.5454E-01	.1067E+01
.8842E+00	.9303E+05	.7992E-01	.2082E-01	.6275E-01	.1066E+01
.8947E+00	.8015E+05	.9478E-01	.1529E-01	.7345E-01	.1068E+01
.9053E+00	.6859E+05	.1087E+00	.1109E-01	.8659E-01	.1072E+01
.9158E+00	.5764E+05	.1318E+00	.7797E-02	.1037E+00	.1079E+01
.9263E+00	.4778E+05	.1621E+00	.5331E-02	.1252E+00	.1092E+01
.9368E+00	.3917E+05	.1534E+00	.3525E-02	.1527E+00	.1113E+01
.9474E+00	.3168E+05	.1372E+00	.2226E-02	.1901E+00	.1143E+01
.9579E+00	.2471E+05	.2935E+00	.1296E-02	.2477E+00	.1169E+01
.9684E+00	.1810E+05	.6380E+00	.6695E-03	.3445E+00	.1172E+01
.9789E+00	.1164E+05	.1237E+01	.2710E-03	.5423E+00	.1240E+01
.9895E+00	.5106E+04	.2299E+01	.5185E-04	.1242E+01	.1748E+01

PIPE LENGTH = 2 FEET, INSIDE DIAMETER = 1/4 INCH
SOURCE PRESSURE = 20 PSIA, SINK PRESSURE = 15 PSIA

Z/L	RE	F	MA2	V/U	PHI
.1053E-01	.6110E+03	.2756E-01	.1076E-04	-.2694E+00	.1300E+01
.2105E-01	.1325E+04	.1496E-01	.5067E-04	-.1244E+00	.1238E+01
.3158E-01	.1939E+04	.1032E-01	.1085E-03	-.8530E-01	.1229E+01
.4211E-01	.2658E+04	.7550E-02	.2039E-03	-.6249E-01	.1230E+01
.5263E-01	.3277E+04	.6114E-02	.3102E-03	-.5100E-01	.1230E+01
.6316E-01	.4005E+04	.5010E-02	.4633E-03	-.4201E-01	.1230E+01
.7368E-01	.4632E+04	.4328E-02	.6204E-03	-.3665E-01	.1230E+01
.8421E-01	.5375E+04	.3734E-02	.8350E-03	-.3189E-01	.1231E+01
.9474E-01	.6007E+04	.3341E-02	.1046E-02	-.2884E-01	.1230E+01
.1053E+00	.6783E+04	.2958E-02	.1329E-02	-.2591E-01	.1231E+01
.1158E+00	.7405E+04	.2715E-02	.1596E-02	-.2398E-01	.1229E+01
.1263E+00	.8226E+04	.2442E-02	.1956E-02	-.2201E-01	.1231E+01
.1368E+00	.8882E+04	.2264E-02	.2291E-02	-.2070E-01	.1230E+01
.1474E+00	.9642E+04	.2090E-02	.2721E-02	-.1930E-01	.1230E+01
.1579E+00	.1046E+05	.1920E-02	.3154E-02	-.1838E-01	.1231E+01
.1684E+00	.1118E+05	.1801E-02	.3664E-02	-.1733E-01	.1230E+01
.1789E+00	.1195E+05	.1687E-02	.4173E-02	-.1668E-01	.1230E+01
.1895E+00	.1282E+05	.1570E-02	.4813E-02	-.1588E-01	.1231E+01
.2000E+00	.1365E+05	.1479E-02	.5430E-02	-.1541E-01	.1230E+01
.2105E+00	.1447E+05	.1394E-02	.6176E-02	-.1479E-01	.1230E+01
.2211E+00	.1531E+05	.1320E-02	.6908E-02	-.1445E-01	.1229E+01
.2316E+00	.1628E+05	.1242E-02	.7833E-02	-.1396E-01	.1230E+01
.2421E+00	.1722E+05	.1179E-02	.8727E-02	-.1372E-01	.1229E+01
.2526E+00	.1818E+05	.1112E-02	.9816E-02	-.1335E-01	.1231E+01
.2632E+00	.1910E+05	.1064E-02	.1087E-01	-.1319E-01	.1227E+01
.2737E+00	.2017E+05	.1010E-02	.1220E-01	-.1290E-01	.1229E+01
.2842E+00	.2124E+05	.9606E-03	.1350E-01	-.1281E-01	.1227E+01
.2947E+00	.2242E+05	.9047E-03	.1512E-01	-.1260E-01	.1230E+01
.3053E+00	.2354E+05	.8716E-03	.1670E-01	-.1256E-01	.1226E+01
.3158E+00	.2478E+05	.8290E-03	.1867E-01	-.1242E-01	.1229E+01
.3263E+00	.2598E+05	.7912E-03	.2061E-01	-.1244E-01	.1226E+01
.3368E+00	.2734E+05	.7478E-03	.2305E-01	-.1235E-01	.1228E+01
.3474E+00	.2870E+05	.7199E-03	.2549E-01	-.1241E-01	.1224E+01
.3579E+00	.3024E+05	.6839E-03	.2856E-01	-.1239E-01	.1226E+01
.3684E+00	.3178E+05	.6557E-03	.3167E-01	-.1249E-01	.1222E+01
.3789E+00	.3349E+05	.6226E-03	.3558E-01	-.1252E-01	.1225E+01
.3895E+00	.3517E+05	.5987E-03	.3958E-01	-.1268E-01	.1221E+01
.4000E+00	.3707E+05	.5660E-03	.4463E-01	-.1278E-01	.1223E+01
.4105E+00	.3898E+05	.5458E-03	.4992E-01	-.1297E-01	.1218E+01
.4211E+00	.4114E+05	.5193E-03	.5663E-01	-.1313E-01	.1220E+01
.4316E+00	.4335E+05	.4951E-03	.6387E-01	-.1339E-01	.1216E+01
.4421E+00	.4587E+05	.4709E-03	.7314E-01	-.1361E-01	.1216E+01
.4526E+00	.4846E+05	.4538E-03	.8341E-01	-.1392E-01	.1210E+01
.4632E+00	.5143E+05	.4346E-03	.9678E-01	-.1422E-01	.1210E+01
.4737E+00	.5451E+05	.4153E-03	.1121E+00	-.1462E-01	.1203E+01
.4842E+00	.5807E+05	.3937E-03	.1328E+00	-.1505E-01	.1202E+01
.4947E+00	.6170E+05	.3874E-03	.1570E+00	-.7776E-02	.1198E+01

.5158E+00	.6173E+05	.3975E-03	.1573E+00	.1127E-02	.1197E+01
.5263E+00	.6149E+05	.8464E-03	.1551E+00	.1413E-02	.1180E+01
.5368E+00	.6064E+05	.1784E-02	.1437E+00	.2051E-02	.1165E+01
.5474E+00	.6000E+05	.3365E-02	.1441E+00	.2514E-02	.1145E+01
.5579E+00	.5899E+05	.5443E-02	.1376E+00	.3103E-02	.1129E+01
.5684E+00	.5816E+05	.7802E-02	.1329E+00	.3475E-02	.1114E+01
.5789E+00	.5710E+05	.1016E-01	.1271E+00	.3895E-02	.1103E+01
.5895E+00	.5618E+05	.1228E-01	.1226E+00	.4149E-02	.1095E+01
.6000E+00	.5510E+05	.1409E-01	.1174E+00	.4446E-02	.1088E+01
.6105E+00	.5413E+05	.1559E-01	.1130E+00	.4643E-02	.1082E+01
.6211E+00	.5306E+05	.1678E-01	.1082E+00	.4871E-02	.1079E+01
.6316E+00	.5206E+05	.1773E-01	.1040E+00	.5038E-02	.1075E+01
.6421E+00	.5096E+05	.1847E-01	.9944E-01	.5251E-02	.1073E+01
.6526E+00	.4990E+05	.1903E-01	.9528E-01	.5423E-02	.1072E+01
.6632E+00	.4875E+05	.1940E-01	.9083E-01	.5648E-02	.1070E+01
.6737E+00	.4764E+05	.1958E-01	.8671E-01	.5847E-02	.1070E+01
.6842E+00	.4647E+05	.1963E-01	.8239E-01	.6098E-02	.1069E+01
.6947E+00	.4535E+05	.1966E-01	.7831E-01	.6350E-02	.1069E+01
.7053E+00	.4417E+05	.1975E-01	.7409E-01	.6654E-02	.1068E+01
.7158E+00	.4300E+05	.1991E-01	.7004E-01	.6970E-02	.1068E+01
.7263E+00	.4176E+05	.2012E-01	.6588E-01	.7341E-02	.1067E+01
.7368E+00	.4052E+05	.2035E-01	.6186E-01	.7734E-02	.1066E+01
.7474E+00	.3922E+05	.2060E-01	.5778E-01	.8183E-02	.1066E+01
.7579E+00	.3792E+05	.2087E-01	.5385E-01	.8665E-02	.1065E+01
.7684E+00	.3657E+05	.2118E-01	.4990E-01	.9207E-02	.1064E+01
.7789E+00	.3521E+05	.2158E-01	.4608E-01	.9803E-02	.1063E+01
.7895E+00	.3379E+05	.2206E-01	.4228E-01	.1047E-01	.1061E+01
.8000E+00	.3236E+05	.2261E-01	.3862E-01	.1121E-01	.1060E+01
.8105E+00	.3087E+05	.2327E-01	.3500E-01	.1203E-01	.1058E+01
.8211E+00	.2937E+05	.2406E-01	.3155E-01	.1295E-01	.1057E+01
.8316E+00	.2781E+05	.2500E-01	.2818E-01	.1399E-01	.1055E+01
.8421E+00	.2625E+05	.2614E-01	.2500E-01	.1516E-01	.1053E+01
.8526E+00	.2462E+05	.2749E-01	.2191E-01	.1649E-01	.1052E+01
.8632E+00	.2301E+05	.2910E-01	.1903E-01	.1801E-01	.1050E+01
.8737E+00	.2133E+05	.3114E-01	.1628E-01	.1980E-01	.1048E+01
.8842E+00	.1963E+05	.3365E-01	.1375E-01	.2189E-01	.1045E+01
.8947E+00	.1790E+05	.3673E-01	.1137E-01	.2438E-01	.1043E+01
.9053E+00	.1619E+05	.4169E-01	.9243E-02	.2739E-01	.1040E+01
.9158E+00	.1438E+05	.4822E-01	.7273E-02	.3124E-01	.1039E+01
.9263E+00	.1258E+05	.5574E-01	.5548E-02	.3608E-01	.1039E+01
.9368E+00	.1086E+05	.6611E-01	.4076E-02	.4231E-01	.1040E+01
.9474E+00	.9148E+04	.8073E-01	.2835E-02	.5085E-01	.1042E+01
.9579E+00	.7406E+04	.1126E+00	.1824E-02	.6362E-01	.1046E+01
.9684E+00	.5564E+04	.1914E+00	.1020E-02	.8533E-01	.1064E+01
.9789E+00	.3671E+04	.4406E+00	.4423E-03	.1299E+00	.1109E+01
.9895E+00	.1841E+04	.9467E+00	.1112E-03	.2593E+00	.1228E+01

APPENDIX D: One-Dimensional Model, Computer Code

The pages that follow are a listing of the one-dimensional computer code. A warning about the code should be mentioned. As discussed in Chapter VII, the step size used in marching the solution down the pipe depends on the local Mach number. As the Mach number approaches 1, the step size becomes very small. If the initial upstream internal pressure is guessed too small, a problem may result where the step size becomes so small that the solution doesn't progress down the pipe. If this occurs, guessing a larger initial upstream internal pressure will solve the problem.

```
      PROGRAM ONEDF (INPUT,OUTPUT,TAPE1=INPUT,TAPE2=OUTPUT,TAPE3,TAPE4)
C
C  THIS PROGRAM USES A ONE-D COMPRESSIBLE FLOW MODEL WITH FRICTION
C  TO FIND HOW PROPERTIES VARY IN A CLOSED PIPE WITH BLOWING AND
C  SUCTION.  THE BASIC METHOD IS SHAPIRO'S METHOD OF INFLUENCE
C  COEFFICIENTS.
C
C DEFINITION OF VARIABLES
C
C    A      CONSTANT USED IN WALL BLOWING BOUNDARY CONDITION

C    B      CONSTANT USED IN WALL BLOWING BOUNDARY CONDITION
C    C      DUMMY VARIABLE USED IN CALCULATING THE WALL BOUNDARY CONDITION
C    C2     SPEED OF SOUND SQUARED ((FT/SEC)2)
C    D      PIPE INSIDE DIAMETER (FT)
C    DELP   CHANGE IN PO FOR BISECTION METHOD OF FINDING ACTUAL PO
C    DELW   CHANGE IN MASS FLOW RATE DUE TO MASS TRANSFER AT THE WALL

C    DELX   SPACIAL STEP SIZE
C    F      FRICTION COEFFICIENT
C    FF     SHAPIRO'S FRICTION INFLUENCE COEFFICIENT
C    FFP    SHAPIRO'S FRICTION INFLUENCE COEFFICIENT
C    FL     LAMINAR FRICTION COEFFICIENT
C    FT     TURBULENT FRICTION COEFFICIENT
C    FUD    CONSTANT TO ACCOUNT FOR STATISTICAL VARIATION OF POROUS

C            PIPE PROPERTIES
C    FW     SHAPIRO'S MASS ADDITON INFLUENCE COEFFICIENT
C    FWP    SHAPIRO'S MASS ADDITON INFLUENCE COEFFICIENT
C    GAMMA  RATIO OF SPECIFIC HEATS
C    N      STEP COUNTER
C    NM     ITERATION COUNTER
C    NN     NN=1 FOR PREDICTIO LOOP, NN=2 FOR CORRECTOR LOOP
C    P      PRESSURE (LBF/FT2)
C    P2      NEST STEP'S VALUE OF P

C    PEVAP  EVAPORATOR ENVIRONMENT PRESSURE
C    PEX    ENVIORNMENT PRESSURE
C    PCOND  CONDENSER ENVIRONMENT PRESSURE
C    PL     PIPE LENGTH
C    PLM    HALF THE PIPE LENGTH
C    PO     UPSTREAM END OF PIPE PRESSURE
C    PO2    NEXT STEPS TOTAL PRESSURE
C    R      IDEAL GAS CONSTANT FOR AIR
C    RER    RADIAL REYNOLDS NUMBER
C    REY    REYNOLDS NUMBER BASED ON PIPE DIAMETER
```

```
C     RHO   DENSITY ((LBF/SEC^2/FT^4)
C     RHO2  NEXT STEPS DENSITY
C     RHOV  MASS VELOCITY BLOWING THROUGH THE WALL (LBF-SEC/FT^3)
C     RMU   VISCOSITY
C     TO    AIR TEMPERATURE (R)
C     W     LOCAL MASS FLOW RATE
C     W2    NEXT STEP'S LOCAL MASS FLOW RATE
C     WBAR  AVERAGE LOCAL MASS FLOW RATE (CORRECTOR STEP)
C     X     AXAIL LOCATIO
C     X2    NEXT STEPS AXAIL LOCATION

C     XBAR  VARIABLE USED IN LAMINAR TO TURBULENT TRANSITION MODEL
C     XM    LOCAL VELOCITY
C     XM2   NEXT STEP'S LOCAL VELOCITY
C
C   ENTER SPECIFIC PROBLEM VARIABLES
C
        PEVAP=38.90*144
        PCOND=24.50*144
        P0=35.25
        P0=P0*144
        DELP=72
        A=3.636E+9
        B=1.701E+8
        T0=540
        R=1718.
        GAMMA=1.4
        GAMM1=GAMMA/(GAMMA-1)

        D=0.650/12.
        NM=1
1       PL=2.
        PEX=PEVAP
        PLM=PL/2
        DELX=0.01
        FUD=1.07
C
C   INITIALIZE THE VARIABLES AT THE UPSTREAM PIPE END
C
        W =0.0
        XM2=0.0
        X =0.0
        P =P0
        T =T0
        RHO =P0/R/T0
```

```
C
C  USE INCOMPRESSIBLE MODEL TO GET THE STARTING VALUES
C
      C=ABS(P**2-PEX**2)
      RHOV=-(-B+SQRT(B**2+4.*A*C))/(2.*A)*FUD

      C2=GAMMA*P/RHO
      XM22=(4.0*RHOV*DELX/RHO/D)**2/C2
      W2=W-RHOV*DELX*D*3.14*32.2
      X2=X+DELX
      P2=P0/(1.+(GAMMA-1)/2*XM22)**GAMM1
      P02=P0
      RHO2=RHO
C
C  MARCH DOWN THE PIPE FINDING THE FLOW PROPERTIES ALONG THE WAY
C
      N=1
5     CONTINUE
      N=N+1
      IF (X .GT. PLM) PEX=PCOND
      XM2=XM22
      P=P2
      P01=P02
      W=W2
      DELX=0.020*(1.-XM2)**2
      X=X+DELX
C
C  PREDICTOR AND CORRECTOR STEPS
C
      DO 8 NN=1,1
C
C     CALCULATE THE INFLUENCE COEFFICIENTS
C
      XM2BAR=(XM2+XM22)/2.
      CON1=1.+(GAMMA-1)/2*XM2BAR
      CON2=1.-XM2BAR
      CON3=1.+GAMMA*XM2BAR
      CON4=GAMMA*XM2BAR
      FW=2.*CON3*CON1/CON2
      FWP=CON4
C
C    FIND THE MASS ADDED THROUGH THE PIPE WALL

C
      PBAR=(P2+P)/2
      C=PBAR**2-PEX**2
      ID=1
      IF (C .LT. 0.0) ID=-1
      C=ABS(C)
      RHOV=ID*(-B+SQRT(B**2+4.*A*C))/(2.*A)*FUD
      DELW= -RHOV*DELX*D*3.14*32.2
      W2=W+DELW
      IF (W2 .LT. 0) GO TO 30
```

```
C
C     FIND THE FRICTION FACTOR AND THE FRICTION INFLUENCE COEFFICIENT
C
      T=T0/CON1
      RMU=2.27E-08*SQRT(T**3)/(T+198.6)

      WBAR=(W+W2)/2
      REY=4*WBAR/3.14/D/RMU/32.2
      RER=RHOV*D/RMU
      XBAR=((X-1.00)/.25)**2
      FL=16/REY*1.2337*EXP(1.20*XM2)
C     FL=16/REY
      BETA=ABS(RER/REY)
      FSTAR=0.046/REY**0.2
      FT=FSTAR*(1+55*REY**.1*EXP(1.2*XM2)*BETA**0.9*FL/D**0.1)
C     FT=FSTAR
      F=FT-(FT-FL)*EXP(-.412*XBAR)
      IF (X .LE. 1.0) F=FL
      FF=CON4*CON1/CON2*4*F/D

      FFP=CON4/2*4*F/D
C     FF=0.0
C     FFP=0.0
C
C     FIND THE CHANGE IN MACH NUMBER AND PRESSURE DUE TO FRICTION AND
C     MASS ADDITION
C
      XM22=EXP(ALOG(XM2)+FF*DELX+FW*ALOG(W2/W))
      P02=EXP(ALOG(P01)-FFP*DELX-FWP*ALOG(W2/W))
      P2=P02/(1.+(GAMMA-1)/2*XM22)**GAMM1
8     CONTINUE
C
9     WRITE(2,*) X/PL,P2/P0,W2
C
C CHECK FOR CONVERGENCE AND GUESS A NEW VALUE FOR P0
C
      IF (X .GT. PL) GO TO 10
      IF (N .EQ. 2500) GO TO 40
      GO TO 5
10    CONTINUE
      GO TO 40
      IF (W2 .LT. .001) GO TO 40
      NM=NM+1
      WRITE(2,*) 'NM=',NM,'P0=',P0
```

```
      IF (NM .GT. 8) GO TO 40
      DELP=DELP/2
      PO=PO+DELP
      GO TO 1
30    DELP=DELP/2
      GO TO 40
      PO=PO-DELP
      NM=NM+1
      IF (NM .GT. 8) GO TO 40
      WRITE (2,*) 'NM=   ',NM,'PO=    ',PO
      GO TO 1
40    STOP
      END
```

BIBLIOGRAPHY

1. Ivanovskii, M. N, V. P. Sorokin, and I. V. Yagodkin. The Physical Principles of Heat Pipes. New York: Oxford University Press, 1982.

2. Berman, A. S. "Laminar Flow in Channels with Porous Walls," Journal of Applied Physics, 24 (9): 1232-1235, Sept. 1953.

3. Schlichting, H. Boundary-Layer Theory. Seventh Edition, McGraw-Hill Book Company, 1979.

4. Brady, J. K. "Flow Development in a Porous Channel and Tube," Physics of Fluids, 27 (5): 1061-1067, May 1984.

5. Friedman, M. and Gillis, J. "Viscous Flow in a Pipe with Absorbing Walls," Journal of Applied Mechanics, Transactions of the ASME, 819-822, December 1967.

6. Kinney, R. B. "Fully Developed Frictional and Heat Transfer Characteristics of Laminar Flow in Porous Tubes," International Journal of Heat and Mass Transfer, 11: 1393-1401, 1968.

7. Rathby, G. "Laminar Heat Transfer in the Entrance Region of Circular Tubes and Two-Dimensional Rectangular Ducts with Wall Suction and injection," Journal of Heat and Mass Transfer, Vol. 14, 223-243, 1971.

8. Terrill, R. M. and Thomas, P. W. "On Laminar Flow Through a Uniform Porous Pipe," Applied Science Research, 21: 37-67, August 1969.

9. Terrill, R. M. "An Exact Solution for Flow in a Porous Pipe," Journal of Applied Mathematics and Physics, 33: 547-552, July 1982.

10. Terrill, R. M. "Laminar Flow in a Porous Tube," Journal of Fluids Engineering, 105: 303-307, Sept 1083.

11. Chi, S. W. Heat Pipe Theory and Practice. New York: McGraw-Hill Book Company, 1976.

12. Dunn, P. and D. A. Reay. Heat Pipes (Second Edition). London: Perganon Press, 1978.

13. Cotter, T. P. "Theory of Heat Pipes," LA-3246-MS, Los Alamos Scientific Laboratories, Los Almos, N. M., 1965.

14. Yuan, S. W. and Finkelstein, A. B. "Laminar Pipe Flow With Injection and Suction Through a Porous Wall," Transactions of the ASME: 719-724, May 1956.

15. Knight, B. W. and B. B. McInteer. "Laminar Incompressible Flow in Channels with Porous Walls," LADC-5309, Los Alamos Scientific Laboratory, Los Alamos, N. M., 1965.

16. Wageman, W. E. and Guevara, F. A. "Fluid Flow Through a Porous Channel," The Physics of Fluids, 3 (6): 878-881, Nov-Dec 1960.

17. Bankston, C. A. and H. J. Smith. "Vapor Flow in Cylindrical Heat Pipes," Transactions of ASME, Journal of Heat Transfer, 95: 371-376, 1973.

18. Van Ooijen, H. and C. J. Hoogendoorn. "Numerical Calculations on the Vapor Flow in a Flat-Plate Heat Pipe with Asymmetrical Boundary Conditions," Third International Heat Pipe Conference: Palo Alto Califonia, 1978.

19. Van Ooijen, H. and C. J. Hoogendoorn. "Experimental Pressure Profile along the Vapor Channel of a Flat-Plate Heat Pipe," Forth International Heat Pipe Conference: London, 1981.

20. Levy, E. K. "Theoretical Investigation of Heat Pipes Operating at Low Vapor Pressures," Transactions, ASME Journal for Industry: 547, November, 1968.

21. Kemme, J. E. "Heat Pipe Capability Experiment," IEEE Therionic Conversion Specialist Conference, Nov. 1966, Houston, Texas.

22. Bystrov, P. I. and A. N. Popov. "The Supersonic Flow of Vapor in the Condensation Zone of High Temperature Heat Pipes," Third International Heat Pipe Conference: Palo Alto, California, 21-26, 1978.

23. DeMichele, D. W. A Numerical Solution to Axial Symmetric Compressible Flow with Mass Injection and its Application to Heat Pipes. PhD Dissertation, Department of Nuclear Engineering, University of Arizona, 1970.

24. Von Vises, R. "Bermerkugen Zur Hydrodynamik," ZAMM 7, 425-431, 1927.

25. Tien. C. L. and A. R. Rohani. "Analysis of the Effects of Vapor Pressure Drop on Heat Pipe Performance," Journal of Heat and Mass Transfer, 17: 61-67, 1974.

26. Busse. C. A. and F. C. Prenger. "Numerical Analysis of the Vapor Flow in Cylindrical Heat Pipes," Fifth International Heat Pipe Conference: Tsukuba, Japan, 19-24, 1984.

27. Haug, F. and C. A. Busse. "Pressure Recovery in a Cylindrical Heat Pipe at High Radial Reynolds Numbers and at High Mach Numbers," AIAA 20th Thermophysics Convention: Williamsburg, Virginia, 1985.

28. Quaile, J. P., and Levy, E. K. "Laminar Flow in a Porous Tube With Suction," Journal of Heat Transfer, Transactions of the ASME, 66-71, February 1975.

29. Aggarwal, M. A., Hollingsworth, M. A., and Mayhew, Y. R. "Experimental Friction Factors for Turbulent Flow with Suction in a Porous Tube," International Journal of Heat and Mass Transfer, 15: 1585-1602, Pergamon Press 1972.

30. Beam, J. E. "Transient Heat Pipe Analysis," AIAA 20th Thermophysics Conference: Williamsburg, Virginia, 1985.

31. Chang, W. S. Heat Pipe Startup from the Supercritical State. PhD Thesis, Georgia Institute of Technology, Atlanta, Georgia, 1981.

32. Colwell, G. T. "Transient Heat Pipe Operation in the Near Critical Region," Forth International Heat Pipe Conference: London, 7-10, 1981.

33. Klein, D. and Catton, I. "Transient Analysis of Heat Pipe Vapor Dynamics," Preedings of 4th Symposium on Space Nuclear Power Systems, Albuquerque, New Mexico, January 1987.

34. Ransom, V. "Athena Heat Pipe Transient Model," same as 33.

35. Costello, F., Montague, A., Merrigan, M., and Reid, R. A Detailed Transient Model of a Liquid-Metal Heat Pipe," same as 33.

36. Colwell, G. T. "Transient Heat Pipe Modeling at Georgia Tech," same as 33.

37. Hall, M., and Doster, J., "Transient Thermohydraulic Heat Pipe Modleing," same as 33.

38. Cebici, T. "Behavior of Turbulent Flow near a Porous Wall with Pressure Gradient," AIAA Journal, Vol. 8, No. 12, 2152-2156, December 1970.

39. Doshi, M. R. and Gill, W. N. "Turbulent Flow in a Tube With Wall Suction," Journal of Heat Transfer, 251-252, May 1974.

40. Kays, W. M. and Moffat, R. J. Studies in Convection, Vol 1, Academic Press, London, 213-319, 1975.

41. Kinney, R. B. and Sparrow, E. M. "Turbulent Flow, Heat Transfer, and Mass Transfer in a Tube With Surface Suction," Journal of Heat Transfer, 117-125, February 1970.

42. Merkine, L., Solan, A., and Winograd, Y. "Turbulent Flow in a Tube With Wall Suction," Journal of Heat Transfer, 242-244, May 1971.

43. Van Driest, E. R. "On Turbulent Flow Near a Wall," Journal of Aerospace Science, Vol. 23, No. 11, 1007-1011, November 1956.

44. Brosh, A. and Winograd, Y. "Experimental Study of Turbulent Flow in a Tube With Wall Suction," Journal of Heat Transfer, 338-342, August 1974.

45. Eroshenko, V. M., Ershov, A. V., and Zaichik, L. I. "Calculation of Turbulent Flow of an Incompressible Fluid in a Circular Tube With Suction Through Porous Walls," Fluid Dynamics, Translated from Russian, Vol. 17, No. 4, 559-564, July-August 1982.

46. Shapiro, A. H. The Dynamics and Thermodynamics of Compressible Fluid Flow. Vol. 1, The Ronald Press Company, New York, 1953, pp 238-241.

47. Bean, H. S. Fluid Meters, Their Theory and Application, Sixth Edition, 1971, The Americal Society of Mechanical Engineers. New York.

48. Muskat, M., The Flow of Homogeneous Fluids Through Porous Media, J. W. Edwards, Inc. Ann Arbor, Michigan, 1946.

49. Anderson, A. A., Tannehill, J. C. and Pletcher, R. H., Computational Fluid Mechanics and Heat Transfer. McGraw Hill Book Company, 1984.

50. Cebeci, T. and Smith, A. M. O., Analysis of Turbulent Boundary Layers. Academic Press, New York, 1974.

51. Baldwin, B. S. and Lomax, H., "Thin Layer Approximation and Algebraic Model for Separated Turbulent Flows," AIAA 16th Aerospace Sciences Meeting, Huntsville Alabama, January 1978.

52. Dhawan, S. and Narasimha, R. "Some properties of Boundary Layer Flow during the Transition from Laminar to Turbulent Motion," Journal of Fluid Mechanics, Vol. 3. Part 4, 418-436, 1958.

53. MacCormack, R. W. "The Effect of Viscousity in Hypervelocity Impact Cratering," AIAA Paper No. 69-354, 1969.

54. MacCormack, R. W. and Baldwin, B. S., "A Numerical Method for Solving the Navier-Stokes Equations with Application to Shock-Boundary Layer Interaction," AIAA 13th Aerospace Sciences Meeting, Pasadena, California, January 1975.

Vita

Jerry Bowman [redacted] graduated from Capital High School in Boise in 1972. From 1973 to 1975 he served a mission for The Church of Jesus Christ of Latter-day Saints in Uruguay, South America. In 1978 he graduated Magna Cum Laude from Brigham Young University, receiving a BS in Mechanical Engineering. From 1978 to 1982 he served as a commisioned officer in the United States Navy. During that time he taught Mathematics, Heat Transfer, Thermodynamics and Fluid Mechanics at the Naval Nuclear Power School in Orlando, Florida. In 1982 he received a MSE in Mechanical Engineering from the University of Central Florida. Also in 1982 he accepted a commision as a Captain in the United States Air Force. From 1982 to 1984 he worked as a Space Shuttle Systems Engineer at the National Aeronautics and Space Administrations Kennedy Space Center, Florida. In June of 1984 he began Doctoral studies at the Air Force Institute of Technology studying Aeronautical Engineering.

[redacted]

UNCLASSIFIED
SECURITY CLASSIFICATION OF THIS PAGE

REPORT DOCUMENTATION PAGE

Form Approved OMB No 0704-0188

AD-A182592

1a. REPORT SECURITY CLASSIFICATION UNCLASSIFIED	1b. RESTRICTIVE MARKINGS
2a. SECURITY CLASSIFICATION AUTHORITY	3 DISTRIBUTION/AVAILABILITY OF REPORT APPROVED FOR PUBLIC RELEASE; DISTRIBUTION UNLIMITED.
2b. DECLASSIFICATION/DOWNGRADING SCHEDULE	
4. PERFORMING ORGANIZATION REPORT NUMBER(S) AFIT/DS/ENY/87	5. MONITORING ORGANIZATION REPORT NUMBER(S)
6a. NAME OF PERFORMING ORGANIZATION SCHOOL OF ENGINEERING 6b. OFFICE SYMBOL (If applicable) AFIT/ENY	7a. NAME OF MONITORING ORGANIZATION
6c. ADDRESS (City, State, and ZIP Code) AIR FORCE INSTITUTE OF TECHNOLOGY WRIGHT-PATTERSON AFB, OHIO 45433	7b. ADDRESS (City, State, and ZIP Code)
8a. NAME OF FUNDING/SPONSORING ORGANIZATION 8b. OFFICE SYMBOL (If applicable)	9 PROCUREMENT INSTRUMENT IDENTIFICATION NUMBER
8c. ADDRESS (City, State, and ZIP Code)	10 SOURCE OF FUNDING NUMBERS PROGRAM ELEMENT NO. / PROJECT NO / TASK NO / WORK UNIT ACCESSION NO

11. TITLE (Include Security Classification)
SIMULATED HEAT-PIPE VAPOR DYNAMICS

12. PERSONAL AUTHOR(S)
W. JERRY BOWMAN, M.S.E., CAPT, USAF

13a. TYPE OF REPORT	13b TIME COVERED	14. DATE OF REPORT (Year, Month, Day)	15 PAGE COUNT
PhD DISSERTATION	FROM ____ TO ____	1987 MAY	227

16. SUPPLEMENTARY NOTATION

17. COSATI CODES			18 SUBJECT TERMS (Continue on reverse if necessary and identify by block number)
FIELD	GROUP	SUB-GROUP	
20	04		HEAT PIPE ,FRICTION COEFFICIENT, FRICTION FACTOR, INJECTION, SUCTION, EXTRACTION, BLOWING

19. ABSTRACT (Continue on reverse if necessary and identify by block number)

DISSERTATION CHAIRMAN: JAMES E. HITCHCOCK
PROFESSOR OF MECHANICAL ENGINEERING

20. DISTRIBUTION/AVAILABILITY OF ABSTRACT ☒ UNCLASSIFIED/UNLIMITED ☐ SAME AS RPT ☐ DTIC USERS	21 ABSTRACT SECURITY CLASSIFICATION UNCLASSIFIED
22a. NAME OF RESPONSIBLE INDIVIDUAL JAMES E. HITCHCOCK, PhD	22b TELEPHONE (Include Area Code) 513-255-3517 22c OFFICE SYMBOL AFIT/ENY